Non-Uniform Heat Transfer in Thermal Regenerators

Jensen, Jesper Buch

Publication date:
2011

Document Version
Publisher's PDF, also known as Version of record

Non-Uniform Heat Transfer in Thermal Regenerators

Jesper Buch Jensen

Ph.D. Thesis

Risø DTU

November 2011

Preface

This thesis was prepared at the Fuel Cells and Solid State Chemistry Division at Risø DTU with Nini Pryds, Christian Bahl, and Brian Elmegaard as supervisors. The project has been financed by the Programme Commission on Energy and Environment (EnMi) (Contract no. 2104-06-0032) which is part of the Danish Council for Strategic Research. I would like to express my gratitude to my supervisors for their support and guidance throughout the project, as well as Kurt Engelbrecht for his advice and for useful discussions.

During the research project, I have visited the Solar Energy Laboratory at the Department of Mechanical Engineering, University of Wisconsin-Madison in the United States for a period of five months. During this visit, the main part of the regenerator model described in the thesis was developed and numerous good results were obtained. I owe Professors Gregory Nellis and Sanford Klein my sincerest thanks for their advice and hospitality throughout my visit.

I have had many useful discussions and received a lot of support from my office mates, Kaspar Kirstein Nielsen, Rasmus Bjørk, and Dan Eriksen, for which I am very grateful. I would also like to thank them for being great office mates in general and always keeping spirits high in (and out of) the office.

I would like to thank Jørgen Geyti, who has provided excellent technical assistance, particularly with the modifications that have been made to the experimental setup. Likewise, Finn Saxild and Kristian Nim Sørensen have been great to provide technical assistance, which has been of much value.

Dennis Christensen is thanked for his contributions to the experimental work and for useful discussions is this respect.

Finally, I would like to thank my many other colleagues and friends at Risø DTU and at the University of Wisconsin-Madison who have provided help and encouragement throughout the years.

July 5, 2011
Jesper Buch Jensen

Contents

Abstract

This thesis presents investigations on the heat transfer in complex heat exchangers in general and in regenerative heat exchangers (regenerators) in particular. The motivation for this work is a result of inconsistencies obeserved in the results from a series of experiments on active magnetic regenerators (AMRs) with parallel plates. The results suggest that random variations in the regenerator geometries causes maldistributed fluid flow inside the regenerators, which affects the regenerator performance.

In order to study the heat transfer processes in regenerators with non-uniform geometries, a numerical model, which simulates a single-blow operation in a parallel-plate regenerator, was developed and used to model the heat transfer under various conditions.

In addition to the modeling of the heat transfer, a series of experiments on passive regenerators with non-uniform, but precisely controlled, geometries was performed. The objective of performing these experiments was in part to evaluate the direct applicability of the model, which only simulates one half of the regenerator cycle, to a practical situation where the regenerator is running continuously by comparing the results gained. Additionally, the experiments gave real comparative results, whereas the model to a certain degree more served to provide insight to the heat transfer processes taking place inside the regenerators, something that would be - if not impossible - then highly impractical to do experimentally.

It has been found that non-uniformity in the plate spacings of non-uniform regenerators can have a significant impact on the regenerator effectiveness, particularly for regenerators with small plate spacings. The observed reductions in effectiveness have furthermore been found to alter the optimim plate spacing, and decreasing the plate spacing beoynd a certain point can even hurt the performance.

Inter-channel heat transfer effects - or thermal cross-talk - have also been investigated and the results show that not only the size of the plate spacings, but also their mutual order, can affect the heat transfer significantly.

Resumé

I denne afhandling bliver en række undersøgelser af varmeoverførsel i komplekse varmevekslere og termiske regeneratorer med parallelle plader præsenteret. Disse enheder bliver brugt i mange sammenhænge, men i her er der især fokuseret på anvendelsen af aktive magnetiske regeneratorer (AMR'er) i forbindelse med magnetisk køling ved stuetemperatur.

Magnetisk køling er en teknologi, hvor der produceres køling ved hjælp af et varierende magnetfelt og et såkaldt magnetokalorisk materiale. Ved stuetemperatur vil feltet typisk blive produceret af en kraftig permanent magnet, hvilket kræver relativt meget magnetisk materiale per magnetiseret volumen.

En AMR skal derfor være kompakt og have en høj varmeoverførsel per volumen, hvilket for regeneratorer med parallelle plader, betyder at plade- og kanaltykkelserne skal være så små som muligt. Dog har det vist sig at der opstår betydelige variationer i kanaltykkelserne når parallel-plade regeneratorer med kanaltykkelser på 0.1 til 1 mm fremstilles.

Det er derfor blevet undersøgt, hvordan disse variationer påvirker effektiviteten af regeneratorerne og resultaterne viser betydelige reduktioner i effektiviteten for regeneratorer med ujævnt fordelte kanaltykkelser. Ydermere er det blevet fundet, at det ikke nødvendigvis giver bedre varmeoverførsel at have tyndere kanaler, da de relative afvigelser typisk stiger når kanalerne bliver tyndere.

Ydermere har det vist sig at effektiviteten ikke kun bestemmes af, hvor stor variationen i kanaltykkelserne er, men i høj grad også, hvilke nabokanaler, hver enkelt kanal har. Denne effekt vil naturligvis udlignes i regeneratorer med mange kanaler, men for regeneratorer hvor antallet af kanaler er i størrelsesordenen 20 eller mindre kan disse tilsyneladende tilfældige variationer være ganske store.

Symbols

a	Slope of temperature difference as a function of heat load (eqs. 8.5 and 8.6)	K/W
A_c	Cross section area	m^2
AF	Augmentation factor	
AR	Aspect ratio (p. 67)	
A_s	Surface area	m^2
b	Constant for element function	
Bi	Biot number (eq. 5.19)	
Br	Brinkman number (eq. 5.5)	
c	Specific heat capacity	J/(kg K)
C	A constant (eq. 9.6)	
C_R	Capacity ratio (eq. 6.3)	
COP	Coefficient of performance (eq. 1.4)	
d	Depth of regenerator in z-direction (fig. 5.1)	m
D_h	Hydraulic diameter (eq. 1.7)	m
E	Energy	J
$FWHM$	Full width a half maximum	
h	Heat transfer coefficient	$\mathrm{W}/(\mathrm{m}^2\ \mathrm{K})$
H	Magnetic field	T/μ_0
i	Index	
j	Index	
k	Thermal conductivity	W/(m K)

K	Number of nodes assigned to element	
K_{R}	A constant (eq. 9.3)	
$\hat{l}$	Length dimension	
L	Length of regenerator (fig. 5.1)	m
L_{e}	Hydrodynamic entry length	m
m	Mass	kg
$\dot{m}$	Mass flow rate	kg/s
$\hat{m}$	Mass dimension	
M	Magnetization	T/μ_0
M_{R}	Regenerator performance parameter (eq. 9.2)	
n	Number of input variables	
N	Number of channels in regenerator	
NTU	Number of transfer units (eq. 1.5)	
Nu	Nusselt number (eq. 1.6)	
p	Probability density function	
P	Pressure	Pa
Pe	Peclet number (p. 67)	
P_{w}	Wetted perimeter	m
q	Thermal energy	J
$\dot{q}$	Heat transfer rate	W
r	Rank of dimensional matrix	
R	Thermal resistance	K/W
Re	Reynolds number (eq. 1.14)	
R_k	Ratio of thermal conductivity of fluid to thermal conductivity of solid (p. 67)	
R_{M}	Ratio of thermal mass of fluid to solid	
$\mathbf{R}_{\mathrm{N}}$	Vector of normally distributed random numbers	
R_α	Ratio of thermal diffusivity of fluid to thermal diffusivity of solid (p. 67)	
s_N	Standard deviation	
s_N^*	Relative standard deviation (p. 67)	
S	Entropy	J/K
S_{R}	Regenerator performance parameter (eq. 9.5)	
t	Time	s

$\hat{t}$	Time dimension	
t_{B}	Blow period	s
T	Temperature	K
$\hat{T}$	Temperature dimension	
T_{C}	Curie temperature	K
ΔT_{ad}	Adiabatic temperature change	K
u	Fluid velocity in x-direction	m/s
$\mathbf{u}$	Fluid velocity vector	
U	Overall heat transfer coefficient	$\mathrm{W/(m^2\ K)}$
v	Number of independent variables	
V	Volume	$\mathrm{m^3}$
$\dot{V}$	Volumetric flow rate	$\mathrm{m^3/s}$
w	Channel width (fig. 5.1)	m
$\mathbf{w}$	Channel width distribution	
w_{pl}	Plate width (fig. 5.1)	m
W	Work	J
x	Spatial coordinate along length of regenerator (fig. 5.1)	
x_2	Spatial coordinate along horizontal direction in image plane (fig. 3.1)	
y	Spatial coordinate along width of regenerator (fig. 5.1)	
y_2	Spatial coordinate along vertical direction in image plane (fig. 3.1)	
z	Spatial coordinate along depth of regenerator (fig. 5.1)	
z_2	Spatial coordinate along direction perpendicular to image plane (fig. 3.1)	

Greek symbols

α	Thermal diffusivity	m^2/s
ε_{Reg}	Regenerator effectiveness (eq. 1.11)	
ε_{SB}	Single blow effectiveness (eq. 1.8)	
η	Porosity (p. 67)	
θ	Angle	degrees
μ	Viscosity	Pa s
μ_0	Vacuum permeability	T m/A
ρ	Density	kg/m^3
ϕ	Element function	
Φ	Utilization (eq. 1.13)	

Subscripts

amb	Ambient
bulk	Bulk
cold	Cold end of regenerator
cond	Conduction
conv	Convection
eq	Equivalent
E	Electronic
f	Fluid
fin	Final
hot	Hot end of regenerator
HL	Heat load
i	In
in	Inlet
init	Initial
L	Lattice
m	Mean
max	Maximum
M	Magnetic
net	Net
nom	Nominal

o	Out
p	Peak value
s	Solid
t	Transferred between fluid and solid
tot	Total

Miscellaneous

$\dot{a}$	Per unit time
a'	Per unit depth
a''	Per unit area
$\bar{a}$	Mean value
$\langle a \rangle$	Expectation value
a^*	Relative (dimensionless) value
$\mathbf{a}$	Vector

Abbreviations

AISI	American Iron and Steel Institute
AMR	Active Magnetic Regenerator
HEX	Heat Exchanger
MCE	Magnetocaloric Effect
Risø DTU	Risø National Laboratory for Sustainable Energy, Techincal University of Denmark
SLS	Selective Laser Sintering

Chapter 1

Introduction

1.1 Outline

The thesis is structured as follows: In this initial chapter, an introduction to magnetic refrigeration and the regenerator theory that is used for the heat transfer analysis in this thesis is presented. Furthermore, a brief introduction to the issue with non-uniformity in regenerators is given.

The second chapter describes the experimental setup, which has been used both for the initial experiments on active magnetic regenerators (AMRs) and subsequent experiments on passive regenerators.

In the third chapter, the method used for measuring the geometries of the regenerators is described.

The fourth chapter presents the experiments performed on AMRs that led to the development of the model, which is described in the fifth chapter.

The sixth and seventh chapters each present a series of simulations that were performed using the model and analysis of the results provide an understanding of the process of heat transfer in various versions of irregular regenerators.

In the eighth chapter, experiments that were performed on a series of passive regenerators are presented and an analysis of the results, which includes comparison with numerical results, is undertaken.

The ninth chapter presents an alternative series of simulations that model geometries of actual passive regenerators which were fabricated for the purpose.

Finally a summary of the results obtained from the investigations is presented together with an overview of the conclusions that have been reached and an outlook on possible future work.

1.2 Regenerator Theory

Refrigeration and air conditioning accounts for a relatively large fraction of today's energy consumption. According to surveys, 30 % of the electricity consumption in US homes and 24 % in commercial buildings (in 2001 and 2003, respectively) is used for refrigeration and air conditioning [1, 2].

A very widespread method used for refrigeration is based on the vapour compression cycle, which consists of compression and expansion of a refrigerant. The refrigerants used are most commonly chloro-fluoro-carbon (CFC), hydro-chloro-fluoro-carbon (HCFC), and hydro-fluoro-carbon (HFC) gases. The former two have high ozone depletion potentials and all three have high global warming potentials, and the uses of these refrigerants are being regulated by international protocols [3, 4].

Magnetic refrigeration is an alternative technology to compression-based refrigeration which utilizes a varying magnetic field in order to heat and cool a refrigerant. The refrigerants used in magnetic refrigeration are solid state materials with zero ozone depletion potential and zero global warming potential.

1.2.1 The Magnetocaloric Effect

Magnetic refrigeration is based on the magnetocaloric effect (MCE), which is an effect exhibited by all magnetic materials. The effect causes a temperature change when the material is subjected to a varying magnetic field. The temperature change is a result of a transfer of energy from a magnetic state to a thermal state which is caused by the change in the magnetization of the material.

Figure 1.1 illustrates the spin alignment in a paramagnetic material in a magnetic field and in zero field. In zero field, the magnetic spins are randomly oriented, but when a field is applied, the spins will align in the direction of the field. This alignment will cause an entropy change, which, under adiabatic conditions, is converted into a temperature change.

(a) Zero field **(b)** Non-zero field

Figure 1.1: Spin alignment in a paramagnetic material in zero field and in a non-zero field. In zero field, the spins are randomly aligned and the magnetic entropy is high. In the non-zero field, the spins are aligned parallel to the field direction and the magnetic entropy is low.

The total entropy of the material can be written as the sum of the magnetic entropy, S_{M}, the lattice entropy, S_{L}, and the electronic entropy, S_{E} [5,6]

$$S_{\mathrm{tot}} = S_{\mathrm{M}} + S_{\mathrm{L}} + S_{\mathrm{E}}. \tag{1.1}$$

The magnetic entropy is the entropy due to misalignment of the magnetic spins, the lattice entropy is the entropy due to lattice vibrations, and the electronic entropy is the entropy due to movement of free electrons. Generally, the lattice and electronic contributions only depend on the temperature, although they in some cases also may depend on the magnetic field [7–9].

At zero field, where the spins in the material are randomly aligned, the magnetic entropy, S_{M}, is high. When a magnetic field is applied, the spins will align, and the magnetic entropy decreases. Under adiabatic conditions, the total entropy is conserved, so the lattice and electronic entropies will increase, which causes an increase in temperature.

Likewise, if the field is removed, the orientation of the magnetic spins will randomize, giving an increase in the magnetic entropy and thus a decrease in temperature. If the material does not exhibit any magnetic hysteresis, the process will be reversible and the material will return to its initial temperature.

The magnetocaloric effect of a material is usually reported as either the adiabatic temperature change, ΔT_{ad}, or the isothermal entropy change, ΔS_{M}, which are illustrated in Figure 1.2 for a material with a paramagnetic/ferromagnetic transition. The adiabatic temperature change is the temperature change gained for a given field change under adiabatic conditions and the isothermal entropy change is the entropy change when changing the field under isothermal conditions.

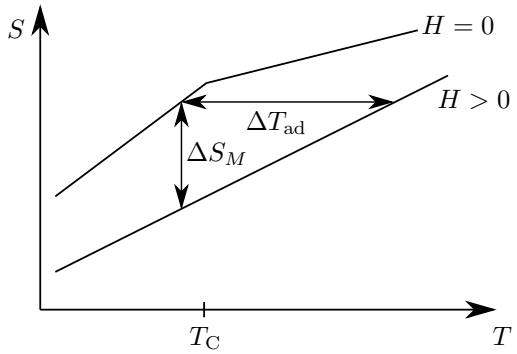

Figure 1.2: Entropy as a function of temperature for a paramagnetic/ferromagnetic material in zero field and non-zero field. A change in the applied field under adiabatic conditions causes a temperature change, ΔT_{ad}, and a field change under isothermal conditions causes a change in magnetic entropy. T_{C} is the Curie (transition) temperature of the material.

For materials where the magnetization is a continuous function of temperature, the isothermal entropy change is given by

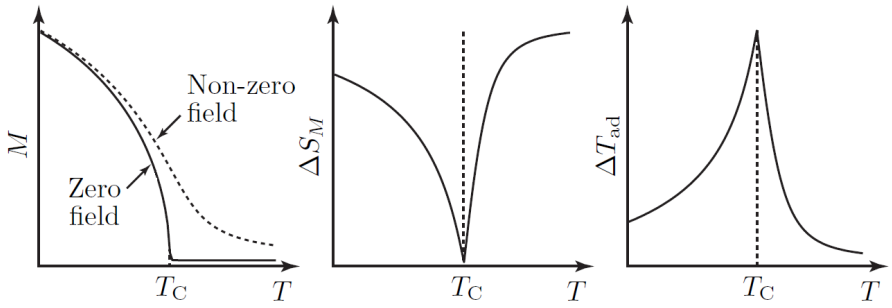

Figure 1.3: Magnetization, entropy change and adiabatic temperature change of a paramagnetic/ferromagnetic material with transition temperature T_C. Figure adapted from reference [11].

$$\Delta S_M = \mu_0 \int_{H_{init}}^{H_{fin}} \left(\frac{\partial M}{\partial T} \right)_H \mathrm{d}H, \tag{1.2}$$

where μ_0 is the vacuum permeability, H is the magnetic field, M is the magnetization, and T is the temperature. The "init" and "fin" subscripts denote the initial and final state, respectively. The adiabatic temperature change is given as [10]

$$\Delta T_{ad} = -\mu_0 \int_{H_{init}}^{H_{fin}} \frac{T}{c} \left(\frac{\partial M}{\partial T} \right)_H \mathrm{d}H, \tag{1.3}$$

where c is the specific heat capacity.

Usually, the magnetization decreases when the temperature increases, which means that $\frac{\partial M}{\partial T}$ is negative. Therefore, an increase in magnetic field usually gives a negative ΔS_M and a positive ΔT_{ad}. It is apparent from Equations 1.2 and 1.3, that the magnetocaloric effect not necessarily is the same for a field change e.g. from 0 T to 1 T as it is from 0.5 T to 1.5 T.

A substantial number of magnetocaloric materials are known, but for room temperature magnetic refrigeration, gadolinium is used as a benchmark material [10]. Gadolinium has a paramagnetic/ferromagnetic phase transition at 20°C and an adiabatic temperature change of approximately 3.5 K when magnetizing from 0 to 1 T [12–15]. Figure 1.3 shows the magnetization, the adiabatic temperature change, and the isothermal entropy change as functions of temperature. The largest gradient in the magnetization occurs at the Curie temperature, which means that ΔS_M and ΔT_{ad} peak near this temperature.

1.2.2 Principles of Regenerator Operation

In order to utilize the magnetocaloric effect for continuous refrigeration, regenerative heat exchangers can be used. A regenerative heat exchanger, or

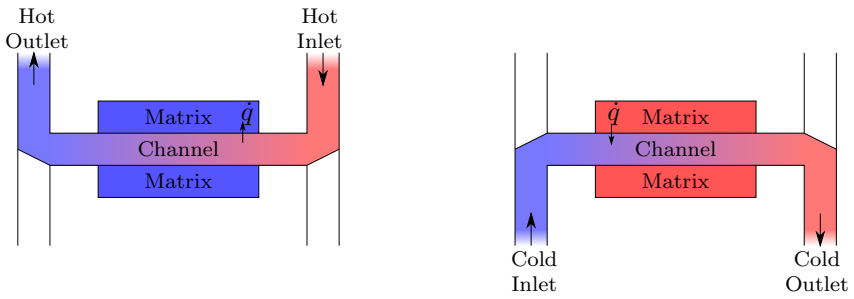

(a) Hot-to-cold blow

(b) Cold-to-hot blow

Figure 1.4: Operation of a passive regenerator. During the hot-to-cold blow, hot fluid moves through the regenerator depositing some of its thermal energy in the matrix. During the cold-to-hot blow, cold fluid moves through the regenerator absorbing the deposited thermal energy. In this way, heat is transferred from the hot inlet fluid to the cold outlet fluid.

regenerator, is a thermal device used for storage and transfer of heat between a hot and a cold fluid. In a regenerator, the temperature changes can be accumulated, such that it is possible to refrigerate to temperature differences that are several times larger than ΔT_{ad}.

Regenerators are not only used in magnetic refrigeration, but can be found in numerous applications in different fields, for example air preheaters [16], cryocoolers [17], and air conditioners and dehumidifiers [18].

This section presents an overview of the principles of operation of different types of regenerators.

Passive Regenerators

A regenerator consists of a solid regenerator matrix through which there is a periodically alternating flow of fluid. Regenerators can generally be divided into passive and active regenerators. In a passive regenerator, thermal energy is transferred indirectly from a hot fluid to a cold fluid via a solid material (the matrix) as illustrated in Figure 1.4.

The regenerative cycle of a passive regenerator consists of two periods. During the first period (the hot-to-cold blow period), the hot fluid flows through the matrix, transferring some of its thermal energy to the matrix. During the second period (the cold-to-hot blow period), the cold fluid flows through the regenerator, absorbing the thermal energy that was transferred from the hot fluid during the hot-to-cold blow period.

In the design shown in Figure 1.4, the hot and the cold fluids are essentially the same fluid, but the fluid in one end of the regenerator (the hot end) is hotter than the fluid in the other end (the cold end), and by alternately heating and cooling the regenerator matrix, heat is transferred from the hot inlet to the cold outlet.

Another passive regenerator design is the wheel-type regenerator shown in Figure 1.5. In this regenerator, the hot fluid and the cold fluid are completely separated, which minimizes the mixing of the fluids and allows for continuous fluid flow. This regenerator consists of two channels, where hot fluid flows through the top channel and cold fluid flows through the bottom channel. Inside the channels, the fluids pass through a rotating matrix, such that the upper half of the matrix is continuously heated and the lower part is continuously cooled. In this way, heat is indirectly transferred from the hot fluid to the cold fluid with minimal mixing of the two fluids.

This type of design can be found in air conditioning systems, where heat in the outgoing stream of air is recovered and reused in the ingoing stream (or vice versa), thus reducing the energy used for re-heating or re-cooling of the ingoing air, and in air preheaters where a contaminated hot fluid exchanges heat with a non-contaminated cold fluid.

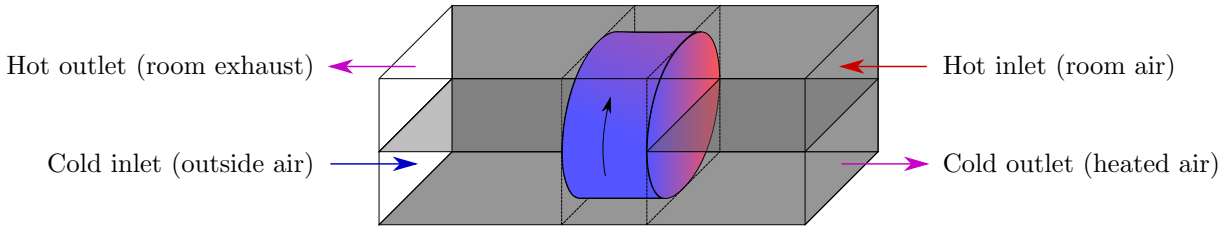

Figure 1.5: Wheel-type passive regenerator. In the top channel hot fluid passes through the regenerator matrix, depositing thermal energy. The matrix rotates and when a heated part of the matrix moves to the bottom channel, it is cooled by the cold fluid, which in turn is heated up.

Active Regenerators

An active regenerator is similar to a passive regenerator, except that the heat transfer is not caused by the two fluids having different temperatures. In an active regenerator, the matrix actively adds and removes heat from the fluids during the operation which creates a temperature difference.

For magnetic refrigeration, an active magnetic regenerator (AMR) is used, which is a type of regenerator that utilizes the magnetocaloric effect to heat and cool the matrix during operation.

The Magnetic Ericsson Refrigeration Cycle The first room temperature magnetic refrigeration device was constructed by Brown [19] in 1976. The design of this device is illustrated in Figure 1.6 and it used the magnetic Ericsson refrigeration cycle for providing refrigeration. A T-S diagram for this cycle is shown in Figure 1.7, which corresponds to the operations in Figure 1.6.

The device consists of a magnetocaloric matrix material (in this case gadolinium) which is submerged in a heat transfer fluid (an alcohol-water mixture)

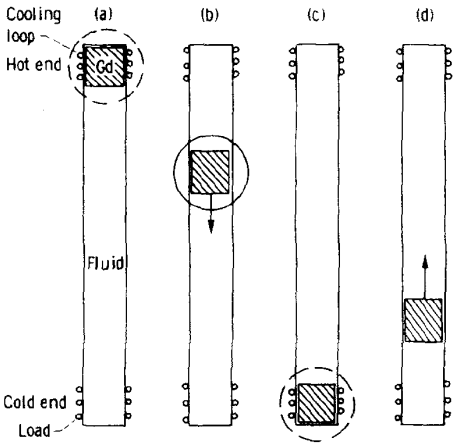

Figure 1.6: Magnetic refrigeration machine described in reference [19]. (a) at the hot end, a bed of gadolinium is magnetized and thermal energy is transferred isothermally to a hot reservoir. (b) the bed is moved to the cold end while magnetized. (c) the bed is demagnetized isothermally and thus absorbs thermal energy from the cold reservoir. (d) the demagnetized bed is moved to the hot end and the cycle can be repeated. Figure taken from reference [19].

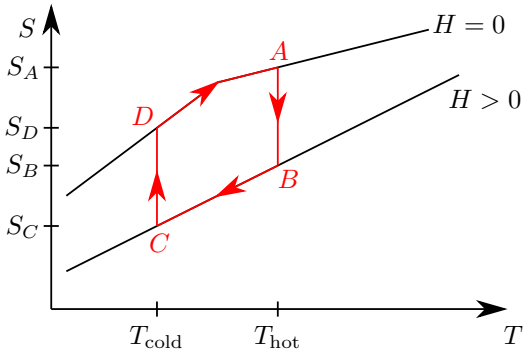

Figure 1.7: Entropy and temperature of material during Ericsson cycle.

and can be moved between two heat exchangers. The cycle consists of four steps:

a) The matrix is magnetized in the hot end of the regenerator, while being in contact with the hot heat exchanger. Magnetizing the material generates heat which is removed by the heat exchanger. This reduces the entropy of the matrix from S_{A} (at point A) in to S_{B} (at point B) in Figure 1.7 while maintaining a constant temperature.

b) The matrix, which is now magnetized, is moved from the hot end to the cold end of the machine, which reduces its temperature to T_{cold} (point C).

c) At the cold end, the magnetic field is removed isothermally, which increases the entropy to S_{D} (at point D) and heat is therefore absorbed by the matrix.

d) The matrix is then returned to the hot end in a demagnetized state, and the cycle can be repeated.

The AMR cycle More recent magnetic refrigeration systems use the AMR cycle, which was introduced in references [20,21] in 1982 and uses near adiabatic magnetization and demagnetization to regenerate a temperature gradient.

In an AMR, the matrix has a temperature gradient, and each matrix segment goes through a unique cycle depending on its temperature. A series of cascading cycles builds up a temperature gradient that can be significantly larger than the adiabatic temperature change of the matrix material.

The cycle is illustrated in Figure 1.8 and the T-S diagram for the cycle is shown in Figure 1.9. The regenerator in Figure 1.8 consists of a regenerator matrix which is surrounded by a heat transfer fluid. Each end of the regenerator is connected to a heat exchanger - the left end to a cold heat exchanger and the right end to a hot heat exchanger.

Initially, the regenerator is in the state a in Figure 1.8 and at point A in Figure 1.9. The regenerator then goes through four steps which comprise the AMR cycle:

b) The matrix is magnetized, which increases its temperature to $T_{\mathrm{hot}+}$ (point B). As the temperature of the matrix increases, the temperature of the heat transfer fluid also increases.

c) The fluid is displaced toward the hot end and thus the heated fluid is moved to the hot heat exchanger where excess heat is removed. This brings the temperature down to T_{hot} (point C).

d) The matrix is then demagnetized, which reduces its temperature to $T_{\mathrm{cold}-}$ (point D), and thus cools the fluid in contact with the matrix.

e) The fluid is displaced toward the cold end, which moves the cooled fluid to the cold heat exchanger and heats the matrix to T_{cold}. The cooled fluid at the cold heat exchanger absorbs heat from a cooling load which, under steady state conditions, returns the regenerator to its initial state (point A).

1.2.3 Performance Metrics

In order to evaluate the performance of an AMR refrigeration system, a number of different metrics can be used. For refrigeration systems in general, the coefficient of performance (COP) is usually used. The COP is defined as the ratio of transferred heat (i.e. the cooling power), q, to the work consumed by the system, W

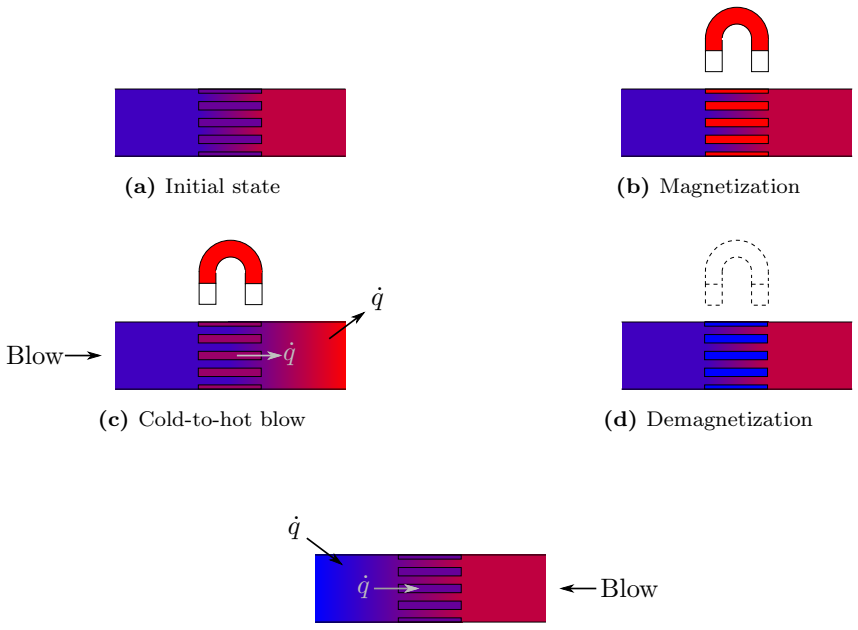

(a) Initial state

(b) Magnetization

(c) Cold-to-hot blow

(d) Demagnetization

(e) Hot-to-cold blow

Figure 1.8: Magnetic refrigeration cycle. (a) the regenerator is in its initial state, in which there during steady-state operation is a temperature gradient along the regenerator. (b) the matrix is magnetized and thus heats up. This causes the fluid in contact with the matrix to heat up as well. (c) the (hot) fluid is displaced toward the hot end and thermal energy is rejected to the hot heat exchanger. (d) The matrix is demagnetized which causes the matrix and nearby fluid to cool down. (e) the (cold) fluid is displaced toward the cold end where thermal energy is absorbed from the cold heat exchanger. This returns the regenerator to the state in (a) and the cycle can be repeated.

$$COP = \frac{q}{W}. \tag{1.4}$$

For conventional household refrigeration systems, this value is typically around three, which means that for every unit of energy the system consumes, three units of thermal energy is transferred from the cold side to the hot side[1].

To evaluate the overall amount of heat transfer in a regenerator system, the number of transfer units, NTU, can be used. The NTU is given by

$$NTU = \frac{hA_\mathrm{s}}{\dot{m}c_\mathrm{f}}, \tag{1.5}$$

where h is the convective heat transfer coefficient, A_s is the (wetted) surface area, $\dot{m}$ is the mass flow rate, and c_f is the specific heat capacity of the fluid.

[1]For magnetic refrigeration units, COP values of up to ten have been reported [22].

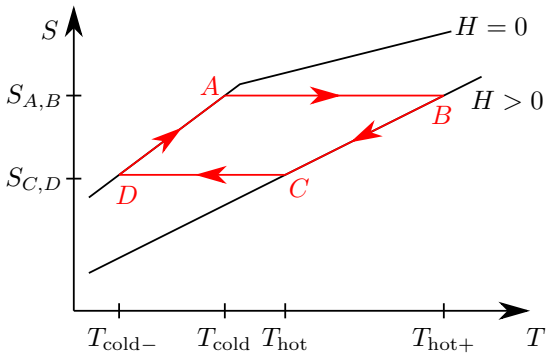

Figure 1.9: Entropy and temperature of material during AMR cycle.

The NTU can be regarded as a dimensionless size of a regenerator because it describes how much heat that can be transferred for a given mass flow rate and specific fluid heat capacity. The NTU requires knowledge of the heat transfer coefficient, which for simple regenerator geometries such as uniformly distributed parallel plates, can be estimated by correlations or it can be experimentally found.

For flow in ducts, the Nusselt number, Nu, can be used to characterize the local heat transfer. The Nusselt number is given by

$$Nu = \frac{hD_{\mathrm{h}}}{k_{\mathrm{f}}}, \tag{1.6}$$

where k_{f} is the thermal conductivity of the fluid and D_{h} is the hydraulic diameter of the duct. The hydraulic diameter is defined as

$$D_{\mathrm{h}} = \frac{4A_{\mathrm{c}}}{P_{\mathrm{w}}}, \tag{1.7}$$

where A_{c} is the cross-sectional area of the duct and P_{w} is the wetted perimeter.

In the work presented in this thesis, investigations have been performed on complex regenerator geometries, where the fluid flow characteristics vary throughout the regenerators. For fluid flows in channels of different widths and heat transfer between the channels, the heat transfer coefficient becomes ill-defined and difficult to estimate reliably. The methods for estimating the heat transfer coefficient of a regenerator require that the regenerator geometry is uniform (see e.g [23, 24]).

The regenerator effectiveness is therefore also used. For single-blow processes, the effectiveness is defined as the ratio of thermal energy transferred from the regenerator matrix to the heat transfer fluid at a given time, $q_{\mathrm{t}}(t = t_1)$, to the maximum ratio of thermal energy that can be transferred, which is equal to the heat transferred at $t \to \infty$. This quantity can also be termed the non-dimensional heat storage (as defined in reference [25]), but in this thesis it will be called the single-blow effectiveness, or $\varepsilon_{\mathrm{SB}}$. It is defined as

$$\varepsilon_{\mathrm{SB}}(t = t_1) = \frac{q_{\mathrm{t}}(t = t_1)}{q_{\mathrm{t}}(t \to \infty)}. \tag{1.8}$$

The heat transfer at time t_1 is found by integrating the heat transfer rate

$$q_{\mathrm{t}}(t = t_1) = \int_0^{t_1} \dot{q}_{\mathrm{t}}(t)\mathrm{d}t \tag{1.9}$$

and, if constant material properties are assumed, the heat transfer when $t \to \infty$ is given by

$$q_{\mathrm{t}}(t \to \infty) = \int_0^{\infty} \dot{q}_{\mathrm{t}}(t)\mathrm{d}t = \rho_{\mathrm{s}} c_{\mathrm{s}} V_{\mathrm{s}} (T_{\mathrm{init}} - T_{\mathrm{in}}), \tag{1.10}$$

where ρ_{s} is the density of the solid, c_{s} is the specific heat capacity of the solid, V_{s} is the volume of the solid, and T_{init} and T_{in} are the initial and inlet temperatures, respectively. The single-blow effectiveness will have a value between zero and one, corresponding to the fraction of thermal energy that has been removed (or added) at a given time.

The regenerator effectiveness is useful for analysing single blow processes, but can be difficult to determine experimentally because it requires detailed knowledge of heat transfer rates inside the regenerator.

For regenerative processes, however, it is more convenient to express the effectiveness in terms of thermal energy transferred from the cold fluid to the hot fluid. The regenerative effectiveness is thus given as the ratio of thermal energy transferred during a given single blow, q_{t}, to the thermal capacity of the fluid that has passed through the regenerator, $q_{\mathrm{max,f}}$, i.e. [26]

$$\varepsilon_{\mathrm{reg}} = \frac{q_{\mathrm{t}}(t)}{q_{\mathrm{max,f}}}. \tag{1.11}$$

The transferred energy is still defined as in Equation 1.9. The thermal capacity of the fluid is given by

$$q_{\mathrm{max,f}} = \dot{m} c_{\mathrm{f}} t (T_{\mathrm{init}} - T_{\mathrm{in}}). \tag{1.12}$$

In the present work, the effectiveness is evaluated as a function of utilization, Φ. The utilization is the ratio of the thermal mass of the displaced heat transfer fluid at a given time and the thermal mass of the matrix, i.e.

$$\Phi = \frac{\dot{m}_{\mathrm{f}} c_{\mathrm{f}} t}{m_{\mathrm{s}} c_{\mathrm{s}}}, \tag{1.13}$$

where $\dot{m}_{\mathrm{f}}$ is the fluid mass flow rate and m_{s} is the mass of the solid regenerator matrix.

The flow in a channel is also characterized by its Reynolds number, Re, which is given by

$$Re = \frac{\rho_\mathrm{f} D_\mathrm{h} u_\mathrm{m}}{\mu}, \tag{1.14}$$

where ρ_f is the density of the fluid, u_m is the mean fluid velocity, and μ is the viscosity of the fluid.

The Reynolds number generally correlate the viscous behaviour of fluid flow. For flow in ducts, this behavior also depends on other factors, such as geometry and surface roughness, but generally flows with $Re \leq 10^3$ can be assumed to be laminar [27].

1.2.4 Overview of Regenerator Analysis

Different methods exist for calculating the performance of a regenerator. A series of one dimensional methods consists of direct closed form calculation of the steady state [24] or simulation-type calculations cycled to equilibrium (i.e. steady-state) [28–30]. An early numerical model using a one dimensional approach was presented in references [31,32] for a general case of a regenerator, and many specialized models have been developed since, e.g. for AMRs [33–46], preheaters [47], and cryocoolers [48–50].

The one dimensional solutions are very general and can include a low number of independent variables, depending on the formulation. However, they require that a number of assumptions can be made about the regenerator and the flow conditions. The regenerator geometry, for example, must be completely homogeneous with infinite conduction in the transverse direction and zero conduction in the longitudinal direction, and the flow must be completely uniform with no velocity or temperature profiles. This assumption is correct for fine grained packed beds and may be appropriate for other geometries with acceptable accuracy. For regenerators with larger features, such as parallel plates, however, this assumption does not necessarily hold and the results obtained using this type of model may not be adequate.

Furthermore, for this type of solution, knowledge of the overall heat transfer coefficient is required. This is normally found through correlations [51, 52], but these are also only valid under certain conditions, and are not necessarily applicable to complicated flow patterns.

For parallel plates, the heat transfer in the dimension along the plate width must be modeled as well. A few two-dimensional models based on a single repeating plate and channel have been developed (recently) for parallel-plate geometries (AMRs: [53–55]), which take into account both transverse and longitudinal conduction and do not require prior knowledge of the heat transfer coefficient. The two-dimensional models also allow for more accurate modeling of heat losses and have been found to provide more precise results than one dimensional models for certain geometries [56].

Plate and channel widths, however, are not necessarily uniform in parallel-plate regenerators. This means that different channels may have different flow rates and temperature profiles, which may affect the performance of the regenerators. Only a few models consider the effect of non-uniform plate spacings. In reference [57], the effect of having two halves of a regenerator with different plate spacings in a Stirling-type cryocooler is examined. In this case, reductions in COP of 15 % or more were found for regenerators with plate spacing variations that are only ±10% of the nominal plate spacing. Reference [58] examines fabrication and testing procedures for thermoacoustic Stirling engines, where ±10% deviations in plate spacing lead to 30% variations in flow resistance.

1.3 Motivation

Parallel-plate regenerators with small dimensions are receiving interest for several applications because of their theoretically high thermal performance (i.e. high heat transfer coefficient due to a large specific surface area) and low pressure drops [59, 60]. In AMRs, the need to produce compact, high performance regenerators is particularly essential because the volume over which high magnetic field changes can be generated are limited when using permanent magnets.

Although the theoretical performance of parallel-plate regenerators is high [57, 61], the experimentally measured performance is typically less than what is expected [55, 57, 58], and it is generally accepted that flow maldistribution of the heat transfer fluid caused by non-uniformity in the flow channels is one of the causes of the discrepancy. The extent of this effect, however, is rarely addressed.

There will always be some degree of variation in plate spacing and plate flatness that results from the fabrication of a parallel-plate regenerator, which causes non-uniform channels for the flow of the heat transfer fluid. As the spacing becomes smaller, the relative variation in the plate spacings becomes larger, assuming the same manufacturing techniques and tolerances. Figure 1.10 shows an example of a ceramic parallel-plate regenerator that has been constructed at Risø DTU[2]. Even with the naked eye, the irregularities in the plate spacings of this regenerator are visible.

As noted above, many models that examine parallel-plate regenerators are based on a repeating single channel or are one dimensional and therefore require a correlation in order to calculate the heat transfer coefficient. The correlation is the embodiment of a separate solution to the detailed differential equations for mass, momentum, and energy under some limiting conditions (e.g., steady-state, negligible axial conduction, etc.) that may not be appropriate for parallel-plate regenerators with non-uniform plate spacing.

In the current work, a mathematical model of a regenerator has been developed, which can simulate the heat transfer in regenerators with arbitrary distributions of parallel plates. A number of theoretical distributions have been

[2]Risø National Laboratory for Sustainable Energy, Techincal University of Denmark

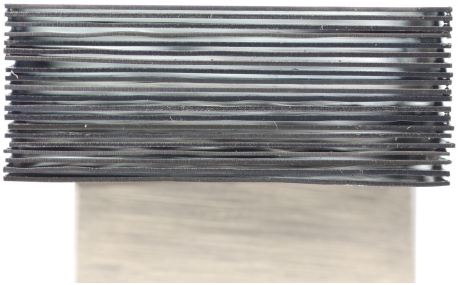

Figure 1.10: Photography of the cross section of an assembled stack of plates for an AMR. Non-uniformity in the plate spacing is clearly visible.

modeled as well as a variety of random distributions and the effect of flow maldistribution due to non-uniform plate spacings has been investigated for a wide range of parallel-plate regenerators with different geometries.

The modeling results have been supplemented by experimental investigations on a series of regenerators that have been fabricated to have different degrees of non-uniformity in the plate spacings.

The scope of this work is to investigate the heat transfer effects that are responsible for the loss of performance in non-uniform parallel-plate regenerators and to study the correlation between the channel width distributions, the fluid flow conditions, and the heat transfer characteristics inside the regenerators.

Furthermore, it will be addressed, under which conditions the extent of performance loss is most significant, and how altering the regenerator geometry changes this.

Chapter 2

Experimental Setup

2.1 Introduction

In this chapter, the setup of a test machine, which has been used for various experiments on regenerators, is presented. Initially, a series of experiments on AMRs were performed in order to investigate the effects of various modifications to their geometries.

The results from these experiments necessitated the development of a mathematical model, which simulates a single-blow process in the regenerators. These simulations result in a single-blow effectiveness of regenerative heat exchangers in general terms. This is useful because it provides a very general description and a detailed understanding of the heat transfer phenomena, which is applicable not only to regenerators, but to a variety of heat transfer problems. However, in a reciprocating device, the losses of effectiveness - and thereby heat transfer - may have an accumulating effect on the temperature gradient between the hot and the cold end of the regenerator, which also is an essential performance metric for a regenerator system.

In order to investigate the effect of non-uniformity of the plate spacings in reciprocating parallel-plate regenerators, additional experiments have therefore been performed on passive regenerators with stainless steel and aluminum plates.

2.2 Regenerator Test Machine

The experiments have been performed using a magnetic refrigeration test machine constructed at Risø DTU. The machine is constructed in a modular fash-

ion such that individual components can be removed or replaced, depending on the requirements of a particular experiment. This means that the machine is not limited to running with AMRs, but can also run with passive regenerators.

The test machine setup is illustrated in Figure 2.1 for both the passive and the active configuration.

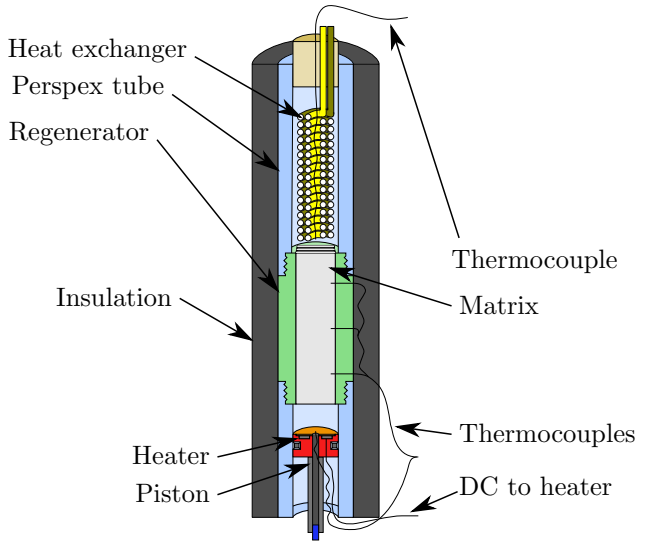

(a) Passive configuration

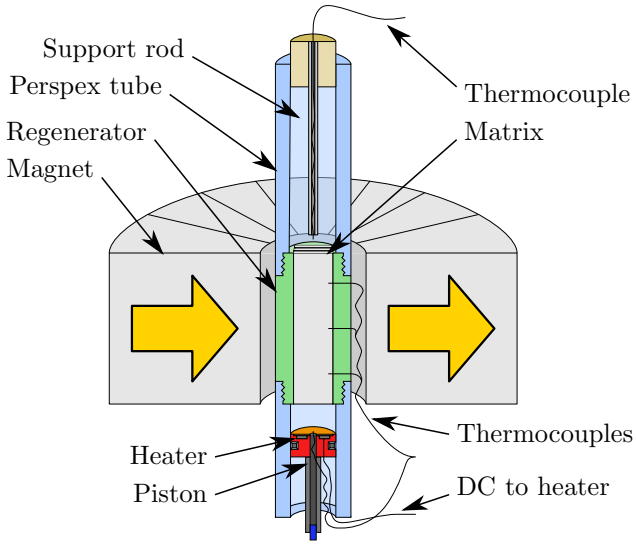

(b) AMR configuration

Figure 2.1: Cross-section of test machine setup in the passive configuration and in the active magnetic configuration.

2.2.1 Regenerators

The main component of the test machine is the regenerator. A number of different regenerators have been fabricated for testing in the machine. These regenerators can be divided into three types, which are described below. A more thorough description of the specific geometric properties of the individual regenerators and their usage in relation to the experiments can be found in the corresponding sections for each experiment series.

Active Magnetic Regenerators

A set of regenerators have been produced for use in the AMR experiments. The regenerators are all 4 cm long and have been produced by rapid prototyping in an acrylic, using a Polyjet process. Ribs are "printed" into the sides of the slots in the rapid prototyping process (which means that the accuracy of the regenerators are not as high as for the passive regenerators). Gadolinium plates are slit in between these ribs and held in place by retainers which are attached to the ends of the regenerators using screws.

Six different regenerators, shown in Figure 2.2, have been manufactured. The nominal regenerator is the base case, and the other five regenerators are variations of this. The middle right regenerator, which is denoted the "nominal" regenerator, contains 11 plates with a width of 0.9 mm and 9 channels with a width of 0.9 mm. The top and bottom plates flush against the wall of the regenerator housing. The bottom left regenerator is denoted the "half-channel" regenerator and has channels of half width at the top and bottom in order to reduce the heat transfer to the walls and make the heat transfer from the top and bottom plates more regular.

The bottom right regenerator, denoted the "narrow" regenerator, is similar to the nominal regenerator, but has a channel width of 0.6 mm, which is expected to give an increased heat transfer per unit mass flow.

In order to further investigate the effect of heat transfer through the walls on the performance, a regenerator with hollow walls (top) has been constructed using Selective Laser Sintering (SLS). This is expected to significantly reduce the heat transfer through the walls, but also significantly reduces the mechanical strength of the regenerator housing.

The middle left regenerator is denoted the "radial" regenerator and has the same average channel width, but arranged radially. This geometry is investigated in order to evaluate the impact on the regenerator performance for a rotating device.

Passive Stainless Steel Regenerators

Geometry Three different passive regenerators with stainless steel matrices have been fabricated. Each regenerator consists of a regenerator housing which

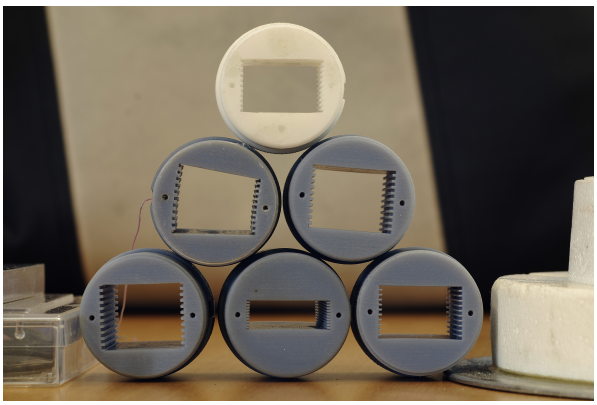

Figure 2.2: Housings of the regenerators used in the AMR experiments. Top: regenerator with hollow walls. Middle left: Regenerator with radially oriented plates. Middle right: Regenerator with 0.9 mm plate spacings and no gaps between end plates and the walls of the housing. Bottom left: Regenerator with 0.9 mm plate spacings and gaps with the width of a half plate between end plates and the walls of the housing. Bottom middle: Regenerator with 0.2 mm plates of a ceramic material and 0.5 mm plate spacings (no gap). Bottom right: Regenerator with 0.5 mm plate spacings (no gap).

contains a pair of plate holders and a pair of retainers, as shown in Figure 2.3. AISI 304 stainless steel plates are inserted into the grooves of the plate holders and the plate holders are slided into the housing.

The housing, plates, and retainers are re-used, but since the plate holders define the plate spacings, different sets are used in each of the regenerators.

Regenerator Housing The regenerator housing is a single cylindrical piece of nylon with a diameter of 40 mm and a rectangular slot that is 24 mm wide and 20 mm high. When the plate holders are inserted, the regenerator cross section is 20 mm by 20 mm and its length is 10 cm. The housing has a thread at either end for attaching it to the test machine and holes in the side for temperature measurements. Due to its complex geometry, the housing has been manufactured by SLS rapid prototyping.

When designing the regenerator housing, two factors are particularly important to consider: heat losses and heat regeneration in the housing. Heat loss from the regenerator to the surroundings impairs the effectiveness of the regenerator and must be negligible, compared to the heat transfer inside the regenerator. This is partly achieved by choosing an insulating material for the regenerator housing, i.e. a material with a low thermal conductivity, and partly by adding a layer of insulation on the outside of the regenerator and the thermal reservoirs.

It is also important to minimize passive heat regeneration in the housing. If not completely insulating, the walls of the housing can store thermal energy locally at one point in the cycle and release it at another. This effect will tend to even out the temperature gradient along the length of the regenerator, which will

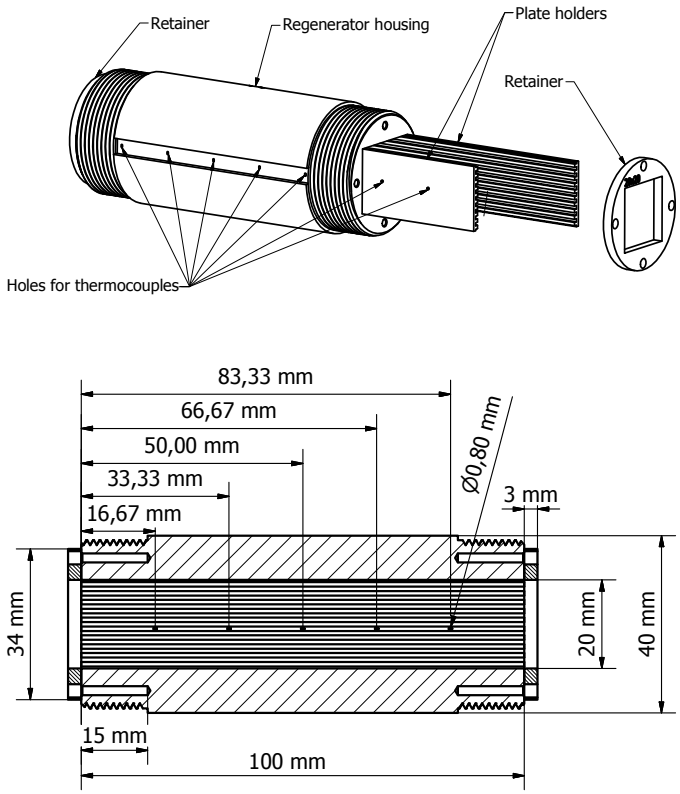

Figure 2.3: Geometry, dimensions, and assembly of the regenerator components used in the passive regenerator experiments.

reduce its performance. In order to minimize this effect, the housing material should have a low thermal diffusivity.

The regenerator housing has been manufactured in nylon, which has a low conductivity (0.13 W/(m K)) and a low diffusivity (6.0×10^{-8} m^2/s); and it can be used with rapid prototyping.

Plate Holders In order to keep the plates in their desired positions, a plate holder is slided into each side of the slot in the regenerator housing. The plate holders are 100 mm × 20 mm × 2 mm plates, which flush against the side walls of the housing slot. One side of each plate holder has 9 whole trenches with a width of 1 mm and a depth of 1 mm, and 2 half trenches with a width of 0.5 mm that hold the plates fixed inside the regenerator housing according to a predefined distribution. One pair of plate holders is manufactured for each distribution of plate spacings with a corresponding distribution of trench spacings.

When using rapid prototyping, the geometry is fabricated layer by layer, either by irradiating the material, which heats it up, causing it to solidify locally, or by depositing small amounts of material, thus "printing" the geometry. The

layer thickness is 0.15 mm, which defines the maximum precision that can be achieved in a single direction (along the vertical axis when printing). The average channel width in the final regenerators is 1 mm, so with a precision of 0.15 mm, the most uniform regenerator that can be constructed would have a standard deviation of approximately 15 %, which is much too inaccurate for the experiments. The plate holders are therefore precision machined, which is done with an accuracy of 0.02 mm.

However, in order to make the plate spacing distribution as close to the intended distribution as possible, the plates are tightly fitted into the grooves, which means that the plate holders are subjected to stress during assembly and operation of the test machine.

While nylon has great thermal properties for surrounding the regenerator matrix, it is not very durable and would be likely to break when machining it or using it in the regenerator assembly. The plate holders are therefore produced in polystyrene, which is more durable and still has a low thermal conductivity (0.15 W/(m K)) and diffusivity (1.1×10^{-7} m^2/s).

Assembly and Retainers The regenerators are assembled by fitting 9 stainless steel plates (AISI 304) with a width of 1 mm each into the trenches in the plate holders and sliding the plate holders into the slot in the regenerator housing.

In order to keep the plates and the plate holders fixed during operation of the test machine, a retainer is attached to each end of the regenerator housing. The retainers are also produced by rapid prototyping in nylon and are attached to the housing with four screws each.

Passive Aluminum Regenerators

A series of regenerators with aluminum palates have also been constructed for use in passive regenerator experiments. These regenerators have been constructed with nominal plate spacings of 0.74, 0.4, 0.2, and 0.1 mm, respectively, and with a plate width of 0.4 mm.

The regenerators consist of a 4 cm long housing with a slot for plates that is 20 mm wide and has a height determined by the channel distribution. The housing is manufactured by SLS rapid prototyping, like the stainless steel regenerators. The plates in the slots are separated by wires with the same thickness as the nominal plate spacing and are glued together using epoxy glue. These regenerators have been fabricated by Kurt Engelbrecht[1].

[1] Risø DTU

2.2.2 Machine Assembly and Peripherals

Tubes

Hollow perspex tubes are used as cold and hot thermal reservoirs at the top and bottom of the machine, respectively. The tubes are attached to either end of the regenerator using the threads in the housing and have an inner diameter of 34 mm and an outer diameter of 40 mm, which give them a larger bore cross-section than the regenerators. The test machine assembly with the tubes and other peripheral components attached is illustrated in Figure 2.1.

In one of the AMR experiments, the top tube is replaced with a copper pipe, but in the rest of the experiments, the Perspex tube is used.

Piston and Heater

The tube at the bottom of the regenerator is defined to be the hot reservoir for the AMR experiments and the cold end for the passive regenerator experiments. The tube at the top is defined to be the cold reservoir in the AMR experiments and the hot reservoir in the passive regenerator experiments.

The reason for switching the reservoirs in this way, is that a heater in the piston is used to apply a heat load, $\dot{q}_{HL}$, to the cold reservoir in the AMR experiments, but in the passive regenerator experiments, it provides heating of the hot reservoir.

In the bottom tube, a piston displaces the heat transfer fluid and a resistive heating element in the piston supplies a heat load for the regenerator to absorb. In order to prevent the heat transfer fluid from coming into contact with the heating element, it is attached to the back side of a thin copper disk which acts as the front of the piston. The heater, however, is relatively small, which means that its effect is limited to 2 W or less. The maximum heat load for the piston has not been tested, so the maximum heat load that has been used is 1.6 W.

A small hole is drilled through the center of the piston and the piston rod, which is used in order to drain the heat transfer fluid from the test machine and to support a thermocouple used for temperature measurements of the fluid near the piston.

Heat Exchanger

In the passive regenerator experiments, a heat exchanger is attached to the top tube using a rubber bung. The heat exchanger consists of two concentric helices of copper pipe which are connected at the bottom.

Water at ambient temperature is pumped through the copper pipe with the heat exchanger inlet connected to the outer helix and the outlet connected to

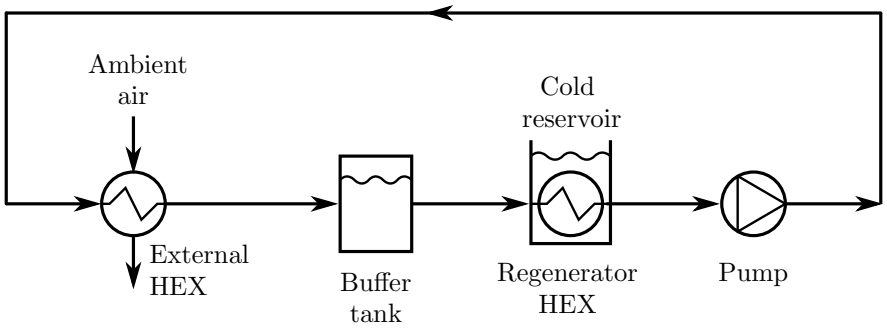

Figure 2.4: Heat exchanger setup. A water/ethanol-mixture at ambient temperature is pumped from a buffer tank through the regenerator heat exchanger. When exiting the regenerator heat exchanger the fluid moves through the pump and an external heat exchanger where the thermal energy absorbed from the regenerator is rejected to the surroundings.

the inner helix. The inlet water is first pumped through an external liquid-to-air heat exchanger to cool it to ambient temperature and then through a buffer tank in order to even out temperature fluctuations. The heat exchanger setup is shown in Figure 2.4.

Magnet

When using an AMR in the test machine, a 1.1 T magnet is fitted to the frame of the machine, such that the regenerator can be moved in and out of its field.

The magnet is a Hallbach array consisting of 16 NdFeB elements that are arranged as a hollow cylinder around the regenerator. The inner diameter of the magnet is 42 mm, such that the regenerators fit inside the bore, the outer diameter is 120 mm, and the height is 50 mm [62].

Stepper Motors

The piston is mounted on a slide, which, along with the regenerator, tubes, and heat exchanger is mounted on a second slide. Each slide is attached to a stepper motor using a worm gear, and can be moved independently of each other. The first slide can move the piston relative to the tubes and regenerator and the second slide can move the regenerator (including the piston) relative to the magnet.

Insulation

In order to minimize the thermal losses to the surroundings, a layer of insulation covers the regenerator and tubes when the machine is used for passive experiments. During AMR experiments, clearance is required for moving the

regenerators relative to the magnet and the insulation cannot be attached. The insulation layer has a thickness of 13 mm and consists of closed cell insulation foam. A slit is cut in the side of the insulation for the thermocouples.

Sealing

The threads between the regenerator and the tubes are sealed using Teflon tape. This, however is not sufficient to completely seal the connections in the test machine, so a layer of silicone is added after assembly. The holes in the regenerator used for temperature measurement are likewise sealed with silicone.

An x-shaped o-ring (a quad-ring or x-ring) is used in order to seal the gap between the piston and the bottom tube and the channel in the piston rod is sealed using a plastic plug, which can be removed when draining the machine.

2.2.3 Temperature Regulation

In order to be able to control the ambient temperature and to keep it constant throughout experiments, the test machine is placed inside a temperature-controlled cabinet. A programmable thermostat has been installed and a fan ensures mixing of the air in the cabinet. In order to expand the temperature range of the cabinet, a 40 W heating element (a light bulb) is also mounted inside the cabinet, which allows the ambient temperature of the experiment to go above the ambient temperature in the laboratory.

Using the cabinet, it is possible to keep the temperature of the test machine constant consistently within ± 1 K of the set point temperature.

2.2.4 Temperature Measurement

During the experiments, temperatures are measured using six 0.13 mm diameter (36 gauge) E-type thermocouples with Teflon insulation. As shown in Figure 2.1, thermocouples are placed at the piston, at the heat exchanger, and on the frame of the test machine, as well as inside the regenerator.

The regenerators allow for up to five thermocouples to be attached along the length of the regenerator, as shown in Figure 2.3. Due to the threads, however, the thermocouples cannot be placed closer to the ends (inlet and outlet) of the regenerator than 17 mm.

The thermocouples are connected to an ice-point reference unit, which maintains a known reference temperature of 0°C. This unit, however, only supports up to six thermocouples, which limits the number of thermocouples that can be used in each experiment. Thermocouples are therefore only installed in the top, middle, and bottom holes of the regenerators and the remaining two holes are sealed during the experiments.

2.2.5 System Control and I/O

The pump for the hot reservoir heat exchanger and the fan for the external heat exchanger are powered by an external power supply and a second external power supply is used to power the heating element in the piston.

In order to provide a given heater effect, an appropriate fixed current is supplied to the heater. The resistance of the heater has been measured to 31.7 Ω, so the currents shown in Table 2.1 are used.

Power [W]	**Current** [mA]
0.4	112.3
0.8	158.9
1.2	194.6
1.6	224.7

Table 2.1: Heater power and corresponding current values.

These currents are too low for the built-in ammeter in the power supply to measure precisely and an external flux meter is therefore used for current measurements.

The stepper motors are powered by a power supply, which is controlled from a PC, and a Keithley 2700 multimeter is used to measure the thermocouple signals. The signals are processed by the PC, which runs two Labview programs, one for motor control and one for temperature measurements.

2.3 Thermal Characterization

In this section, two series of experiments that have been performed in order to evaluate the heat transfer characteristics of the experimental setup are presented. In the first series of experiments, the thermal losses from the test machine and the reduction in thermal losses achieved by adding the insulating layer are investigated and compared to the heat transfer through the heat exchanger.

In the second series of experiments, the machine is run with no heat load in order to determine if there are any "natural" thermal gradients in the system and to estimate the accuracy and reliability of the temperature measurements.

2.3.1 Thermal Losses

The thermal loss experiments have been performed with the test machine in an idle state, i.e. no movement of the regenerator or piston and no applied heat load in the heater. In the experiments, the overall heat transfer coefficient, U, is calculated for each of the following three configurations:

1. The default configuration: With the heat exchanger and the insulation mounted.
2. Without the heat exchanger, but with the insulation.
3. With neither the heat exchanger, nor the insulation.

The heat transfer in configuration (1) is the base heat transfer away from the machine under normal operating conditions. Configuration (2) gives the heat loss to the surroundings without the heat transfer through the heat exchanger and configuration (3) gives the heat loss without insulation. The effect of adding the insulation can then be evaluated by comparing with the results from configurations (2) and (3).

The experiments have been run with a height of the bottom reservoir of 3 mm and a height of the top reservoir of 15 mm, which corresponds to 94 ml of heat transfer fluid. A passive stainless steel regenerator with a distribution of plate spacings with a relative standard deviation of 50 % has been used for the experiments. The heat transfer fluid that has been used is a mixture of 75 % (by volume) deionized water and 25 % ethylene glycol-based commercial antifreeze.

The drained test machine is prepared in the appropriate configuration and allowed to reach an equilibrium temperature while the temperature control cabinet is set to 22°C. Meanwhile, 94 ml of heat transfer fluid is heated to approximately 70°C by submerging a glass beaker containing the fluid into hot water. When the heat transfer fluid has reached the desired temperature, it is poured into the test machine, and the test machine is allowed to return to thermal equilibrium, while the temperatures are measured.

The reference time, $t = 0$, is defined as the end of the pouring operation, such that the test machine cools down for $t \geq 0$, approaching the ambient temperature as $t \to \infty$.

Since the heating and the pouring of the heat transfer fluid changes its temperature and because it is difficult to control these processes accurately, the initial temperature in the three different configurations is not the same. The regenerator, tubing and insulation are at a different temperature at the moment of pouring and therefore absorbs some of the thermal energy, which means that the system takes a short time to reach a well defined rate of heat transfer to the surroundings. The development of the temperature profile at small times ($t \lesssim 30$ s) may therefore be unreliable.

In order to determine the heat transfer coefficient, the mean bulk temperature of the heat transfer fluid and the ambient temperature are used. The total heat flux from the fluid is given by the relation

$$\dot{q} = U A_{\mathrm{s}} (T_{\mathrm{bulk}} - T_{\mathrm{amb}}), \tag{2.1}$$

where U is the overall heat transfer coefficient, T_{bulk} is the bulk fluid temperature, and T_{amb} is the ambient temperature.

The fluid temperature is measured at the piston, T_P, at the heat exchanger, T_HEX, and at three locations inside the regenerator, T_t (top), T_m (middle), and T_b (bottom). In order to find the bulk fluid temperature, an average temperature, weighed by the fluid volume in each part of the regenerator, is used. The bulk fluid temperature is thus given by

$$T_\mathrm{bulk} = \frac{V_\mathrm{res,b}T_\mathrm{P} + V_\mathrm{reg,void}(T_\mathrm{t} + T_\mathrm{m} + T_\mathrm{b})/3 + V_\mathrm{res,t}T_\mathrm{HEX}}{V_\mathrm{res,b} + V_\mathrm{reg,void} + V_\mathrm{res,t}}, \tag{2.2}$$

where $V_\mathrm{res,b}$ is the volume of the bottom reservoir, $V_\mathrm{reg,void}$ is the void volume of the regenerator, and $V_\mathrm{res,t}$ is the volume of the top reservoir.

The heat transfer rate is found by taking the derivative of the bulk temperature

$$\dot{q} = \frac{\mathrm{d}T_\mathrm{bulk}}{\mathrm{d}t} V_\mathrm{bulk}\rho_\mathrm{f}c_\mathrm{f}, \tag{2.3}$$

where $V_\mathrm{bulk} = V_\mathrm{res,b} + V_\mathrm{reg,void} + V_\mathrm{res,t}$. In order to get a smooth $\mathrm{d}T_\mathrm{bulk}/\mathrm{d}t$, a linear regression is performed for each point over the range of the 50 nearest neighboring points, which corresponds to approximately 280 s. The derivative is then taken as the slope of this line. In this way, rapid measurement fluctuations are smoothed out and more stable values for the heat transfer coefficient are found.

The product of the heat transfer coefficient and the area, UA_s, is used in order to evaluate the heat losses. This gives the heat transfer in units of W/K and makes it unnecessary to define the area A_s. A definition of this area might be ambiguous which could cause unintended effects on U.

The temperature differences and the derivatives of the bulk temperature measured for the three configurations are shown in Figure 2.5a and b, respectively, as a function of time. The corresponding calculated heat transfer coefficients are shown in Figure 2.6.

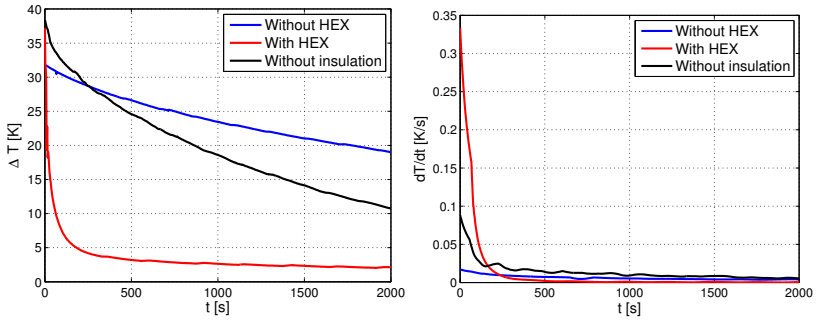

(a) Difference between the bulk and ambient temperatures.

(b) Derivative of bulk temperature.

Figure 2.5: Development of temperature difference and derivative as functions of time for the three different test machine configurations.

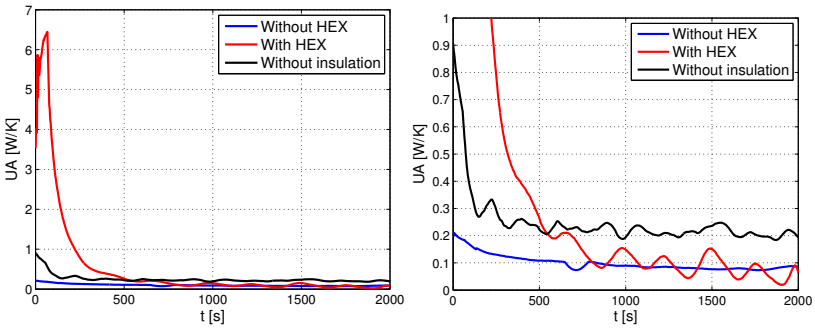

Figure 2.6: Calculated value of the overall heat transfer coefficient multiplied by the heat transfer area, UA_s, as a function of time for the three different test machine configurations at different time scales.

It can be seen that the heat transfer is much higher and that the bulk temperature drops much more quickly when the heat exchanger is mounted. The heat transfer coefficient when the heat exchanger is attached decreases with time and at around 700 s, it becomes approximately equal to the heat transfer coefficient of the configuration without the heat exchanger, but with insulation. This is because the heat exchanger rapidly cools down the fluid in the top reservoir, bringing it close to the ambient temperature. The fluid in the rest of the test machine is not cooled directly by the heat exchanger but by heat losses to the surroundings, which occur at approximately the same rate as in the configuration without the heat exchanger and with insulation.

Figure 2.7, shows the measured temperatures in the configuration with the heat exchanger. As time increases, the temperature of the top reservoir decreases rapidly, whereas the temperatures further away from the heat exchanger decrease more slowly.

It can be seen that the temperatures in the bottom of the machine initially are significantly lower than the temperatures in the top. This is due to the liquid being poured from the top of the machine. While the hot liquid falls to the bottom of the machine, heat is removed by the components it passes, thereby reducing the temperature of the fluid at the bottom. The liquid at the top does not give off as much heat when poured and is therefore initially at a higher temperature. With the heat exchanger attached, however, the rate of heat transfer is greater at the top, and the temperature at the heat exchanger rapidly falls below the temperatures of the rest of the system. Figure 2.7b shows the temperatures in the system after they have reached equilibrium.

In Figure 2.6b, it can be seen that the heat loss is reduced approximately by a factor of 2 when the insulating layer is added. The results also show that the heat losses to the surroundings can be neglected without introducing significant errors when using the heat exchanger.

The heat transfer coefficient can be seen to fluctuate more in the configurations without insulation and with heat exchanger than in the configuration with insulation and no heat exchanger. This is because the temperature control cabinet

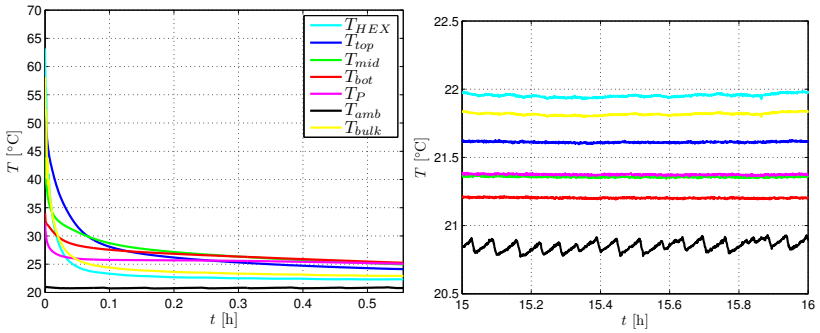

Figure 2.7: Development of the measured temperatures as functions of time for the configuration with heat exchanger and with insulation. The figure on the right shows the temperatures when the machine has reached thermal equilibrium. T_{HEX} is the temperature at the heat exchanger in the top reservoir, T_{t}, T_{m}, and T_{b} are the temperatures of the top, middle, and bottom thermocouples in the regenerator, respectively, T_{amb} is the ambient temperature, and T_{bulk} is the bulk temperature, calculated using Equation 2.2

runs an on/off temperature regulation with a compression refrigeration system[2], which causes the temperature to vary in cycles of around five minutes. Because the thermal contact between the fluid and the surroundings is much better when there is no insulation or when the heat exchanger is mounted, the fluid temperature is more sensitive to the fluctuations in the ambient temperature in theses configurations

Figure 2.8a shows the temperature development as a function of time for the configuration with insulation, but without heat exchanger. The cutout shown in Figure 2.8b shows that all the temperatures come to an equilibrium within 0.3 K.

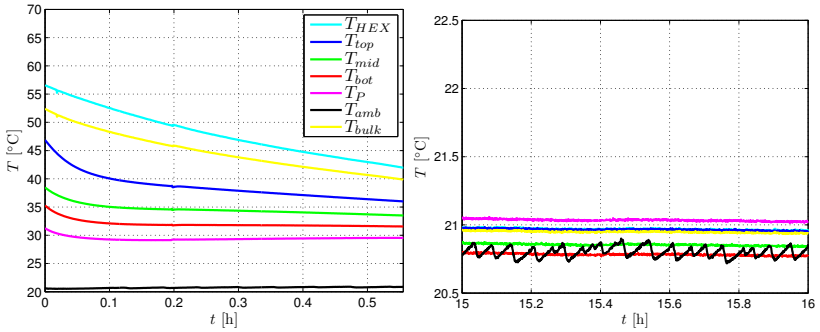

Figure 2.8: Development of the measured temperatures as functions of time for the configuration without heat exchanger but with insulation. The figure on the right shows the temperatures when the machine has reached thermal equilibrium.

[2]In this case, a magnetic refrigerator would be advantageous.

The temperature development for the configuration with insulation and heat exchanger, shown in Figure 2.7b, shows variations of the equilibrium temperatures of up to 2.2 K, with the heat exchanger temperature being the highest. The temperatures decrease as the distance from the heat exchanger increases, approaching the ambient temperature.

This indicates that the the heat exchanger fluid has a temperature that is higher than the ambient temperature, and thus applies a small heat load to the top reservoir when the regenerator is idle. This can be due to heat input from the pump and viscous dissipation, or temperature gradients in the cabinet.

When running the machine with an applied heat load, the higher temperature in the heat exchanger only means that the temperatures are increased by up to 2.2 K relative to the ambient temperature. This will give a slightly higher heat loss, but will otherwise not affect the experiments. Given the large difference between heat loss and heat transfer through the heat exchanger, this effect is assumed to be negligible.

Since the thermostat for the temperature control has not been calibrated, the ambient temperature is constant around 20.8°C, although the set point temperature is 22°C. Besides changing the thermal properties of the materials by a minuscule amount, this only shifts the temperature range of the experiments, and has no effect of the physical processes that are involved.

2.3.2 Axial Conduction in the System

In order to estimate the thermal conduction in the system, an experiment has been performed, where a heat load is applied, but the piston and regenerator are not moving. The system is then allowed to reach a steady state where the temperature profile is constant. The measured steady state temperature profile is plotted in Figure 2.9, and it can be seen that the temperature decreases by 9.9 °C across the length of the regenerator.

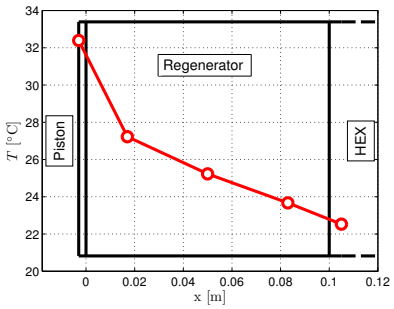

Figure 2.9: Temperatures measured in the regenerator with heat exchanger and insulation at thermal equilibrium when a heat load of 1.6 W is applied at the piston which is kept stationary.

The applied heat load is 1.6 W, which means that the the overall axial heat transfer coefficient is $(UA_s)_{ax} = \dot{q}/\Delta T = 0.16$ W/K. It should be noted, how-

ever, that since the conductivity of the regenerator matrix usually is an order of magnitude larger than the conductivity of the heat transfer fluid, the axial conduction inside the regenerator may be significantly larger.

Chapter 3

Measuring Plate Spacings

3.1 Introduction

In order to measure the widths of the plate and channel distributions of fabricated regenerators, a photogrammetric approach has been used. This technique is often used for creating two or three dimensional maps from aerial photos, but can also be used for measuring distances at smaller scales from photos.

The method used here consists of acquiring a series of images of the regenerators under controlled conditions (constant distance, angle, lighting conditions, etc.) using a digital camera, correcting the images for distortions, and then measuring regenerator features from the images.

This approach has the advantage that it is highly versatile as measurements can be made on virtually any geometry as long as the features that are measured are clearly visible and that measurements can be made over large areas. The plate spacings in a series of similar aluminum regenerators have been measured using a laser scanner, as described in Section 9.3, which is more accurate, but the stainless steel regenerators are larger and do therefore not fit into the scanner. Another option for measuring the plate spacings is optical microscopy, but this method can only acquire images of small patches of the regenerator. With the photogrammetric approach, images of the whole area of interest can be analyzed using a simple setup without specialized equipment.

3.2 Photogrammetry Setup

A compact digital camera[1] has been used for acquiring images. The camera is mounted on an arm, which is attached to a stand and enables it to be rotated around two axes (the x_2- and y_2-axes) and moved up and down (along the z_2-axis) as illustrated in Figure 3.1. A second arm used for holding the samples, which can also be rotated around the x_2- and y_2-axes, is mounted on another stand.

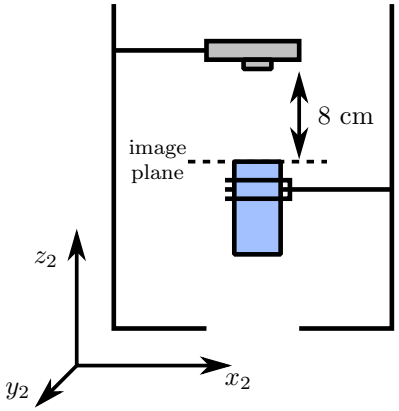

Figure 3.1: Photogrammetry setup.

The distance between the camera and the image plane is kept constant at 8 cm and both the camera and the samples are aligned horizontally.

In order for the measurements to be reproducible, all samples have been measured under identical lighting conditions. To minimize errors due to reflections or uneven lighting, an indirect light source has been used to illuminate the samples.

3.3 Correction for Distortion

In order to correct for lens distortion, the Matlab plugin described in reference [63] has been used. When using this, a series of images are acquired of a checkered pattern consisting of black and white squares. The corners of this pattern are then analyzed and a set of calibration parameters are calculated, which can be used for removing lens distortion in other images.

A plate with a pattern consisting of 61 squares with a side length of 3 mm, which is shown in Figure 3.2, was used for the calibration.

10 images of the calibration pattern have been acquired with the pattern at various angles, θ, as specified in Table 3.1. The approximate locations of the

[1] of the type "Olympus stylus", model "1010"

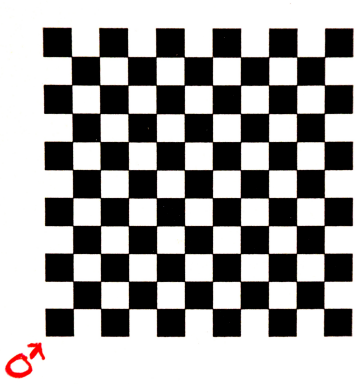

Figure 3.2: Calibration pattern.

corners in the calibration pattern are then manually entered in the calibration plugin and the pattern is automatically recognized. Since the pattern is completely uniform, any deviations in the images are due to distortions, and are accordingly corrected for by the calibration software, which calculates a set of calibration parameters to use for correcting other acquired images.

#	θ_{x2} [deg]	θ_{y2} [deg]
1	0	0
2	0	0
3	0	15
4	0	15
5	0	-15
6	0	-15
7	15	0
8	15	0
9	-15	0
10	-15	0

Table 3.1: Calibration angles.

In order to visualize the effect of the calibration, a compound image is produced for each calibration: The original and the corrected image are both converted to black and white, and the two images are superimposed as illustrated in Figure 3.3a. Pixels which are either white or black in both images retain their color, but pixels where the color differs are colored in red or blue. By using this approach shifted pixels can be seen as red or blue areas in the compound image.

Figure 3.3b shows an example of such an image, based on the original image shown in Figure 3.3c. The red and blue pixels are not clearly visible, but in the cut-out in Figure 3.3d, it can be seen that the corrections are on the order of ± 1 pixel.

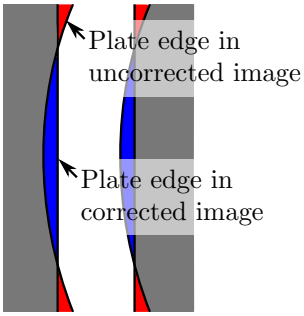

(a) Correction sketch

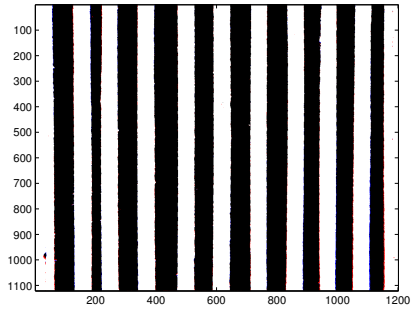

(b) Correction for lens distortion

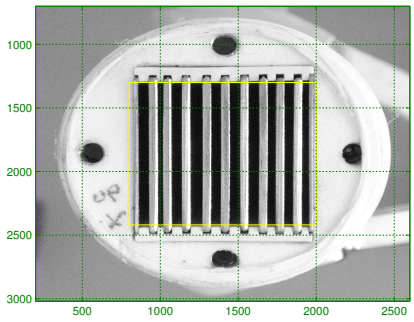

(c) Regenerator image

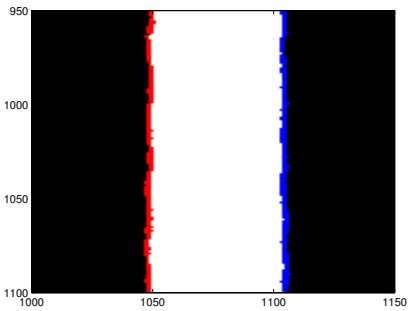

(d) Cut-out of (b)

Figure 3.3: Correction for lens distortion. (a): sketch of the visualization of the correction of the distortion in images (b) and (d). (b) and (d): Corrected and uncorrected images of the search area. Red and blue pixels show areas where the correction changes the pixel positions. These pixels are not clearly visible in (b) because the correction is only a few pixels. (c): sample image of a regenerator used for measuring the channel width distribution. The yellow box indicates the area where the plate edges are measured.

3.4 Procedure for Analysis

A Matlab script has been written to analyze the sample images and find the channel widths. The script searches the area shown in Figure 3.3c for plate edges and measures the distances between these edges.

The acquired image is converted to gray scale and is rotated so the plates are approximately aligned in the vertical direction. The approximate positions of each plate edge is then entered manually, and a range of 19 pixels for the AMRs and 15 pixels for the passive regenerators surrounding the approximate location is searched for the actual edge.

The plate edge is defined as the maximum gradient over three pixels, so the script searches for the largest gradient in the appropriate direction (left edges have positive gradients and right edges have negative gradients) and sets the middle pixel as the edge location.

The edge location procedure is repeated for every line in the y_2-direction within

the boundaries. When the edge location has finished, each edge is fitted to a straight line and this line is used for the distance measurements. Fitting the edge to a line requires that the plates are almost perfectly flat. For the stainless steel plates this is the case - Figure 3.4a shows a single plate edge from Figure 3.4b and it can be seen that this plate edge indeed is almost perfectly flat.

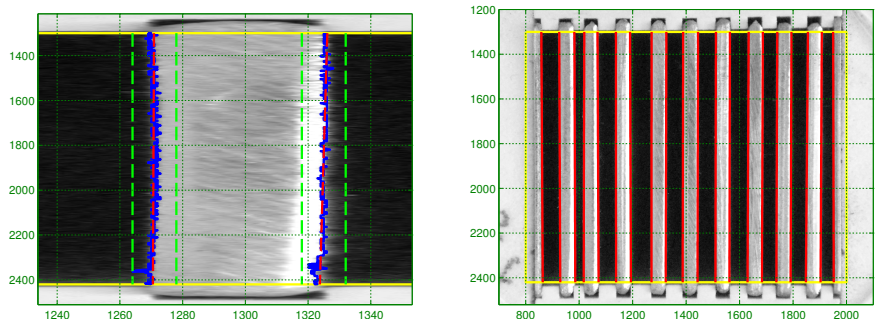

(a) Edge **(b)** Regenerator

Figure 3.4: Example of edge location for (a) a single plate, and (b) regenerator. The solid yellow and the dashed green lines are the search boundaries. The blue lines show the location of the maximum gradient for each line of pixels and the red lines are linear fits of the blue lines.

Figure 3.4b shows an example of the edge location of the uniform regenerator. The yellow box defines the boundaries for the edge location. The sides close to the plate holders are excluded from the search since the procedure is unable to properly differentiate between plates and plate holders. The green dashed lines are the search ranges for each edge, the blue lines are the found edges, and the red lines are the fitted lines.

The channel width is calculated for each point on the left side of the channel (a right plate edge) as the shortest distance to the right side (a left plate edge), using the fitted edges. The channel width, measured in pixels, is then the mean of this distance. If the plates are not completely parallel, there will be some variation in these distances. The standard deviation of the distances used for a mean value ranges from 0 to 3.5×10^{-2} mm for all the measured channel widths, which means that the plates are parallel with a relatively high precision.

In order to convert the values from pixels to mm, we use that the distance from the first plate edge on the left to the last plate edge on the right is approximately 19 mm. The resolution of the images are all approximately 67 px/mm or 0.015 mm/px.

3.5 Test Measurements

3.5.1 Independence of Lighting Angle

The measurements of the channel widths have all been conducted several times at different angles relative to the light source in order to ensure that no errors are introduced by uneven lighting conditions.

The uniform regenerator has been measured on the face in the up-direction at three different angles: 0°, 45°, and 90° rotation relative to the x_2-direction. The measured channel widths are shown in Table 3.2 and show that the channel width measurements are consistent within 0.013 mm, or 1.3 % of the mean channel width.

θ_{z2} [deg]	**Channel widths** [mm]									
0	1.0078	0.9575	1.0384	1.0534	1.0002	0.9402	0.9917	0.9927	1.0604	0.9578
45	1.0047	0.9608	1.0390	1.0517	0.9955	0.9399	0.9905	0.9985	1.0578	0.9615
90	1.0041	0.9556	1.0365	1.0479	1.0055	0.9407	0.9943	0.9935	1.0509	0.9711

Table 3.2: Uniform channel widths measured at various angles.

3.5.2 Measurements of a Known Sample

In order to ensure that the measurements are correct and to estimate the accuracy and reproducibility of the method, the channel width distribution has been measured on one of the aluminum regenerators. The distributions of the aluminum regenerators have also been measured by laser-optometry which has resolution of 5 μm.

The regenerator has a nominally uniform distribution with a channel width of 0.74 mm and plate widths of 0.4 mm. The measured channel widths are plotted in Figure 3.5 for each of the photogrammetric measurements and for the laser measurement.

The maximum difference between measurements of the same channel width is in channel number 16, where the difference is 0.021 mm. This corresponds to a deviation of 2.9 % of the mean plate spacing (or 2.1 % if the nominal plate spacing is 1 mm, as is the case for the stainless steel regenerators). This is only slightly greater than the resolution of the images, which was 0.015 mm/px, which indicates that the resolution of the digital photos is the main limitation on the measurement accuracy.

The deviations among the photogrammetric measurements are an order of magnitude smaller, which indicates that the errors to some degree are systematic. The standard deviation for the four different measurements of the individual channels is on average 0.33 % of the mean channel width.

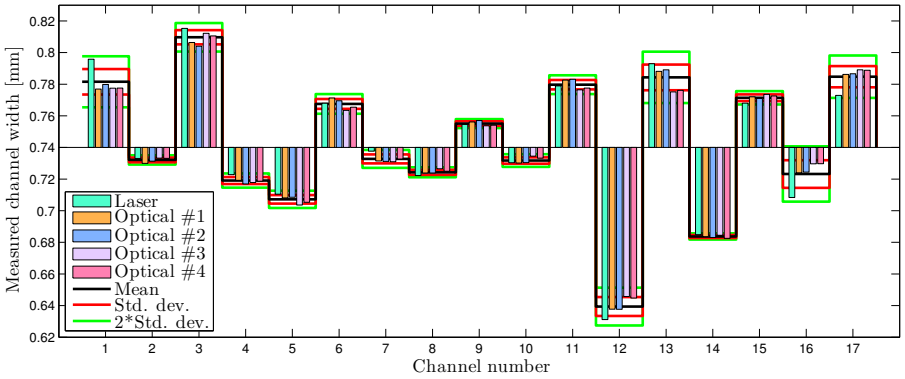

Figure 3.5: Channel widths in a regenerator with 0.4 mm aluminum plates, measured using two different techniques. The green bars show the measurements made using a laser scanner and the other bars show repeated measurements made using the photogrammetric approach described in this Chapter. The black line shows the meas for all five measurements and the red and green lines show one and two standard deviations, respectively.

Chapter 4

Experiments on Active Magnetic Regenerators

4.1 Introduction

Several magnetic refrigeration devices utilizing AMRs have been constructed (see e.g. references [64–67]). Many experiments have been performed using these and other machines or test devices in order to optimize operating parameters for given designs, e.g. in references [11, 68–73].

The experiments presented in this chapter focus on investigations of various modifications to the regenerator geometry, which have been implemented in order to investigate possible ways to optimize the geometries of AMRs for the test machine.

Experiments have been performed on four different regenerators and the effects of these modifications are evaluated. Furthermore, an experiment has been performed with a modified thermal reservoir at the top (i.e. the hot end) of the test machine.

4.2 Regenerators

The four tested regenerators all consist of 10 plates of gadolinium with dimensions 40 mm × 25 mm × 0.9 mm and use water as heat transfer fluid. Due to the ribs holding the plates, the regenerator channels are 23 mm deep and 40 mm long. The fabrication of the regenerators is described in more detail in Section 2.2.1. In addition to the overall geometry, the four regenerators have the following characteristics:

1. Nominal: The nominal regenerator. This regenerator has nine channels, each with a width of 0.9 mm and a depth of 23 mm. The outermost plates flush directly against the walls of the regenerator housing.

2. Half channels: This regenerator is identical to the nominal regenerator, except that the end plates do not flush against the walls of the housing. Instead, channels of 0.45 mm (half width) separate the outermost plates and the walls.

3. Radial channels: In this regenerator, the plates are not parallel. Instead, they are varying such that one side of the regenerator follows a circle with a radius of 75 mm and the other side a circle with a radius of 100 mm. This corresponds to the regenerator being a segment of a ring of thickness 25 mm and an outer diameter of 100 mm. Otherwise, it is identical to the nominal regenerator.

4. Narrow channels: This is the nominal regenerator, but with 0.6 mm channel widths instead of 0.9 mm. The numbers of plates and channels are still the same, which means that the volume of the regenerator is smaller than the volume of the nominal regenerator.

5. Copper heat exchanger: This is an alternative configuration where the narrow regenerator is used. The Perspex tube at the top of the test machine (see Figure 2.1) is replaced with a copper pipe which acts as a heat exchanger. In later experiments (see Chapter 8), an active heat exchanger is added to the setup at this end to keep it at a constant, controlled, temperature. That heat exchanger is described in Section 2.2.2, but in the current series, the more simple version is used.

The tested regenerators are pictured in Figure 2.2. Also pictured, is a regenerator with hollow walls (the white regenerator). The testing and comparison of this regenerator is not covered in this thesis but is described in reference [62] (in Appendix B.3). Furthermore, a regenerator with 0.1 mm spacings is depicted, but this regenerator is constructed for use with ceramic plates of 0.4 mm width, so this regenerator has not been tested with gadolinium and is therefore not covered in this thesis.

4.3 Experiments

The regenerators have been tested using the test machine in the configuration illustrated in Figure 2.1b. The experiments have been run with an applied magnetic field varying between 0 and 1.1 T, which causes the temperature of the regenerator matrices to change during the regenerative cycle. The magnetocaloric effect of gadolinium has been found to give an adiabatic temperature change of approximately 3.5 K and a magnetic entropy change of approximately 3.2 J/(kg K) in a field change from 0 to 1.0 T [12–15].

An average fluid velocity of 10 mm/s and a fluid displacement of 20 mm, i.e. 50 % of the regenerator length, have been used in all the experiments. The

fluid velocity and displacement are both defined for the fluid flowing inside the regenerator. The velocity and displacement of the piston in the test machine is therefore smaller by a factor which is given by the ratio between the cross sectional void area of the reservoir and that of the regenerator. Since the fluid displacement is kept constant in the experiments, the utilization, varies depending on the porosity of the regenerators. The utilization in the experiments on the nominal and radial regenerators is 1.0, the utilization for the half-channel regenerator is 1.1, and the utilization for the narrow regenerator is 0.67.

The heat load that is applied in the piston has been varied between 0 and 1.6 W during the experiments. The operating parameters used in the experiments are summarized in Table 4.1

Parameter	**Value**	**Unit**
Fluid velocity (u_{m})	10	mm/s
Fluid displacement	20 (50)	mm (%)
Piston heat load ($\dot{q}_{\mathrm{HL}}$)	0-1.6	W
Utilization (Φ)	0.67-1.1	-

Table 4.1: Operating parameters for AMR experiments.

4.4 Results

The measured temperature differences between the hot end (bottom) and the cold end (top) of the test machine have been plotted in Figure 4.1 as functions of the applied heat load for all the tested regenerators. It can be seen that the temperature difference decreases approximately linearly as a function of the heat load although the slope and position of the lines vary.

It is observed that the temperature difference at zero heat load is around 8 K for all the regenerators with only slight variations. However, the temperature differences at a heat load of 1.6 W vary from approximately 0 K to -8 K.

It should be noted that a negative temperature difference corresponds to the "cold" end (at the bottom) of the regenerator being hotter than the "hot" end (at the top). When running the machine with an AMR, heat is transported from the bottom reservoir to the top reservoir, which causes the bottom reservoir to cool down. At low heat loads, this means that the bottom reservoir is colder than the top reservoir - hence the "cold" and "hot" denominations - but if a sufficiently large heat load is applied in the bottom reservoir, the temperature of this reservoir becomes greater than the temperature of the top reservoir and thus a negative temperature difference is achieved.

In Figure 4.1, it can be seen that the temperature difference as a function of heat load for the radial regenerator is less linear than the other regenerators.This could either be because the temperature does not depend linearly on the heat load or it could indicate that the measurement errors in this experiment are greater than the measurement errors in the other experiments.

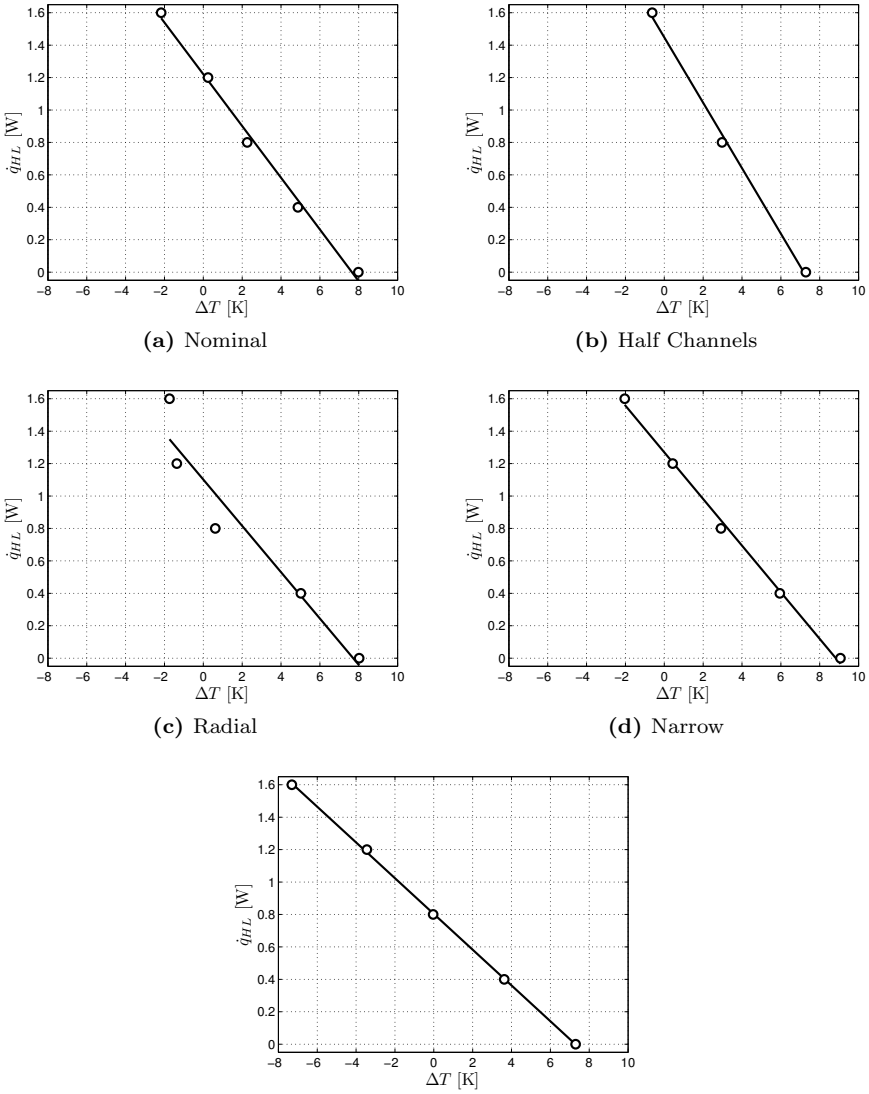

(a) Nominal

(b) Half Channels

(c) Radial

(d) Narrow

(e) Copper pipe

Figure 4.1: Measured temperature span as a function of applied heat load for all the tested AMRs.

In other experiments on AMRs, which are similar to the experiments conducted here, the temperature difference as a function of heat load are found to be approximately linear, see e.g. references [65–67, 69–71]. In reference [67], however, the results show that at high operating frequencies (4 Hz), the temperature profile becomes non-linear. The non-linearity occurs as a decrease in temperature difference at high heat loads which grows at an increasing rate as the heat load increases. In the radial regenerator, however, the opposite, i.e. a decrease in the rate of change of the temperature difference at high heat loads, is observed. This might indicate that the non-linearity is due to errors in the experiment.

If we nevertheless assume that the temperature difference is approximately linear as a function of the heat load, the regenerator performance under the given experimental conditions can be described by two factors. Here, the no-load temperature span and the no-temperature span heat load, i.e. $\Delta T(\dot{q}_{\mathrm{HL}} = 0\ \mathrm{W})$ and $\dot{q}_{\mathrm{HL}}(\Delta T = 0\ \mathrm{K})$, respectively, are used. These quantities, which have been found by interpolating along the fitted lines, are shown in Figure 4.2 for all the experiments along with the estimated standard deviations.

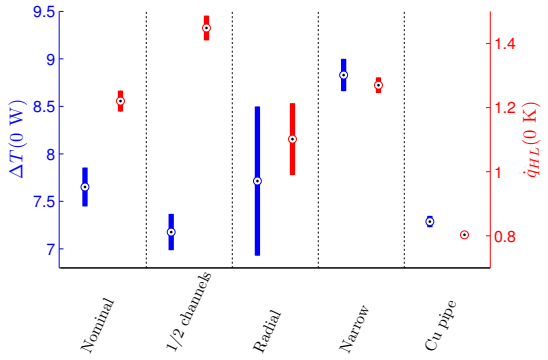

Figure 4.2: No-load temperature spans and no-span heat loads found from linear fits for all the tested AMRs.

As it has also been found from Figure 4.1, the no-load temperature span varies in the proximity around 8 K for all the regenerators. The no-span heat load of the nominal regenerator is 1.2 W and is higher for the half-channel and narrow regenerators and lower for the radial regenerator and the configuration with the copper pipe.

4.5 Discussion

The errors in the measurements are relatively large, which makes it difficult to conclusively identify trends in several of the experiments. It can be seen, that the no-load temperature span in the regenerator with narrow channels is significantly greater, which could be caused by the smaller utilization. However, when attaching the copper pipe, it can be seen that both the no-load temperature span and the no-span temperature difference decrease significantly. This is

unexpected, since the copper pipe is only expected to change the temperature of the top reservoir. However, the pipe might cause the temperature in the reservoir to be more uniform, which would reduce the temperature difference between the two ends at all heat loads. Moreover, the thread of the pipe extends to cover part of the outside of the regenerator housing, which to some extend might give additional heat transfer in this area and thus impact the regenerator operation in a similar way as heat losses to the surroundings.

In reference [70], the temperature difference versus heat load curves were measured systematically for varying utilizations, which should correspond to a change in effectiveness (see e.g. reference [26]). In that study, it can be seen that the curves are all linear and approximately parallel, which indicates that increasing the utilization would be expected to increases both the no-load temperature span and the no-span heat load.

This, however is not the case in the present experiments. The half-channel regenerator shows a higher heat load but a lower temperature difference; the radial regenerator shows higher temperature differences but a lower heat load; and the narrow regenerator and the copper pipe configuration show increases and decreases in both temperature difference and heat load, respectively.

The inconsistencies in the observed trends may be due to the modifications of the regenerators, but since the variations in the measured data - particularly in the no-load temperature span - are relatively small, they could also be attributed to experimental errors.

There are a number of possible sources of error in the experiments: The temperature measurement at the bottom end of the test machine is performed close to the piston and the mixing of fluid in either reservoir is not perfect. Both of these factors may influence the actual measurements but are not expected to alter the observed trends. The ambient temperature is kept at a room temperature of approximately 26°C, but varies from 24.3°C to 27.2°C in the actual experiments. The magnetocaloric effect of gadolinium is quite sensitive to temperature, so even slight changes in the ambient temperature in an experiment could change the results significantly. (In subsequent experiments, the test machine has been placed inside a temperature controlled cabinet and variations in ambient temperature are therefore minimal). In reference [74] (Appendix B.5), however, variations in ambient temperature were investigated for similar regenerators, using both modeling and experimental data. There, it was found that variations in performance do occur, but the variations are too small to completely explain the discrepancies observed in the current study.

Visual inspection of the regenerators reveals that the plate spacings tend to vary. The average width of the channels in a regenerator is not the same for all channels and the width of a given channel varies along from one side of the regenerator to the center or to the other side.

After the experiments had been performed, the half-channel regenerator was reassembled and the channel width distribution was measured using the setup described in Chapter 3. The measured end of the regenerator is shown in Figure 4.3. When measuring the plate distribution, a window of ±9 pixels was

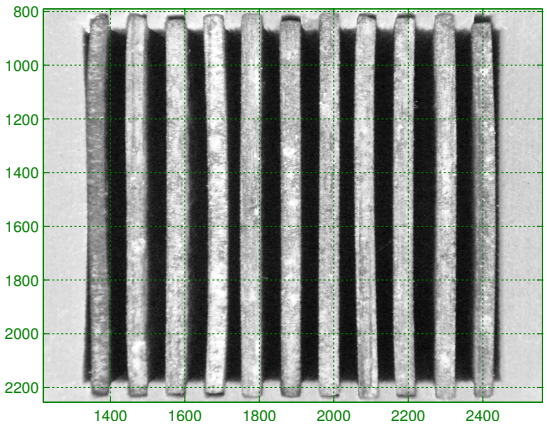

Figure 4.3: Measured cross section of the half-channel AMR.

used(see also Section 3.4 for details on this procedure). The average channel widths of the measured regenerator are shown in Figure 4.4. The standard deviation of the channel width is 0.10 mm, which corresponds to 11 % of the mean width, and the widest and narrowest channels are 1.03 mm (+0.13 mm) and 0.73 mm (-0.17 mm), respectively.

The measured channel widths are based on the average width of each channel along the depth direction (the y_2-direction). The width of a given channel, however, is not necessarily the same everywhere in the channel. Along the depth of the channels, the measured (average) channel width of a given channel, deviates on average by 0.04 mm, or 3 %, from the actual channel width at a given position. Even though this is less than the standard deviation of 11 % of the average channel widths, it may still affect the fluid flow and heat transfer in the regenerators. This variation is, of course, much greater for the radial regenerator since variations in this direction are intentionally introduced in the

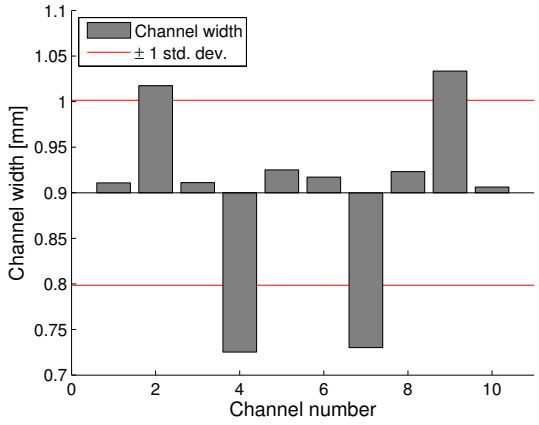

Figure 4.4: Measured channel widths of the half-channel AMR. Only whole channels are included in this measurement.

design of the regenerator.

It can be seen from the imaged cross section shown in Figure 4.3 that, besides the variations in the (whole) channels that have been measured, the widths of the half channels exhibit great variation. This is mainly due to the walls of the regenerator not being entirely flat but may nonetheless have a significant effect of the flow rate in the half channels.

Variations in the plate spacings of this magnitude means that the possibility of significant reductions of performance in the regenerators cannot be neglected. If this is the case, the effects of these variations need to be investigated, and if not negligible, an experimental procedure should be developed where the effects are either excluded, or accounted for in the data analysis and evaluation of performance.

Reference [74] (in Appendix B.5) presents a "2.5"-dimensional finite difference model of an AMR. Results of simulations run using the model are compared to equivalent experiments, which have been performed using the same equipment.

The comparison showed that the experimental regenerator performance was lower (in terms of no-load temperature span and no-span heat load) for the experiments than predicted by the model. Possible causes of this discrepancy were initially identified as heat losses to the surroundings, variations in the ambient temperature, and impurities in the matrix material (commercial grade gadolinium).

Including heat losses to the surroundings and variations in ambient temperature in the simulations did account for some of the discrepancy. Impurities in the gadolinium, and subsequently demagnetization effects [75], was accredited as possible cause for the rest. Non uniform channels, however, might also be a significant contributing factor since the experiments were carried out using a regenerator with a geometry that is similar to that of the nominal regenerator.

Gadolinium, which is often used for magnetic refrigeration applications, is a very soft material which easily exhibits plastic deformation. It has a yield strength of only 15 MPa [76], whereas stainless steel, for comparison, has yield strengths on the order of 900 MPa, depending on the type and treatment [77]. Therefore, it is often difficult to retain the shape of gadolinium plates in regenerators, which means that thin plates of gadolinium will have a greater tendency to be irregularly shaped than similar plates of hard metals such as stainless steel or aluminum. The ductility furthermore means that thin plates more easily can be deformed during assembly or operation of regenerators, which could result in irregular channel geometries.

4.6 Non-Uniformity Investigations

Due to the large variations in channel widths observed in these experiments, it has been decided to investigate the effects of non uniform plate spacings on the regenerators. Initially, a numerical model simulating multiple channels will be developed in order to investigate the heat transfer during a single-blow process,

and then a series of experiments will be performed in order to evaluate whether the single-blow results accurately estimate the losses during cyclic operation. The goal of this investigation is to determine the significance of non uniformly distributed (but parallel and equally spaced) channels in regenerators.

The study will be targeted toward regenerators in general, but since there is very great variety in materials, operating conditions, geometries etc. for different types of regenerators, the parameter space used in simulations and experiments will be based around typical values used in magnetic refrigeration.

Chapter 5

Regenerator Model with Multiple Channels

5.1 Introduction

A model describing a single blow process in a regenerator has been developed in order to investigate the heat transfer mechanisms taking place in regenerators with complex geometries. The model has been developed specifically to simulate parallel plate regenerators and consists of a number of parallel plates where the plate spacings can be freely varied[1].

This model will be used to investigate the heat transfer in various parallel plate regenerators with a range of different plate spacing distributions and geometries in order to determine the effects of non-uniform plate distributions on the regenerator performance.

The model and the results obtained using the model are also presented in references [78–80] (also shown in Appendix B). Reference [78] covers a series of simulations which are presented in Chapter 6 and part of Chapter 7. Reference [79] covers a different series of simulations, which are also presented in Chapter 7. Reference [80] covers the simulations presented in Chapter 9, which consist of a series of simulations of experimental regenerators.

5.2 Model Description

The model is a two-dimensional transient finite element model of a single-blow process in a parallel-plate regenerator. The model simulates a time span where

[1] The plate widths can also be varied, but this feature is not utilized in the present work.

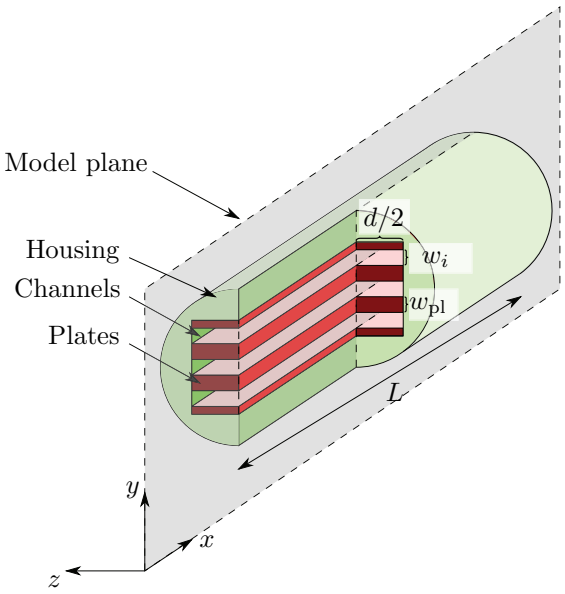

Figure 5.1: Cross section of the modeled geometry. The model can simulate an arbitrary number of plates and channels, but in the presented results, 10 channels and 9 whole plus 2 half plates have been used. The model only considers the xy-plane and the housing is assumed to be perfectly insulating.

the fluid and matrix initially is in thermal equilibrium. Fluid at a different temperature enters through a number of inlets, which causes an internal heat transfer to take place in the regenerator and results in the regenerator matrix heating up or cooling down.

5.2.1 Geometry

The regenerator geometry that has been modeled consists of a number, $N-1$, of parallel plates which all have equal widths, w_{pl}, and lengths, L. The plates are separated by N fluid channels with widths w_i, which are not necessarily equal. At either side of the top and bottom channel, two additional plates of width $w_{\mathrm{pl}}/2$ are modeled. The geometry of the modeled regenerator is shown in Figure 5.1.

The regenerator is modeled with its walls being perfectly insulating and the depth of the regenerator, d, is considered to be large compared to the widths of the channels and the plates. Edge effects at the sides of the regenerator are therefore neglected, and the model only considers the two dimensions of the xy-plane (as defined in Figure 5.1).

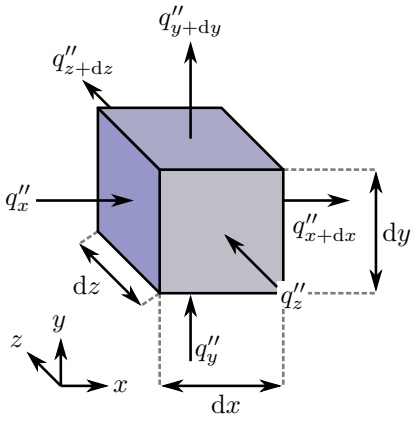

Figure 5.2: Control volume for an arbitrary point in the regenerator. The heat flux is separated into x-, y- and z-components flowing through the faces of the control volume. Each side of the volume has an infinitesimal length, $\mathrm{d}x$, $\mathrm{d}y$, and $\mathrm{d}z$, respectively.

5.2.2 Governing Equations

If we consider a control volume in the regenerator with infinitesimal side lengths, $\mathrm{d}x$, $\mathrm{d}y$, and $\mathrm{d}z$, as illustrated in Figure 5.2, the heat flux through the faces of this volume must be balanced with the change of thermal energy stored within the volume. The heat fluxes are defined such that positive heat fluxes flow in the positive x-, y-, and z-directions.

Two different thermal processes transfer heat in this system: conduction and convection. The conductive heat flux in the x-direction, $\dot{q}''_{\mathrm{cond},x}$, is given by

$$\dot{q}''_{\mathrm{cond},x} = -k\frac{\partial T}{\partial x}. \tag{5.1}$$

The convective heat is carried by the motion of the fluid, and the convective heat transfer in the x-direction is therefore given by

$$\dot{q}''_{\mathrm{conv},x} = \rho c u T. \tag{5.2}$$

The difference between the thermal energy entering the control volume at x and the thermal energy exiting the control volume at $x + \mathrm{d}x$ by conduction is given by

$$\frac{\partial \dot{q}''_{\mathrm{cond},x}}{\partial x} = -k\left.\frac{\partial T}{\partial x}\right|_x + k\left.\frac{\partial T}{\partial x}\right|_{x+\mathrm{d}x} = \frac{\partial}{\partial x}\left(-k\frac{\partial T}{\partial x}\right) \tag{5.3}$$

and the difference between the thermal energy entering and exiting by convection is given by

$$\frac{\partial \dot{q}''_{\mathrm{conv},x}}{\partial x} = (\rho c u T)|_x - (\rho c u T)|_{x+\mathrm{d}x} = \frac{\partial}{\partial x}(\rho c u T) \tag{5.4}$$

Similar equations govern the conductive and convective heat transfer in the y- and z-directions and expressions for these directions can be written by replacing the x-coordinate with y or z.

Heat generation is ignored in the model, which means that the amount of thermal energy entering the control volume is equal to the sum of energy exiting the control volume and energy added to the control volume. There are no heat sources in the solid material, but in the fluid, kinetic energy may be converted to thermal energy by viscous dissipation, which will give volumetric heat generation in the fluid.

The criterion for neglecting this effect is that the ratio of viscous dissipation to radial conduction in the system must be small. This ratio is given by the Brinkman number, Br, which is defined as [26]

$$Br_x = \frac{\mu u_{\mathrm{m}}^2}{k_{\mathrm{f}}(T_{\mathrm{s},x} - T_{\mathrm{m},x})}, \tag{5.5}$$

where μ is the fluid viscosity, u_{m} is the mean fluid velocity, $T_{\mathrm{s},x}$ is the surface temperature of the solid, and $T_{\mathrm{m},x}$ is the mean fluid temperature at a given x-position. When the majority of the heat transfer occurs, the temperature difference between the plates and the channels, $T_{\mathrm{s},x} - T_{\mathrm{m},x}$, is close to the temperature difference between the initial and the inlet temperatures, $T_{\mathrm{init}} - T_{\mathrm{in}}$. In the modeling, a temperature difference of 4 K is used, which gives a Brinkman number of 1.5×10^{-3} for an average channel. Since $Br \ll 1$, the effects of viscous dissipation can be ignored in the model.

In order for energy to be conserved in the control volume, the sum of net heat fluxes into the control volume must correspond to a change in temperature, such that

$$\nabla(-k\nabla T) + \nabla(\rho c \mathbf{u} T) = \rho c \frac{\partial T}{\partial t}, \tag{5.6}$$

where $\mathbf{u}$ is the velocity vector.

The first term in Equation 5.6 is the conductive heat flux and the second term is the convective heat flux. With no volumetric heat generation or removal, the sum of these two heat fluxes must be equal to the change in thermal energy of the control volume, which is the third term in Equation 5.6.

Even though the temperatures used in the modeling vary by only 4 K, the modeling results are valid for any temperatures as long as variations in the thermal properties of the materials are negligible, as is shown in Section 5.3. In order to simplify the problem and to make the solution temperature-independent, constant material properties are therefore used. For large temperature changes,

variations in these parameters may have significant effects on the heat transfer, which would not be reflected in the modeling results. However, the purpose of the model is to investigate the heat transfer in systems with complex geometries, and using constant material properties will make any tendencies with respect to geometric variations more clear.

When using constant properties, Equation 5.6 can be simplified to

$$-k\nabla^2 T + \rho c \nabla(\mathbf{u}T) = \rho c \frac{\partial T}{\partial t}. \tag{5.7}$$

Since the fluid only flows in the x-direction, the y- and z-components of $\mathbf{u}$ are zero, and because the flow is fully developed, as described in Section 5.2.4, $\frac{\partial \mathbf{u}}{\partial x} = 0$, which means that the equation can be further simplified to

$$-k\nabla^2 T + \rho c u \frac{\partial T}{\partial x} = \rho c \frac{\partial T}{\partial t}. \tag{5.8}$$

In the definition of the model geometry, it is assumed that $d \gg \bar{w}$, where $\bar{w}$ is the mean channel width, and that the sides of the regenerator are perfectly insulating. Temperature gradients in the z-direction are therefore negligible and it is thus only necessary to model the x- and y-dimensions.

The solution to Equation 5.8 is therefore a two dimensional temperature profile as a function of time, $T(x, y, t)$. This temperature profile is solved for each domain (i.e. each plate and each channel) in the regenerator for a number of time steps. The governing equations in the respective domains are

$$\rho_\mathrm{s} c_\mathrm{s} \frac{\partial T(x,y,t)}{\partial t} + k_\mathrm{s} \nabla^2 T(x,y,t) = 0 \tag{5.9}$$

in the solid and

$$\rho_\mathrm{f} c_\mathrm{f} \frac{\partial T(x,y,t)}{\partial t} + k_\mathrm{f} \nabla^2 T(x,y,t) - \rho_\mathrm{f} c_\mathrm{f} u(y) \frac{\partial T(x,y,t)}{\partial x} = 0 \tag{5.10}$$

in the fluid.

5.2.3 Initial and Boundary Conditions

The external boundaries of the model are the inlets and outlets of the channels, the ends of the plates and the top and bottom sides of the half-width plates. It is assumed that the plate boundaries are insulated ($\dot{q} = 0$), and that the heat transfer by convection at the inlets and outlets is much greater than the heat transfer by conduction, such that it can be assumed that $\dot{q}_\mathrm{cond} \approx 0$ at the inlets and outlets. This corresponds to assuming that the temperatures of the fluid on the sides of the inlets and outlets that are not modeled are completely uniform,

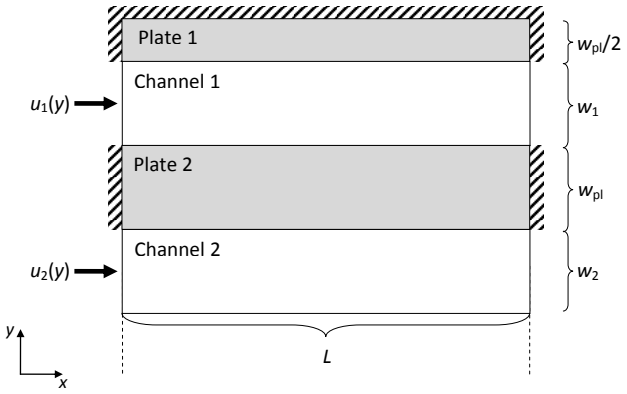

Figure 5.3: Diagram of the modeled geometry with boundary conditions and subdomains (not to scale).

such that the only transfer of thermal energy through these boundaries is due to convection.

The temperature of the fluid entering at the inlets is set to T_{in} and the boundaries and subdomains of the model are shown in Figure 5.3. The insulated boundaries at the top and bottom of the regenerator can be regarded as either flushing against the walls of the regenerator housing (which are adiabatic) or as mirror symmetry lines, such that the modeled regenerator can be considered as a cell in a repeating geometry.

At the beginning of the transient period (at $t = 0$), the temperature of the fluid and the solid is in equilibrium at T_{init}. At $t \geq 0$, fluid at temperature $T_{\text{in}} < T_{\text{init}}$ enters from the inlets with a predefined velocity profile, $u_i(y)$. Due to the cold fluid in the channels, heat begins to transfer from the plates to the channels and is removed from the regenerator through the outlets.

In the following, T_{in} will be used as reference temperature for the thermal energy, such that all the thermal energy initially stored in the regenerator is removed as $t \to \infty$ where the regenerator eventually will reach equilibrium at $T = T_{\text{in}}$, which then corresponds to a thermal energy of zero.

The model works equally well for $T_{\text{in}} > T_{\text{init}}$. In this case the sign of the thermal energies and the heat fluxes is reversed. It does not affect the regenerator performance as the heat transfer mechanisms are the same, only with the direction of the heat transfer being the opposite.

5.2.4 Hydrodynamic Conditions

The fluid flow profiles in the channels can be calculated analytically by making a few assumptions about the flow:

1. It is assumed that the physical properties of the materials are constant within the temperature range of the simulations.

This assumption is already made for the governing equations for the heat transfer, and extending it to the fluid mechanics is appropriate for the same reasons.

2. It is assumed that the fluid flow is laminar and fully developed when it enters through the inlet.

   For the simulations performed in the present work, the average channel has a width of 1 mm and a mean fluid velocity is 5 mm/s. This gives a Reynolds number of 6, which is well within the laminar range ($0.1 \leq Re \leq 1000$ [27]).

   The length over which the fluid is developing after entering the channel, the hydrodynamic entry length for internal flow, L_e, is given by the correlation $L_\mathrm{e}/D_\mathrm{h} = 0.06Re$ [26], where D_h is the hydraulic diameter. For flow between parallel plates, $D_\mathrm{h} = 2w$, which gives an entry length of 0.7 mm. In the simulations, however, the channel widths are varied in different distributions, but the widest possible[2] channel has a width of 2 mm, which gives a Reynold's number of 11 and a hydrodynamic entry length of 2.7 mm. Since the total length of the regenerator is 10 cm, the developing region of the fluid can be ignored without introducing significant errors.

   Neglecting the developing region simplifies the modeling problem significantly since it is not necessary to know the inlet flow conditions.

3. It is assumed that the heat transfer fluid is incompressible. This assumption is required for if the density is to be assumed constant. Neither of these assumptions do generally hold if the heat transfer fluid is a gas, but since the heat transfer fluid used in experiments as well as simulations is liquid water, which has a very low compressibility (0.46 GPa^{-1} [76]), the assumption is appropriate.

4. It is assumed that the depth of the regenerator in the z-direction is much greater than the channel width, i.e. that $d \gg \bar{w}$, such that the fluid flow in each channel can be approximated as a flow between two infinite parallel plates. This is already an inherent assumption in the heat transfer part of the model because only two dimensions are modeled.

Given the above assumptions, the flow profile in each channel as a function of the maximum velocity of that channel, $u_{\mathrm{max},i}$, is given by

$$u_i(y) = u_{\mathrm{max},i}\left(1 - \frac{(y - y_i)^2}{(1/2\ w_i)^2}\right), \tag{5.11}$$

where y_i is the y-coordinate of the center of the ith channel, and the pressure drop along the length of the channel is given by [27]

$$\Delta P_i = \frac{8\mu L}{w_i^2} u_{\mathrm{max},i}. \tag{5.12}$$

[2] with a probability of at least 95 % (see Section 7.2).

The flow is calculated as flowing from one reservoir, which is connected to all the inlets, to another reservoir, which is connected to all the outlets. The fluid flows with a predefined overall volumetric flow rate, $\dot{V}$. This means that the fluid flow in all the channels of a given regenerator will be driven by the same pressure drop and the pressure drop is therefore the same in all channels of a given regenerator, i.e.

$$\Delta P_i = \Delta P. \tag{5.13}$$

The pressure drop, however, depends on the overall flow rate and on the channel widths and may therefore vary from one modeled regenerator to another.

The volumetric flow rate in the individual channels is given by

$$\dot{V}_i = \frac{dw_i^3 \Delta p}{12\mu L} \tag{5.14}$$

and the total flow rate can thus be written

$$\dot{V} = \sum_{i=1}^{N} \dot{V}_i = \frac{d\sum_{i=1}^{N}(w_i^3)}{12\mu L}\Delta p. \tag{5.15}$$

Substituting Equation 5.12 into Equation 5.15 gives the relationship between the overall flow rate and the width and velocity of the channels in the regenerator

$$\frac{\dot{V}}{d} = \dot{V}' = \frac{2}{3}\frac{\sum_{i=1}^{N}(w_i^3)}{w_i^2}u_{\max,i}, \tag{5.16}$$

where $\dot{V}'$ is the volumetric flow rate per unit depth. This equation is valid for all channels in a given regenerator and rearranging it gives the maximum fluid velocity of a channel as a function of channel widths in the regenerator

$$u_{\max,i} = \frac{3}{2}\frac{w_i^2}{\sum_{i=1}^{N}(w_i^3)}\dot{V}'. \tag{5.17}$$

For flow between parallel plates, the mean fluid velocity is simply $u_{\mathrm{m}} = 2/3 \cdot u_{\max}$.

It should be noted that the fluid velocity in a given channel not only is a function of the width of the channel that is being considered, but is a function of the whole distribution of channels in the particular regenerator.

Using Equation 5.17, the maximum fluid velocity of each channel is found, and the flow profile is then calculated using Equation 5.11. Figure 5.4 shows the calculated flow profiles and flow rates for a regenerator with channels of various widths.

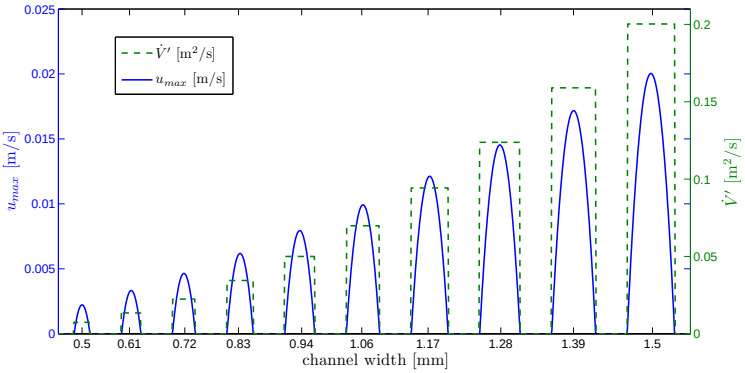

Figure 5.4: Fluid velocity profiles and volumetric flow rate per unit depth in a regenerator with various channel widths. The values on the x-axis denotes the width of each channel.

5.2.5 Model Implementation

The model has been implemented using the commercially available software Comsol [81]. This program uses the finite element method to solve the temperature profile in all elements in a given mesh. This mesh divides the geometry into a number of elements, each of which is associated to a number of nodes as illustrated in Figure 5.5.

When using the finite element method, the temperature in each (ith) element is approximated to a function of the form

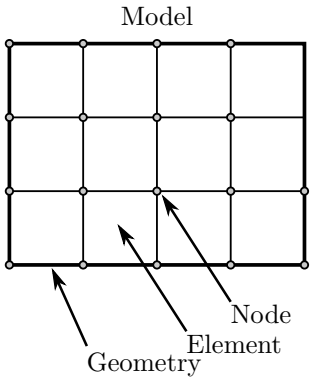

Figure 5.5: Concept of finite element model. The geometry consists of a number of elements, which can have different properties, and the elements and boundaries are connected by nodes. In the present model, the elements are rectangular, but in finite element models in general, the elements are commonly triangular, such that non-rectangular geometries can be more accurately approximated.

$$T(x_i, y_i) = \sum_{j=1}^{K} b_{i,j}\phi_j(x, y), \tag{5.18}$$

where $b_{i,j}$ is a constant for the jth node of the ith element, K is the number of nodes assigned to the ith element, and ϕ_j is some (element) function for the jth node.

The element functions create a simple polynomial interpolation of order $K-1$ between the K constants, which describes the temperature in the model at a given time step. The particular solution is found by Comsol using the solver described in reference [82]. For a more thorough description of this method, see reference [83].

Since the geometric objects in the model are rectangular, a rectangular mesh has been used for the discretization of the regenerator. In the simulations presented in this thesis, a mesh with 128 elements in the x-direction in both plates and channels, 8 elements in the y-direction in the channels, and a single element in the y-direction in the plates have been used. Having only one mesh element across the plates, and thus nodes only at the top and bottom boundaries of the plates, means that the temperature gradient across the plate in the y-direction is an interpolation between the two points at the edges. Furthermore, a time step of 0.005 s has been used in the modeling. The number of elements and the time step size is discussed in Section 5.3.

The nominal geometry, materials, and operating parameters used in the model are based on a regenerator for a test machine built at Risø DTU. The test machine is built for testing AMRs, and the nominal parameters used in the studies presented in this thesis are therefore based on regenerators of this type [64].

The condition for ignoring the temperature distribution in the plates completely is that the Biot number, $Bi \ll 1$, where

$$Bi = \frac{R_{\text{cond}}}{R_{\text{conv}}}, \tag{5.19}$$

where R_{cond} and R_{conv} are the conductive and convective thermal resistances, respectively. This condition can be written as

$$Bi = \frac{w_{\text{pl}}h}{2k_{\text{s}}} \ll 1. \tag{5.20}$$

In the case of uniform, parallel plates, the Nusselt number is approximately 7.541 [26] and is given by

$$Nu = \frac{2h\bar{w}}{k_{\text{f}}}, \tag{5.21}$$

which gives

$$Bi = \frac{Nu}{4} \cdot \frac{w_{\mathrm{pl}}}{\bar{w}} \cdot \frac{k_{\mathrm{f}}}{k_{\mathrm{s}}}. \tag{5.22}$$

Using the values for water and gadolinium in Table A.1, we get that $Bi \approx 0.1 w_{\mathrm{pl}}/\bar{w}$, which is much less than one for porosities close to or less than one. For aluminum and stainless steel, which are also modeled using this model, the thermal conductivities are greater than that of gadolinium, so in these cases, the Biot number can also be expected to be much less than one.

Two different sets of materials have been used: one for modeling of different fixed regenerator plate distributions and for parameter variations of randomly generated distributions (gadolinium and water); and one for experimental investigations of manufactured regenerators with various distributions (stainless steel and an ethylene glycol/water solution).

In the modeling of fixed distributions and parameter variations of random distributions, the magnetocaloric material gadolinium has been used for the matrix material and water for the heat transfer fluid. These simulations only address the heat transfer in the regenerator, so the magnetocaloric properties of gadolinium have not been used.

In a series of subsequent experiments, stainless steel (AISI 304) has been used for the matrix material due to practical reasons: stainless steel plates are more flat and have a more even thickness than gadolinium plates. Furthermore, stainless steel does not deform as easily, which makes it easier to fabricate regenerators with precisely controlled plate spacings. The thermal properties of stainless steel are similar to the thermal properties of gadolinium, and the two different sets of materials are therefore in the same parameter regime. The results when using these materials are therefore still somewhat, although not completely, comparable. The heat transfer fluid used in the experiments is a mixture of 25 % (by volume) of a commercial antifreeze based on ethylene glycol and 75 % deionized water. The simulations used for comparison with the experiments use the same material properties as the experiments. Furthermore, simulations on regenerators with aluminum matrices have been performed. The thermal conductivity of aluminum is much greater than those of gadolinium and stainless steel, but the thermal mass is on the same order of magnitude. The thermal properties of these materials are given in Table A.1.

5.3 Model Validation

In order to verify that the results obtained using the model are sufficiently accurate, a number of different validations have been carried out. First, the mesh configuration and time step size have been tuned by running a version of the model with only one half channel and one half plate for different mesh and time step configurations. In these simulations, however, plates and channels contain the same number of elements.

Since the tuning of the mesh and time step is being performed with a simplified geometry, a second set of simulations has been performed on a model with full 10-channel geometry in order to verify that the accuracy is maintained when using multiple channels.

The heat transfer in the plates and the heat transfer in the channels occur at different rates, which means that the size of the temperature gradients are different. The optimal number of elements is therefore not necessarily the same for plates and channels. A third series of simulations has therefore been run, where the number of elements in the plates is optimized. Since complex geometries are used in the modeling, however, the temperature gradients may be greater for non-uniform distributions, and the number of plate elements must therefore be validated for multiple channels with non-uniform geometries.

Additionally, a simulation of a special case of a uniform regenerator is compared to a known correlation for the heat transfer, which is valid for this particular case.

5.3.1 Mesh Configuration and Time Step Size

The mesh configuration consists of three parameters: the number of elements in the x-direction, the number of elements in the y-direction in the channels, and the number of elements in the y-direction in the plates. The number of elements in the x-direction must be large enough to resolve the temperature gradients that propagate in the regenerator and the number of elements in the y-direction should be large enough to resolve the temperature gradients across the plates and channels. Since the temperature gradients in the plates and in the channels along the x-direction have approximately the same magnitude, the same number of elements is used in this direction for both plates and channels.

Since the thermal diffusivities of the solids are much greater than the thermal diffusivities of the fluids, it can, however, be expected that the temperature gradients along the y-direction are greater in the channels than in the plates. Furthermore, the fluid in in motion and the primary heat transfer process is convection, which means that the required number of mesh elements is larger for the channels.

The size of each time step must be small enough to temporally resolve the movement of the temperature gradient. Typically, in order to get a stable solution, the movement of the thermal front during a single time step should be smaller than the size of the element it is moving through. The velocity of the thermal front is a function of the effectiveness of the regenerator, but for the worst possible regenerator, the velocity profile of this front will approach the velocity of the fluid flow, $u_i(y)$. Regenerators near this limit are not modeled and the velocity of the temperature front in the simulations has been found to typically be approximately $2/3 \cdot \bar{u}_i$.

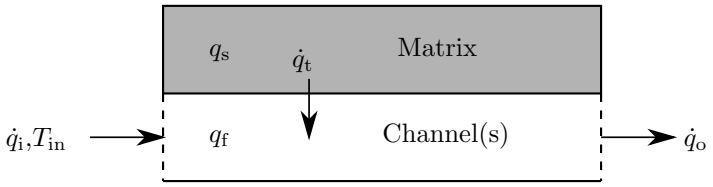

Figure 5.6: Energy balance for a regenerator. $\dot{q}_t$ represents the heat transfer across all internal channel/plate boundaries in the model, even though there may are multiple plates and channels in the model.

5.3.2 Initial Tuning of the Configuration

In the first set of tuning simulations, the number of elements in the plates and in the channels are equal. A series of simulations has been run with the combinations of mesh configurations and time steps shown in Table 5.1. The modeling software comes with a built-in algorithm for determining an appropriate time step. When the time step size is set to "free", the time stepping is completely controlled by this algorithm. When specifying a time step size, this number is used instead[3].

In order to evaluate the accuracy of the model in the different configurations, we consider the energy balance of the system. The total net thermal energy added to the system from the fluid inlet, at a time t_1, is given by

$$q_{\text{in,net}}(t_1) = \int_0^{t_1} \dot{q}_i(t) - \dot{q}_o(t)\mathrm{d}t, \tag{5.23}$$

where $\dot{q}_i(t)$ is the heat flux at the inlet and $\dot{q}_o(t)$ is the heat flux at the outlet. The total thermal energy stored in the system, relative to T_{init}, is the sum of the thermal energy of the solid, q_s, and the thermal energy of the fluid, q_f.

For the time $t \to \infty$, we can thus write

$$q_{\text{in,net}} + q_s + q_f = (V_s c_s \rho_s + V_f c_f \rho_f) \cdot (T_{\text{init}} - T_{\text{in}}) + \Delta E, \tag{5.24}$$

where ΔE is the numerical error, which must be equal to zero for energy to be conserved in the system.

Figure 5.6 illustrate the three interfaces where heat transfer occurs in the regenerator: the inlets ($\dot{q}_i$), the outlets ($\dot{q}_o$), and the plate/channel interfaces ($\dot{q}_t$). Only one plate and one channel are shown in the figure, but multiple plates and channels can be lumped together, such that only the total heat transfer rates need to be considered.

[3]Actually, this is a maximum time step, meaning that if the algorithm determines that smaller time steps are appropriate, it will override the manual value. With the values used in this work, however, this does not happen.

The deviations, ΔE, for the simulations in Table 5.1 is 1.0 % for the configuration of 384 by 16 elements and a maximum time step of 0.01 s, whereas it is 12.0 % for the same mesh but with free time stepping. This dramatic difference in the error shows that a maximum time step is required for the model to be accurate.

The simulations with 128 by 8 elements both give a deviation of the energy balance of 1.5 %, which shows that there is some accuracy to gain by increasing the mesh density, but that decreasing the maximum time step does not provide any significant increase in accuracy. The decrease from an error of 1.5 % to 1.0 %, however requires much longer computation times whereas the decrease in the maximum time step in the worst case only will double the computation time. Since the changes in the temperature profile will be smaller from one time step to another, however, the solution is in practice found more quickly, and only a minor increase in computation time is gained when changing the maximum time step from 0.01 to 0.005 s.

A mesh configuration with 128 elements in the x-direction and 8 elements in the y-direction is therefore used in the channels. Due to the relatively small increase in computation time, the smaller maximum time step of 0.005 s is used in the simulations since the higher temporal resolution makes convergence easier for the solver when simulating irregular geometries.

Since the temperature is proportional to the thermal energy, the numerical errors in calculated temperatures, relative to T_{init}, in the model can, in the worst case, be expected to be on the same order of magnitude as the errors in the thermal energy. The single blow effectiveness is calculated as the ratio of two thermal energies, and the numerical error in effectiveness is therefore also be expected to be within this order of magnitude.

5.3.3 Multiple Channel Validation

The above validation of the model has been performed using a model with one half channel and one half plate. In order to ensure that no errors are introduced when expanding the model to multiple plates and channels, the results from the half-channel model are compared to the results from a uniform 10-channel model.

Figure 5.7 shows the single blow effectiveness of the two models as a function of utilization. Since the volume of the 10-channel model is 20 times larger than

x-elements	y-elements	time step	ΔE
384	16	Free	12 %
384	16	0.01	1.0 %
128	8	0.01	1.5 %
128	8	0.005	1.5 %

Table 5.1: Validation of mesh configurations and time steps. Free time step means that no maximum time step is defined.

the half-channel model, the heat transfer rates are scaled differently, but the effectivenesses are exactly equal. This confirms that the heat transfer in each half channel/half plate cell is the same in both models.

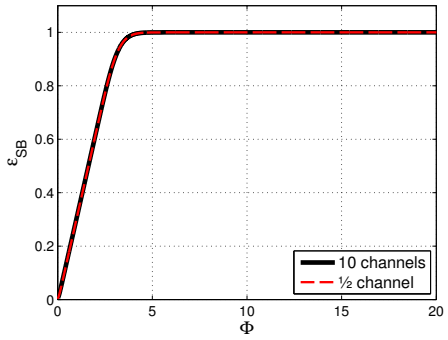

Figure 5.7: Single-blow effectiveness as a function of utilization for a simulation using the half-channel model compared with an equivalent simulation using the 10-channel model.

5.3.4 Number of Elements in Plates

Since non-uniform distributions of plate spacings are being modeled, the single-channel model cannot estimate the expected temperature gradients in the plates adequately. Therefore a regenerator with a highly irregular distribution has been modeled in order to estimate the highest temperature gradient that can be expected in the model.

The modeled channel distribution consists of 10 channels of two different widths. The lower 5 channels have a width of 0.8 mm and the upper 5 channels have a width of 1.2 mm. This gives a relative standard deviation, s_N, of 21 %, but in a highly irregular configuration.

This geometry has been simulated with 128 by 8 and with 128 by 1 elements in each plate. The channels have 128 by 8 elements and the time step is 0.005 s.

The simulation with 8 elements in the y-direction in the plates gives a ΔE value of 1.1 % and the simulation where only one element is used in the y-direction in the plates gives a ΔE of 2.7 %. This indicates that there is some reduction in the accuracy due to decreasing the number of elements in the plates, but the error remains within acceptable levels. In should here be noted that, unlike finite difference modeling, energy conservation is not a part of the formulation of the finite element method. Deviations in the overall energy balance are therefore typically a few percent in finite element models, which is far more than is typically seen in finite difference models.

At the beginning of the simulation, the temperature profile at the inlet is discontinuous, and there is therefore a large temperature gradient at the first column of nodes at the first few time steps. Except at the first two rows of elements during the first 1.4 s, however, the temperature variation within a

plate at any given x-position is at most 0.18 K at all times. Since only a small fraction of the heat transfer takes place close to the inlet during the first 1.4 s, the temperature variations in the plates are considered to be insignificant in comparison with the difference between the plates and channels and the temperature gradients in the channels. When using a single element across the width of the plates, the temperature is being calculated at each surface, but the temperature profiles inside the plates are being interpolated based only on the surface temperatures.

5.3.5 Comparison of Nusselt Numbers

The above validations are all evaluated on the degree of energy conservation observed for a given simulation. In order to verify that the model gives the correct solution for a known case, the Nusselt number has been calculated for a simulation of a uniform regenerator with constant plate temperature and compared to a known value.

The accepted value of the Nusselt number for hydrodynamically fully developed flow between parallel plates of constant temperature is 7.54 [26]. When running the model with a uniform geometry and constant plate temperature, a Nusselt number of 7.64 is found by calculating the convective heat transfer coefficient for the temperature distribution. This value is within 1.4 % of the actual value. Other finite element models of heat transfer in ducts report errors in the range 0.5 - 3.6 % under various conditions [84–86].

5.4 Non-Dimensionalization of Parameters

The number of dependent variables in the system can be reduced by introducing a new set of non-dimensional parameters which are combinations of the existing parameters in the system. This method is often used for decreasing the complexity of problems or to scale experiments and models. Here, it will be used to reduce the number of independent variables that the heat transfer in the system depend on and to generalize the results obtained with the model.

In order to evaluate the performance of a modeled regenerator, the single blow effectiveness, as defined in Section 1.2.3, is used. This is given by

$$\varepsilon_{\mathrm{SB}}(t = t_1) = \frac{q_t(t = t_1)}{q_t(t \to \infty)} \tag{5.25}$$

where

$$q_t(t = t_1) = \int_0^{t_1} \dot{q}_{\mathrm{t}}(t)\mathrm{d}t \tag{5.26}$$

and

Input parameter	Unit	Nominal value
ρ_f	kg/m^3	1000
c_f	J/(kg K)	4200
k_f	W/(m K)	0.6
ρ_s	kg/m^3	7900
c_s	J/(kg K)	240
k_s	W/(m K)	10
u_m	m/s	0.005
$\bar{w}$	m	0.001
w_pl	m	0.001
s_N	m	0.0002
L	m	0.10
T_in	K	273.15
T_init	K	277.15

Table 5.2: Input variables for the model and their nominal values.

$$q_t(t \to \infty) = \int_0^\infty \dot{q}_\mathrm{t}(t)\mathrm{d}t = \rho_\mathrm{s} c_\mathrm{s} V_\mathrm{s}(T_\mathrm{init} - T_\mathrm{in}). \tag{5.27}$$

The effectiveness, however, will be given as a function of utilization, Φ, instead of time.

In order to calculate a solution for a given regenerator system, the model takes the 13 parameters listed in Table 5.2 as input parameters. Based on these input parameters, the solution, and thereby $\varepsilon(\Phi)$ is calculated for the given regenerator.

The initial and inlet temperatures are given the values 273.15 K and 277.15 K, respectively, in all the simulations presented in this thesis. This corresponds to a temperature difference, ΔT, of 4 K. However, since $q(t)$ depends linearly on the temperature difference the way it is defined in Equations 5.26 and 5.27, and because the fluid and solid properties are temperature independent, the function $\varepsilon(\Phi)$ is independent of the temperatures. The difference in single-blow effectiveness between a given regenerator and its corresponding uniform regenerator, $\Delta\varepsilon_\mathrm{SB}(\Phi) = \varepsilon_\mathrm{SB,uni}(\Phi) - \varepsilon_\mathrm{SB}(\Phi)$ will be the same, regardless of the values of ΔT, T_init, and T_in.

This has been validated by running a number of simulations with different combinations of initial and inlet temperatures, which yield exactly the same result in terms of regenerator effectiveness. The tested temperature combinations are shown in Table 5.3, and the resulting effectivenesses are shown as a function of utilization in Figure 5.8

Furthermore, since the density and the specific heat capacity of the materials always appear as the product ρc, we can reduce the four parameters ρ_s, ρ_f, c_s, and c_f to two parameters containing the products $\rho_\mathrm{s} c_\mathrm{s}$ and $\rho_\mathrm{f} c_\mathrm{f}$. For this, the thermal diffusivities of the solid and fluid, respectively, α_s and α_f have been chosen, where

Combination	T_{init} [K]	T_{in} [K]
1	277.15	273.15
2	273.15	277.15
3	1000	900
4	5	1
5	51	50

Table 5.3: Temperature combinations used for validation.

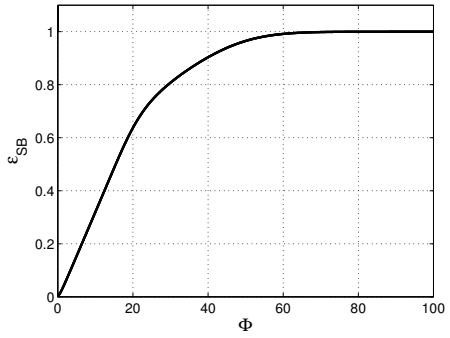

Figure 5.8: Single-blow effectiveness as a function of utilization for regenerators with different combinations of initial and inlet temperatures. All temperature combinations give identical effectiveness curves.

$$\alpha_{\text{f}} = \frac{k_{\text{f}}}{\rho_{\text{f}} c_{\text{f}}} \tag{5.28}$$

and

$$\alpha_{\text{s}} = \frac{k_{\text{s}}}{\rho_{\text{s}} c_{\text{s}}} \tag{5.29}$$

The number of independent input parameters is therefore reduced to 10, including the utilization:

$$\varepsilon_{\text{SB}} = f(\Phi, \alpha_{\text{f}}, \alpha_{\text{s}}, k_{\text{f}}, k_{\text{s}}, u_{\text{m}}, \bar{w}, w_{\text{pl}}, s_N, L) \tag{5.30}$$

The Buckingham Π-theorem states that a physical process involving n variables can be reduced to a relation between $v = n - r$ dimensionless variables, where r is the rank of the dimensional matrix [27]. This does not necessarily mean that the number of independent variables is exactly v since more than r of the dimensional variables can be coupled, but we can reduce the number of dependent variables by at least r. It is, however, impossible to conclusively determine if the number of dependent variables can be reduced further.

The dimensional matrix for the system can be written as:

$$\begin{array}{cccc} \hat{l} & \hat{t} & \hat{m} & \hat{T} \\ \left[\begin{array}{cccc} 0 & 0 & 0 & 0 \\ 0 & 0 & 0 & 0 \\ 2 & -1 & 0 & 0 \\ 2 & -1 & 0 & 0 \\ 1 & -3 & 1 & -1 \\ 1 & -3 & 1 & -1 \\ 1 & -1 & 0 & 0 \\ 1 & 0 & 0 & 0 \\ 1 & 0 & 0 & 0 \\ 1 & 0 & 0 & 0 \\ 1 & 0 & 0 & 0 \end{array}\right] & \begin{array}{l} \Delta\varepsilon_{\mathrm{SB}} \\ \Phi \\ \alpha_f \\ \alpha_s \\ k_f \\ k_s \\ u_{\mathrm{m}} \\ \bar{w} \\ w_{\mathrm{pl}} \\ s_N \\ L \end{array} \end{array}$$

The dimension of each column is indicated above the matrix, where $\hat{l}$ is length, $\hat{t}$ is time, $\hat{m}$ is mass, and $\hat{T}$ is temperature; and the variable contained in each row is indicated to the right. The rank of this matrix is 3, which means that the effectiveness can be expressed as a function of 7 (dimensionless) parameters.

These parameters must contain all the dimensions $\hat{l}$, $\hat{t}$, $\hat{m}$, and $\hat{T}$ in an orthogonal form. The method described in reference [27] has been used to find a suitable set of dimensionless parameters, and these have then been combined in order to create more appropriate forms of the parameters.

The parameters that have been found using this approach are

$$\begin{aligned} R_\alpha &= \frac{\alpha_f}{\alpha_s} && \text{(Ratio of thermal diffusivities)} \\ R_{\mathrm{k}} &= \frac{k_f}{k_s} && \text{(Ratio of thermal conductivities)} \\ Pe &= \frac{u_m L}{\alpha_f} && \text{(Peclet number)} \\ AR &= \frac{L}{\bar{w}} && \text{(Aspect ratio)} \\ \eta &= \frac{\bar{w}}{w_{pl} + \bar{w}} && \text{(Porosity)} \\ s_N^* &= \frac{s_N}{\bar{w}} && \text{(Relative standard deviation)} \\ \Phi &= \frac{\dot{m}_{\mathrm{f}} c_{\mathrm{f}} t}{m_{\mathrm{s}} c_{\mathrm{s}}} && \text{(Utilization)} \end{aligned}$$

The regenerator effectiveness can thus be represented as a function of these seven parameters, instead of ten as in Equation 5.30

$$\varepsilon_{\mathrm{SB}} = f(R_\alpha, R_{\mathrm{k}}, Pe, AR, \eta, s_N^*, \Phi) \tag{5.31}$$

In order to verify that the solution can be accurately described as a function of these dimensionless parameters, a number of simulations have been run, where the dimensional (input) parameters (in Equation 5.30) are independently varied, but in a manner such that the dimensionless values remain constant.

Since the changes in effectiveness are relatively subtle when plotted as $\varepsilon_{\mathrm{SB}}(\Phi)$, the effectiveness of the corresponding uniform regenerator (a regenerator with the same parameters, except $s_N = 0$) has been subtracted from the results. This gives the decrease in effectiveness due to non-uniformity, $\Delta\varepsilon_{\mathrm{SB}}$.

The found $\Delta\varepsilon_{\mathrm{SB}}(\Phi)$-curves are the solid black lines plotted in Figure 5.9. It can be seen that all the solutions with constant dimensionless parameters are equal, which indicates that the set of dimensionless parameters is complete for the model.

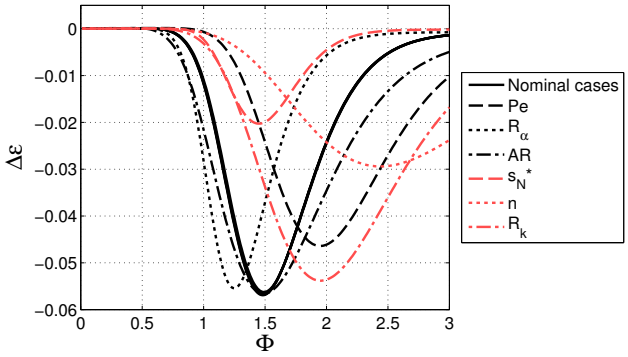

Figure 5.9: Decrease in single-blow effectiveness for variations of both dimensional and dimensionless parameters. The variations of the dimensional parameters are plotted as solid black lines and all overlap. The variations of dimensionless parameters are plotted as non-solid lines. In each variation, the corresponding parameter is set to half its nominal value, and the difference between each curve and the solid black curves correspond to the effect of decreasing the parameter by 50 %.

Furthermore, in order to investigate if any of the dimensionless parameters are redundant, a series of variations of the dimensionless parameters has been simulated as well. The nominal case using the parameters in Table 5.2 has been compared to a series of simulations where the dimensionless parameters one by one are reduced to 50 % of their nominal values. The solutions are overlayed in Figure 5.9 and shows that significant variations in $\Delta\varepsilon_{\mathrm{SB}}$ occur for all variations of the dimensional parameters which indicates that all of the variables in Equation 5.31 are necessary in order to adequately describe the effectiveness. The results also show how variations in the individual parameters can be expected to change the effectiveness of the nominal configuration if all other parameters are being kept constant.

One should be aware that while this reduction of parameters allows us to generalize the results, the basic assumptions used in the model must still be fulfilled in order for the results to be reliable. For example, the model is still only valid in the parameter space where the fluid can be considered incompressible.

In this section, it has been shown that the heat transfer in the modeled regenerators can be expressed as a function of the seven dimensionless parameters that are shown in Equation 5.31. These dimensionless parameters will therefore be used for parameter variations in order to span a greater parameter space for a given number of simulations.

The parameters that have been found not only applies to the model but to regenerators in general as long as the variables shown in Table 5.2 can be assumed to completely describe the heat transfer problem of the regenerator. If the regenerator can be assumed to be uniform, the parameter s_N^* can be disregarded.

Chapter 6

Modeling of Fixed Distributions

6.1 Introduction

In this chapter, a series of regenerators with fixed distributions consisting of channels with only two different channel widths have been simulated. The distributions have been constructed with the same number of channels with identical widths and therefore also the same standard deviation. The order of the channels, however, is varied, which also can affect the heat transfer.

The mean fluid velocity of the flow in a single channel as a function of its width can be found by rearranging Equation 5.12 and using that $u_{\mathrm{m},i} = 2/3\ u_{\mathrm{max},i}$

$$u_{\mathrm{m}} = \frac{\Delta P}{3\mu L} w^2, \tag{6.1}$$

It can be seen that the fluid velocity for a given pressure drop is proportional to the square of the channel width, and since parallel plate regenerators often apply an equal pressure difference to all channels to drive the fluid flow (e.g. by supplying a constant overall flow rate to the channel inlets), even small deviations in channel width can lead to significant deviations in the fluid velocity of a channel.

In a single channel with constant wall temperature, the heat transfer from the walls to the fluid is given by

$$\dot{q}_{\mathrm{t}} = \frac{\dot{m} c_{\mathrm{f}}}{P_{\mathrm{w}}} \left(1 - \exp\left(-\frac{P_{\mathrm{w}} h L}{\dot{m} c_{\mathrm{f}}} \right) \right). \tag{6.2}$$

A lower fluid flow rate gives a smaller heat transfer rate in the channel, which means that the temperature distributions during operation in the regenerator can be expected to become uneven if the channel widths are not equal. This might reduce the overall heat transfer in the regenerators, thus giving reduced regenerator performances.

In order to investigate this effect, a number of different distributions of plate spacings has been simulated using the model described in Chapter 5. In the first part (Section 6.2), a series of distributions which all have the same standard deviation, $s_N = 0.21$ mm are investigated, and the heat transfer in each regenerator is compared to the heat transfer in a corresponding uniform regenerator.

In the second part (Section 6.3), the same distributions, but with different standard deviations are investigated in order to compare equivalent distributions with different degrees of uniformity.

6.2 Constant Channel Width Deviations

6.2.1 Simulations

For the first set of simulations, four different distributions with a constant standard deviation, and a uniform distribution, have been defined. Each distribution, except the uniform, consists of five channels with a width of 0.8 mm (narrow channels) and five channels with a width of 1.2 mm (wide channels), which are distributed according to Table 6.1. The distributions will be referred to as "uniform", "alternating", "2,2", "3,1", and "5,5" in the following. For 10 channels which each have 20 % deviation, the standard deviation, s_N is 0.21.

Distribution	**Std. dev.** [mm]	**Channel widths** [mm]									
Uniform	0	1	1	1	1	1	1	1	1	1	1
Alternating	0.21	0.8	1.2	0.8	1.2	0.8	1.2	0.8	1.2	0.8	1.2
2,2	0.21	0.8	1.2	1.2	0.8	0.8	1.2	1.2	0.8	0.8	1.2
3,1	0.21	0.8	0.8	0.8	1.2	1.2	1.2	0.8	1.2	0.8	1.2
5,5	0.21	0.8	0.8	0.8	0.8	0.8	1.2	1.2	1.2	1.2	1.2

Table 6.1: Fixed distributions used in the simulations. The "channels" column lists the widths of the channels 1-10 from left to right for each of the modeled geometries.

Even though the standard deviation is the same for all the non-uniform distributions, the degree of regularity of the distributions vary because the wide and narrow channels are arranged differently. The velocity in the channels are given by Equation 5.11, and is the same for all channels of the same width. The mean fluid velocities in regenerators with two distinct channel widths, an overall mean fluid velocity of 5 mm/s, and a nominal channel width of 1 mm

are shown in Figure 6.1 as a function of the deviation of the widths from the mean value, Δw.

It can be seen that the fluid velocities depend strongly on the channel distribution, and the heat transfer is therefore also expected to depend on this.

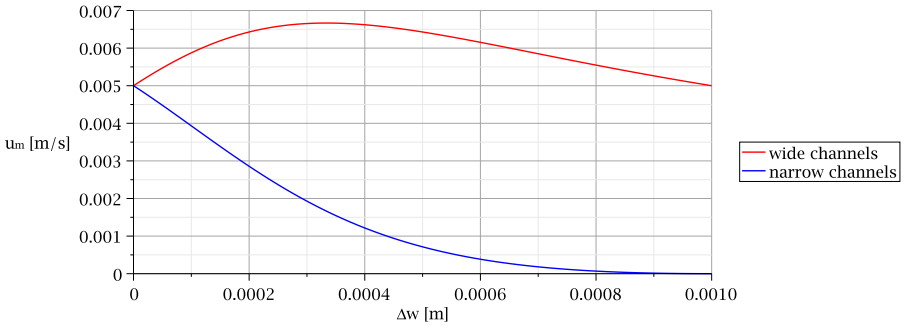

Figure 6.1: Mean fluid velocity in channels of a distribution with two distinct channel widths as a function of the difference between the two widths, Δw. The overall mean fluid velocity is 5 mm/s and the mean channel width is 1 mm.

The distributions in Table 6.1 have been simulated using the dimensions, operating conditions, and simulation parameters shown in Table 6.2, and the material properties of water and gadolinium shown in Table A.1.

Parameter	**Symbol**	**Value**	**Unit**
Geometric dimensions			
Length of regenerator	L	0.1	m
Porosity	η	0.5	-
Mean channel width	$\bar{w}$	$1 \cdot 10^{-3}$	m
Plate width	w_{pl}	$1 \cdot 10^{-3}$	m
Operating conditions			
Initial temperature	T_{init}	277.15	K
Inlet temperature	T_{in}	273.15	K
Total flow rate per unit depth	$\dot{V}'$	$5 \cdot 10^{-5}$	m^2/s
Simulation parameters			
Solution time step		0.1	s
Simulation time		50	s
Max. solver time step		$5 \cdot 10^{-5}$	s

Table 6.2: Values of parameters used in simulations of the fixed regenerator geometries.

6.2.2 Analysis

For each of the modeled distributions, the relative net energy that has been removed from the system, i.e. the integrated axial heat transfer, is plotted in Figure 6.2 as a function of time. The axial heat transfer is defined as the

difference between the heat flux entering the regenerator at the inlet, $\dot{q}_{\mathrm{i}}$, and the heat flux exiting the regenerator at the outlet, $\dot{q}_{\mathrm{o}}$.

The figure shows that the greatest heat transfer occurs in the uniform regenerator, and then in the order: alternating, 2,2, 3,1, 5,5. For $t \to \infty$, the internal energy converges toward zero and the relative removed energy toward one.

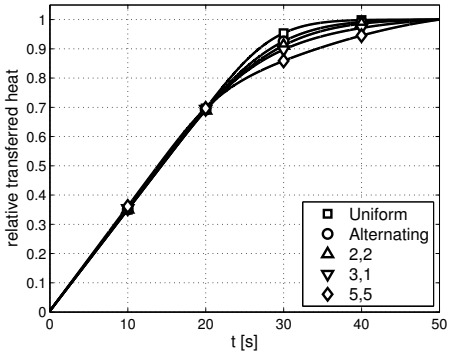

Figure 6.2: Difference in thermal energy entering the regenerator and thermal energy exiting the regenerator as a function of time for each of the modeled regenerators. The thermal energy is normalized such that its value increases form zero to one. Since thermal energy is transferred from the matrix at different rates, the net energy exiting the regenerator also differs for the various regenerators.

The temperature profiles of each of the different geometries at the time where the utilization, $\Phi = 1$ are shown in Figure 6.3. It can be seen that the heat transfer becomes much more uneven as the irregularity of the regenerators increases and increasingly large temperature gradients are observed.

All the regenerator plates in the alternating distribution are equivalent in that all plates are seeing the same surrounding configuration of wide and narrow channels, except for the plates at the edges, which effectively have two identical adjacent channels. This means that, although the heat transfer in the wide and narrow channels differ, all plates have approximately the same heat transfer rate. In the 2,2-distribution, for example, there are 2.5 plates with only narrow adjacent channels, 2.5 plates with only wide adjacent channels, and 5 plates with one of each adjacent channel. In this regenerator, it can be seen that the plates with two wide channels cool down much more quickly than the plates with two narrow channels. In the 5,5-distribution, 4.5 plates have only narrow adjacent channels, 4.5 plates have only wide channels, and only one plate have one of each channel. This means that the maldistribution of fluid flow and heat transfer is even greater.

Figure 6.4 shows the effectiveness of the different regenerators plotted as a function of utilization, and Figure 6.5 shows the difference in effectiveness, relative to the uniform distribution, as a function of utilization.

The difference between the effectiveness, plotted in Figure 6.4, and the relative axial heat transfer, plotted in Figure 6.2, is simply that the effectiveness is

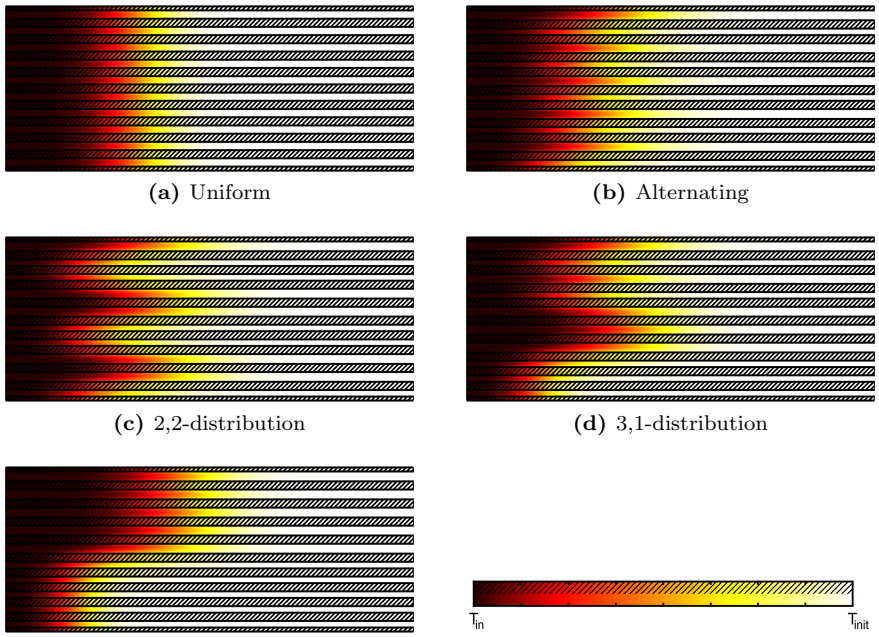

(a) Uniform **(b)** Alternating

(c) 2,2-distribution **(d)** 3,1-distribution

(e) 5,5-distribution

Figure 6.3: Temperature profiles in each of the modeled regenerators at a utilization of one. The heat transfer rate depends on the channel width and irregular geometries will give a lower overall heat transfer. The shaded areas are plates and the non-shaded areas are channels. The geometries are not to scale.

based on the heat transfer between the matrix and the fluid whereas the axial heat transfer is based on the difference between the heat fluxes at the inlets and outlets. From these figures, it can be seen that the more plates there are with only one kind of adjacent channel, the more the effectiveness of the regenerator decreases.

In the beginning of the simulations, at utilizations $\Phi \lesssim 0.25$, the cold fluid is just starting to enter through the inlets, and the heat transfer is thus not affected by neighboring channels. Therefore, the effectiveness in this range is the same for all the regenerators with the channel width deviation of 0.2 mm, but higher for the uniform distribution. For the modeled regenerators, a utilization of 0.25 corresponds to 2.25 s, during which the fluid travels 11 mm.

At utilizations of $0.25 \lesssim \Phi \lesssim 0.5$, the neighboring channels starts to affect the effectiveness, but the "second order" effects of channels further away have still not set in. This happens at $\Phi \approx 0.5$, after 4.5 s, where the effectiveness of the 2,2 and 3,1-distributions starts to split up, and shortly thereafter, the heat transfer reaches a temporary semi steady-state where the difference in effectiveness, $\Delta\varepsilon_{\mathrm{SB}}$, is increasing linearly. At this point, the plates are almost entirely cooled at the inlets and still at $T = T_{\mathrm{init}}$ at the outlets, so the fluid temperatures at the inlets and outlets are constant. A thermal front is moving through the regenerator and progressively cools the plates at increasing x-

positions as time (and utilization) progresses. Since the temperature gradient is greatest near this front, most of the heat transfer occurs in this region. The heat transfer conditions do not change during the interval $0.5 \lesssim \Phi \lesssim 1.6$ because the thermal front is not disturbed in this interval. The rate of reduction in effectiveness is therefore constant due to the rate of heat transfer being constant.

At $\Phi > 1.6$, the temperature fronts in the wide channels reaches the outlets and the heat transfer in the wide channels starts to decrease, since almost all the thermal energy in the plates next to these channels has been removed. The difference in effectiveness continues to increase until a point, where the region of high heat transfer (i.e. the region trailing the thermal front) in the wide channels has exited through the outlets. This occurs at $\Phi \approx 3.5$. At this point, the thermal energy still remaining in the regenerator will mainly be removed by the narrow channels, and since the regenerators with low effectiveness have larger temperature gradients at this point, the rate of change of the effectiveness reverses, and for $\Phi \to \infty$ all regenerators approach an effectiveness of 1.

In practice, however, regenerators of this type have their optimal operating conditions at utilizations in the range $0.2 \lesssim \Phi \lesssim 1$ [68], so for practical applications $\Delta\varepsilon_{\mathrm{SB}}$ can be expected to increase with increasing Φ.

Figure 6.6 shows the temperature profiles along the center of each channel at $\Phi = 1$ for each of the five fixed distributions. As expected, it can be seen that all the channels have the same temperature in the uniform case.

In the alternating regenerator, however, the temperature profiles differ due to the different channel widths. The channel with the lowest temperature, and therefore with the highest heat transfer, is channel number 10. Since the boundary mirrors the geometry, the first channel on the other side of the boundary (which is not modeled), is a wide channel, making channel 10 the only wide channel with a wide neighbor. The heat transfer in this channel is

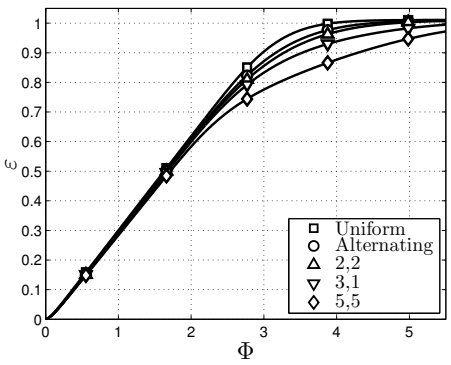

Figure 6.4: Single-blow effectiveness of modeled regenerators as a function of utilization. The difference between this plot and the plot shown in Figure 6.2 is that this is the matrix-to-fluid heat transfer, whereas the plot in Figure 6.2 shows the inlet-to-outlet heat transfer.

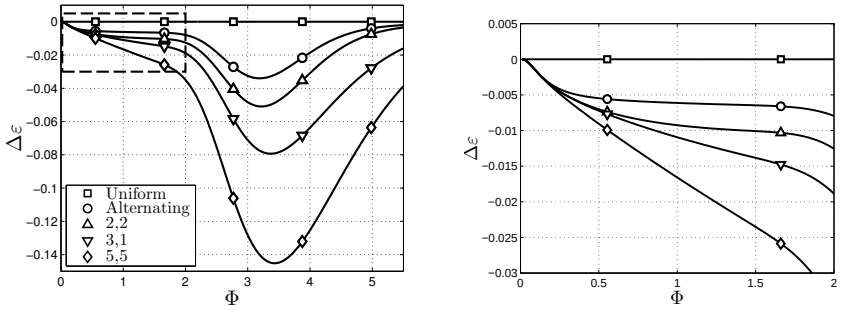

Figure 6.5: Decrease in single-blow effectiveness of regenerators due to non-uniformity as a function of utilization. The right figure is a cut-out showing the area of the dashed line in the left figure.

therefore enhanced compared to the other channels and the heat transfer is increased, which means that the temperature in this channel is lowest.

Likewise, channel 1 is the only narrow channel with a narrow neighbor, which gives this channel a lower heat transfer than the other narrow channels, and it is therefore warmer than the other channels.

The remaining wide channels are almost the same temperature, but due to the "second-order" effects, there are some differences in these channels, too. The coldest of these channels is the channel closest to channel 10 (i.e. channel 8). Since channel 10 is colder than the rest of the channels, this will cause a higher heat transfer (through channel 9) and thus decrease the temperature of this channel. For the same reason, channel 9 is the coldest of the narrow channels. Due to the hot/cold symmetry of the system, the same mechanisms that increase the heat transfer when wide channels are close together, decrease the heat transfer when narrow channels are close together. This means that the hottest narrow channel is channel 3 (because it is close to the hot channel 1) and the hottest wide channel is channel 2 (also because it is close to channel 1). Naturally, the effect of the temperature of a given channel on the heat transfer in another channel decreases with the distance and the number of channels in between. The channels 4 and 6 (wide channels) and 5 and 7 (narrow channels) are therefore almost (pairwise) identical since the channels affecting the heat transfer are at least two channels away.

In the 2,2-distribution, the boundary symmetry is preserved, which means that all narrow and wide channels are equivalent. The temperature profiles are therefore identical in all channels with the same width, as shown in Figure 6.6c.

The 3,1-distribution is symmetrically complicated since all the channels have completely different surroundings. The three first channels (1, 2, and 3) are part of a lump of effectively six narrow channels. There is therefore almost no cross-talk in the first channel, and only little for the second channel, and the temperatures of these channels are therefore high. The next three channels (4, 5, and 6) are all wide and are therefore cold. The temperature difference

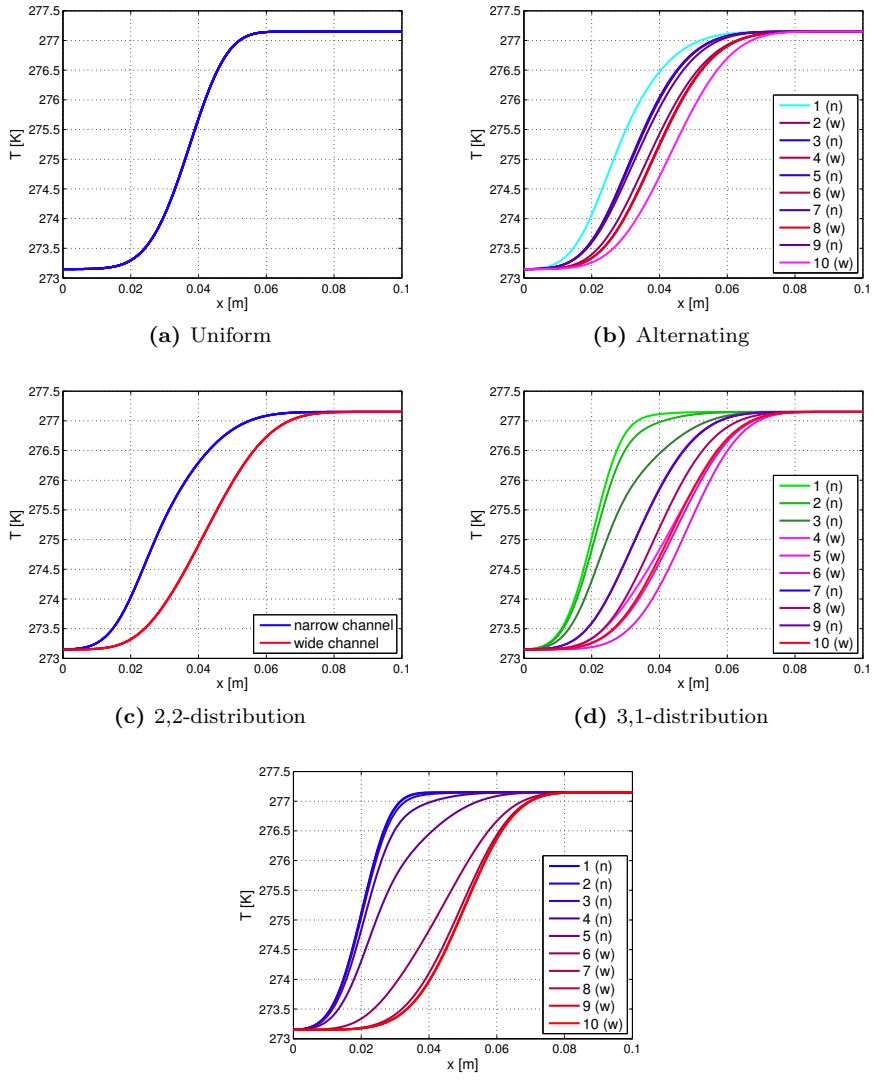

(a) Uniform

(b) Alternating

(c) 2,2-distribution

(d) 3,1-distribution

(e) 5,5-distribution

Figure 6.6: Temperature profiles in the center of each channel at $\Phi = 1$ as a function of x. The legends show the channel numbers, starting at the bottom, and indicates the width of each channel.

between the first group and the second group, however, is large, which gives a lot of cross-talk, thus evening out the difference between channels 3 and 4. The last channel, channel 10, is part of a group of two wide channels and far away from the narrow group, which also gives this channel a low temperature.

In the 5,5-distribution, we see an increasing amount of cross-talk as the distance to the different-width group of channels decreases. The coldest channels are therefore the channels in the top of the regenerator (high channel numbers) and the hottest channels are the channels in the bottom (low channel numbers).

6.2.3 Capacity Ratio

In order to describe the neighboring relationships of the channels in a given regenerator, we can use the capacity ratio. The capacity ratio, is a number for a plate, similar to the utilization, which describes the ratio of the thermal mass of the plate to the average thermal mass of the fluid in the two adjacent channels. The capacity ratio is given by

$$C_{\mathrm{R}} = \frac{m_{\mathrm{s}} c_{\mathrm{s}} t^{-1}}{(\dot{m}_1 + \dot{m}_2) c_{\mathrm{f}}/2}, \tag{6.3}$$

where $\dot{m}_1$ and $\dot{m}_2$ are the mass flow rates in the two channels. By using this number, the flow in both neighboring channels is considered for each plate. Table 6.3 shows the capacity ratios for the plate/channel-configurations that occur in these distributions.

Adjacent channels	**Capacity ratio**
Uniform/uniform	$9.03/t$
Narrow/narrow	$19.8/t$
Wide/narrow	$9.03/t$
Wide/wide	$5.85/t$

Table 6.3: Capacity ratios for all the possible plate/channel-configurations in the fixed distributions.

The more regular distributions will have fewer extreme values of the capacity ratio, and therefore a lower standard deviation of capacity ratios, $s_{\mathrm{N}}(C_{\mathrm{R}}t)$.

The maximum decrease in regenerator effectiveness is plotted as a function of the standard deviation of the capacity ratio multiplied by time in Figure 6.7. It can be seen that the maximum decrease in effectiveness increases approximately exponentially with the standard deviation of the capacity ratio. The results are fitted to an exponential function, which serves as a guide for the eye.

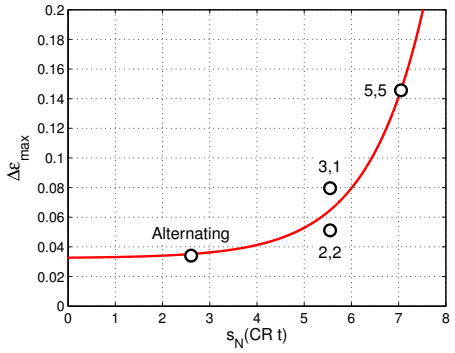

Figure 6.7: Maximum decrease in effectiveness of the fixed distributions as a function of the standard deviation of the capacity ratio.

However, the 2,2 and the 3,1-distributions both have the same number of plates with each configuration of adjacent channels and thereby the same $s_N(C_\mathrm{R}t)$, but still differ slightly in effectiveness. This indicates that it is not sufficient to only consider the directly adjacent channels, but that the distribution as a whole determines overall heat transfer in the regenerator.

The regenerator studied in [57] is in some respects similar to the 5,5-distribution simulated here, in that it consists of a part with only wide channels and a part with only narrow channels. The model in [57] has more channels, but is also divided into multiple stages and uses an expanding gas as heat transfer fluid, which makes it not directly comparable to the current model. The maximum reduction in performance observed in this model, however, is approximately 20 % in a regenerator with 20 % standard deviation of the channel widths. This decrease is close to the maximum decrease of 15 % observed for the 5,5-distribution in the current simulations.

6.3 Varying Channel Width Deviations

The deviation in the channel width in the simulations above is 0.2 mm. Another series of simulations has been performed of regenerators with the same distributions, but with deviations of 0.1, 0.2, 0.3 and 0.4 mm. The decrease in effectiveness for these simulations is shown in Figure 6.8 as a function of utilization.

Not surprisingly, it can be seen that the higher the deviation is, the larger the decrease in effectiveness is. It can, however, also be seen that the effect of changing the distribution from “alternating” to “5,5” has the same order of magnitude as changing the deviation in the channel widths by 0.1 - 0.2 mm.

Figure 6.9 shows the maximum decrease in effectiveness, $\Delta\varepsilon_\mathrm{p}$, as a function of the standard deviation of the capacity ratio multiplied by time.

It can be seen that the behavior of $\Delta\varepsilon_\mathrm{p}$ changes when the deviation in channel width is changed. The 2,2-distributions, for example, approximately exhibits the same effectiveness as the alternating distributions with 0.1 mm larger Δw.

The sum of the capacity ratios of all the plates in a given distribution varies for the different distributions. Generally the increase in capacity ratio for a wide channel is greater than the decrease in capacity ratio for a narrow channel, which means that the total capacity ratio is greater for more irregular distributions. The peak effectiveness loss is shown as a function of the sum of capacity ratios in each regenerator distribution in Figure 6.10.

There is a large spread in the values, but the plot clearly shows a tendency of the effectiveness decreasing when the total capacity ratio increases.

However, it can be seen that the behavior of $\Delta\varepsilon_\mathrm{p}$ is similar for varying $\sum C_\mathrm{R}t$ and for varying $s_N(C_\mathrm{R}t)$. The distributions with large $\sum C_\mathrm{R}t$ also have large standard deviations because the plates with narrow/narrow adjacent channels

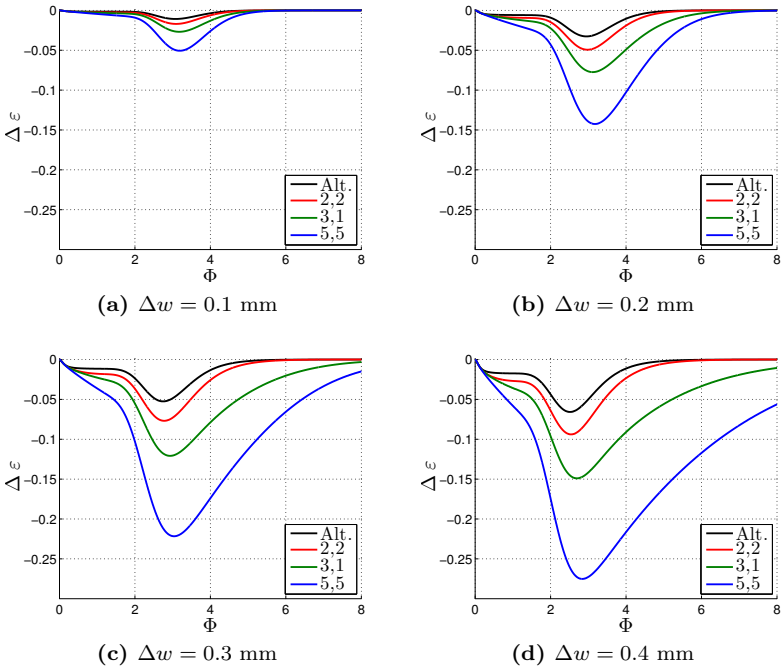

(a) $\Delta w = 0.1$ mm **(b)** $\Delta w = 0.2$ mm

(c) $\Delta w = 0.3$ mm **(d)** $\Delta w = 0.4$ mm

Figure 6.8: Decrease in effectiveness as a function of utilization for the four different fixed distributions with channel width deviations of (a) 0.1 mm, (b) 0.2 mm, (c) 0.3 mm, and (d) 0.4 mm.

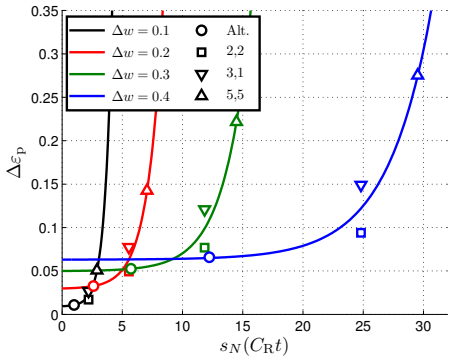

Figure 6.9: Peak effectiveness decrease for fixed distributions with various width deviations as a function of the standard deviation of the capacity ratio.

add more the the overall capacity ratio, compared to the uniform case, than the plates with wide/wide adjacent channels subtract.

The results presented in this section shows that the effectiveness loss in a non-uniform regenerator cannot adequately be described by only the standard deviation of the distribution of plate spacings. The deviations in capacity ratio have been shown to have an equal influence on the effectiveness. The distributions investigated in this chapter, however, are unlikely to be encountered

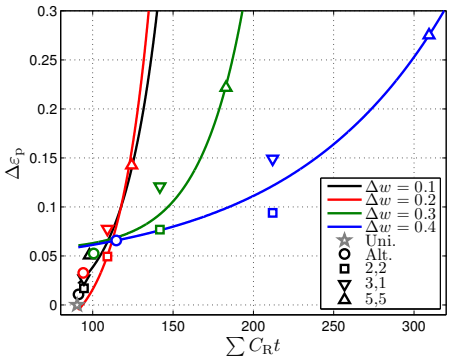

Figure 6.10: Peak effectiveness decrease for fixed distributions with various width deviations as a function of overall capacity ratio, i.e. the sum of capacity ratios in the regenerator.

in real regenerators. In the next chapter regenerators with more plausible distributions are therefore investigated.

Chapter 7

Modeling of Normal Distributions

7.1 Introduction

When constructing parallel-plate regenerators, errors in the intended channel width distributions are inadvertently introduced during the fabrication process. The regenerator geometries investigated in the previous section are all systematic distributions, which have been defined in order to study the effects of different channel widths on the heat transfer in the regenerators. These distributions, however, are unlikely to be encountered in real regenerators. In this chapter, the heat transfer is therefore investigated in a number of regenerators with geometries that are randomly generated from a probability distribution.

The actual probability distribution of the plate spacings in real-life regenerators and the magnitude of the fabrication errors depend on several factors, such as the fabrication technique, the procedure used, and the regenerator materials. In the current investigations, the plate spacings are assumed to follow a normal distribution, which is a good approximation for machined parts [87].

A number of regenerators have been fabricated for use in the experiments described in Chapters 4, 8 and 9. The plate spacings of these regenerators have been measured, and it has been found that the standard deviations introduced by the regenerator fabrication and assembly ranges from 2 % to 26 % of the mean channel width. In the simulations presented in this chapter, regenerators with standard deviations in the range 0 % to 20 % have been investigated. The deviations of the fixed distributions are all 0.2 mm which corresponds to a relative standard deviation of 21 % of the mean width.

In the first part of the investigations (Section 7.2), a series of regenerators with the same basic geometry as the fixed distributions described in the previous chapter, have been modeled. In these simulations, however, the plate spacings follow normal distributions with various standard deviations.

In the second part (Section 7.3), the same simulations are run, but for regenerators with varying geometrical parameters. The relative standard deviation, the aspect ratio, and the porosity of the regenerators are varied, and it is investigated, how the effectiveness is affected by these variations.

7.2 Distributions with Nominal Parameters

In this part, a regenerator with the same parameters as listed in Table A.1 has been simulated. In this series of simulations, however, the plate spacings follow normal distributions with standard deviations of 0 %, 5 %, 10 %, 15 %, or 20 % of the mean value.

The normal distributions are randomly generated and the results therefore vary from one simulation to another. In order to get consistent results, each standard deviation has been run with 20 different, randomly generated, distributions, which gives reliable average values.

The normal distribution is given by the probability density function

$$p(w) = \frac{1}{\sqrt{2\pi}s_N} \exp\left(-\frac{(w-\bar{w})^2}{2s_N^2}\right), \tag{7.1}$$

which is the probability that the channel width of a given channel has the value w, given the mean value $\bar{w}$ and the standard deviation s_N. The probability density of an arbitrary normal distribution with a mean value $\bar{w}$ and a standard deviation s_N is plotted in Figure 7.1. When generating a distribution, the width of a channel can in principle take any value $-\infty < w < \infty$, but the probability is greatest that the value is close to $\bar{w}$. How much the curve spreads out from the mean value is defined by the standard deviation: approximately 68 % of the plate spacings will be in the range $(\bar{w}-s_N) < w < (\bar{w}+s_N)$ and approximately 95 % in the range $(\bar{w}-2s_N) < w < (\bar{w}+2s_N)$.

The random distributions are generated using a pseudo-random number generator, which is built-in to the program Matlab [88]. In order to ensure appropriate variation in the distributions, a time stamp is used as seed. Each random distribution is given by a set of N pseudo-random numbers generated by Matlab using the Mersenne Twister random number generator [89] to generate a random number and then the ziggurat method [90] for transforming it into a normal distribution.

Each distribution generated in this way has a mean value of zero and a standard deviation of one. In order to transform these distributions into distributions with the desired means and standard deviations, the following transformation is used:

$$\mathbf{w} = \bar{w} + s_N \cdot \mathbf{R}_\mathrm{N}, \tag{7.2}$$

where $\mathbf{w}$ is a vector of length N, which contains the channel widths (i.e. the channel width distribution) and $\mathbf{R}_\mathrm{N}$ is the generated list of random numbers from the standard normal distribution.

Since there are no restrictions on the values that can be generated using this method, there is a possibility that the generated list of random numbers contain negative values, which will give negative plate spacings. For obvious reasons, regenerators with negative channel widths cannot be simulated in the model and distributions containing negative values are automatically discarded and a new distribution is generated. For the distributions used here, however, this happens very rarely. For a regenerator with a 20 % standard deviation, only one of every 3×10^7 channels will have a negative value, so this systematic discarding of selected distributions is not expected to affect the results significantly.

At 40 % standard deviaitons, however, approximately 6 % of the generated regenerator distributions will contain negative values, and at this point, the actual distribution of the generated channel widths may become skewed. For large standard deviations, it should therefore be considered to use a type of distribution which excludes negative numbers (e.g. a log-normal distribution).

Figure 7.2 shows the observed decreases in the regenerator effectiveness as a function of utilization for 20 distributions for each of the relative standard deviations: 5 %, 10 %, 15 %, and 20 %. The dashed bands show the standard errors of $\Delta\varepsilon_\mathrm{SB}$, which correspond to the standard deviations of the mean values (the solid line), i.e. $s_N(\Delta\bar{\varepsilon}_\mathrm{SB})$, which is a measure of the variation in the estimated mean of the calculated effectiveness due to the randomness of the generated distributions, and should not be confused by the standard deviation of the channel width distribution ($s_N(\mathbf{w}) = s_N$).

As expected, it can be seen that the effectiveness decreases when the standard deviation increases. The progress of the curves is similar to the fixed

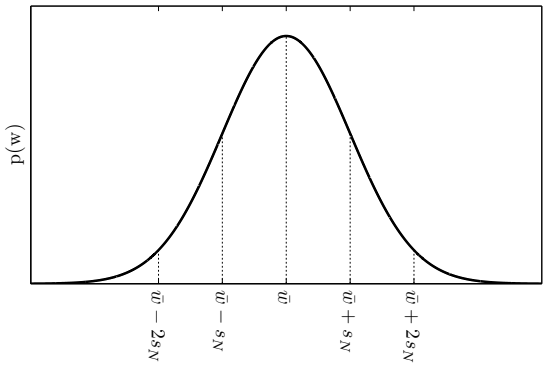

Figure 7.1: Probability density of normal distribution. 68 % of the generated points lie within $\pm s_N$ of the mean and 95 % within $\pm 2s_N$.

distributions, which indicates that the temperature fronts behave in a similar manner.

The curves, however, start splitting up instantly at the beginning, where the fixed distributions would only split up after $\Phi = 0.2$ - 0.5. The only mechanism that caused the fixed distributions to differ, however, was the thermal cross-talk, i.e. the heat transfer between channels during the process. Depending on the width and thermal properties of the plates, it takes some time for the cross-talk to have an effect on the heat transfer. The normal distributions, however, have different channel widths and different standard deviations, and the effectiveness will therefore vary, even if there was no heat transfer between the channels. The variations due to the neighboring relationships of the channels (the cross-talk) then further alter the overall effectiveness of the regenerator.

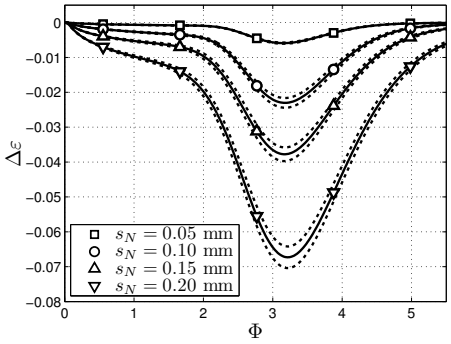

Figure 7.2: Decrease in effectiveness of normal distributions as a function of utilization for various relative standard deviations.

It can be seen that there are significant deviations in the effectiveness of distributions with the same standard deviation. This is partly due to the randomness of the distributions. While some distributions might have a few very wide channels and many channels only slightly narrower than the mean, others can have a few very narrow channels and many slightly wider than average channels, while both distributions still can be normal. Furthermore, as it was found for the fixed distributions, the combination of neighboring channels can have a significant effect on the heat transfer rates.

Since the distributions are randomly generated, there is a wide variety in the combinations of channel widths in the individual distributions, even for distributions with the same standard deviations. In some distributions there will be a few very wide channels and many channels that are only slightly narrower than the mean, and in others all channels will deviate moderately from the mean.

It is a possibility that extreme channel widths affect the effectiveness so much that the effects of the channels closer to the mean are completely overshadowed. In this case, the extreme $\Delta\varepsilon$-curves (the ones that deviate a lot from the mean) should be the ones with the most extreme channel widths. In order to determine if this is the case, some of the distributions with 20 % standard deviations have been plotted in Figure 7.3. The distributions with 20 % stan-

dard deviations have been chosen because they give the greatest variations in effectiveness ($s_N(\bar{\Delta\varepsilon})$). The distributions have been sorted with respect to their effectiveness, and out of the 20 distributions, five have been plotted: the one with the lowest effectiveness (number 1), as well as the ones with the fifth lowest (number 5), tenth lowest (number 10), fifteenth lowest (number 15), and twentieth lowest (number 20, i.e. the one with the highest), effectivenesses. In order to be able to compare the number of extreme widths, the channels have been sorted in order of increasing width.

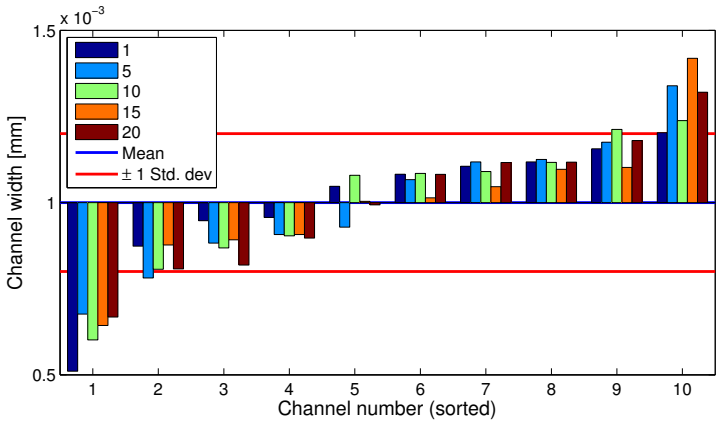

Figure 7.3: Widths of channels of regenerators with 20 % standard deviations by performance. "1" is the regenerator with the lowest effectiveness and "20" is the regenerator with the highest effectiveness. The channel widths are sorted for comparison.

There is no indication that the distributions with the highest or lowest effectiveness have more extreme channel widths, which indicate that the variations in effectiveness for regenerators with identical standard deviations either is due to the overall distributions, or due to particular patterns or combinations in the distributions.

In order to examine the effect of cross-talk, the distributions with the highest and lowest effectiveness have been plotted in Figure 7.4a and 7.4b, respectively. If cross-talk alone causes the variations in effectiveness, we should observe that the decreases in effectiveness that are caused by particularly narrow channels are countered by wider-than-average neighboring channels in regenerators with high effectiveness and are not countered in regenerators with low effectiveness.

In Figure 7.4b, which shows the regenerator with the lowest effectiveness of the 20 % regenerators, it can be seen that the four top channels (channels seven through ten) have widths below average, and that two of them almost are one full standard deviation smaller than the average width. Due to the boundary conditions, this effectively means that there are eight adjacent channels with widths below average. At the bottom of the regenerator, the first three channels are wider than average, which corresponds to six adjacent wide channels. In the results for the regenerators with the fixed distributions, it was found that lumping the wide and narrow channels together has a significant effect

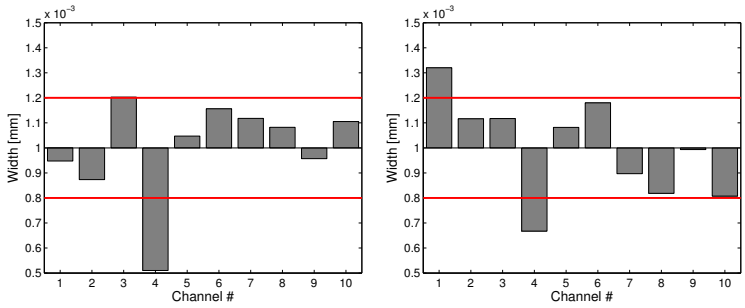

(a) Highest effectiveness **(b)** Lowest effectiveness

Figure 7.4: Channel widths of the 20 % regenerators with the highest and the lowest effectiveness, respecively.

on the effectiveness because it decreases the amount of cross-talk and thus increases the reduction due to non-uniformity. It can be seen that this also has a significant effect in the regenerators with normal distributions.

The regenerator with high effectiveness, shown in Figure 7.4a, has far fewer wide and narrow channels lumped together, which reduces the effect of the non-uniformity and thus gives a high effectiveness.

This indicates that the variations in effectiveness to a large degree are due to the neighboring relationships of the individual channels in the regenerators. This effect is enhanced by the symmetry boundary conditions, and should be reduced if more channels are modeled for the regenerators. More accurate estimates for the mean reduction in effectiveness could be achieved by running more simulations, but in real regenerators, these variations can be expected to occur as well if the distributions of plate spacings deviate from a perfect normal distribution or if the number of channels is low. On the basis of these results, it can thus be expected that the effect of cross-talk is more pronounced in regenerators with a small number of channels as the boundary effects will have more influence on the overall performance. Furthermore, it might be possible to improve the average performance by ensuring that the top and bottom channels have slightly larger widths, but this has not been investigated in further detail.

7.3 Variations of Geometrical Parameters

As described in Section 5.4, the single blow effectiveness of the modeled regenerator systems can be expressed as a function of six different non-dimensional parameters (AR, η, s_N^*, Pe, R_α, and R_k). In this part of the study of normally distributed regenerator channel widths, variations of the geometrical parameters aspect ratio, AR, porosity η, and the relative standard deviation of the channel width distribution, s_N^*, have been investigated in order to determine their effects on the regenerator performance.

7.3.1 Simulations

In this set of simulations, the standard deviation of the channel width has been varied between 0 % and 20 % of the mean channel width, in the same way as in the previous section.

The aspect ratio of parallel-plate regenerators can vary very widely depending on plate width and type of heat transfer fluid. AMRs using gadolinium and water, however, have thermal properties that are very similar to those of the modeled regenerators. AMRs of this type of geometry have been reported to have aspect ratios in the range from 40 to 330 [62, 91–93]. In order to get a sufficient density of data points from the modeling, however, the intermediate range of aspect ratios from 50 to 200 has been modeled using four different values.

AMRs with parallel-plate geometries have been reported to have porosities in the range from 0.23 to 0.52 [62,92–94] and AMRs with porous-bed geometries to have porosities in the range from 0.36 to 0.6 [22,65,66,69]. In reference [68], it is concluded that the optimum porosity for AMRs is around 0.33. In the present simulations, the range of porosities from 0.25 to 0.75 have been modeled, which covers the range of constructed AMR machines.

Each parameter has been modeled with four different, equally spaced values in the aforementioned ranges, which means that the modeled values of the three geometrical parameters are:

$$s_N^* = 0.05, 0.10, 0.15, 0.20, \tag{7.3}$$

$$\eta = 0.25, 0.42, 0.58, 0.75, \tag{7.4}$$

$$AR = 50, 100, 150, 200. \tag{7.5}$$

All combinations of these parameters, 64 in total, have been simulated. Furthermore, since the specific distribution in each simulation is randomly generated, each combination of parameters has been simulated with 20 different distributions (but with the same combination of geometrical parameters). The results in this section thus represent 1280 simulations of 64 parameter variations. The simulated distributions are all generated in the same way as the distributions used in Section 7.2 and the properties of water and gadolinium in Table A.1 have been used.

The input parameters not listed above: the Peclet number and the diffusivity and conductivity ratios, are kept constant at the values shown in Table 7.1, which correspond to the nominal dimensional parameters in Table 6.2.

7.3.2 Results and Discussion

Figure 7.5 shows the variations in single-blow effectiveness as a function of utilization for different porosities, aspect ratios, and relative standard deviations. Figure 7.5a shows the decrease in effectiveness, compared to a uniform

Parameter	Value
R_α	0.027
R_k	0.06
Pe	3500

Table 7.1: Nominal values of the dimensionless parameters that are kept constant.

regenerator, for the regenerators with the lowest porosity, $\eta = 0.25$, and lowest aspect ratio, $AR = 50$, for the four different standard deviations that have been modeled. In this figure, it can be seen that the curves are skewed toward lower utilizations than the utilizations observed in the nominal case in Figure 7.2.

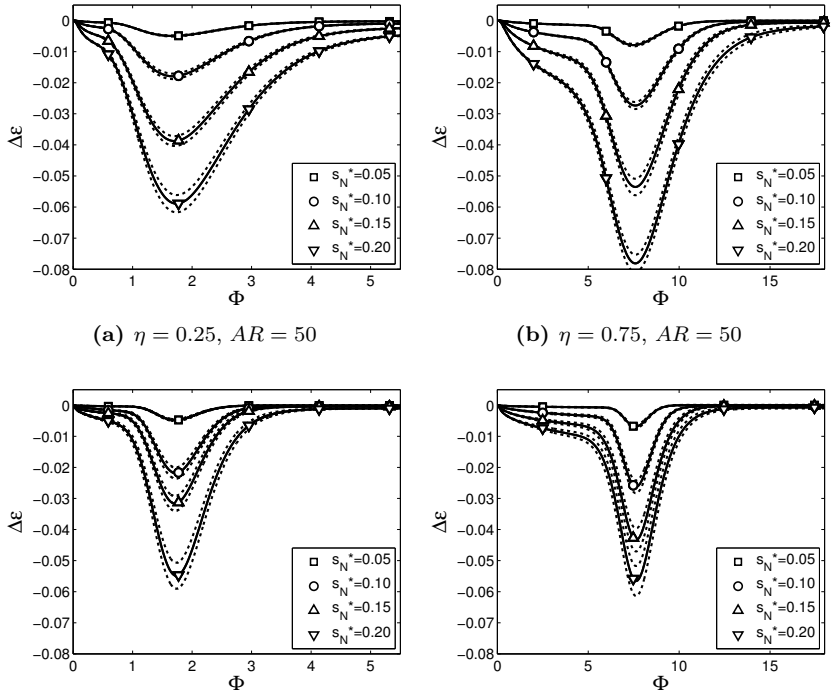

(a) $\eta = 0.25$, $AR = 50$ **(b)** $\eta = 0.75$, $AR = 50$

(c) $\eta = 0.25$, $AR = 200$ **(d)** $\eta = 0.75$, $AR = 200$

Figure 7.5: Decrease in effectiveness for all standard deviations and the highest and lowest modeled values of porosity and aspect ratio.

Figure 7.5b shows the decrease in effectiveness for the regenerators with the highest porosity, $\eta = 0.75$, and the lowest aspect ratio, $AR = 50$. It can be seen that the curves in this case have approximately the same shape, but that they are shifted toward significantly larger utilizations, which indicate that the heat transfer processes are similar, but that they occur, relatively, at greater utilizations (which corresponds to longer time scales) than in the regenerators with low porosity. When the porosity increases, the ratio of fluid volume to

solid volume in the regenerator increases. In the simulations, a constant mass flow rate is used (because the Peclet number is kept constant), so the change in porosity effectively means that the rate of fluid mass flux to solid material, i.e. the utilization, increases. However, since the surface area does not change, the heat flux is not necessarily exactly proportional to the porosity.

Figure 7.5c shows the decrease in effectiveness for the regenerators with the lowest porosity, $\eta = 0.25$, and the highest aspect ratio, $AR = 200$; and Figure 7.5d, the decrease in effectiveness for the regenerators with the highest porosity, $\eta = 0.75$, and the highest aspect ratio, $AR = 200$. It can be seen that the increase in aspect ratio results in slightly more narrow peaks, but with approximately the same peak positions and magnitudes.

In the following, we will use the peak value, $\Delta\varepsilon_\mathrm{p}$ as a measure for the magnitude, the peak position, Φ_p, for the time scale, and the full width at half maximum, $FWHM$, for the peak width.

Table 7.2 shows the average peak positions for the different porosities. Here it can be seen that the peak position increases with the porosity, but also that the deviation in peak position for different values of s_N^* and AR are very low for the same η. This indicates that the peak position, and thereby the time scale of the heat transfer, to some degree depends only on the regenerator porosity and is independent of the aspect ratio and the standard deviation.

η	$\bar{\Phi}_\mathrm{p}$	**std.**	**rel. std.**	$\bar{t}_\mathrm{p}$ [s]
0.25	1.72	0.03	0.02	2.33
0.42	2.55	0.03	0.01	1.59
0.58	4.06	0.04	0.01	1.33
0.75	7.60	0.04	0.00	1.14

Table 7.2: Utilizations where the peak effectiveness occurs for the different porosities that have been modeled. Each utilization corresponds to a certain blow period time, which is listed in the fifth column.

In a regenerator with a geometry where the thermal mass of the fluid is much greater than the thermal mass of the solid, i.e. where $\rho_\mathrm{f} c_\mathrm{f} V_\mathrm{f} \gg \rho_\mathrm{s} c_\mathrm{s} V_\mathrm{s}$, the plates will cool down almost instantaneously when the thermal front of the fluid passes. Neglecting effects of thermal conduction, the peak can thus be expected to occur when $t = L/u_\mathrm{m}$ - at a fluid displacement of 100 % of the regenerator length.

If the ratio $(\rho_\mathrm{f} c_\mathrm{f} V_\mathrm{f})/(\rho_\mathrm{s} c_\mathrm{s} V_\mathrm{s})$ is not infinite, however, the fluid will heat up as it moves through the regenerator, which slows the progression of the thermal front along the length of the regenerator. This delay can be expected to be proportional to the ratio of solid thermal mass to fluid thermal mass, i.e. $(\rho_\mathrm{s} c_\mathrm{s} V_\mathrm{s})/(\rho_\mathrm{f} c_\mathrm{f} V_\mathrm{f})$, which means that the peak can be expected to occur at a fluid displacement of $\left(1 + \frac{\rho_\mathrm{f} c_\mathrm{f} V_\mathrm{f}}{\rho_\mathrm{s} c_\mathrm{s} V_\mathrm{s}}\right) \cdot L$. This corresponds to a utilization of

$$\Phi_\mathrm{p} = \frac{\rho_\mathrm{f} c_\mathrm{f} V_\mathrm{f}}{\rho_\mathrm{s} c_\mathrm{s} V_\mathrm{s}} + 1. \tag{7.6}$$

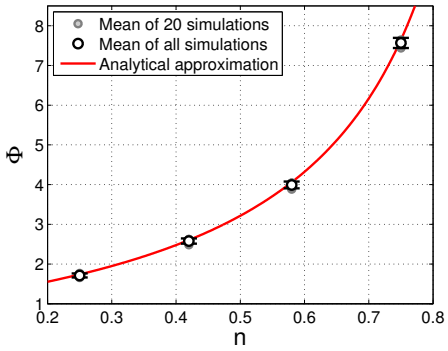

Figure 7.6: Peak position as a function of porosity. The white points are the mean values for all simulations with the given porosity. The gray points are mean values for the 20 simulations with the same combination of porosity, aspect ratio, and relative standard deviation. One gray point is thus plotted for each of these combinations. The error bar indicate the standard deviation of all the simulations with the same porosity (same as the white points).

The peak values calculated by this function are plotted in Figure 7.6 along with the values from the simulations and can be seen to correspond very well. From these results, it can therefore be concluded that the reduction of the effectiveness due to non-uniformity will always increase with the fluid displacement when the fluid displacement is below $\left(1 + \frac{\rho_\mathrm{f} c_\mathrm{f} V_\mathrm{f}}{\rho_\mathrm{s} c_\mathrm{s} V_\mathrm{s}}\right) \cdot L$ and decrease when it is above.

The mean value, and the total and relative standard deviations of the peak magnitude are shown in Table 7.3 for each value of the channel width standard deviation. It can be seen that the magnitude of $\Delta\varepsilon_\mathrm{p}$ increases with the channel width standard deviation, but also that the magnitudes have similar values for all aspect ratios and porosities. The standard deviations of the peak magnitudes are not as small as for the peak positions, but they are still so small as to indicate that the peak magnitude is a strong function of only s_N^* out of the three geometric parameters.

The convective heat transfer in the fluid along the x-direction in a given channel is

s_N^*	$\bar{\Delta\varepsilon}_\mathrm{p}$	**std.**	**rel. std.**
0.05	0.006	0.0012	0.19
0.10	0.021	0.0028	0.13
0.15	0.041	0.0066	0.16
0.20	0.064	0.0076	0.12

Table 7.3: Average magnitude of the peak effectiveness decrease for each relative standard deviation (of the channel width) modeled and corresponding standard deviations.

$$\dot{q}_{\mathrm{conv},i} = \dot{m} c_{\mathrm{f}} T, \tag{7.7}$$

and is thus proportional to the mean fluid velocity in the channel. If we consider the fluid entering the regenerator at the inlet at time $t = 0$, it is, as it reaches the outlet, completely cooled from its inlet temperature, T_{in}, such that it has the same temperature as the plates, i.e. T_{init}. This is not necessarily the case for all regenerators since, if the heat transfer rate between the fluid and solid is not large enough, the fluid may not be completely cooled. In the regenerators simulated in the current work, however, the axial convective heat transfer rate is more limiting, and since this is proportional to the mean fluid velocity, it is therefore assumed that the heat transfer rate between solid and fluid also is proportional to the mean fluid velocity, i.e.

$$\dot{q}_i \propto u_{\mathrm{m},i}. \tag{7.8}$$

Since the pressure drop is equal for all channels in a regenerator, the fluid velocity in the ith channel not only depends on the channel width of that particular channel, but also on the distribution of channel widths in the regenerator.

As shown in Section 5.2, the mean fluid velocity in a given channel is given by

$$u_{\mathrm{m},i} = \frac{w_i^2}{\sum_{j=1}^{N}(w_j^3)} \cdot \dot{V}'. \tag{7.9}$$

The sum in Equation 7.9 can be found from the expectation value of w_i^3, which, for a normal distribution, is given by

$$\langle w_i^3 \rangle = \int_{-\infty}^{\infty} w_i^3 \cdot p(w_i^3) \mathrm{d}x, \tag{7.10}$$

where p is the probability density function for the normal distribution (Equation 7.1). Solving this gives the expectation value

$$\langle w_i^3 \rangle = \bar{w}^3 + 3\bar{w} s_N^2, \tag{7.11}$$

which means that the sum in Equation 7.9 can be expected to be equal to $N(\bar{w}^3 + 3\bar{w} s_N^2)$. The expected value of $\dot{q}$ in a regenerator can then be found using the same approach, which gives

$$\langle \dot{q} \rangle \propto \frac{1 + s_N^{*2}}{\bar{w}^2(1 + 3s_N^{*2})}. \tag{7.12}$$

In the uniform case, $\langle \dot{q} \rangle$ is simply proportional to $1/\bar{w}^2$, which means that the decrease in effectiveness due to non-uniformity is

$$\Delta\varepsilon_{\mathrm{SB}} \approx 1 - \frac{1 + s_N^{*2}}{1 + 3s_N^{*2}}. \tag{7.13}$$

This function is plotted in Figure 7.7 along with the calculated values from the simulations. The gray point show the average decrease in effectiveness for each of the combinations of different aspect ratio and porosity values that have been modeled, and the white points show the average decrease in effectiveness for all simulations with the same relative standard deviation.

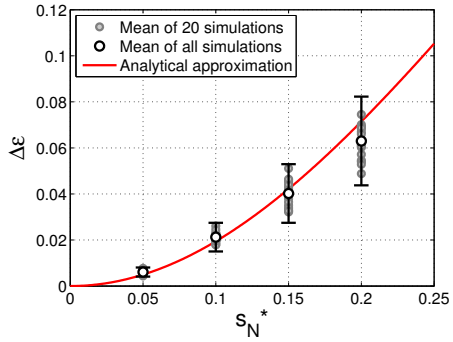

Figure 7.7: Peak magnitude as a function of the relative standard deviation. The white circles are the mean value for all simulations with the given standard deviation and the gray circles are the means for the simulations with the same AR, η, and s_N^*. The error bars show the standard deviations and the red line shows the analytical approximation that is developed.

The mean values (white points) are generally slightly smaller than predicted by the analytical estimate, but this estimate only accounts for differences in the heat transfer due to the width of each channel and the sum of cubed channel widths. Cross-talk between channels augments the heat transfer in regenerators with large standard deviations and is not accounted for in the estimation, which can explain the lower values in the results from the simulations at high standard deviations.

Furthermore, it can be seen from the scattering of the gray points, that there are significant variations between the different values of aspect ratio and porosity; and from the error bars that the variations due to random variations in distributions with the same mean and standard deviation are even greater.

An interesting effect of the relationship suggested in Equation 7.13 is that the worst possible regenerator (i.e. the least uniform) has an effectiveness of 2/3 of the corresponding uniform regenerator.

The standard deviation of a given distribution quantifies how much the channel widths deviate from the nominal width. Clearly larger standard deviations lead to lower effectiveness for any given distribution of channel widths. For distributions that are randomly generated and only shares a mean and a standard deviation in addition to the distributions type, however, rather significant variations are found. It can be seen in Figure 7.7 that some of the regenerators with 20 % standard deviaitons have higher effectiveness that some of the

regenerators with 15 % standard deviations, even though all distributions are generated from a normal distribution.

This can partially be attributed to random variations, and it suggests that the standard deviation of the channel width distribution is not sufficient to accurately describe the variations in heat transfer observed for non-uniform regenerators. The same conclusion was reached in Chapter 6, and this only cements the fact that the specific neighboring relationships in the distributions also need to be accounted for.

Table 7.4 shows the average full width at half maximum, $\bar{FWHM}$, for the individual values of aspect ratio, porosity, and channel width standard deviation, respectively. It can be seen that the full width at half maximum is a monotonically decreasing function of the aspect ratio and a monotonically increasing function of the porosity and standard deviation. It is generally desirable to have a sharp peak with a low $FWHM$, since the effectiveness will have higher values, but the primary parameter to consider in this respect is $\Delta\varepsilon_{\mathrm{p}}$.

Increased peak widths can be expected to give greater decreases in effectiveness for utilizations near the peak. However, since the peak position and magnitude varies significantly for variations in the geometrical parameters, the variations in peak width are of secondary importance when evaluating the effects of these variations on the effectiveness of regenerators.

AR	$\bar{FWHM}$	**std.**	**rel. std.**
50	2.72	0.87	0.32
100	2.00	0.65	0.33
150	1.54	0.59	0.38
200	1.35	0.52	0.38
η	$\bar{FWHM}$	**std.**	**rel. std.**
0.25	0.99	0.14	0.14
0.42	1.42	0.40	0.28
0.58	1.80	0.52	0.29
0.75	2.72	0.81	0.30
s_N^*	$\bar{FWHM}$	**std.**	**rel. std.**
0.05	1.50	0.62	0.41
0.10	1.70	0.72	0.42
0.15	1.95	0.83	0.43
0.20	2.21	0.99	0.45

Table 7.4: Average $FWHM$ values for different aspect ratios, porosities, and relative standard deviations (of channel widths), respectively, and their corresponding standard deviations.

Chapter 8

Experiments with Varying Plate Spacing Deviations

8.1 Introduction

In this chapter, the effectiveness of three different regenerator geometries has been investigated in a series of experiments. Three regenerators with nominal relative standard deviations of 0 (uniform), 20 %, and 50 % have been constructed and tested in the test machine.

When constructing the regenerators, small fabrication errors are inadvertently introduced and the resulting relative standard deviations are therefore not exactly 0, 20 %, and 50 %, respectively. The regenerators, however, will nonetheless be referred to using their nominal standard deviations.

8.2 Regenerators

The fabrication method for the regenerators is described in detail in Section 2.2.1. In all the regenerators, the nominal mean widths of both the plates and the channels are 1 mm, and the plate material is stainless steel (AISI 304). Stainless steel has been used because it is easier to achieve flat plates with a precise thickness with this material than with gadolinium. The relevant thermal properties: conductivity, specific heat capacity, and density are, as shown in Table A.1, similar to those of gadolinium, which means that the results of these tests in terms of effectiveness are similar to gadolinium regenerators.

Both the nominal and the measured geometries of the three tested regenerators are shown in Table 8.1. The two non-uniform geometries are based on the same

randomly generated distribution, but the deviations from the mean channel width have been scaled by different factors.

8.3 Regenerator Measurements

The distributions of plate spacings in the three regenerators have been measured using the photogrammetric approach described in Chapter 3.

Since it is only the plate spacing distributions at the inlet and outlet ends of the regenerator that are measured, both ends (designated as the "up" and "down" directions according to how they are mounted in the test machine) are compared. Furthermore, in order to ensure accurate measurements, each end of the regenerators is measured twice with its plates parallel to the x_2-direction and twice with its plates parallel to the y_2-direction with x_2 and y_2 defined as in Figure 3.1.

The average measurement of the channel width of each of the channels in the regenerators is shown in Table 8.1.

Ch. widths [mm]	**Uniform**		**20 % std. dev.**		**50 % std. dev.**	
Channel no.	**Measured**	**Nominal**	**Measured**	**Nominal**	**Measured**	**Nominal**
1	0.98	*1.00*	1.09	*1.08*	1.21	*1.20*
2	0.97	*1.00*	0.61	*0.64*	0.10	*0.10*
3	1.04	*1.00*	1.12	*1.09*	1.22	*1.23*
4	0.96	*1.00*	1.26	*1.30*	1.70	*1.75*
5	0.99	*1.00*	1.03	*1.04*	1.12	*1.10*
6	1.03	*1.00*	1.17	*1.17*	1.34	*1.43*
7	1.02	*1.00*	1.05	*1.09*	1.18	*1.23*
8	0.98	*1.00*	0.93	*0.85*	0.69	*0.63*
9	1.04	*1.00*	1.01	*0.99*	1.00	*0.98*
10	0.99	*1.00*	0.73	*0.74*	0.44	*0.35*

Table 8.1: Measured and nominal channel widths for the experimental regenerators.

The relative standard deviations for these three distributions are 2.9 %, 19.9 %, and 46.8 % for the "uniform", "20 %", and "50 %" distributions, respectively. All the measured channel widths are within 0.09 mm, or 9 %, of the corresponding nominal width, which shows that the actual channel width distributions are close to the nominal distributions. Since the heat transfer can vary significantly if the distributions vary, this is a requirement if comparisons are to be made based on the standard deviation values.

8.4 Regenerator Geometries and Experimental Procedure

The regenerators have been tested with various values of heat load and utilization using the test machine in its passive configuration as illustrated in Figure 2.1a. Before each test, the appropriate regenerator is mounted in the test machine and the interfaces between the various parts are sealed using silicone. When the silicone has cured, the heat transfer fluid, which is a mixture of 75 % (by volume) water and 25 % ethylene glycole, is added. The insulation is attached, and the heat exchanger is turned on and the cabinet is then allowed to reach an equilibrium temperature before initializing the experiments.

The regenerators have been tested at four different utilizations and with four different heat loads. The utilization is varied by varying the fluid displacement length, keeping the remaining parameters constant.

The regenerators have been tested with fluid displacements of 1/3, 2/3, 3/3, and 4/3 of the regenerator length, L, which corresponds to utilizations of 0.74, 1.48, 2.22, and 2.95, respectively.

The heat load has been varied between 0.4 W and 1.6 W in steps of 0.4 W, and the remaining operating parameters used in the experiments are shown in Table 8.2.

Parameter	**Symbol**	**Value**	**Unit**
Fluid displacement	-	0.033 - 0.133	[m]
Plate width	w_{pl}	1×10^{-3}	[m]
Mean channel width	$\bar{w}$	1×10^{-3}	[m]
Regenerator length	L	0.1	[m]
Mean fluid velocity	u_{m}	0.01	[m/s]
Solid material	-	Stainless steel	
Fluid material	-	Water + ethylene glycol	
Porosity	η	0.5	-
Aspect Ratio	AR	100	-
Relative std. dev.	s_N^*	0 - 0.5	-
Peclet number	Pe	10042	-
Diffusivity ratio	R_α	0.026	-
Conductivity ratio	R_k	0.027	-

Table 8.2: Operating parameters for the experiments.

For each combination of utilization and heat load, the regenerator is run until a cyclical steady state is reached. The steady state is considered to have been reached when there is no significant change in the temperature difference from one cycle to another over a period of at least 30 minutes.

The experiments are run in succession, which means that the temperature profiles in the regenerator at the beginning of the experiments may not be the same for all the experiments. This, however, does not alter the steady-state of the test machine setup.

8.5 Temperature Measurements

As described in Chapter 2, the temperatures in the regenerator are measured in the middle of the 10 cm long regenerator and 17 mm from either end of the regenerator (see Figure 2.3). The temperatures are measured in the middle of the sixth channel which has a width of 1 mm + $0.85 \cdot s_N$, i.e. a channel that, in the non-uniform regenerators, is wider than average.

Not measuring the temperatures at the ends of the regenerator will give rise to some measurement error. Since the temperature gradient in the regenerator is unknown, the exact magnitude of this error cannot be accurately estimated. However, it can be assumed that the gradient at any given time will have the same sign at all points in the regenerator, i.e. that the temperature will increase steadily from the cold end to the hot end. Furthermore, it is expected that if the temperature difference between the two ends of the regenerator changes by some fraction, the temperature difference between the measured "end" points will change by approximately the same fraction.

The temperature differences that are measured at the thermocouple positions are therefore used to estimate the regenerator effectiveness as described in the next section. Even though this procedure may introduce some measurement error, the results are still assumed to be accurate for comparison of the different regenerators.

During steady state operation, the measured temperatures at the ends of the regenerator will cycle as shown in Figure 8.1.

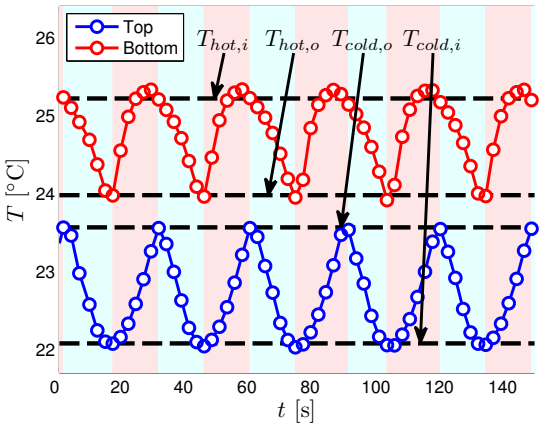

Figure 8.1: Measured temperatures in a uniform regenerator at a heat load of 1.6 W and a fluid displacement of 4/3 of the regenerator length.

Ideally, the hot and cold inlet temperatures should be constant at the temperatures of the hot and cold reservoirs, respectively. In practice, however, the temperature oscillates as it, at the beginning of a given blow period is equal to the outlet temperature of the previous blow period. During the blow period,

fluid will enter at the inlet, and the measured temperature will approach that of the reservoir.

The mixing of the fluid in the reservoirs, however, is not perfect, and it can therefore be expected that temperature gradients exist in the reservoirs as well. This has been found to be most pronounced at the hot end because the piston moves with the fluid, which means that it only is the fluid in contact with the piston that is being heated. At the cold end, the fluid flows through the heat exchanger while heat is being exchanged, which is expected to minimize the temperature gradients in the cold reservoir.

In order to calculate the regenerator effectiveness, we need to find the temperature difference between the inlet at the hot end and the outlet at the cold end during the hot-to-cold blow, ΔT_1, and the difference between the two inlet fluids, ΔT_2, as illustrated in Figure 8.2.

The measured temperatures for the uniform regenerator with a utilization of 2.95 and an applied heat load of 1.6 W are shown in Figure 8.1. The beginning of the hot-to-cold blow period is determined by the local minimum of the bottom temperature and the beginning of the cold-to-hot blow period as the local maximum of the top temperature. The hot-to-cold periods are shaded in red and the cold-to-hot periods are shaded in blue. The dashed lines indicate the mean temperatures over the last 30 minutes of the data series.

It can be seen that the temperatures oscillate synchronously and have approximately equal amplitudes. It is therefore assumed that the temperature difference ΔT_1 can be approximated as the difference between the temperatures $T_{\text{hot,i}}$ and $T_{\text{cold,o}}$ and that the temperature difference ΔT_2 as the difference between $T_{\text{hot,i}}$ and $T_{\text{cold,i}}$.

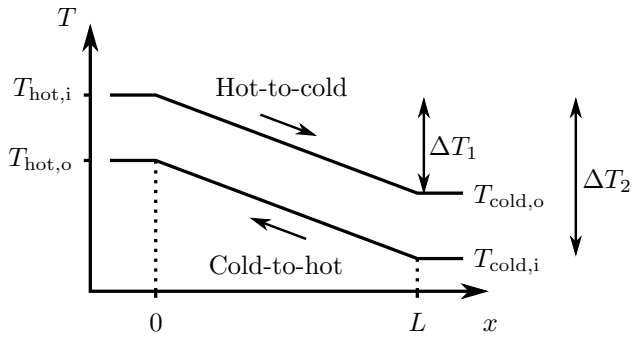

Figure 8.2: Approximate temperature profiles in the regenerator during steady state at the beginning of the blow periods.

In order to determine the maximum possible heat transfer, the difference between the two inlet temperatures is required. Since all the blow lengths are significantly longer than the distance between the regenerator ends and the thermocouples (it is at least 33 mm), it is assumed that the inlet temperature at the hot end can be estimated by the maximum temperature that the

fluid reaches at the hot end during the hot-to-cold blow period and likewise that the inlet temperature at the cold end can be estimated by the minimum temperature that the fluid reaches at the cold end during the cold-to-hot blow.

Since the temperatures are measured in channels that are wider than the average channel, the fluid flow rates near the thermocouples will be greater than the average flow rates. This effectively increases the fluid displacement, but may also introduce some measurement error for the non-uniform regenerators, an effect which can be expected to increase when the standard deviation of the channel distribution increases.

8.6 Data Analysis

8.6.1 Single-Blow Effectiveness

The single-blow effectiveness of a regenerator is given as (Equation 1.8)

$$\varepsilon_{\mathrm{SB}} \equiv \frac{q_{\mathrm{t}}}{q_{\mathrm{max,s}}}, \tag{8.1}$$

where q_{t} is the thermal energy transferred from the matrix to the solid at a given time and $q_{\mathrm{max,s}}$ is the maximum thermal energy that can be transferred from the matrix to the fluid. This effectiveness is initially zero and approaches unity as the time increases.

The maximum thermal energy that is transferred from the solid to the fluid can be calculated as

$$q_{\mathrm{max,s}} = m_{\mathrm{s}} c_{\mathrm{s}} (T_{\mathrm{hot,in}} - T_{\mathrm{cold,in}}) = m_{\mathrm{s}} c_{\mathrm{s}} (\Delta T_2), \tag{8.2}$$

where ΔT_2 is the difference between the hot inlet fluid and the cold inlet fluid. The transferred thermal energy at time t_{B} is given by

$$q_{\mathrm{t}} = \int_0^{t_{\mathrm{B}}} \dot{m} c_{\mathrm{f}} (T(x=0) - T(x=L)) \mathrm{d}t. \tag{8.3}$$

The temperatures at the two ends oscillate between the respective inlet and outlet temperatures, but the oscillations are synchronous. Therefore, the temperature difference ΔT_1, which is illustrated in Figure 8.2, is used. The transferred thermal energy is thus given by

$$q_{\mathrm{t}} = \dot{m} c_{\mathrm{f}} t_{\mathrm{B}} \Delta T_1. \tag{8.4}$$

The measured values of ΔT_1 and ΔT_2 are plotted as functions of the applied heat load for different utilizations in Figures 8.3 and 8.4, respectively. In these

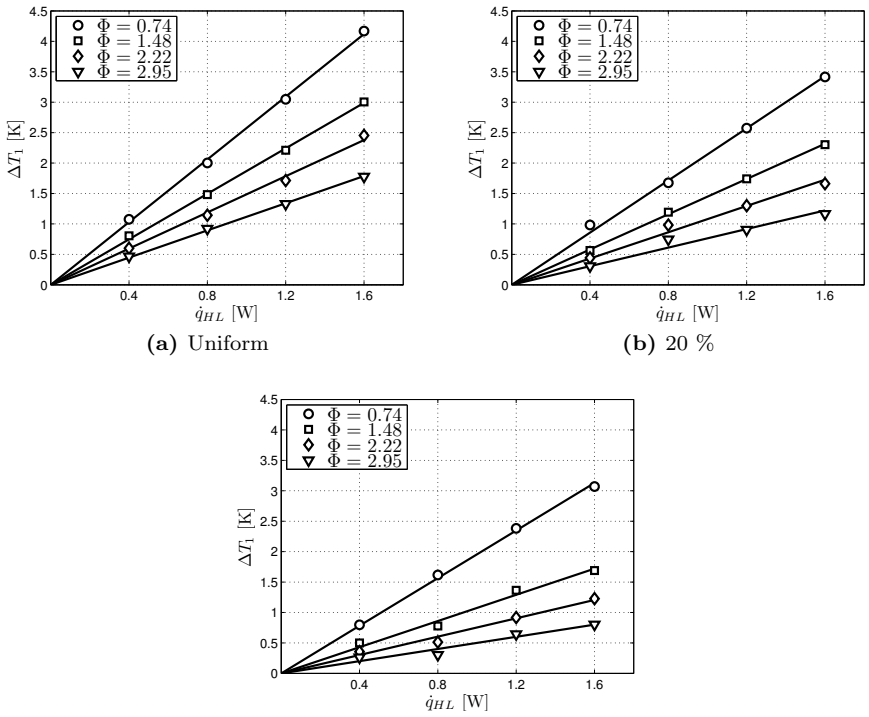

(a) Uniform **(b)** 20 %

(c) 50 %

Figure 8.3: Measured values of ΔT_1 as a function of the applied heat load for the three regenerators.

figures, it can be seen that both of the temperature differences increase approximately linearly with the applied heat load. Furthermore, it can be seen that the temperature differences are greater for smaller utilizations. This is because the overall thermal resistance of the regenerators in the axial direction decreases when the utilization increases, which causes the rate of heat transfer from the hot end to the cold end to increase, thus reducing the temperature of the hot end (if the cold end is at a constant temperature).

In order to calculate the effectiveness of the tested regenerators, we use that the temperature differences in the regenerators are approximately linear functions of the applied heat load (as seen in Figures 8.3 and 8.4). In order to increase the statistical accuracy of the measurements, the temperature differences have been fitted to linear functions. Since a heat load of zero does not give any temperature difference, the functions are forced to go through the origin. The slope of ΔT_1 as a function of the heat load is denoted a_1 and is given by

$$a_1 = \frac{\Delta T_1}{\dot{q}_{\mathrm{HL}}} \tag{8.5}$$

and the slope of ΔT_2 as a function of the heat load is denoted a_2 and is given by

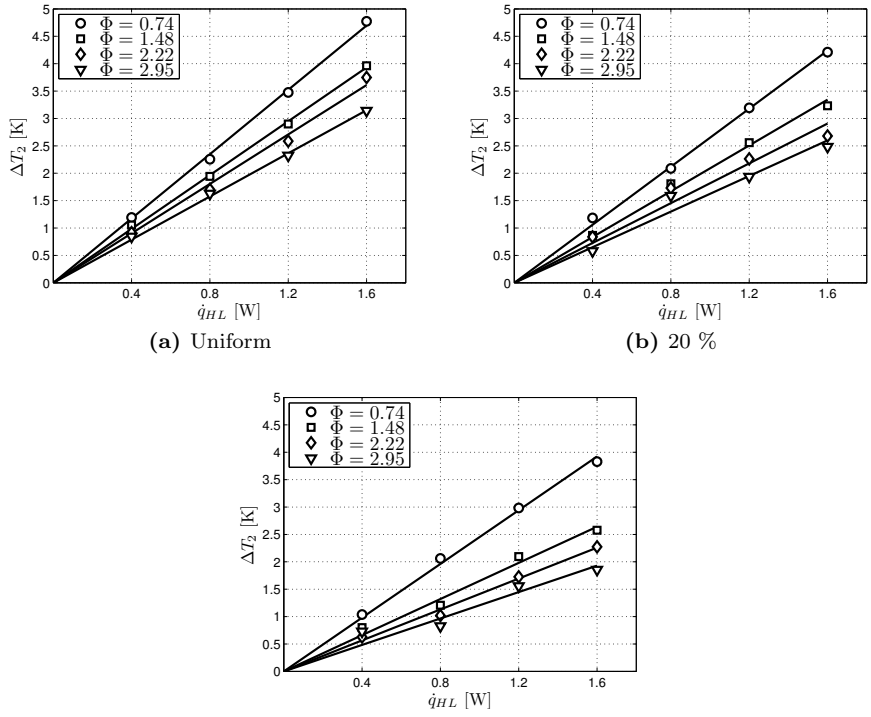

(a) Uniform **(b)** 20 %

(c) 50 %

Figure 8.4: Measured values of ΔT_2 as a function of the applied heat load for the three regenerators.

$$a_2 = \frac{\Delta T_2}{\dot{q}_{\mathrm{HL}}}, \tag{8.6}$$

where $\dot{q}_{\mathrm{HL}}$ is the applied heat load. These slopes are plotted in Figures 8.5a and 8.5b, respectively, as functions of utilization for each of the tested regenerators. The error bars in the plots show the standard deviations of the fitted lines.

Using Equations 8.2 and 8.4, the single blow effectiveness (Equation 8.1) is given by

$$\varepsilon_{\mathrm{SB}} \equiv \frac{q_{\mathrm{t}}}{q_{\mathrm{max,s}}} = \frac{\Delta T_1}{\Delta T_2} \frac{\dot{m} c_{\mathrm{f}} t_{\mathrm{B}}}{m_{\mathrm{s}} c_{\mathrm{s}}} \tag{8.7}$$

which can be written in terms of the fitted slopes as

$$\varepsilon_{\mathrm{SB}} = \frac{a_1}{a_2} \Phi. \tag{8.8}$$

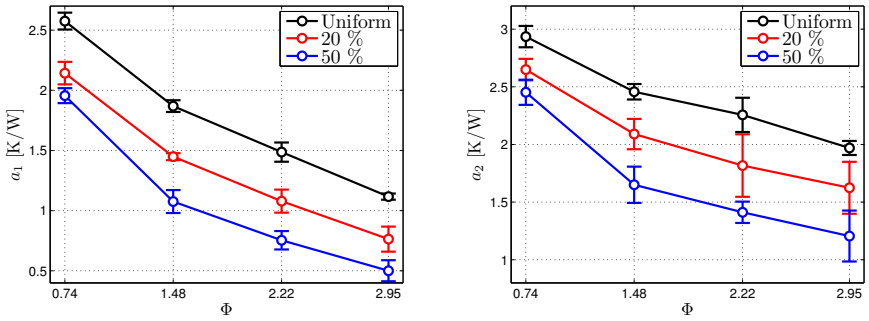

(a) a_1 **(b)** a_2

Figure 8.5: Slopes of the plots of temperature difference as a function of heat load, calculated from the fitted lines for (a) ΔT_1 and (b) ΔT_2.

The experimentally found single blow effectiveness for each of the tested regenerators is plotted in Figure 8.6 as a function of utilization. The corresponding effectiveness found by modeling the regenerators is also shown in the figure.

It can be seen that the effectiveness decreases when the standard deviation increases. This is the case for both the experimental and simulated experiments. The simulations, however, result in higher effectiveness than the experiments, which is discussed in more detail in Section 8.7.

8.6.2 Regenerative Effectiveness

For single blow processes, the single blow effectiveness gives an intuitive figure for the amount of thermal energy that is being transferred in the regenerator. However, for reciprocating devices, it is more appropriate to use an effectiveness which is defined as the ratio of transferred energy to the thermal energy of the fluid that has entered the regenerator [26], i.e.

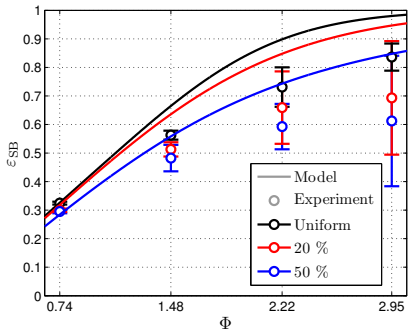

Figure 8.6: Single-blow effectiveness of regenerators as a function of utilization. The symbols show the experimentally found values and the lines show the values found by modeling.

$$\varepsilon_{\mathrm{Reg}} \equiv \frac{q_{\mathrm{t}}}{q_{\mathrm{max,f}}}, \tag{8.9}$$

where $q_{\mathrm{max,f}}$ is the thermal energy of the fluid that has entered the regenerator through the inlet during a given blow period. This effectiveness, which will be referred to as the regenerative effectiveness, corresponds to the amount of thermal energy being transferred from the hot fluid to the cold fluid, relative to the excess thermal energy of the hot fluid, i.e. the maximum possible heat transfer between the two fluids. The maximum fluid energy is given by

$$q_{\mathrm{max,f}} = \dot{m}\ c_{\mathrm{f}}\ t_{\mathrm{B}}(T_{\mathrm{hot,i}} - T_{\mathrm{cold,i}}), \tag{8.10}$$

which can be written in terms of the temperature differences as

$$q_{\mathrm{max,f}} = \dot{m}\ c_{\mathrm{f}}\ t_{\mathrm{B}}(\Delta T_2). \tag{8.11}$$

The regenerative effectiveness is therefore given as

$$\varepsilon_{\mathrm{Reg}} = \frac{\Delta T_1}{\Delta T_2} \tag{8.12}$$

or, in terms of the slopes of the ΔT-curves, as

$$\varepsilon_{\mathrm{Reg}} = \frac{a_1}{a_2}. \tag{8.13}$$

This effectiveness is calculated as the relative amount of heat that is transferred from the hot fluid during the hot-to-cold blow period to the cold fluid during the cold-to-hot period during steady state operation. It can as such not be found from single blow data because they only contain information about the current single blow, whereas the regenerative effectiveness depends on the steady state. However, it can be seen from Equations 8.8 and 8.13 that the two different effectivenesses differ by a factor of Φ when calculated for the experimental data.

The regenerative effectiveness for the simulations are therefore estimated to be approximately equal to $\varepsilon_{\mathrm{SB}}/\Phi$. The regenerative effectiveness is plotted in Figure 8.7 for experiments as symbols and for simulations as solid lines.

8.7 Discussion

8.7.1 Error Sources

The experimentally found effectivenesses are lower than the corresponding values found in the simulations. This may be due to the error sources introduced

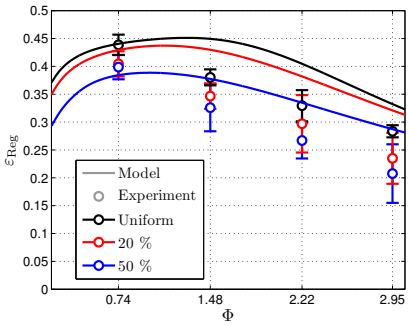

Figure 8.7: Regenerative effectiveness of regenerators with various standard deviations. Solid lines are simulations and points are experimental data.

in the temperature measurements that were discussed in Section 8.5 and imperfections in the experiment.

Three main sources of measurement errors were identified, namely variations in ΔT_1 during the cycles, the distance between the ends of the regenerators and the thermocouples, and imperfect mixing of fluid in the reservoirs. Particularly the latter contribution can be expected to reduce the measured effectiveness, but other factors, such as thermal losses and regeneration in the regenerator housing, may also influence the results.

If the mixing of the fluids in the thermal reservoirs is not perfect, the average inlet temperature will be lower during the hot-to-cold blow period and higher during the cold-to-hot blow period. However, since the maximum transferable energy is defined from the maximum and minimum temperatures under the assumption that the inlet temperatures are constant, the actual transferable energy may be lower in practice. This will lead to decreased values of the effectiveness, as is observed in the plots.

Moreover, there may be a significant contribution to the deviations between the experiments and simulations due to the way that the effectiveness is calculated from the temperature measurements. In the calculations it is assumed that the difference between the temperatures at the two ends of the regenerator is constant and the blow periods are determined by the local extrema in the temperature as a function of time. However, the local extrema do not always occur at exactly the same time and the temperature differences between the two ends are only approximately constant.

It can be seen in the results of both the experiments and the simulations that the effectiveness decreases with increasing plate spacing deviations. If we consider the peak regenerative effectiveness in the simulations, a reduction of 3 % is observed at a standard deviation of 20 % and a reduction of 14 % is observed at a standard deviation of 50 %.

8.7.2 Entrained Fluid

In reference [25], a simplified model, which ignores entrained fluid, shows that, in cases where entrained fluid can be ignored, the effectiveness approaches an ideal value of

$$\varepsilon_{\mathrm{Reg}} = \frac{NTU}{NTU + 2} \tag{8.14}$$

for (infinitely) small utilizations. However, for the model, the regenerative effectiveness peaks at a utilization greater than zero. This peak in regenerative effectiveness could be explained by the fact that the model considers entrained fluid.

If the thermal mass of the entrained fluid is not much smaller than the thermal mass of the solid, which is the case in the current experiments, the blow length becomes smaller than the regenerator length at small utilizations, which may reduce the heat transfer surface area and thereby the regenerative effectiveness.

If we approximate the Nusselt number to 7.54, which is a generally accepted value for flow between (uniformly spaced) parallel plates (see Section 5.3.5), we get an NTU of 1.8 for the flow rate used in the experiments. This gives an ideal regenerative effectiveness of 0.48, which is slightly higher than the peak values for the uniform regenerator and indicates that the entrained fluid has a significant effect on the heat transfer at low utilizations.

In Figure 8.7 it can be seen that the regenerative effectiveness does not approach an ideal value at $\Phi \to 0$, but it rather approaches zero. This can be explained by the entrained fluid slowing down the heat transfer process at low values of the utilization. At higher utilizations, the effect of the entrained fluid becomes less significant and the regenerative effectiveness reaches a maximum at utilizations around one.

The effect of entrained fluid has been investigated in references [95, 96]. It was found, however, that the entrained fluid has a positive effect of the regenerator effectiveness, particularly for small values of NTU. Reference [95] presents a general analysis of the effect of entrained fluid on the regenerator effectiveness and proposes an augmentation factor for NTU for small utilizations ($NTU < 130$), such that

$$NTU^* = AF \cdot NTU. \tag{8.15}$$

It was found that $AF \approx 1 + 1.76R_{\mathrm{M}} + R_{\mathrm{M}}^2$ where R_{M} is the ratio of thermal mass of the entrained fluid and the matrix (approximately equal to one in the present case). In the current experiments, $AF = 3.8$, which gives an ideal regenerator effectiveness of 0.78. It is thus assumed that the ideal regenerator effectiveness can be expected to lie in the range from 0.48 to 0.78 for the tested configuration of the uniform regenerator.

8.7.3 Initial Temperature Distribution

Besides the measurement errors and the effects of entrained fluid, the deviations could also be explained by the single blow process with the step change in temperature being more effective than a single blow during a developed steady-state. The main physical difference between the modeled single blow situation and the situation measured in the experiments, is the initial temperature profile at the beginning of the single blow (both in the experiments and in the simulations). We know that the initial temperature profile in the regenerator is uniform in the simulated situation, but the temperature profile in the experimental case is unknown.

In order to investigate the effect of the initial temperature profile, two different cases have been modeled in a pair of test simulations of a uniform regenerator. In the first case, the temperature is initially uniform and at $t = 0$, fluid at a different temperature enters regenerator. In the second case, the regenerator starts with a linear temperature profile, where the initial temperature at the inlet is equal to the temperature of the fluid entering the regenerator. The single blow effectiveness is plotted for both cases in Figure 8.8.

Furthermore, results from a regenerator model presented in reference [97] are also plotted in this figure. The model, which is described in reference [98] is a single blow model that assumes that the fluid is a gas with a very low heat capacity, such that the fluid displacement becomes very large for a given utilization.

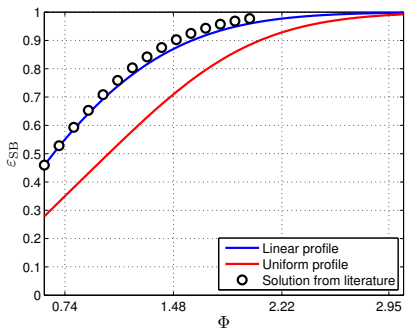

Figure 8.8: Calculated single blow effectiveness using different methods. Red line: single blow model using uniform temperature profile; blue line: single blow model using linear temperature profile; circles: solution from reference [97].

It can be seen that the effectiveness of the regenerator with the step change in the temperature is smaller than the effectiveness of the regenerator with the initially linear temperature profile. The effectiveness from the references is slightly greater than the effectiveness of the regenerator with the initially linear temperature profile, which indicates that the model in the references approximately corresponds to a regenerator with a linear temperature profile. If the heat capacity is very low, the cooling of the matrix will be more even, so it can be expected that the temperature profile is close to being linear in that case.

Solution for Cowper Stoves

In reference [99], the temperature profiles of regenerators in Cowper stoves are analyzed. A Cowper stove is a type of regenerator where air for a furnace is preheated before entering the furnace. In contrast to a counterflow heat exchanger, where the temperature profile is completely linear, it was found that it only is linear in the middle part of a regenerator. Near the ends of the regenerator, the temperature profile curves off, forming a slanted "s"-shape as depicted in Figure 8.9. Depending on the size of the regions of the curved temperature profiles, the profiles become more or less similar to a linear profile. For the tested regenerators, it is assumed that the actual initial temperature profiles are somewhere in between the linear profile and the step change.

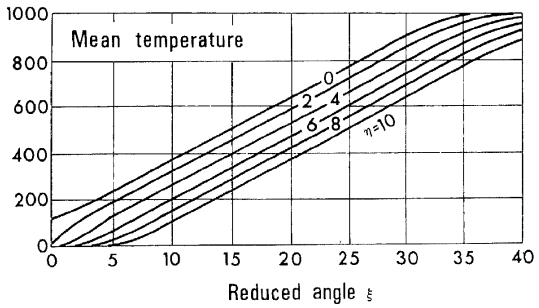

Figure 8.9: Temperature profiles calculated for Cowper stove regenerators. The different lines represent different solutions and the reduced angle is a coordinate for the position in the regenerator. Figure taken from reference [99].

In the model presented in [98], it is assumed that the heat transfer fluid is a gas with a much smaller thermal mass than the matrix, which gives very long fluid displacements for a given utilization compared to the situation in the current experiments. Furthermore, a constant wall temperature is assumed in the cited model, which may be the case in regenerators with gases with low thermal masses, but definitely is not the case for the currently investigated regenerators.

Solution for AMR

In reference [11], the temperature profile in AMRs have been investigated for various aspect ratios using two independently developed heat transfer models. Figure 8.10a shows the calculated temperature profiles at the beginning of a hot-to-cold blow period for a porosity of 1/3, a utilization of 0.27, and an aspect ratio of 50 and Figure 8.10b shows the temperature profile for a similar regenerator with an aspect ratio of 17.

It can be seen that the temperature profile in the regenerator with the high aspect ratio is significantly more s-shaped than in the regenerator with the low aspect ratio. Since the only parameter that changes in this study is the channel width, the regenerator with the low aspect ratio has more resistance to

heat transfer in the transverse (y-) direction than the regenerator with the high aspect ratio. This means that the regenerator with more even heat transfer has a significantly more linear temperature gradient than the regenerator with larger gradients in the y-direction.

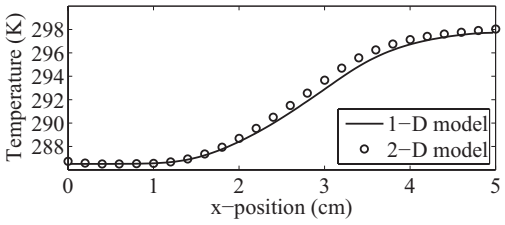

(a) $AR = 50$

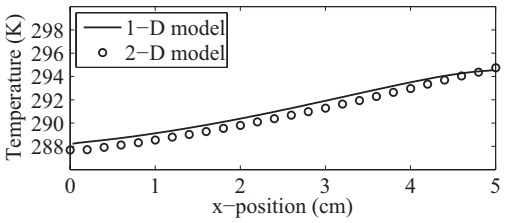

(b) $AR = 17$

Figure 8.10: Temperature profiles calculated for AMRs with various aspect ratios. Figure taken from reference [11]. Plots at additional intermediate aspect ratios can be found in the reference.

8.8 Conclusions

On the basis of the analysis above, it is implied that the differences between the experimentally found effectiveness and the simulated effectiveness possibly are due to inadequate mixing of the fluids in the reservoirs and it is furthermore indicated that the regenerators under the investigated conditions are more accurately represented by an initially uniform regenerator temperature than an initially linear regenerator temperature.

The experimental results show that maldistribution of the fluid flow due to an inhomogeneous distributions of plate spacings reduces the effectiveness of the regenerators significantly. The magnitude of this effect is on the same order as what was found in the modeling, which was presented in Chapters 6 and 7. Furthermore, the actual effectivenesses of the regenerators are relatively accurately simulated by the model despite the calculated values being slightly greater than the experimentally found values.

Additional accuracy might be obtained by either ensuring proper mixing of the fluid in the thermal reservoirs in the experiments, or by modeling time-dependent inlet temperatures. Furthermore, an error source (of unknown magnitude) could be avoided by ensuring that the temperatures are measured ex-

actly at the ends of the regenerators, although this will require a redesign of the experimental setup.

Chapter 9

Modeling of Experimental Regenerators

9.1 Introduction

When producing regenerators, the goal generally is to create a geometry that resembles the intended (or nominal) geometry as closely as possible. The degree to which the final product deviates from the nominal geometry can depend on the fabrication method used as well as the characteristics of the nominal geometry. For a given fabrication method, it is assumed that the relative standard deviation of the channel width distribution becomes greater when the plate spacing is reduced. Whether the absolute standard deviation is affected will be investigated in this chapter.

Theoretically, the performance of a perfectly uniform parallel plate regenerator increases as the plate spacing is reduced, but as has been found in previous chapters, the reduction in performance due to non-uniformity also increases with decreasing plate spacings. In this chapter, it is therefore investigated, how the actual performance in real fabricated regenerators behaves when the plate spacing is decreased.

The results presented in this chapter is the product of the contributions of several researchers. The main contribution by this author is developing and adapting the model to simulate a series of experimental regenerators and running part of the simulations as well as participating in discussion and analysis of the results.

The fabrication of the regenerators has been performed mainly by Kurt Engel-

brecht[1], the measurements of the regenerators mainly by Dennis Christensen[2], and the management and analysis of the results of the simulations mainly by Kaspar Nielsen[1]. Furthermore, Kaspar Nielsen and Kurt Engelbrecht have run parts of the simulations as well.

In order to provide a coherent description of the results found in this investigation, however, all the aforementioned contributions will be described in this chapter as a whole, although some of them are due to the work of other contributors.

9.2 Regenerators

Four different regenerators have been constructed as described in Section 2.2.1. The regenerators have nominal plate spacings of 0.1 mm, 0.2 mm, 0.4 mm, and 0.74 mm, respectively and a plate width of 0.4 mm.

The plates are made of aluminum and the heat transfer fluid is water. Each regenerator consists of 18 plates with dimensions of 40 mm $\times$ 25 mm $\times$ 0.4 mm and 17 channels. A length of metal wire of a thickness corresponding to the plate spacing is placed at either side of each channel in a stack of plates, and the sides, the top and the bottom of the stack are coated with a layer of epoxy glue and mounted in a regenerator housing. The periphery of the stack is sealed with silicone in order to prevent fluid bypassing the regenerator channels by flowing around the regenerator stack.

When inserting the stack into the housing, some of the channels at the ends of the regenerator may become covered with epoxy. The width of these channels cannot be measured and they are therefore disregarded in the modeling.

9.3 Measurements

The channel widths of each of the regenerators have been measured using a Vantage Laser Scanner. The laser scanner has been used to image the cross section at both ends of each regenerator, thus giving a total of eight different measured regenerator geometries. The two ends of the regenerators will be denoted as the "up" and the "down" directions, according to how they are mounted in the test machine.

The resolution of the measurements are 5 μm is the x_2-direction, i.e. the direction normal to the plates, and 20 μm in the y_2-direction, i.e. the direction along the depth of the regenerator (the same coordinate system as shown in Figure 3.1 is used). The laser scanner measures the three spatial coordinates of the surface topology, but in this case, since the information in the z_2-direction only consists of "plate" and "void", the measurements were truncated to only

[1] Risø DTU
[2] University of Copenhagen

one of two possible values, representing either (x_2, y_2) coordinates with plates or (x_2, y_2) coordinates with channels.

Figure 9.1 shows an example of the measurement process. The image is initially represented by the raw measurement data which contains the whole regenerator face and part of the housing (a). These data contain some measurement noise, which is filtered by averaging the value (plate/channel) of each pixel by a number of surrounding pixels (b). The data is then rotated and cropped such that only channels that are not obstructed by epoxy are included (c).

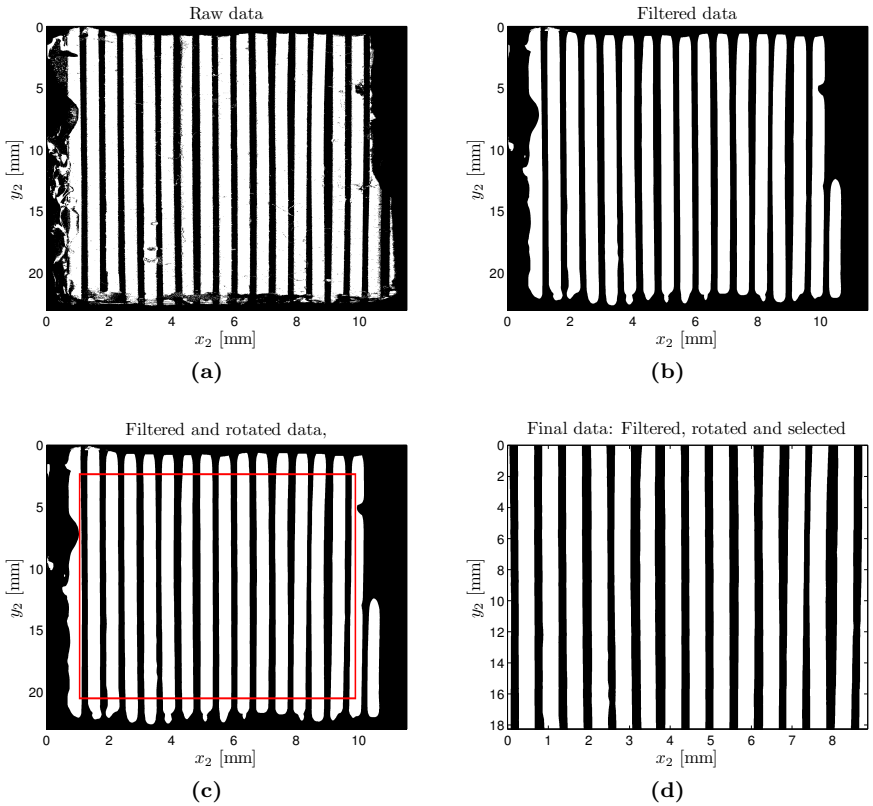

Figure 9.1: Example of measurement procedure for channel width distributions when using laser scanning. This regenerator is the regenerator with 0.2 mm plate spacings.

The cropped section is analyzed line by line (d) and the plate spacing is defined by the average spacing for all the analyzed lines in a given channel. Figure 9.2 shows the measured plate spacings for each of the regenerators. The error bars denote the standard deviations for each measured width.

Figure 9.3a shows the standard deviations of the measured width as a function of the nominal width. It can be seen that the standard deviation is approximately 0.03 mm - 0.04 mm, although the 0.4 mm regenerator has a significantly greater standard deviation in the "up"-direction. The measured plate distribution for this particular regenerator end is shown in Figure 9.4 and it

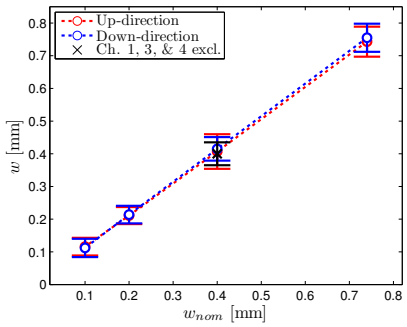

Figure 9.2: Measured channel widths as function of the nominal channel width for all the measured regenerators. The error bars denote the standard deviations of the measurements.

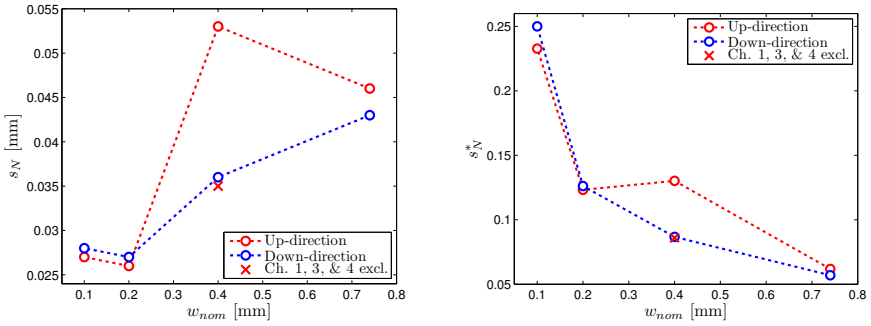

(a) Absolute standard deviation **(b)** Relative standard deviation

Figure 9.3: Standard deviations of the measured channel widths. The standard deviations agree on both sides of the regenerators if the bent plates are excluded.

can be seen that the first and the fourth plates are bending. Excluding the neighboring channels of these plates from the measurement gives a standard deviation of 0.035 mm, which is much closer to the standard deviation for the "down"-direction of the same regenerator.

The standard deviation increases slightly when the nominal plate spacing is increased, but it increases by a factor less than two for a more than sevenfold increase in the nominal separation. Figure 9.3b shows the relative standard deviations in percent, and it can be seen that the relative standard deviation increases rapidly for decreasing plate spacings. This means that the decrease in effectiveness can be expected to be much greater for regenerators with small plate spacings, even though these theoretically have higher absolute effectiveness.

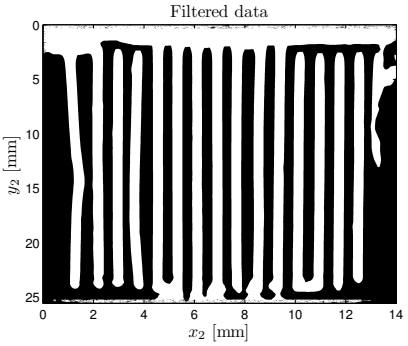

Figure 9.4: Filtered image of the channels in the 0.4 mm regenerator in the up-direction. It can be seen that plates number one and four are slightly bent.

9.4 Simulations

In order to estimate the effect of inaccuracy in the fabrication process, the regenerators have been modeled using the single blow model described in Chapter 5. The model is essentially identical to the model used for the simulations of regenerators presented in Chapters 6 and 7, but has been modified to model a variable number of plates and channels. The measured geometries of the up and down ends of each regenerator have been averaged, excluding plates number one and four in the 0.4 mm up regenerator end, and the average distributions have been modeled.

Each of the distributions have been modeled at the following values of the mass flow rates per unit depth, $\dot{m}/d$: 4.5, 9, 15, 18, and 25 g/(m s), where

$$\dot{m}/d = \rho_{\mathrm{f}} u_{\mathrm{m}} \bar{w}. \tag{9.1}$$

The parameters for model configuration, operating conditions, and geometry used in the simulations are shown in Table 9.1. The materials properties for water and aluminum are shown in Table A.1.

Parameter	**Value**	**Unit**
Solid	Al	
Fluid	Water	
w_{pl}	0.4	[mm]
$\bar{w}$	0.1-0.74	[mm]
d	20	[mm]
L	40	[mm]
T_{init}	273.15	[K]
T_{in}	283.15	[K]

Table 9.1: Simulation parameters used in the modeling of the experimental regenerators.

In addition to the measured distributions, a series of normal distributions with a constant standard deviation of 0.035 mm, but with plate spacings varying from 0.08 mm to 0.8 mm has been simulated. The same deviations, which are shown in Table 9.2 for a mean of zero are used for all the simulations, but the mean value is offset by different amounts.

Distribution	**Std. dev.** [mm]	**Channel width deviations** [mm]						
Normal	0.035	+0.006	-0.025	-0.003	+0.010	-0.027	-0.009	+0.011
		-0.055	+0.031	+0.073	+0.029	-0.009	+0.013	-0.031

Table 9.2: Deviations in the randomly generated distribution that has been used in the modeling. When defining the particular distributions to simulate, these deviations are added to the mean channel widths starting in the top left corner with channel number 1 and ending in the bottom right corner with channel number 14. This gives a distribution with a given mean and a standard deviation of 0.035 mm.

Furthermore, in order to compare the results for the non-uniform regenerators, corresponding uniform regenerators with different mean plate spacings have been modeled using a single channel model.

9.5 Results

9.5.1 Measured Distributions

In order to evaluate the heat transfer in the regenerators, two methods for evaluation of performance, described in reference [100], have been adopted. The first uses the maximum slope of the temperature breakthrough curve and the second uses the time interval between reaching temperature changes of 20 % and 80 % as described below. Using these methods, the regenerator effectiveness is evaluated from the variation of the fluid temperature at the outlet as a function of time during a single blow.

The mean temperature at the regenerator outlet as a function of time is used to evaluate the effectiveness. Two properties are calculated from the temperature curve: the maximum slope and the difference between the time where the temperature at the outlet has changed 20 % and the time where the temperature has changed 80 % of the maximum temperature difference. These two properties are represented by the perameters S_{R} and M_{R}, respectively. M_{R} is defined as

$$M_{\mathrm{R}} = K_{\mathrm{R}}(1-\eta)^2 \max\left(\frac{\mathrm{d}\bar{T}_{\mathrm{f}}(x=L)}{\mathrm{d}t}\right), \tag{9.2}$$

where K_{R} is given by

$$K_{\mathrm{R}} = \frac{(\rho_{\mathrm{s}} c_{\mathrm{s}} L)^2}{\rho_{\mathrm{f}} c_{\mathrm{f}} u_{\mathrm{m}} \Delta T_{\max}}, \tag{9.3}$$

where $\Delta T_{\max}$ is the maximum temperature change. $\bar{T}_{\mathrm{f}}(x = L)$ is the velocity-weighted (i.e. thermal mass-weighted) mean temperature of the fluid at the outlet, which is given by

$$\bar{T}_{\mathrm{f}}(x = L) = \frac{\sum_{i=1}^{N} \bar{T}_{\mathrm{o},i} u_{\mathrm{m},i} w_i}{\sum_{i=1}^{N} u_{\mathrm{m},i} w_i}, \tag{9.4}$$

where $\bar{T}_{\mathrm{o},i}$ is the mean fluid temperature at the outlet of the $i$the channel.

The parameter S_{R} is defined as

$$S_{\mathrm{R}} = \frac{C}{1 - \eta}(t_{80} - t_{20}), \tag{9.5}$$

where t_{20} and t_{80} are the times where the temperature change has reached 20 % and 80 %, respectively, of the maximum value. C is a constant, which is given by

$$C = \frac{\rho_{\mathrm{f}} c_{\mathrm{f}} u_{\mathrm{m}}}{c_{\mathrm{s}} \rho_{\mathrm{s}} L}. \tag{9.6}$$

The maximum slope, t_{20}, and t_{80} are illustrated in Figure 9.5. The calculated values of M_{R} and S_{R} for the measured channel width distributions are shown in Figure 9.6 as a function of channel width for each of the tested flow rates.

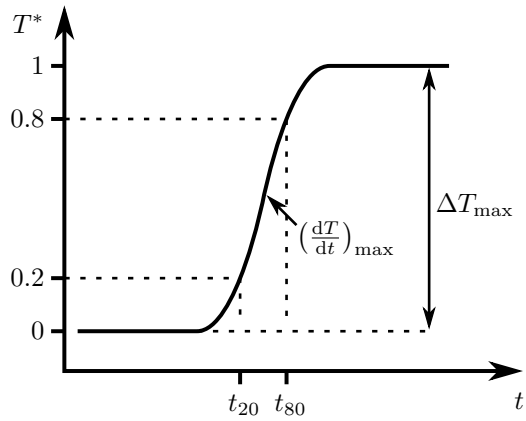

Figure 9.5: Sketch of temperature breakthrough curve. If the temperature increases from $T^* = 0$ to $T^* = 1$, t_{20} is where $T^* = 0.2$ and t_{80} is where $T^* = 0.8$.

T^* is a normalized temperature given by

$$T^* = \frac{T - T_{\text{init}}}{T_{\text{in}} - T_{\text{init}}}. \tag{9.7}$$

t_{20} and t_{80} are the times where T^* reaches 0.2 and 0.8, respectively and the maximum slope is where $\mathrm{d}T/\mathrm{d}t$ is greatest.

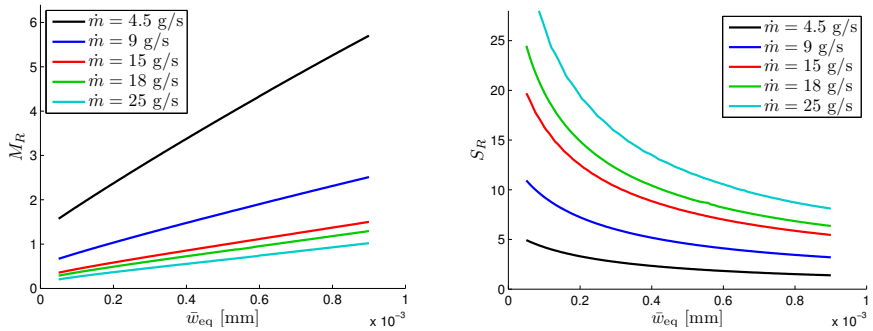

Figure 9.6: Measured M_{R} and S_{R} for the tested regenerators as functions of the equivalent channel width.

In Figure 9.6, it can be seen that the M_{R}-value increases with increasing equivalent channel width and decreases with increasing flow rate. The S_{R}-value, on the contrary, increases with the the flow rate and decreases with the equivalent channel width.

The M_{R}- and S_{R}-values have also been calculated for the uniform distributions, and for each measured distribution, an equivalent uniform distribution with the same M_{R}- and S_{R}-values is found. This gives an equivalent plate spacing, w_{eq}, for the non-uniform regenerators which corresponds to the plate spacing that a uniform regenerator with the same performance would have.

In Figure 9.7, the equivalent channel width is plotted as a function of the actual mean channel width for the measured regenerators. It can be seen that the normalized equivalent channel width increases to values significantly above one at low mean channel widths. The effect is greatest at high flow rates, but eventually converges around 30 g/s.

As expected, the effect diminishes as the relative standard deviation decreases and becomes insignificant at approximately 6 %, which is in accordance with the results found in Chapter 6. It can furthermore be seen that the equivalent channel widths are greater in the "down" direction than in the "up" direction at 0.1 mm channel width. This is due to randomness in the distributions, but can be seen to have an effect on the heat transfer.

For flow between parallel plates, we know that the Nusselt number is approximately 7.541 [26]. Using this correlation, we can estimate an equivalent convective heat transfer coefficient in the system, h_{eq}, as a function of the equivalent hydraulic diameter, and thereby as a function of the equivalent channel width.

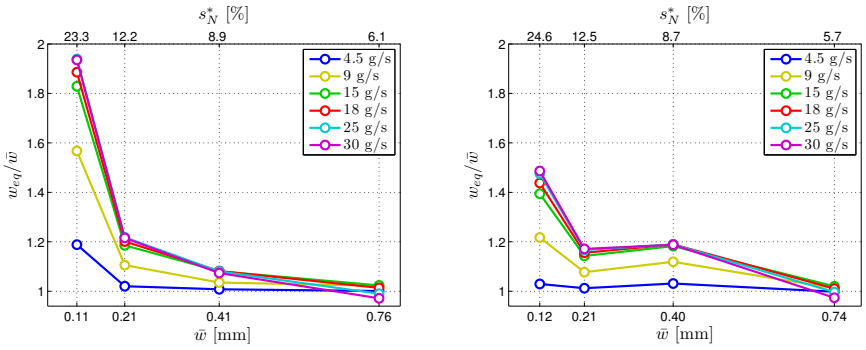

(a) **(b)**

Figure 9.7: Calculated equivalent channel widths, normalized with the mean channel widths, as functions of the actual measured mean channel widths for the experimental regenerators at various flow rates.

Figure 9.8 shows the calculated h_{eq} values for each of the measured regenerators as a function of their equivalent (uniform) channel widths for all the simulated fluid flow rates.

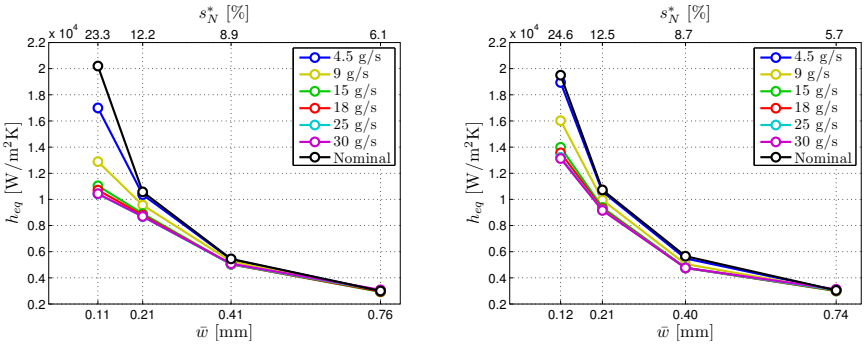

(a) up-direction **(b)** down-direction

Figure 9.8: Calculated equivalent heat transfer coefficient as a function of the channel width in (a) the up-direction and (b) the down-direction.

It can be seen that the heat transfer coefficient generally increases for increasing flow rates and for decreasing channel widths, which indicates that the effectiveness increases. These results, however, are based on only four different channel width distributions and the data are therefore relatively coarse. Furthermore, although the variations in the absolute standard deviation are small, they are not small enough to be considered completely negligible.

In the regenerators with 0.1 mm average channel width, it can be seen that the smaller equivalent channel widths give slightly greater heat transfer coefficients.

9.5.2 Normal Distribution

In order to achieve a more consistent calculation of the equivalent heat transfer coefficient with a higher density of data points, a series of channel width distributions that have been randomly generated from a normal distribution has been simulated (see Table 9.2). In this series of distributions, the mean channel width is varied while the absolute standard deviation is kept constant at $s_N = 0.035$ mm. In this way, the relative standard deviation is being varied in a similar way as in the fabricated regenerators such that the two cases are comparable.

The random distributions have been modeled with mass flow rates of 4.5 g/(m s) and 18 g/(m s) and the (equivalent) heat transfer coefficients have been calculated in the same way as for the measured distributions. The heat transfer coefficients of these two simulations, and the simulation of the corresponding uniform (nominal) hydraulic diameter, are plotted in Figure 9.9 as a function of nominal channel width and relative standard deviation.

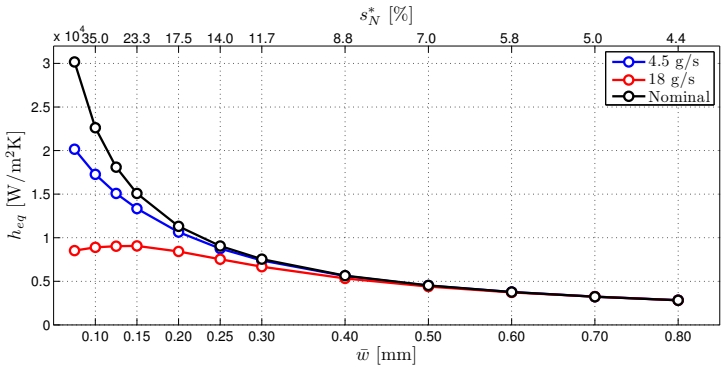

Figure 9.9: Calculated equivalent heat transfer coefficients as a function of the mean channel width at different flow rates for the random distributions and for the corresponding nominal (uniform) distribution.

For the uniform distribution, it can be seen that the heat transfer coefficient increases for decreasing equivalent channel widths as expected. This is also the case for the distribution with the high flow rate, but for the low flow rate, a peak in the heat transfer coefficient is observed at an equivalent channel width of approximately 0.15 mm. This indicates that, for the given configuration and standard deviation, there is a point, where decreasing the nominal channel width actually can harm the overall performance of the regenerator.

Since the distributions of channel widths in the non-uniform cases and in the equivalent uniform case are not the same, the pressure drops can also be expected to vary. Since the pressure drop decreases with the square of the channel width, the pressure drops are lower for the non-uniform regenerators than for the corresponding uniform regenerators with the same mean channel width.

Figure 9.10 shows the ratio of the pressure drop in the non-uniform regenerator to that of the equivalent regenerator as a function of mean channel width. It

can be seen that the pressure drop decreases by up to 35 %, but since the loss of heat transfer for the same equivalent channel width is much greater, the non-uniformity still results in a significantly worse performance, even if the decreased pressure drop is accounted for.

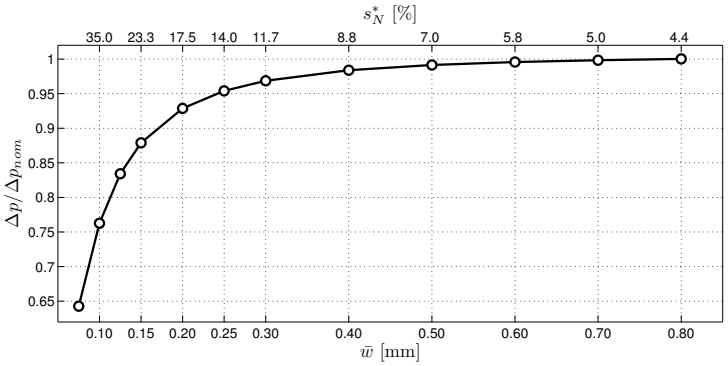

Figure 9.10: Ratio of actual pressure drop to the nominal pressure drop as a function of the mean channel width for the random distributions.

9.5.3 Evaluation of Thermal Cross-Talk

As described in Section 6.2.2, inter-channel heat transfer - or cross talk - affects the influence of non-uniformity in the regenerators. If a particularly narrow channel in a regenerator has wide neighboring channels, the performance loss due to the narrow channel is outweighed to a greater degree, than if the neighboring channels were also narrow.

This means that in a regenerator with great differences between neighboring channels, the effect of non-uniformity is smaller than in a regenerators with small differences between neighboring channels.

The "down"-faces of the 0.1 mm and 0.74 mm regenerators have been modeled in two configurations with a flow rate of 18 g/(m s). In the first configuration, the regenerators are simply run with the geometries as they have been measured, but in the second configuration the channels are rearranged and sorted by increasing width, such that the first channel in the regenerator is the narrowest and the last channel is the widest.

The temperature breakthrough curves for all the channels of the four simulations are shown in Figure 9.11a-d. It can be seen that the variations in the temperatures of the sorted configurations are significantly greater than in the unsorted configurations. This is due to the cross talk being minimized in the sorted configuration which gives greater variation in the temperatures. In the unsorted configurations, the neighboring relationships are random, and the effects of wide/narrow channels are countered by narrow/wide adjacent channels to a greater degree.

In addition to the two configurations described above, the two channel width distributions have been simulated as a collection of insulated single channels.

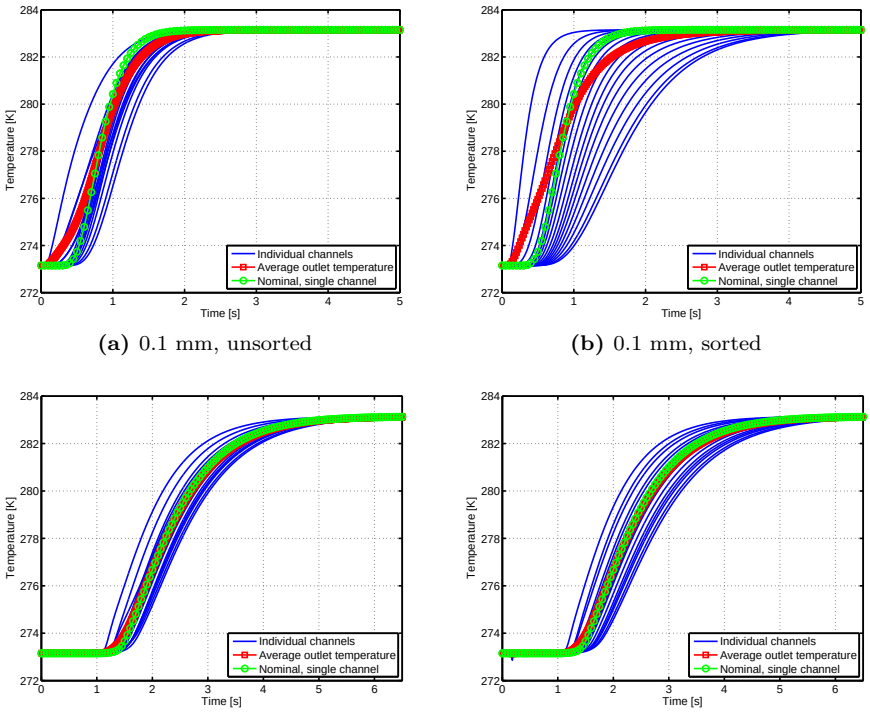

(a) 0.1 mm, unsorted

(b) 0.1 mm, sorted

(c) 0.74 mm, unsorted

(d) 0.74 mm, sorted

Figure 9.11: Temperature breakthrough curves for the 0.1 mm and 0.74 mm regenerators in sorted and unsorted configurations.

In this way, it is ensured that there is no heat transfer between the individual channels, such that the effects of cross-talk are completely eliminated. The breakthrough curves for the widest and the narrowest channels of the single channel, sorted, and unsorted configurations are plotted in Figure 9.12 for nominal channel width of 0.1 mm.

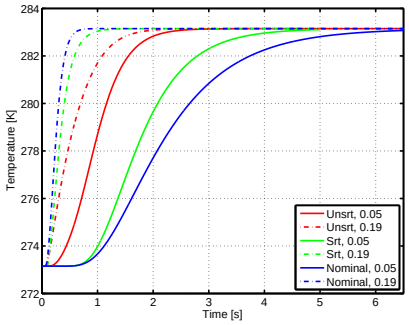

Figure 9.12: Temperature breakthrough curves for only the widest and narrowest channels of the sorted and unsorted configurations of the 0.1 mm regenerator and for two uniform regenerators with the same channel widths.

It can be seen that the single channel temperature curves differ most, which gives a lower effectiveness. There is significantly less variation in the sorted configuration, but still much more than in the unsorted configuration. It should be noted, however, that these results are specific for the fabricated aluminum regenerators, and since the thermal conductivity of aluminum is very high, the effect of cross-talk can be expected to be more pronounced than in similar regenerators with plate materials of lower conductivity.

It has been shown that, under specific conditions, the effective heat transfer coefficient of a regenerator may be reduced if the plate spacing is reduced. This assumes that the absolute magnitude of the fabrication errors are constant, but this has been found to be true for the fabrication method that was used for the investigated regenerators. It is ongoing future work to test the results for the fabricated regenerators experimentally.

Chapter 10

Summary

10.1 Conclusion

In this thesis, a series of experiments on parallel-plate active magnetic regenerators (AMRs) has led to investigations on the heat transfer processes in such devices. A mathematical model has been developed in order to simulate the heat transfer processes when the distributions of plate spacings are not uniform and experiments have been performed to extend the investigations.

It has been found that non-uniformity in the plate spacing distributions can affect the effectiveness of regenerators significantly, but also that the magnitude of the effect varies and depends on both geometry and operating parameters.

Correlations between the decrease in effectiveness and the geometrical properties of regenerators have been studies and expressions for the approximate decrease in effectiveness have been developed.

Furthermore, thermal cross-talk in regenerators - an effect where thermal energy transferred between the channels in a regenerator - has been investigated. It has been found that, while certain observations can be made from the mean and standard deviation of a given channel width distribution, the thermal interactions of all channels in the context of the whole distribution must be considered in order to achieve a complete description of the overall heat transfer.

It has also been found that the pressure drop in non-uniform regenerators is lower than in corresponding uniform regenerators. However, this effect is due to the maldistributed flow in the channels and is approximately an order of magnitude smaller than the reduction if heat transfer and thus do not counter the loss of thermal effectiveness.

In experimentally fabricated regenerators, it has been found that the relative standard deviation of the distributions generally range between around 2 % and 25 % of the mean channel width, being significantly greater at small channel widths. Experimental results have been obtained for series of passive regenerators. These results are subject to some errors, mainly due to improper mixing of fluid and restrictions in positioning of thermocouples, but agreement between modeling and experimental results has nonetheless been found. It has furthermore been found that the single-blow data obtained in the modeling can be used to estimate performance during regenerative operation.

The effectiveness of regenerators has been found to depend strongly on the standard deviation of the channel width distribution as well as the utilization that the regenerator operates at. However, regenerators with relative standard deviations of less than 5 % have been found to generally have reductions in effectiveness of less than 1 %.

10.2 Outlook

The model has been developed with the purpose of investigating the effects of non-uniformity on the heat transfer between parallel plates. Therefore, some simplifications have been made which makes it more suitable for studying these effects. However, it remains to be determined, exactly to which degree these results are accurate for AMRs.

In the model that has been developed, a uniform temperature profile is assumed as an initial condition. This gives a steep temperature gradient in the modeled regenerator during operation. However, the actual temperature profile in a regenerator depends on many factors, but if it can be approximated prior to the simulation, more accurate estimates could be achieved for the regenerative heat transfer in regenerators. Alternatively, the model could be run iteratively as a reciprocating regenerator instead of simulating only a single-blow process. Furthermore, active regeneration could be implemented in such a model by adding an appropriate heat generation term in the governing equation for the regenerator matrix.

The experimental results were obtained using a test machine at Risø DTU, but a few limitations in the setup introduced avoidable errors in the results. At the moment of this writing, the test machine is undergoing testing of a redesign, which has been based on these findings. More appropriately located temperature measurement has been added and the heating element and piston configuration has been completely rebuild, such that the temperature in the thermal reservoir to a greater degree can be kept uniform and constant.

Bibliography

[1] US Department of Energy. Residential energy consumption survey, 2001.

[2] US Department of Energy. Commercial buildings energy consumption survey, 2003.

[3] Secretariat for The Vienna Convention for the Protection of the Ozone Layer & The Montreal Protocol on Substances that Deplete the Ozone Layer. The montreal protocol on substances that deplete the ozone layer, 2000.

[4] United Nations Framework Convention on Climate Change. Kyoto protocol to the united nations framework convention on climate change, 1998.

[5] A.M. Tishin. Magnetocaloric effect in the vicinity of magnetic phase transition. *Journal of Magnetism and Magnetic Materials*, 184(1):62–66, 1998.

[6] A.M. Tishin and Y.I. Spickin. *The Magnetocaloric Effect and Its Applications*. Institute of Physics, 2003.

[7] M.K. Chattopadhyay, M.A. Manekar, and S.B. Roy. Magnetocaloric effect in $CeFe_2$ and Ru-doped $CeFe_2$ alloys. *Journal of Physics D: Applied Physics*, 39(6):1006–1011, 2006.

[8] S. Gama, A.A. Coelho, A. De Campos, A. Magnus, G. Carvalho, F.C.G. Gandra, P.J. Von Ranke, and N.A. De Oliveira. Pressure-induced colossal magnetocaloric effect in MnAs. *Physical Review Letters*, 93(23):237202, 2004.

[9] R. Burriel, L. Tocado, E. Palacios, T. Tohei, and H. Wada. Square-shape magnetocaloric effect in Mn_3GaC. *Journal of Magnetism and Magnetic Materials*, 290-291:715–718, 2005.

[10] K.A. Gschneidner, V.K. Pecharsky, and A. Tsokol. Recent developments in magnetocaloric materials. *Reports on Progress in Physics*, 68(6):1479–1539, 2005.

[11] T.F. Petersen. *Numerical modelling and analysis of a room temperature magnetic refrigeration system.* PhD thesis, Risø National Laboratory, Techincal University of Denmark, 2007.

[12] S.Y. Dan'kov, A.M. Tishin, V.K. Pecharsky, and K.A. Gschneidner. Magnetic phase transitions and the magnetothermal properties of gadolinium. *Physical Review B: Condensed Matter and Materials Physics*, 57:3478–3490, 1998.

[13] S.M. Benford and G.V. Brown. T-S diagram for gadolinium near the Curie temperature. *Journal of Applied Physics*, 52:2110–2112, 1981.

[14] J.S. Lee. Evaluation of the magnetocaloric effect from magnetization and heat capacity data. *Physica Status Solidi*, 7:1765–1768, 2004.

[15] R. Bjørk, C.R.H. Bahl, and M. Katter. Magnetocaloric properties of $LaFe_{13-x-y}Co_xSi_y$ and commercial grade Gd. *Journal of Magnetism and Magnetic Materials*, 322:3882–3888, 2010.

[16] D.A. Reay. A review of gas-gas heat recovery systems. *Journal of Heat Recovery Systems*, 1(1):3–41, 1981.

[17] R. Radebaugh. Development of the pulse tube refrigerator as an efficient and reliable cryocooler. In *Proceedings of the Institute of Refrigeration*, volume 96, pages 11–31, 1999.

[18] S. Jain, P.L. Dhar, and S.C. Kaushik. Evaluation of liquid dessicant based evaporative cooling cycles for typical hot and humid climates. *Heat Recovery Systems and CHP*, 14(6):621–632, 1994.

[19] G.V. Brown. Magnetic heat pumping near room temperature. *Journal of Applied Physics*, 47(8):3673–3680, 1976.

[20] J. Barclay and W. Steyert. Active magnetic regenerator, patent, June 1982.

[21] J.A. Barclay. Theory of an active magnetic regenerative refrigerator. *NASA Conference Publication*, pages 375–387, 1983.

[22] C. Zimm, A. Jastrab, V.K. Sternberg V. Pecharsky, K.A. Gschneidner Jr, M. Osborne, and I. Anderson. Description and performance of a near-room temperature magnetic refrigerator. *Advances in Cryogenic Engineering*, 43:1759–1766, 1998.

[23] F.P. Incropera, D.P. Dewitt, T.L. Bergman, and A.S. Lavine. *Introduction to Heat Transfer.* John Wiley & Sons, 5th edition, 2007.

[24] T.E.W. Schumann. Heat transfer: A liquid flowing through a porous prism. *Journal of The Franklin Institute*, 208(3):405–416, 1929.

[25] F.W. Schmidt and A.J. Willmott. *Thermal Energy Storage and Regeneration.* McGraw-Hill, 1981.

[26] G.F. Nellis and S.A. Klein. *Heat Transfer.* Cambridge University Press, 2009.

[27] F.M. White. *Fluid Mechanics*. McGraw-Hill, 6th edition, 2008.

[28] C.E. Iliffe. Thermal analysis of contra-flow regenerative heat exchanger. *Proceedings of the Institution of Mechanical Engineers*, 159(44):363–371, 1948.

[29] A.N. Nahavandi and A.S. Weinstein. A solution to the periodic-flow regenerative heat exchanger problem. *Journal of Applied Sciences Research*, 10(1):335–348, 1961.

[30] T.J. Lambertson. Performance factors of periodic-flow heat exchanger. *Transactions of the American Society of Mechanical Engineers*, 159:586–592, 1958.

[31] A.J. Willmott and E.W. Voice. Development of theoretical methods for calculating thermal performance of hot blast stove. *Journees Internationales de Siderurgie*, pages 473–482, 1962.

[32] A.J. Willmott. Digital computer simulation of a thermal regenerator. *International Journal of Heat and Mass Transfer*, 7(11):1291–1302, 1964.

[33] A.J. Degregoria. Modeling the active magnetic regenerator. In R.W. Fast, editor, *Advances in Cryogenic Engineering: Proceedings of the 1991 Cryogenic Engineering Conference*, volume 37B, pages 867–873, 1991.

[34] L.D. Kirol and J.I. Mills. Numerical analysis of thermomagnetic generators. *Journal of Applied Physics*, 56(3):824–828, 1984.

[35] A. Smaïli and R. Chahine. Thermodynamic investigations of optimum active magnetic regenerators. *Cryogenics*, 38(2):247–252, 1998.

[36] J.C. Hu and J.H. Xiao. New method for analysis of active magnetic regenerator in magnetic refrigeration at room temperature. *Cryogenics*, 35(2):101–104, 1995.

[37] C.P. Jeffreson. Prediction of breakthrough curves in packed beds: I. applicability of single parameter models. *American Institute of Chemical Engineers Journal*, 18(2):409–416, 1972.

[38] K. Engelbrecht, G.F. Nellis, and S.A. Klein. The effect of internal temperature gradients on regenerator matrix performance. *Journal of Heat Transfer*, 128(10):1060–1069, 2006.

[39] L. Zhang, S. A. Sherif, A.J. DeGregoria, C.B. Zimm, and T. N. Veziroglu. Design optimization of a 0.1-ton/day active magnetic regenerative hydrogen liquefier. *Cryogenics*, 40(4-5):269–278, 2000.

[40] J. He, J. Chen, and C. Wu. The influence of heat-transfer laws on the performance characteristics of a magnetic stirling refrigeration cycle. *International Journal of Ambient Energy*, 24(2):75–82, 2003.

[41] L. Zhang, S.A. Sherif, T. N. Veziroglu, and J. W. Sheffield. Second law analysis of active magnetic regenerative hydrogen liquefiers. *Cryogenics*, 33(7):667–674, 1993.

[42] Z. Yan and J. Chen. The characteristics of polytropic magnetic refrigeration cycles. *Journal of Applied Physics*, 70(4):1911–1914, 1991.

[43] Z. Yan and J. Chen. The effect of field dependent heat capacity on the characteristics of the ferromagnetic Ericsson refrigeration cycle. *Journal of Applied Physics*, 72(1):1–5, 1992.

[44] F. Shir, L. Yanik, R.D. Shull, L.H. Bennett, and E.D. Torre. Room temperature active regenerative magnetic refrigeration: Magnetic nanocomposites. *Journal of Applied Physics*, 93(10):8295–8297, 2003.

[45] A.M. Rowe and J. A. Barclay. Ideal magnetocaloric effect for active magnetic regenerators. *Journal of Applied Physics*, 93(3):1672–1676, 2003.

[46] K.K. Nielsen, J. Tusek, K. Engelbrecht, S. Schopfer, A. Kitanovski, C.R.H. Bahl, A. Smith, N. Pryds, and A. Poredos. Review on numerical modeling of active magnetic regenerators for room temperature applications. *International Journal of Refrigeration*, 34(3):603–616, 2011.

[47] J.P. Harvey, C.S. Kirkconnell, and P.V. Desai. A fast and accurate regenerator numerical model. In R.G. Ross, editor, *Cryocoolers 13*, pages 455–461. Springer US, 2005.

[48] K. Muralidhar and K. Suzuki. Analysis of flow and heat transfer in a regenerator mesh using a non-Darcy thermally non-equilibrium model. *International Journal of Heat and Mass Transfer*, 44(13):2493–2504, 2001.

[49] S.K. Andersen, H. Carlsen, and P.G. Thomsen. Numerical study on optimal stirling engine regenerator matrix designs taking into account the effects of matrix temperature oscillations. *Energy Conversion and Management*, 47(7-8):894–908, 2006.

[50] J.D. Jones. Performance of a stirling engine regenerator having finite mass. *Journal of Engineering for Gas Turbines and Power*, 108(4):669–673, 1986.

[51] S. Whitaker. Forced convection heat transfer correlations for flow in pipes, past flat plates, single cylinders, single spheres, and for flow in packed beds and tube bundles. *American Institute of Chemical Engineers Journal*, 18(2):361–371, 1972.

[52] D.G. Osborne and F.P. Incropera. Laminar, mixed convection heat transfer for flow between horizontal parallel plates with asymmetric heating. *International Journal of Heat and Mass Transfer*, 28(1):207–217, 1985.

[53] T.F. Petersen, N. Pryds, A. Smith, J. Hattel, H. Schmidt, and H.J. Høgaard Knudsen. Two-dimensional mathematical model of a reciprocating room-temperature active magnetic regenerator. *International Journal of Refrigeration*, 31(3):432–443, 2008.

[54] P.A. Oliveira, P.V. Trevizoli, J.R. Barbosa Jr., and A.T. Prata. Numerical analysis of a reciprocative active magnetic regenerator. In P.W. Egolf, editor, *Proceedings of the Third IIF-IIR International Conference on Magnetic Refrigeration at Room Temperature*, pages 283–294, 2009.

[55] K.K. Nielsen, C.R.H. Bahl, A. Smith, R. Bjørk, N. Pryds, and J. Hattel. Detailed numerical modeling of a linear parallel-plate active magnetic regenerator. *International Journal of Refrigeration*, 32(6):1478–1486, 2009.

[56] T.F. Petersen, K. Engelbrecht, C.R.H. Bahl, B. Elmegaard, N. Pryds, and A. Smith. Comparison between a 1D and a 2D numerical model of an active magnetic regenerative refrigerator. *Journal of Physics D: Applied Physics*, 41:105002, 2008.

[57] D. Gedeon. Flow circulations in foil-type regenerators produced by non-uniform layer spacing. In R.G. Ross, editor, *Cryocoolers 13*, pages 421–430. Springer US, 2005.

[58] S. Backhaus and G.W. Swift. Fabrication and use of parallel plate regenerators in thermoacoustic engines. *Proceedings of the 36th Intersociety Energy Conversion Engineering Conference*, 1:453–458, 2001.

[59] F. Duprat and G. Lopez Lopez. Comparison of performance of heat regenerators: Relation between heat transfer efficiency and pressure drop. *International Journal of Energy Research*, 25(4):319–329, 2001.

[60] J.A. Barclay and S. Sarangi. Selection of regenerator geometry for magnetic refrigerator applications. *Cryogenic Processes and Equipment*, pages 51–58, 1984.

[61] I. Ruhlich and H. Quack. Investigations on regenerative heat exchangers. In R.G. Ross, editor, *Cryocoolers 10*, pages 265–274. Springer US, 2002.

[62] K. Engelbrecht, J.B. Jensen, C.R.H. Bahl, and N. Pryds. Experiments on a modular magnetic refrigeration device. In P.W. Egolf, editor, *Proceedings of the Third IIF-IIR International Conference on Magnetic Refrigeration at Room Temperature*, pages 431–436, 2009.

[63] J.Y. Bouguet. *Camera Calibration Toolbox for Matlab Documentation.* Computer Vision Research Group, Dept. of Electrical Engineering, California Institute of Technology, 2010.

[64] C.R.H. Bahl, T.F. Petersen, N. Pryds, and A. Smith. A versatile magnetic refrigeration test device. *Review of Scientific Instruments*, 79, 2008.

[65] T. Okamura, K. Yamada, N. Hirano, and S. Nagaya. Performance of a room-temperature rotary magnetic refrigerator. *International Journal of Refrigeration*, 29(8):1327–1331, 2006.

[66] A.M. Rowe, A. Dikeos, and A. Tura. Experimental studies of a near-room temperature magnetic refrigeration. In P.W. Egolf, editor, *Proceedings of the First IIF-IIR International Conference on Magnetic Refrigeration at Room Temperature*, page 325–334, 2005.

[67] C. Zimm, A. Boeder, J. Chell, A. Sternberg, A. Fujita, S. Fujieda, and K. Fukamichi. Design and performance of a permanent magnet rotary refrigerator. *International Journal of Refrigeration*, 29:1302–1306, 2006.

[68] K.K. Nielsen, C.R.H. Bahl, A. Smith, N. Pryds, and J. Hattel. A comprehensive parameter study of an active magnetic regenerator using a 2D numerical model. *International Journal of Refrigeration*, 33(4):753–764, 2010.

[69] M.A. Richard, A.M. Rowe, and R. Chahine. Magnetic refrigeration: Single and multimaterial active magnetic regenerator experiments. *Journal of Applied Physics*, 95(4):2146–2150, 2004.

[70] G.H. Yao, M.Q. Gong, and J.F. Wu. Experimental study on the performance of a room temperature magnetic refrigerator using permanent magnets. *International Journal of Refrigeration*, 29:1267–1273, 2006.

[71] K. Engellbrecht, C.R.H. Bahl, and K.K. Nielsen. Experimental results for a magnetic refrigerator using three different types of magnetocaloric material regenerators. *International Journal of Refrigeration*, 34:1132–1140, 2011.

[72] M. Frischmann. *Heat Transfer Coefficient Using Liquid Heat Transfer Fluids for use in Active Magnetic Regenerative Refrigeration*. PhD thesis, University of Wisconsin-Madison, 2009.

[73] Q. Gao, B.F. Yu, C.F. Wang, B. Zhang, D.X. Yang, and Y. Zhang. Experimental investigation on refrigeration performance of a reciprocating active magnetic regenerator of room temperature magnetic refrigeration. *International Journal of Refrigeration*, 29:1274–1285, 2006.

[74] K.K. Nielsen, R. Bjørk, J.B. Jensen, C. R. H Bahl, N. Pryds, A. Smith, A. Nordentoft, and J. Hattel. Magnetic cooling at Risø DTU. In *Proceedings of the 8th IIR Gustav Lorentzen Conference on Natural Working Fluids*, 2008.

[75] D. Christensen, K.K. Nielsen, C.R.H. Bahl, and A. Smith. Demagnetizing effects in stacked rectangular prisms. *Journal of Physics D: Applied Physics*, 44, 2011.

[76] W.M. Haynes and D.R. Lide, editors. *CRC Handbook of Chemistry and Physics*. Taylor and Francis Group, LLC, 91st edition, 2010.

[77] P.L. Mangonon and G. Thomas. Structure and properties of thermal-mechanically treated 304 stainless steel. *Metallurgical Transactions*, 1:1587–1594, 1970.

[78] J.B. Jensen, K. Engelbrecht, C.R.H. Bahl, N. Pryds, G.F. Nellis, S.A. Klein, and B. Elmegaard. Modeling of parallel-plate regenerators with non-uniform plate distributions. *International Journal of Heat and Mass Transfer*, 53(23-24):5065–5072, 2010.

[79] J.B. Jensen, C.R.H. Bahl, K. Engelbrecht, B. Elmegaard, and N. Pryds. Analysis of single blow effectiveness in non-uniform parallel plate regenerators. *International Journal of Heat and Mass Transfer*, In press, 2011.

[80] K.K. Nielsen, K. Engelbrecht, D.V. Christensen, and J.B. Jensen. Degradation of the performance of microchannel heat exchangers due to flow maldistribution. *In preparation*.

[81] Comsol AB, Göteborg, Sweden. *Comsol Physics User's Guide*, 2008. version 3.5a.

[82] T.A. Davis. A column pre-ordering strategy for the unsymmetric-pattern multifrontal method. *ACM Transactions on Mathematical Software*, 30(2):165–195, 2004.

[83] D.W. Pepper and J.C. Heinrich. *The Finite Element Method*. Taylor and Francis Group, LLC, 2006.

[84] A.L. Nayak and P. Cheng. Finite element analysis of laminar convective heat transfer in vertical ducts with arbitrary cross-sections. *International Journal of Heat and Mass Transfer*, 18(2):227–236, 1975.

[85] H.M.S. Bahaidarah, M. Ijaz, and N.K. Anand. Numerical study of fluid flow and heat transfer over a series of in-line noncircular tubes confined in a parallel-plate channel. *Numerical Heat Transfer, Part B Fundamentals*, 50(2):97–119, 2006.

[86] G. Saha, S. Saha, M. Quamrul Islam, and M.A. Razzaq Akhanda. Natural convection in enclosure with discrete isothermal heating from below. *Journal of Naval Architecture and Marine Engineering*, 4:1–13, 2007.

[87] C. Zhang and H.P. Wang. Robust design of assembly and machining tolerance allocations. *IIE Transactions*, 30:17–29, 1998.

[88] The MathWorks Inc., Natick, Massachusetts. MATLAB, version 7.10.0, 2010.

[89] M. Matsumoto and T. Nishimura. Mersenne twister: A 623-dimensionally equidistributed uniform pseudorandom number generator. *ACM Transactions on Modeling and Computer Simulation*, 8:3–30, 1998.

[90] G. Marsaglia and W.W. Tsang. The ziggurat method for generating random variables. *Journal of Statistical Software*, 5:1–7, 2000.

[91] C.R.H. Bahl, K. Engelbrecht, R. Bjørk, D. Eriksen, A. Smith, and N. Pryds. Design concepts for a continuously rotating active magnetic regenerator. In P.W. Egolf, editor, *Proceedings of the Fourth IIF-IIR International Conference on Magnetic Refrigeration at Room Temperature*, pages 351–358, 2010.

[92] P. Clot, D. Viallet, F. Allab, A. Kedous-Lebouc, J.M. Fournier, and J.P. Yonnet. A magnet-based device for active magnetic regenerative refrigeration. *IEEE Transactions on Magnetics*, 39(5):3349–3351, 2003.

[93] Y.B. Tang, Y.G. Chen, B.M. Wang, Q.X. Xue, and M.J. Yu. A room-temperature magnetic refrigerator using heat exchange of free convection. In A. Poredos and A. Sarlah, editors, *Proceedings of the Second IIF-IIR International Conference on Magnetic Refrigeration at Room Temperature*, volume 1, pages 359–362, 2007.

[94] C. Zimm, J. Auringer, A. Boeder, J. Chells, S. Russek, and A. Sternberg. Design and initial performance of a magnetic refrigerator with a rotating permanent magnet. In A. Poredos and A. Sarlah, editors, *Proceedings of the Second IIF-IIR International Conference on Magnetic Refrigeration at Room Temperature*, page 341–347, 2007.

[95] G.F. Nellis and S.A. Klein. Regenerative heat exchangers with significant entrained fluid heat capacity. *International Journal of Heat and Mass Transfer*, 49:329–340, 2006.

[96] D.E. Daney and R. Radebaugh. Non-ideal regenerator performance- the effect of void volume fluid heat capacity. *Cryogenics*, 24 (9):499–501, 1984.

[97] B.S. Baclic and G.D. Dragutinovic. *Operation of Counterflow Heat Exchangers*. Computational Mechanics Publications, 1998.

[98] B.S. Baclic and G.D. Dragutinovic. Asymmetric-unbalanced counterflow thermal regenerator problem: Solution by the Galerkin method and meaning of dimensionless parameters. *International Journal of Heat and Mass Transfer*, 34(2):483–498, 1991.

[99] H. Hausen. *Heat exchangers: design and theory sourcebook*, chapter Survey of the heat transfer theories in regenerators, pages 207–222. McGraw-Hill, 1975.

[100] P.J. Heggs and D. Burns. Single-blow experimental prediction of heat transfer coefficients: A comparison of four commonly used techniques. *Experimental Thermal and Fluid Science*, 1:243–251, 1988.

[101] P. Jacobsson and B. Sundqvist. Thermal conductivity and electrical resistivity of gadolinium as functions of pressure and temperature. *Physical Review B: Condensed Matter and Materials Physics*, 40(14):9541–9551, 1989.

[102] R.H. Bogaard, P.D. Desai, H.H. Li, and C.Y. Ho. Thermophysical properties of stainless steels. *Thermochimica Acta*, 218:373–393, 1993.

[103] Å. Melinder, editor. *Thermophysical Properties of Liquid Secondary Refrigerants*. Tables and Diagrams for the Refrigeration Industry. International Institute of Refrigeration, 1997.

Appendix A

Material Properties

This table lists the thermal properties of all the materials used in either simulations or experiments in this thesis. Unless otherwise specified, all properties are evaluated under atmospheric conditions, at a temperature of 20°C, and in zero field. The water/ethylene glycol is a mixture of 25 %, by volume, of ethylene glycol (commercial antifreeze) and 75 % water.

Material	**Property**	**Value**	**Unit**	**Reference**
Gadolinium	density	7900	kg/m^3	[76][a]
	thermal conductivity	10	W/(m K)	[101]
	specific heat capacity	240	J/(kg K)	[76][a]
Stainless steel	density	7900	kg/m^3	[76]
	thermal conductivity	15	W/(m K)	[76]
	specific heat capacity	500	J/(kg K)	[102]
Aluminum	density	2700	kg/m^3	[76]
	thermal conductivity	240	W/(m K)	[76]
	specific heat capacity	900	J/(kg K)	[76]
Water	density	1000	kg/m^3	
	thermal conductivity	0.6	W/(m K)	[76]
	specific heat capacity	4200	J/(kg K)	[76]
Water/ethylene glycol	density	1030	kg/m^3	[103]
	thermal conductivity	0.4	W/(m K)	[103]
	specific heat capacity	3900	J/(kg K)	[103]

Table A.1: Thermal properties of materials used in simulations and experiments. All properties are evaluated in zero field and at 20°C, unless another temperature is noted.

[a] evaluated at 25°C

Appendix B

Publications

This appendix contains a number of publications that has been published in connection with the Ph.D. project presented in this thesis. First, articles that have been published in peer-reviewed scientific journals are listed in chronological order and then an article published in conference proceedings is listed.

List of publications

B.1 Modeling of Parallel-Plate Regenerators with Non-Uniform Plate Distributions

This article was published in International Journal of Heat and Mass Transfer in November 2010. The article covers the modeling of the fixed regenerator geometries that was also described in Chapter 6 and the modeling of the regenerators with nominal normal geometries, i.e. the geometries that have the same parameters as the fixed geometries, but are generated from normal distributions. The latter geometries are described in Section 7.2.

International Journal of Heat and Mass Transfer 53 (2010) 5065–5072

Contents lists available at ScienceDirect

International Journal of Heat and Mass Transfer

journal homepage: www.elsevier.com/locate/ijhmt

Modeling of parallel-plate regenerators with non-uniform plate distributions

Jesper B. Jensen [a,*], Kurt Engelbrecht [a], Christian R.H. Bahl [a], Nini Pryds [a], Gregory F. Nellis [b], Sanford A. Klein [b], Brian Elmegaard [c]

[a] Fuel Cells and Solid State Chemistry Division, Risø National Laboratory for Sustainable Energy, Frederiksborgvej 399, P.O. Box 49, Building 779, DK-4000 Roskilde, Denmark
[b] Department of Mechanical Engineering, University of Wisconsin-Madison, Engineering Research Building, 1500 Engineering Drive, Madison, WI 53706-1687, USA
[c] Department of Mechanical Engineering, Technical University of Denmark, Nils Koppels Allé, Building 404, DK-2800 Kgs. Lyngby, Denmark

ARTICLE INFO

Article history:
Received 30 November 2009
Received in revised form 28 June 2010
Accepted 16 July 2010
Available online 17 August 2010

Keywords:
Regenerator
Modeling simulation
Distribution
Non-uniform
Performance

ABSTRACT

A two-dimensional finite element model describing the performance of parallel-plate regenerators with arbitrary channel width distributions has been developed in order to investigate the effect of non-uniform plate spacing on the performance of regenerators. Results for a series of hypothetical plate spacing distributions are presented in order to understand the impact of spacing non-uniformity. Simulations of more realistic distributions where the plate spacings follow normal distributions are then discussed in order to describe the deviation of the performance of a regenerator relative to one with uniform spacing as a function of the standard deviation of the plate distribution. It has been shown that the most significant reduction in performance occurs when a volume of fluid between 100% and 200% of the regenerator void volume is displaced in a single blow.

1. Introduction

Regenerators are found in numerous applications in different fields, ranging from cryocoolers [1] to dehumidifiers [2]. Extensive effort has been put into the development of mathematical models of regenerators that are generally applicable and take into account the complex heat transfer interactions that occur between the matrix and the fluid, see e.g. [3,4]. Parallel-plate regenerators with small dimensions (spacings of 1 mm or less) are receiving interest for several applications because of their theoretically high thermal performance (i.e., high heat transfer coefficient due to a large specific surface area) with low pressure drops [5,6]. The geometry has been investigated as a means to reduce regenerator size in various regenerator systems, particularly in active magnetic regenerative refrigerators. Although the theoretical performance of parallel-plate regenerators is high [7,8], the experimentally measured performance is typically less than what is expected [7,9]. It is generally accepted that flow maldistribution of the heat transfer fluid caused by non-uniformity in the flow channel widths is one of the causes of the discrepancy. This paper studies the effect of non-uniform flow channel distribution on the performance of a parallel-plate regenerator undergoing a single-blow process.

There will always be some degree of variation in plate spacing and plate flatness that results from the fabrication of a parallel-plate regenerator, which causes non-uniform channels for the flow of the heat transfer fluid. As the spacing becomes smaller, the relative variation in plate spacing becomes larger assuming the same manufacturing techniques and tolerance. Many models that examine parallel-plate regenerators are based on a repeating single channel or are one dimensional and therefore require a correlation in order to calculate the heat transfer coefficient. The correlation is the embodiment of a separate solution to the detailed differential equations for mass, momentum, and energy under some limiting conditions (e.g., steady-state, negligible axial conduction, etc.) that may not be appropriate for parallel-plate regenerators with non-uniform plate spacing. Only a few models consider the effect of non-uniform plate spacings. Gedeon [7] has examined the effect of having two halves of a regenerator with different plate spacings in a Stirling-type cryocooler. In this case, reductions in COP of 15% or more were found for regenerators with plate spacing variations that are only ±10% of the nominal plate spacing. Backhaus and Swift [10] have examined fabrication and testing procedures for thermoacoustic Stirling engines, where ±10% deviations in plate spacing lead to ~30% variations in flow resistance.

In order to investigate the effect of non-uniform plate spacing, a two-dimensional transient model of a single-blow process in a parallel-plate regenerator has been developed using the finite element modeling software Comsol Multiphysics [11]. The model accounts

* Corresponding author. Tel.: +45 4677 4762.
E-mail address: jbuj@risoe.dtu.dk (J.B. Jensen).

0017-9310/$ - see front matter © 2010 Elsevier Ltd. All rights reserved.
doi:10.1016/j.ijheatmasstransfer.2010.07.058

Nomenclature

c	specific heat capacity (J/kg K)
E	internal energy (J)
k	thermal conductivity (W/m K)
L	length (m)
m	mass (kg)
N	number of channels
$\dot{q}$	heat transfer rate (W)
s_N	standard deviation of width (mm)
t	time (s)
T	temperature (K)
w	width (mm)
u	fluid velocity (m/s)
$\bar{u}$	average fluid velocity in channel (m/s)
$\dot{V}'$	volumetric fluid flow rate per unit depth (m^2/s)
x	spatial dimension along axial direction (m)
y	spatial dimension along transverse direction (m)
Greek symbols	
Δ	difference
ε	regenerator effectiveness
ρ	density (kg/m^3)
Φ	utilization
Subscripts	
ch	channel
f	fluid
i	channel or plate index
in	inlet
init	initial
max	maximum
ov	overall
pl	plate
s	solid
t	transferred across internal boundaries
tot	total
uni	uniform case

for dispersion and conduction in the fluid in both the axial and transverse directions as well as axial conduction in the plates. Transverse conduction in the plates has been found to have an insignificant effect on the heat transfer (for the geometry and materials used here), and the temperature gradient associated with transverse conduction in the plates has therefore been modeled using only a single element. The model consists of a total of 10 regenerator plates (9 whole plates and 2 half plates) and 10 channels. The paper focuses on the impact of the distribution of the channels on the performance of the device.

This paper is meant to be a general study of the performance of parallel-plate regenerators with non-uniform distributions. However, the baseline conditions used to carry out the simulation are based on materials and regenerator geometries that are similar to those used in active magnetic regenerators (AMRs) for magnetic refrigeration [12]. AMRs require that a relatively high magnetic field is applied to the regenerator, and the cost and complexity of an AMR setup therefore depends strongly on the size of the regenerator. The performance per volume is crucial in such applications and therefore the plate spacings in parallel-plate AMRs are often very small and difficult to control with high precision. This combination creates a situation where large relative deviations in the plate spacing can exist, which can affect the performance of the regenerator strongly.

The aim of the paper is to describe the change in regenerator performance that results from spacing non-uniformity relative to the performance of the same regenerator with uniform spacing. The study was carried out for a regenerator with a specific geometry consisting of plates made of gadolinium and subjected to a flow of water. The results found in this study provide some insight into the behavior of such regenerators in situations where the deviation in the uniformity of the plate spacing is comparable to the size of the spacing.

2. Physical model and formulation

The modeled geometry consists of a stack of 11 individual plates, separated by 10 channels, and is illustrated in Fig. 1. The model is 2-dimensional with fluid flow along the x-direction and the y-direction perpendicular to the channel. The width of the first and last plates is only half of the width of the rest of the plates and these end plates have fluid contacting only one side.

The temperature in the regenerator is found by solving the governing equations for transient heat transfer in the solid and the fluid parts of the regenerator, respectively. The governing equation in the solid is

$$\rho_s c_s \frac{\partial T_s}{\partial t} - k_s \nabla^2 T_s = 0, \tag{1}$$

where ρ_s is the density of the plate, c_s is the specific heat capacity of the plate, T_s is the temperature, t is time, and k_s is the thermal conductivity of the plate. The governing equation in the fluid is

$$\rho_f c_f \frac{\partial T_f}{\partial t} - k_f \nabla^2 T_f = -\rho_f c_f u \frac{\partial T_f}{\partial x}, \tag{2}$$

where ρ_f is the density of the fluid, c_f is the specific heat capacity of the fluid, T_f is the fluid temperature, k_f is the thermal conductivity of the fluid, and u is the local fluid velocity.

The fluid flow has been modeled for a situation where all the channels are connected to the same hot and cold reservoirs and where the overall fluid flow rate is constant. This means that the pressure drop along each channel is identical for all channels in a given regenerator, but also, since the total volumetric flow rate is kept constant, that the pressure drop may vary from one regenerator to another.

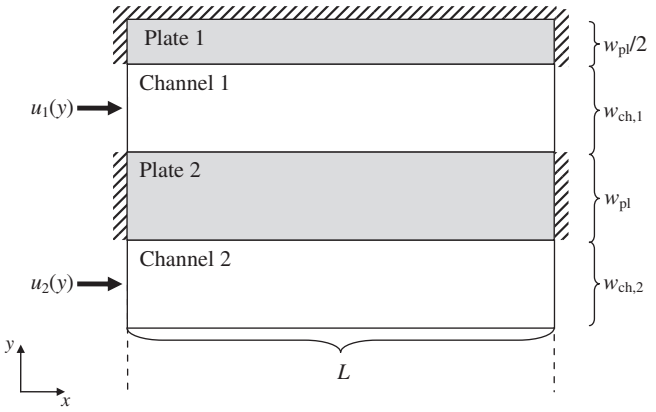

Fig. 1. Illustration of the geometry of the regenerator (not to scale). The geometry repeats up to Plate 11, which, like Plate 1, is of width $\frac{w_{pl}}{2}$.

The applied velocity profile is fully developed throughout the whole regenerator. Regardless of the inlet velocity profile, the flow will become fully developed within the first few nodes in the model, so it is assumed that the results obtained using this profile will be applicable for regenerators with different inlet velocity profiles as well.

The velocity profile has been calculated analytically and used as input to the model. A solution to the momentum equation, where it is assumed that the flow is laminar, incompressible, and viscous and that the fluid properties are constant has been used. The fluid velocity within the ith channel, u_i, is given by

$$u_i(y) = u_{\max,i}\left(1 - 4\frac{(y - y_i)^2}{w_{\mathrm{ch},i}^2}\right), \tag{3}$$

where y_i is the y-coordinate in the middle of the ith channel, and $w_{\mathrm{ch},i}$ is the width of the ith channel. $\dot{V}'$ is the total volumetric flow rate per unit length in the transversal direction not modeled (the z-direction), and the maximum fluid velocity in the ith channel is given by

$$u_{\max,i} = \frac{3w_{\mathrm{ch},i}^2}{2\sum_{i=1}^{N}\left(w_{\mathrm{ch},i}^3\right)}\dot{V}'. \tag{4}$$

The solid and the fluid are initially at the same temperature, T_{init}, throughout the whole regenerator. At time $t = 0$, fluid begins to enter the channels at an inlet temperature, T_{in}, that is lower than the initial temperature. When the fluid leaves the regenerator, it is assumed that the convective heat flux is much larger than the conductive heat flux, such that the thermal conduction at the regenerator outlet is negligible. Furthermore, no exchange of heat with the surroundings is assumed, so all other external boundaries are adiabatic and the heat flux is continuous across all internal domains.

The material properties are assumed to be constant with values consistent with those at room temperature. The reason for choosing constant material properties is that in the range of temperature where the regenerator operates, i.e., around room temperature, the effects of temperature variations are assumed to be negligible. Also, the primary objective is to study the impact of plate spacing variation and this effect can be examined without including the complications associated with non-uniform properties. Eqs (1) and (2) are solved using the UMFPACK method (version 4.2) [13] with Comsol Multiphysics. The governing equations are discretized according to a predefined mesh consisting of a number of rectangular elements. At each intersection of the mesh lines, the governing equations are solved using the finite element method with the commercially available software.

Since the accuracy of the model is sensitive to the discretization of the mesh and time step size, a sensitivity analysis was carried out to assure that the solution to the model was accurate with the selected mesh configuration. Based on this analysis, the mesh in the model was chosen to consist of 128 elements in the axial direction, eight elements across each channel in the transverse direction, and a single element across each plate in the transverse direction. The maximum time step taken by the solver was chosen to be 0.005 s. The CFL number, which is the ratio of the length that the heat wave travels in a single time step to the size of the mesh elements in that direction, is $u\Delta t/\Delta x = 0.64$. This mesh and time step configuration has been chosen based on the sensitivity analysis because it provides deviations in the energy balance of less than 1% over a wide range of regenerator geometries. It has been found that the maximum deviation in the energy balance for all simulations performed in this paper occurs in the regenerator with the 5,5 configuration (see Section 3 below) and is at most 0.74% during the simulation. The materials properties, the simulation parameters, and the geometry of the regenerator used in the simulations are shown in Table 1.

Table 1
Values of constant properties and parameters.

Parameter	Symbol	Value	Unit
Geometric dimensions			
Length of regenerator	L	0.1	m
Porosity		0.5	–
Mean channel width		1×10^{-3}	m
Plate width	w_{pl}	1×10^{-3}	m
Material properties			
Conductivity of fluid[a]	k_f	0.6	W/m K
Density of fluid	ρ_f	1000	kg/m^3
Specific heat capacity of fluid[a]	c_f	4200	J/kg K
Conductivity of solid[b]	k_s	10	W/m K
Density of solid[c]	ρ_s	7900	kg/m^3
Specific heat capacity of solid[c]	c_s	240	J/kg K
Operating conditions			
Initial temperature	T_{init}	277.15	K
Inlet temperature	T_{in}	273.15	K
Total flow rate per unit depth	$\dot{V}'$	5×10^{-5}	m^2/s
Simulation parameters			
Solution time step		0.1	s
Simulation time		50	s
Max solver time step		5×10^{-5}	s

[a] From [14], evaluated at 20 °C.
[b] From [15], evaluated at 20 °C.
[c] From [14], evaluated at 25 °C.

One of the assumptions used when developing the model is that conduction in the transverse direction in the plates can be neglected (i.e., that the plates are almost uniform in temperature in the y-direction). In order to verify that the error associated with this assumption is not significant, a model identical to the current model, but with eight elements in each plate (in the y-direction) has been run with the 5,5-distribution (see Table 2). The reason for choosing the 5,5-distribution is that it gives the largest temperature difference between two channels, and therefore is expected to have the largest plate temperature gradient. In this model, transverse conduction in the plate is not neglected, and the results of the simulation show that the maximum temperature difference within the plate never exceeds 0.14 K at any axial location other than the inlet boundary where the temperature is discontinuous at time $t = 0$ due to the initial and boundary conditions. Neglecting the conduction in the transverse direction is therefore justified. In order to provide an additional validation of the model, the Nusselt number has been calculated for a regenerator with uniform distribution and constant plate temperature. The calculated overall Nusselt number for this regenerator converges toward a value of 7.64 as the flow becomes thermally fully developed; this value is within 1.4% of the accepted value of 7.54 for thermally and hydrodynamically fully developed flow between parallel plates with constant temperature [16].

3. Simulations

The geometry and materials of the regenerator that has been modeled are similar to those used in the experimental setup described in [17] and consist of water flowing over a gadolinium matrix (gadolinium is a widely used benchmark material for AMR matrices). Choosing a specific set of geometrical and material parameters limits the generality of the study, but gives qualitative insight to the heat transfer effects in regenerators in general. A series of regenerators with various fixed distributions of plate spacings has been modeled in order to understand the impact of channel distribution on regenerator performance. Subsequently, a

Table 2
Channel widths and standard deviations of simulated distributions.

Distribution	Standard deviation (mm)	Channel width (mm)									
Uniform	0	1	1	1	1	1	1	1	1	1	1
Alternating	0.21	0.8	1.2	0.8	1.2	0.8	1.2	0.8	1.2	0.8	1.2
2,2	0.21	0.8	1.2	1.2	0.8	0.8	1.2	1.2	0.8	0.8	1.2
3,1	0.21	0.8	0.8	0.8	1.2	1.2	1.2	0.8	1.2	0.8	1.2
5,5	0.21	0.8	0.8	0.8	0.8	0.8	1.2	1.2	1.2	1.2	1.2
Normal (1)	0.05	20 different, randomly generated									
Normal (2)	0.10	20 different, randomly generated									
Normal (3)	0.15	20 different, randomly generated									
Normal (4)	0.20	20 different, randomly generated									

number of simulations were run in which the regenerator plate spacing distribution was randomly assigned using a normal distribution with various standard deviations. These simulations were modeled in order to investigate the impact of plate distribution on performance in more realistic scenarios. These scenarios are, of course, only realistic in terms of the distributions of plate spacings. The model still assumes that the plates are perfectly flat and parallel, which is not necessarily the case in real regenerators.

Four different fixed distributions, all using two different channel widths, 0.8 mm (narrow) and 1.2 mm (wide), have been modeled. The distributions of narrow and wide channels were as follows: (1) alternating wide and narrow channels (termed "Alternating" in the paper), (2) a repeating configuration with two wide channels followed by two narrow channels followed by two wide channels followed by two narrow channels with single channels at the top (wide) and bottom (narrow) that ensure symmetry (termed "2,2" in the paper), (3) three adjacent narrow channels and three adjacent wide channels followed by alternating channels (termed "3,1" in the paper), and (4) five adjacent wide channels followed by five adjacent narrow channels (termed "5,5" in the paper). In each distribution above, the same number of wide and narrow channels is used and therefore the standard deviation of each of these distributions is the same, 0.21 mm, for the channel widths of 0.8 mm and 1.2 mm. Each of these simulations therefore has the same mean and standard deviation and yet the results show that the performance varies based on the sequence of wide and narrow channels.

Four different normal distributions have also been modeled. The normal distributions have mean widths of 1 mm and standard deviations of 0.05 mm, 0.10 mm, 0.15 mm, and 0.20 mm. The specific distribution of the channel width is randomly generated for each simulation using the mean and standard deviation. Due to limitations in computational capabilities, only 10 channels have been modeled in each simulation. However, because only 10 channels are modeled, there are some variations in the performance of the regenerators with normal distributions. That is, each time the distribution is randomly generated, the result will be different and so the performance will be different, even though the mean and standard deviation are the same. In order to reduce the uncertainty of the results, each normal distribution (i.e., each value of standard deviation) is simulated with 20 different randomly generated distributions, and the average of the resulting performances is reported. We have chosen to use 20 different distributions for each configuration as it has been found that this number gives an acceptable precision of the regenerator performance obtained for a given normal distribution.

Due to the symmetry boundary conditions at the top and bottom of the modeled regenerator, the distributions of the channel widths are effectively repeating (i.e., the simulation is consistent with an arbitrarily large regenerator having the same set of 10 plates mirrored and repeated over and over). This means that the random distributions are not random on a scale of more than 10 plates. However, as shown in Section 4 below, the effect of the width of a given channel on the heat transfer from a given plate diminishes quickly the further apart the plate and channel are. Therefore it is assumed that by using 10 channels, the overall effect of having a repeating geometry is negligible.

Preliminary simulation results with various plate widths, suggest that plate width has an insignificant impact on the performance compared to the channel width as long as the porosity is close to 0.5. In the present simulations the plate width was held constant while varying only the width of the channel. The different distributions that have been modeled are summarized in Table 2.

4. Results and discussion

In order to describe the performance of the regenerators in the most general way, the regenerator effectiveness has been used as a figure of merit. The regenerator effectiveness is defined as the ratio of the thermal energy transferred from the regenerator matrix to the fluid in a single blow to the maximum thermal energy that can be transferred, i.e.,

$$\varepsilon = \frac{E_t}{E_{tot}}, \tag{5}$$

where E_t is the thermal energy transferred from the matrix to the fluid and E_{tot} is the total thermal energy that can be transferred. The solution at any time step is the solution to a single blow with that particular period. Therefore, the effectiveness as a function of time can be written as

$$\varepsilon(t) = \frac{\int_0^t \dot{q}_t dt}{m_s c_s (T_{init} - T_{in})}, \tag{6}$$

where $\dot{q}_t$ is the heat transfer rate across the plate/channel interfaces and m_s is the mass of the matrix. The figure of interest, however, is the relative change in effectiveness as compared to a perfectly uniform regenerator, $\Delta\varepsilon = \varepsilon_{uni} - \varepsilon$. This quantity indicates how much of the regenerator performance is lost when the plate distribution becomes non-uniform. This difference is given as a function of the utilization, which is defined as

$$\Phi = \frac{\dot{m}_f c_f t}{m_s c_s}, \tag{7}$$

where $\dot{m}_f$ is the mass flow rate of the fluid. As the time, $t \to \infty$, $\Phi \to \infty$, and thus $E_t \to E_{tot}$. Therefore, it can be expected, that $\lim_{\Phi\to\infty} \varepsilon = 1$. For AMR applications, the optimal value of Φ is in the range $0.2 \leqslant \Phi \leqslant 1$ [18], and we thus expect that most AMRs operate within this range.

4.1. Fixed distributions

The temperature distributions in the regenerators with the fixed distributions are shown in Fig. 2 at the time where the utilization is unity. It can be seen that the heat transfer from the plates to the fluid is much larger for the wide channels than for the nar-

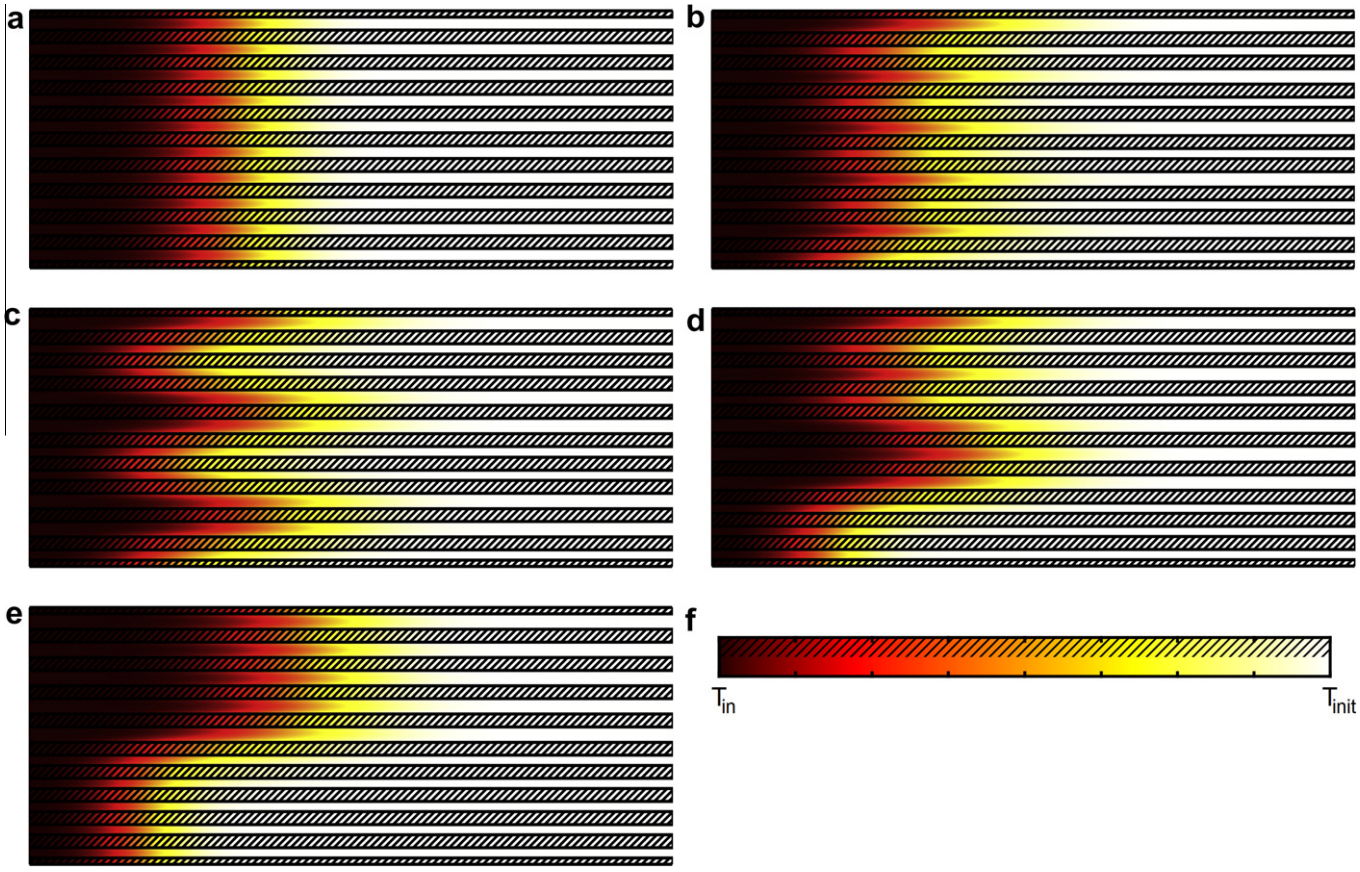

Fig. 2. Temperature profile in the regenerators with fixed distributions at $\Phi = 1$ (not to scale). The shaded areas are plates and the non-shaded areas are channels. (a) Uniform distribution; (b) alternating distribution; (c) 2,2-distribution; (d) 3,1-distribution; (e) 5,5-distribution.

row channels, which means that plates adjacent to wide channels cool down much faster than plates adjacent to narrow channels. This occurs because the fluid flow rate in the wide channels is significantly larger than the fluid flow rate in the narrow channels.

The model uses the initial and inlet temperatures 277.15 K and 273.15 K, respectively, but since the material properties are assumed to be constant, the temperatures are scalable, such that the results presented in this paper are applicable for any combination of initial and inlet temperatures.

Fig. 2a shows the uniform distribution and, as expected, all channels have identical temperature distributions. In Fig. 2b, which shows the temperature distribution in the alternating regenerator, it can be seen that the heat moves faster in the wide channels than in the narrow channels. Still, due to the symmetry, all of the narrow channels have almost identical temperature distributions, as do all of the wide channels. There is some asymmetry, mostly in the top and bottom channels, which is due to the mirror symmetry at the top and bottom boundaries. The mirror symmetry effectively means that there are two identical channels next to each other (on either side of the boundary), which breaks the alternating pattern and introduces the irregular heat flow at the edges. If the edge asymmetry is disregarded, the alternating distribution provides identical heat transfer conditions for all plates because every plate has one wide channel and one narrow channel next to it.

The 2,2-distribution, shown in Fig. 2c, has 5 plates which, like in the alternating regenerator, have one wide and one narrow channel. In this regenerator, however, 2.5 plates have two wide and 2.5 plates have two narrow neighboring channels (the top and bottom plates are only half plates). Since the narrow channels transfer less heat from the plates, the plates with two narrow channels will cool down much more slowly than the plates with two wide channels. This behavior will affect the temperature of the fluid in the channels, such that the plates with one wide and one narrow channel will experience a conductive heat flux from the narrow channel to the wide channel. This is not only making the overall heat transfer less efficient but can result in negative or infinite values of the local heat transfer coefficient if the temperature difference between two adjacent plates is too high, which makes the local regenerator performance difficult to assess. If calculated directly, the Nusselt number and the number of transfer units both become discontinuous and thus do not represent the system well.

Fig. 2d shows the 3,1-distribution, which not only has the same number of wide and narrow channels as the 2,2-distribution (and all the other fixed distributions, except the uniform), but also has the same number of plates with two narrow channels, plates with two wide channels, and plates with one narrow and one wide channel. In this distribution, however, the plates with only narrow channels and the plates with only wide channels are lumped together, as opposed to the 2,2-distribution, where they are evenly distributed.

In the 5,5-distribution, shown in Fig. 2e, there is only one plate with a wide and a narrow channel. The rest have either only wide or only narrow channels as their neighbors. This geometry increases the cooling rate of the plates with only wide channels, since most of the wide channels are not indirectly cooling the narrow channels (at least not to nearly the same degree). The cooling of the plates with only narrow channels, however, happen at a much slower rate because it is not being augmented by the wide channels; thus decreasing the overall rate of cooling.

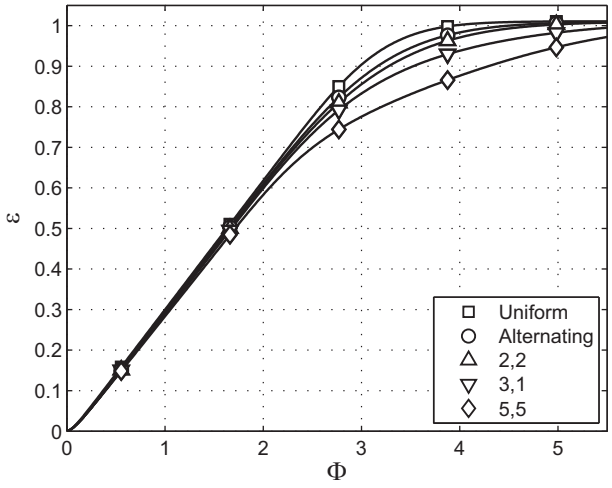

Fig. 3. Effectiveness of regenerators with fixed distributions as a function of utilization.

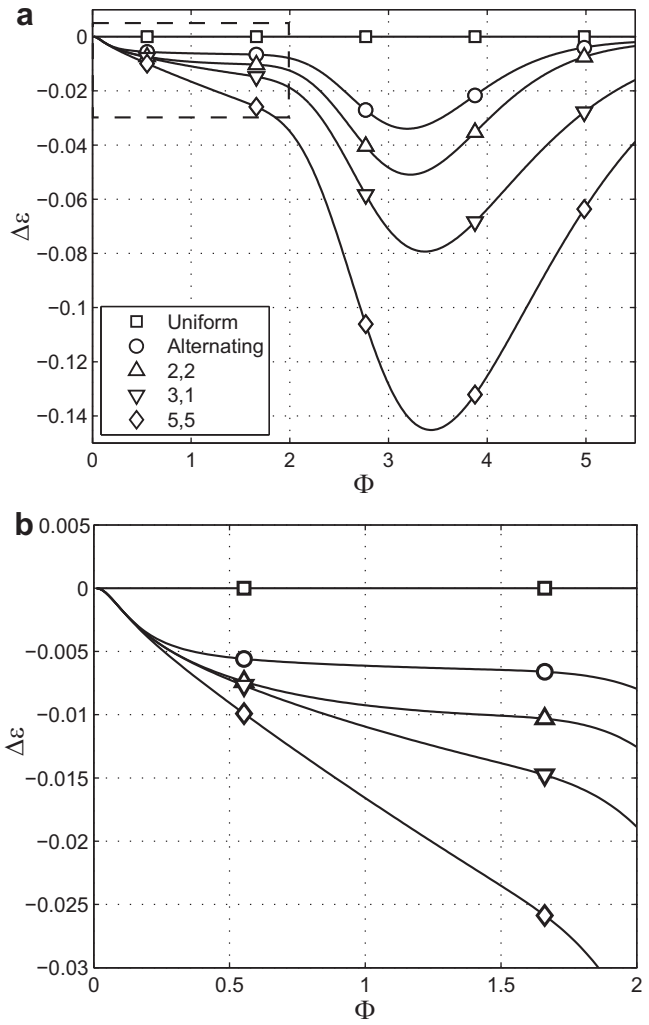

Fig. 4. (a) Change in effectiveness compared to a uniform plate spacing (defined as the relative difference in transferred energy) as a function of utilization in fixed distributions. (b) Cutout of selected area.

The regenerator effectiveness for each of the distributions in Fig. 2 is plotted as a function of utilization for the fixed distributions in Fig. 3. The difference in effectiveness of each of the distributions compared to the uniform distribution is plotted in Fig. 4. It can be seen that the regenerators with the more evenly distributed channel widths have better performances with the uniform distribution providing the best performance. The effectiveness is reduced by up to 14.5% for the 5,5-distribution, whereas the maximum reduction is only 3.4% for the alternating distribution and in between for the intermediate distributions 3,1 and 2,2. These results show that distributions with the same mean and standard deviation can be affected very differently by having non-uniform distributions of channels depending on the sequencing of the channels. If the regenerator geometry has many wide channels or many narrow channels together, then the impact on performance will be significantly larger than if the non-uniformity is distributed more evenly.

In the plots in Figs. 2 and 4, it can be seen that there is a certain spatial region within each distribution where most of the heat transfer is occurring at a particular time. This region of high heat transfer is moving from the inlet to the outlet as the simulation progresses. As long as this region remains within the regenerator the total rate of heat transfer will be approximately constant and therefore the reduction in performance will be approximately linear in time. This behavior is highlighted in Fig. 4b which shows that the decrease in performance is approximately linear in the interval $0.3 \lesssim \Phi \lesssim 1.6$.

For small utilizations, $\Phi \lesssim 0.5$, the fluid is just starting to enter, and the heat transfer from a plate to a given channel does not depend on the neighboring channels since the changes in temperature has not yet moved through the plates. All channels in the uniform regenerator will therefore experience the same heat transfer. In the non-uniform regenerators, all narrow channels will experience the same heat transfer and all wide channels will experience the same heat transfer, regardless of the widths of neighboring channels. After the utilization reaches approximately 0.2, the channels will start to experience different plate temperatures depending on the temperatures of the neighboring channels, and the effectiveness will begin to differ. This will happen first at the interfaces, where e.g. a narrow channel first will "see" that there is a wide channel at the other side of the plate. In the 2,2 and the 3,1-distributions, the numbers of plates with wide/narrow, narrow/narrow, and wide/wide channel combinations, however, is the same, which means that the heat transfer will not differ until the temperature change mediates all the way to the middle of the channel. The middle of the channel will at that time be affected by both neighboring channels and at that time (where $\Phi > 0.5$) the effectivenesses will start deviating. When the region of high heat transfer reaches the outlet, the contribution to the heat transfer from the wide channels decreases dramatically (because this part of the region leaves first). Because the narrow channels now contribute more to the heat transfer, the performance will decrease more rapidly until the entire region of high heat transfer has left the regenerator. After that, the remaining thermal energy will transfer slowly and eventually all of the regenerators will reach the same final temperature leading to $\Delta\varepsilon = 0$ as $\Phi \to \infty$. Since the more irregular distributions are less efficient, it takes longer for the region of high heat transfer to exit the regenerator, which means that the minimum $\Delta\varepsilon$ value shifts to higher values of Φ for the more irregular distributions.

To a first approximation, the number of identical channels adjacent to one another can be considered in order to rank the different distributions. The higher the number of adjacent identical channels, the higher $|\Delta\varepsilon|$ is observed. The 2,2 and 3,1-distributions, however, have the same number of adjacent identical channels, but still show different performances. This indicates, that the width of a given channel also has a significant effect on the heat transfer from plates that it is not directly adjacent to. However,

e.g. in the 5,5-distribution, the temperature profiles of the top and bottom channels that are far from narrow or wide channels, respectively, are practically identical, which indicates that the effect of channel width diminishes relatively quickly as a function of distance (or as a function of other channels that the effect must mediate through).

The regenerator studied in [7] is in some respects similar to the 5,5-regenerator in that it is separated into a part with only wide channels and a part with only narrow channels, except that the number of channels is larger. The model, however, is not completely comparable because it consists of multiple stages and features expansion of the heat transfer fluid, but the maximum reduction in performance observed for 20% deviations in channel width is approximately 20%, which is comparable to the maximum decrease found for the 5,5-regenerator.

4.2. Random distributions

Each of the random distributions has been simulated 20 times with different randomly generated distributions. The average value of $\Delta\varepsilon$ has been plotted as a function of Φ for all of the normal distributions that were considered in Fig. 5. The standard deviation of $\Delta\varepsilon$ for the 20 simulations is used to plot the bands surrounding each result.

The same general shape of the curves is seen for the random distributions as was observed for the fixed distributions shown in Fig. 4. The length of the linear region decreases with increasing standard deviation because the region of high heat transfer increases in size. Since the regularity of the distributions is the same, the maximum decrease in effectiveness occurs at the same Φ only its magnitude and spread changes with the standard deviation. Comparing the random distributions to the fixed distributions shows that a normal distribution is better than the 3,1-distribution and worse than the 2,2-distribution with the same standard deviations.

Ref. [9] covers a number of experiments performed on a regenerator similar to the regenerator examined in the current paper. The experiments were compared with a cyclical model of a regenerator including thermal losses to the surroundings (but assuming uniform regenerator geometry). Only the no-load temperature span was examined in these experiments, but it was found that the experimental data would start deviating at a utilization of approximately 0.5–0.6. The deviations would increase for increasing piston stroke lengths up to approximately 20% at a utilization of approximately 2. The performance of the regenerator is thus smaller than the one predicted from the model. These results illustrate the need for a model that takes into an account the deviation in the channels width as well as set of experiments which include plate distributions. This is our ongoing future work.

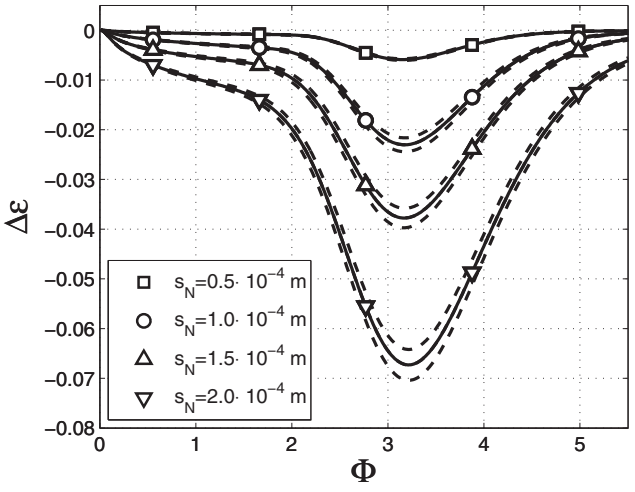

Fig. 5. Change in effectiveness of regenerators with normal distributions compared to a uniform regenerator as a function of utilization. The dashed bands are standard deviations.

5. Conclusion

A model describing the heat transfer in parallel-plate regenerators with arbitrary distributions of channel widths has been developed. The model has been checked for energy conservation and validated by comparison with the fully developed Nusselt number for parallel plates.

The heat transfer in a series of hypothetical channel distributions has been investigated in order to understand the effect of non-uniform spacing on regenerator performance. Furthermore, a series of realistic cases, where the deviations from uniformity are assigned randomly using a normal distribution with specific characteristics, has been investigated and used to establish a relationship between the manufacturing accuracy and the performance of regenerators.

It has been found that non-uniform distributions in regenerators degrade the performance relative to a regenerator with a uniform distribution – for the modeled regenerator geometry, by up to 3% under realistic operating conditions and up to 14% in all simulations. The reduction for the modeled geometry has been found to be greatest when $2 \lesssim \Phi \lesssim 5$, which is outside the optimal operating range. Furthermore, it has been found that the reduction not only depends on the standard deviation of the distribution, but also on the details of the distribution with regard to the sequence and order of wide and narrow channels.

The degree of non-uniformity of the plate spacings affects the performance in different stages. If we consider the fixed distributions, then, for very small utilizations, the performance simply depends on the number of wide and narrow channels, and, of course, on their sizes. For intermediate utilizations, the combination of neighboring channels also affects the performance, and for larger utilizations the second nearest neighbors also plays a role. The number of neighbors to consider increases with utilization, and the utilization for which more neighbors need to be considered depends on the particular regenerator (e.g. in a regenerator with infinite transverse conduction, all channels would have to be considered at all times).

Acknowledgements

The authors would like to acknowledge the support of the Programme Commission on Energy and Environment (EnMi) (Contract no. 2104-06-0032) which is part of the Danish Council for Strategic Research.

References

[1] R. Radebaugh, Development of the pulse tube refrigerator as an efficient and reliable cryocooler, Proc. Inst. Refrig. 96 (1999–2000) 11–31.
[2] S. Jain, P.L. Dhar, S.C. Kaushik, Evaluation of liquid desiccant based evaporative cooling cycles for typical hot and humid climates, Heat Recovery Syst. CHP 14 (6) (1994) 621–632.
[3] B.S. Baclic, P.J. Heggs, Unified regenerator theory and reexamination of the unidirectional regenerator performance, in: J.P. Hartnett, T.F. Irvine (Eds.), Advances in Heat Transfer, vol. 20, Academic Press Inc., 1990, pp. 133–179.
[4] T.E.W. Schumann, Heat transfer: a liquid flowing trough a porous prism, J. Franklin Inst. 308 (3) (1929) 405–416.
[5] F. Duprat, G.L. Lopez, Comparison of performance of heat regenerators: relation between heat transfer efficiency and pressure drop, Int. J. Energy Res. 25 (2001) 319–329.

[6] J.A. Barclay, S. Sarangi, Selection of Regenerator Geometry for Magnetic Refrigerator Applications, Cryogenic Processes and Equipment, ASME, 1984.
[7] D. Gedeon, Flow Circulations in Foil-Type Regenerators Produced by Non-Uniform Layer Spacing, Cryocoolers, vol. 13, Springer, US, 2004.
[8] I. Ruhlich, H. Quack, Investigations on Regenerative Heat Exchangers, Cryocoolers, vol. 10, Kluwer Academic/Plenum Publishers, New York, 1999.
[9] K.K. Nielsen, C.R.H. Bahl, A. Smith, R. Bjørk, N. Pryds, N. Hattel, Detailed numerical modeling of a linear parallel-plate active magnetic regenerator, Int. J. Refrig. 32 (6) (2009) 1478–1486.
[10] S. Backhaus, G.W. Swift, Fabrication and use of parallel plate regenerators in thermoacoustic engines, Proceedings of the 36th Intersociety Energy Conversion Engineering Conference, ASME, 2001.
[11] Comsol Multiphysics User's Guide, ver. 3.5a, Comsol AB, Göteborg, 2008.
[12] K.A. Gschneidner Jr., V.K. Pecharsky, A. Tsokol, Recent developments in magnetocaloric materials, Rep. Prog. Phys. 68 (6) (2005) 1479–1539.
[13] T.A. Davis, A column pre-ordering strategy for the unsymmetric-pattern multifrontal method, ACM Trans. Math. Softw. 30 (2) (2004) 165–195.
[14] D.R. Lide (Ed.), CRC Handbook of Chemistry and Physics, 90th ed., CRC Press, Taylor and Francis, Boca Raton, FL, 2009 (Chapter 6 12).
[15] P. Jacobsen, B. Sundqvist, Thermal conductivity and electrical resistivity of gadolinium as functions of pressure and temperature, Phys. Rev. B 40 (14) (1989) 9541–9551.
[16] G.F. Nellis, S.A. Klein, Heat Transfer, Cambridge, New York, 2009, pp. 665–667.
[17] K. Engelbrecht, J.B. Jensen, C.R.H. Bahl, N. Pryds, Experiments on a modular magnetic refrigeration device, in: Proceedings 3rd International Conference on Magnetic Refrigeration at Room Temperature, IIR/IIF, 2009.
[18] K.K. Nielsen, C.R.H. Bahl, A. Smith, N. Pryds, J. Hattel, A comprehensive parameter study of an active magnetic regenerator using a 2D numerical model, Int. J. Refrig. 33 (2010) 753–764.

B.2 Analysis of Single-Blow Effectiveness in Non-Uniform Parallel-Plate Regenerators

This article was published in the International Journal of Heat and Mass Transfer in June 2011. The article covers the parameter variations of regenerator geometries described in Section 7.3.

International Journal of Heat and Mass Transfer 54 (2011) 4746–4751

Contents lists available at ScienceDirect

International Journal of Heat and Mass Transfer

journal homepage: www.elsevier.com/locate/ijhmt

Analysis of single blow effectiveness in non-uniform parallel plate regenerators

J.B. Jensen [a,*], C.R.H. Bahl [a], K. Engelbrecht [a], B. Elmegaard [b], N. Pryds [a]

[a] Fuel Cells and Solid State Chemistry Division, Risø National Laboratory for Sustainable Energy, Frederiksborgvej 399, P.O. Box 49, Building 779, DK-4000 Roskilde, Denmark
[b] Department of Mechanical Engineering, Technical University of Denmark, Nils Koppels Allé, Building 404, DK-2800 Kgs. Lyngby, Denmark

ARTICLE INFO

Article history:
Received 19 October 2010
Received in revised form 25 May 2011
Accepted 25 May 2011
Available online 27 June 2011

Keywords:
Regenerator
Modeling
Distribution
Non-uniform
Performance

ABSTRACT

Non-uniform distributions of plate spacings in parallel plate regenerators have been found to induce loss of performance. In this paper, it has been investigated how variations of three geometric parameters (the aspect ratio, the porosity, and the standard deviation of the plate spacing) affects this loss in a single blow model of a parallel-plate regenerator. Simple analytical functions for the magnitude and the time scale of the reduction of performance are presented and compared to numerical results.

1. Introduction

A regenerator is a type of heat exchanger operating in a cyclical mode, where hot and cold fluids alternately exchange heat with a solid matrix. In this way, thermal energy is indirectly transferred between the fluids through the matrix. Regenerators are used in numerous applications, such as cryogenic cooling and dehumidifying or preheating of air [1–3]. Magnetic refrigeration is another example where the matrix itself generates and absorbs heat as a part of the process [4,5].

Extensive effort has been made to describe the performance characteristics of regenerators in general terms under various limiting conditions, particularly under the assumption of uniform geometry [6–10].

However, non-uniform distributions of plate spacings and fluid flows have been reported to reduce the performance of parallel-plate heat exchangers and regenerators, e.g. in [11–14].

In [11], a study has been conducted, which shows that significant reductions in single blow performance occur for regenerators with large standard deviations in the distribution of plate spacings. The study has been made for a regenerator based on the active magnetic regenerator used in [15], and shows reductions of up to 7% for regenerators with 20% standard deviations of the plate spacings.

In this study, the heat transfer during a single blow operation is investigated for regenerators with different distributions of plate spacings. The single blow operation corresponds to one half cycle of the regeneration process. A number of simulations have been performed of a single blow with various normal distributions of plate spacings, and the single-blow performances of non-uniform regenerators are compared to the single-blow performances of uniform regenerators.

The reduction of performance due to the non-uniformity of a regenerator is found numerically as a function of the three geometrical parameters: standard deviation, aspect ratio, and porosity; and correlations for the magnitude and timescale of this reduction are presented.

2. Numerical model

The heat transfer in the regenerators has been simulated using a 2-dimensional finite element model which has been developed using the commercially available software Comsol [16].

The model consists of 10 channels, separated by 9 plates, with half plates on the exterior sides of the first and last channels. The regenerator (the fluid and the matrix material) is initially in thermal equilibrium at the temperature T_0, which is different from the temperature of the fluid entering the regenerator through the inlet, T_{in}.

In the model, the governing equation for the solid is

$$\rho_s c_s \frac{\partial T}{\partial t} - k_s \nabla^2 T = 0, \quad (1)$$

where ρ_s is the density of the solid, c_s is the specific heat capacity of the solid, T is the temperature, t is the time, and k_s is the thermal conductivity of the solid; and the governing equation for the fluid is

* Corresponding author. Tel.: +45 4677 4762.
E-mail address: jbuj@risoe.dtu.dk (J.B. Jensen).

0017-9310/$ - see front matter © 2011 Elsevier Ltd. All rights reserved.
doi:10.1016/j.ijheatmasstransfer.2011.05.031

Nomenclature

Symbols

AR	aspect ratio = $L/\bar{w}$
c	specific heat capacity (J/kg K)
h	heat transfer coefficient (W/m^2 K)
j	rank of dimensional matrix
k	thermal conductivity (W/m K)
l	number of independent variables
L	regenerator length (m)
m	mass (kg)
$\dot{m}$	mass flow rate (kg/s)
n	porosity
N	number of channels
p	number of parameters
P	blow period (s)
Pe	Peclet number = $u_m\bar{w}/\alpha_f$
q	thermal energy (J)
R_α	ratio of thermal diffusivities
R_k	ratio of thermal conductivities
s_N	standard deviation of plate spacing distribution (m)
s_N^*	relative standard deviation of plate spacing distribution
t	time (s)
T	temperature (K)
u	fluid velocity (m/s)
w	channel width (m)
$\bar{w}$	average channel width (m)

Greek symbols

α	thermal diffusivity (m^2/s)
Δ	difference
ε	effectiveness
μ	fluid viscosity (N s/m^2)
ρ	density (kg/m^3)
Φ	utilization

Subscripts

0	initial
f	fluid
i	channel index
in	inlet
m	mean
max	maximum
pl	plate
s	solid
uni	uniform

$$\rho_f c_f \frac{\partial T}{\partial t} - k_f \nabla^2 T = -\rho_f c_f u \frac{\partial T}{\partial x}, \tag{2}$$

where ρ_f is the density of the fluid, c_f is the specific heat capacity of the fluid, k_f is the thermal conductivity of the fluid, and u is the local fluid velocity. The materials properties are assumed to be constant.

The boundary conditions are constant fluid temperature at the channel inlet and a zero-gradient temperature at the channel outlet. All other external boundaries are assumed to be adiabatic.

The fluid velocity used in Eq. (2) is calculated analytically as a steady, fully developed, laminar flow with a constant pressure drop across the regenerator. The details of this calculation are described in [11]. The total fluid flow rate is the same in all simulations, but since the distributions of plate spacings vary, the pressure drop can vary from one distribution to the next. The actual pressure drop across the regenerators, however, varies only ±2% or less in equivalent simulations, even though the distributions of plate spacings are random.

The model is identical to the model used in [11] and a more detailed description of the model can be found there.

3. Non-dimensionalization

In this study, we have investigated the effectiveness of a single blow in regenerators with different distributions of channel spacings as a function of utilization.

The utilization is given by the ratio of the thermal mass of the fluid that has entered the regenerator and the thermal mass of the solid

$$\Phi = \frac{\dot{m}_f c_f P}{m_s c_s}, \tag{3}$$

where $\dot{m}_f$ is the mass flow rate of the fluid and m_s is the mass of the solid. The effectiveness is defined as the fraction of heat that has been transferred from the plates to the channels to the total amount of heat that can be transferred

$$\varepsilon = \frac{q(\Phi)}{q_{max}}, \tag{4}$$

where q_{max} is given by

$$q_{max} = m_s c_s \Delta T \tag{5}$$

and $\Delta T = T_{in} - T_0$ is the difference between the initial and the inlet temperatures. The decrease in effectiveness induced by the non-uniformity of the plate spacings is then given by

$$\Delta\varepsilon = \varepsilon - \varepsilon_{uni}, \tag{6}$$

where ε_{uni} is the effectiveness of a uniform regenerator.

In order to limit the number of variables governing the system, a set of six non-dimensional parameters, which govern $\Delta\varepsilon(\Phi)$ is proposed and validated. Furthermore, the strength of their dependencies is evaluated in order to determine if any of the parameters can be neglected.

3.1. Proposition

The model calculates the heat transfer from the plates to the channels as a function of time from the 11 input parameters ρ_f, ρ_s, c_f, c_s, k_f, k_s, u_m, $\bar{w}$, w_{pl}, s_N, and L. Here, u_m is the average fluid velocity, $\bar{w}$ is the average channel width, w_{pl} is the plate width, s_N is the standard deviation of the channel width distribution, and L is the length of the regenerator.

While a solution can be found for any combination of these parameters, they are not all independent and all solutions are therefore not unique. For example, the governing equations are functions of only the product ρc, and not the individual values of ρ and c. Therefore we can use the diffusivity, $\alpha = k/(\rho c)$, as an input parameter and get solutions that are generally applicable for the product ρc.

Since the heat flux anywhere in the regenerator is proportional to the local temperature gradient, it is also proportional to the temperature difference $T_0 - T_{in}$. The heat flux is therefore independent of the absolute values of the initial and inlet temperatures, and depends only on their difference, ΔT. However, since we are

evaluating the solutions in terms of the ratio of two heat transfer rates, the temperature difference cancels out (in Eq. (4)) and the solution is thus independent of the input temperatures altogether.

This reduces the number of independent input parameters, p, to 9. According to Buckingham's Π-theorem, the number of independent variables is $l = p - j$, where j is the rank of the dimensional matrix. The rank of the current dimensional matrix has been calculated using Matlab [17] and is $j = 3$, which means that $l = 6$.

We therefore need six non-dimensional parameters as independent input variables. In this paper, we will use the following variables:

- The Peclet number, $Pe = \frac{u_m \bar{w}}{\alpha_f}$.
- The ratio of thermal diffusivity of the solid and the fluid, $R_\alpha = \frac{\alpha_f}{\alpha_s}$.
- The ratio of thermal conductivity of the solid and the fluid, $R_k = \frac{k_f}{k_s}$.
- The relative standard deviation of the distributions of plate spacings, $s_N^* = \frac{s_N}{\bar{w}}$.
- The regenerator porosity, $n = \frac{w}{w_{pl}+w}$.
- The aspect ratio of the regenerator, $AR = \frac{L}{\bar{w}}$.

3.2. Validation

In order to validate the choice of non-dimensional parameters and in order to estimate the strength of the dependencies for each of the variables, a series of parameter variations has been performed.

A set of the 11 (not necessarily independent) dimensional input parameters, as defined in Section 3.1, has been selected as the nominal case, which gives a set of nominal non-dimensional parameters. The nominal values are based on an active magnetic regenerator consisting of gadolinium and water, and are shown in Tables 1 and 2. The dimensional parameters have been varied in five simulations in a way, such that all the dimensional parameters are varied, but the non-dimensional parameters remain unchanged. The $\Delta\varepsilon(\Phi)$ values found in these simulations are plotted as solid lines in Fig. 1.

It can be seen that the $\Delta\varepsilon(\Phi)$ function remains unchanged when the dimensional parameters are varied, as long as the non-dimensional parameters are kept constant.

Furthermore, in order to determine if any of the non-dimensional groups are redundant, a series of simulations have been run, where each of the non-dimensional parameters are set to 50% of its nominal value. $\Delta\varepsilon(\Phi)$ for these simulations is plotted as the non-solid lines in Fig. 1 and shows variations in $\Delta\varepsilon(\Phi)$ for all the non-dimensional parameters.

4. Simulations

In the current study, we have focused on the effect of varying the geometrical parameters s_N^*, n, and AR .

Table 1
Nominal values of dimensional parameters.

Parameter	Nominal value	Unit
ρ_f	1000	kg/m^3
ρ_s	7900	kg/m^3
c_f	4200	J/(kg K)
c_s	240	J/(kg K)
k_f	0.6	J/(m s)
k_s	10	J/(m s)
u_m	0.005	m/s
$\bar{w}$	0.001	m
w_{pl}	0.001	m
s_N	0.0002	m
L	0.10	m

Table 2
Nominal values of non-dimensional parameters.

Parameter	Nominal value
Pe	35
R_α	0.027
R_k	0.06
s_N^*	0.2
n	0.50
AR	100

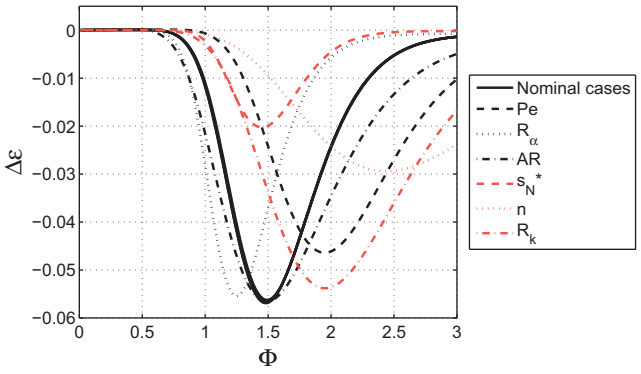

Fig. 1. $\Delta\varepsilon$ as a function of Φ. The solid black lines are simulations with constant non-dimensional parameters and the non-solid lines are individual variations where the non-dimensional parameters are set to 50% of their nominal values. The legend indicates which parameter is being varied.

The distributions of plate spacings of a series of passive regenerators, which have been fabricated for use in a different experiment, have been measured. The plates in the regenerators consist of Al or steel, and have average plate spacings ranging from 0.1 mm to 1 mm. The standard deviations of the distributions in these regenerators have been found to be between 7% and 26%, with smaller plate spacings giving larger relative standard deviations. In this study, we have chosen to cover standard deviations from 0 (the uniform case) up to 20%.

For the regenerator porosity, we have focused on the range 0.25–0.75 because extreme values close to 0 or 1 rarely are seen in regenerators.

A very wide range of aspect ratios are used for different regenerators, and the aspect ratio can become very high, if thin plates are used. If we focus on regenerators that use Gd plates, however, the aspect ratio is typically in the range $40 < AR < 330$ (see e.g. [15,18–20]).

Combinations of the following parameter values have been used for the simulations in this study:

$$s_N^* = \{0.05, 0.10, 0.15, 0.20\}, \tag{7}$$

$$n = \{0.25, 0.42, 0.58, 0.75\}, \tag{8}$$

$$AR = \{50, 100, 150, 200\}. \tag{9}$$

The remaining parameters are kept constant at the nominal values shown in Table 2.

Each modeled regenerator consists of 10 channels with widths given by a normal distribution. In order to ensure that the results are representative for an average regenerator, a new random normal distribution is generated before each simulation. Since the modeled regenerators contain only 10 channels, however, the $\Delta\varepsilon$ found in two simulations with the same input parameters may vary. In order to reduce these variations, 20 identical simulations are performed for each combination of parameters and the mean

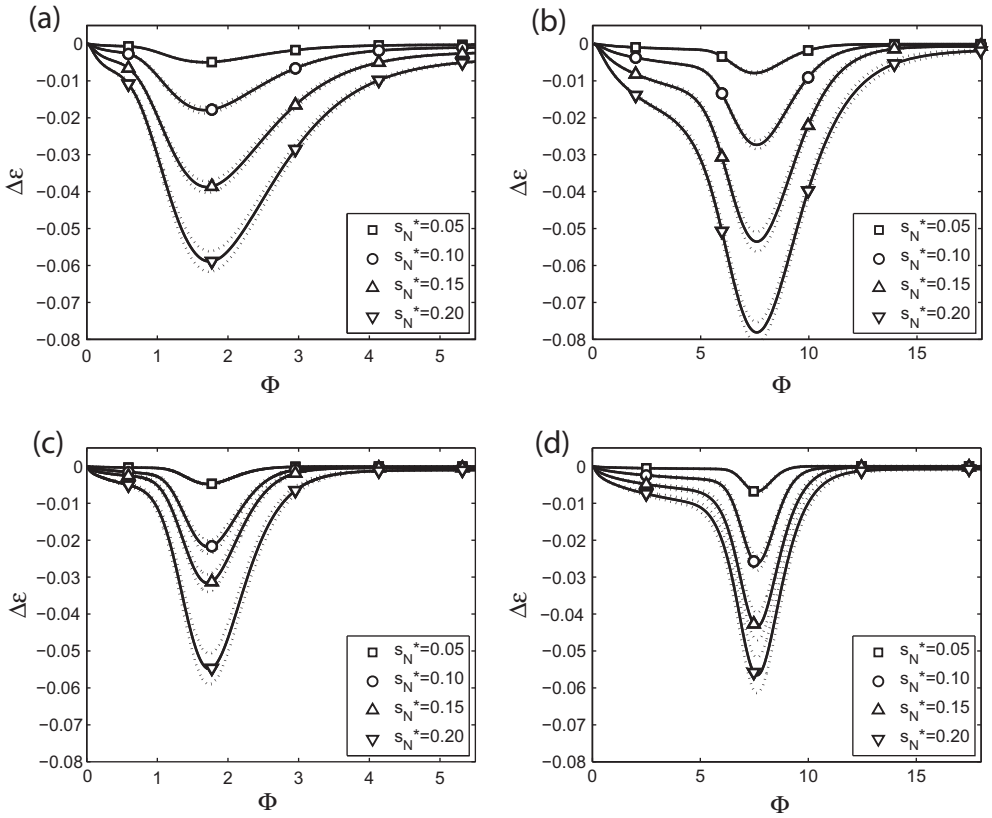

Fig. 2. Examples of $\Delta\varepsilon$ vs. Φ for all values of s_N^*. (a) $n = 0.25$, $AR = 50$; (b) $n = 0.75$, $AR = 50$; (c) $n = 0.25$, $AR = 200$; (d) $n = 0.75$, $AR = 200$.

result of these 20 simulations is used. This number of equivalent simulations has been found to give an acceptable accuracy of the average solution, as described in [11].

5. Results and discussion

In Fig. 2, the decrease in effectiveness compared to the uniform case, $\Delta\varepsilon$, has been plotted as a function of utilization, Φ, for the cases with the extreme values of AR and n.

Variations of the characteristic peak shape, which was also found in [11], can be observed for the different combinations of s_N^*, AR, and n. It can be seen that the magnitude of $\Delta\varepsilon$ increases when the standard deviation, s_N^*, is increased and that the peak position shifts toward larger values of Φ when the porosity increases. For increasing aspect ratio, the peaks become compressed in that both the peak magnitude and the peak width becomes smaller. The peak position, however is unchanged when the aspect ratio is varied. The variation in $\Delta\varepsilon$ as a function of aspect ratio is minor compared to the variation as a function of s_N^*.

Because fluid and solid initially are in equilibrium, there will be a confined region where the temperature difference between the solid and the fluid is significantly larger than in the rest of the regenerator, and the heat transfer will mainly take place within this region. This region starts at the inlet and gradually moves toward the outlet. In front of this region, both the solid and the fluid temperature will be close to the initial temperature, and behind the region, the solid and the fluid will both be close to the inlet temperature. It was found in [11] that the peak occurs when this region reaches the outlet.

Increasing the aspect ratio effectively corresponds to increasing the length of the regenerator (or decreasing the channel width). This means that the extent of the region of high heat transfer relative to the regenerator length decreases when the aspect ratio is increased. Due to the decrease in the size of the region where the heat transfer takes place, the width in Φ of the peak also decreases.

The peak values of $\Delta\varepsilon$ are plotted in Fig. 3 as a function of the relative standard deviation, s_N^*. The gray points are the mean peak values for each of the 16 combinations of AR and n and the white points are the overall mean peak value for the $16 \cdot 20$ combinations with a given value of s_N^*, i.e. each white point is the mean of 320 peak values with the same s_N^*, but different AR and n.

The error bars indicate the standard deviations for the overall mean peak values. The large standard deviations indicate that the deviations of the peak value can vary significantly from one regenerator to another, if the distribution of plate spacings vary. However, this is due to each regenerator distribution being modeled

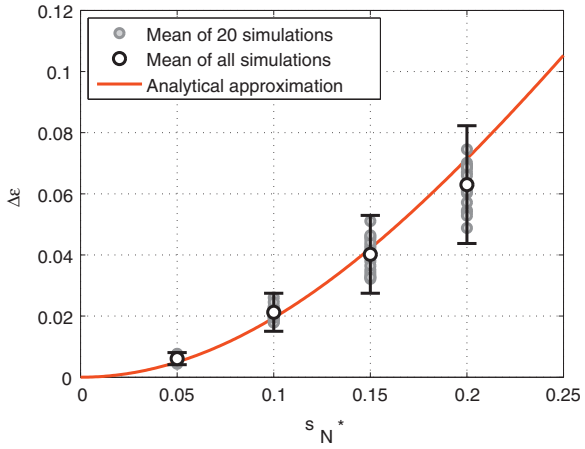

Fig. 3. Peak magnitude as a function of relative standard deviation. The gray points are mean values for the 20 equivalent simulations and the white points are mean values for all simulations with the same relative standard deviation.

with only 10 channels, and the mean of 20 simulations can be expected to represent the solution for a regenerator with an infinite number of channels (as is also indicated by the dotted bands in Fig. 2).

An analytical approximation is also plotted in Fig. 3. This approximation is based on the assumption that the heat transfer from the solid to the fluid in a given channel is proportional to the convective heat transfer coefficient, h, and the fluid velocity, $u_{m,i}$:

$$q_i \propto h \cdot u_{m,i}. \tag{10}$$

Because the pressure drop is constant in all channels in a given regenerator and the total volume flow rate is equal for all regenerators, the fluid velocity in a given channel depends not only on the channel width, but also on the distribution of channel widths in the regenerator. The mean fluid velocity in a given channel, i, is given by [21]

$$u_{m,i} = \frac{w_i^2}{12\mu L}\Delta p_i, \tag{11}$$

where w_i is the width of the ith channel, μ is the viscosity of the fluid, and Δp_i is the pressure drop in the ith channel. Since the pressure drop is equal for all channels,

$$\Delta p_i = \Delta p, \tag{12}$$

where Δp is the overall pressure drop. The volumetric flow rate in the i th channel, $\dot{V}_i$, is given by [21]

$$\dot{V}_i = \frac{dw_i^3 \Delta p}{12\mu L}, \tag{13}$$

and the overall flow rate, $\dot{V}$, is therefore

$$\dot{V} = \sum_{i=1}^{N} \dot{V}_i = \frac{d\sum_{i=1}^{N}(w_i^3)}{12\mu L}\Delta p. \tag{14}$$

Isolating Δp and substituting it into Eq. (11) gives the mean fluid velocity in the ith channel

$$u_{m,i} = \frac{w_i^2}{\sum_{i=1}^{N}(w_i^3)} \cdot \dot{V}', \tag{15}$$

where $\dot{V}'$ is the volume flow rate per unit depth of the regenerator. The sum in Eq. (15) can be found from the expectation value of w_i^3, which for a normal distribution is given by [22]

$$\langle w_i^3 \rangle = \int_{-\infty}^{\infty} \frac{w_i^3}{s_N\sqrt{2\pi}} \exp\left(-\frac{(w_i - \bar{w})^2}{2s_N^2}\right) dw_i, \tag{16}$$

where $\bar{w}$ is the mean channel width and s_N is its standard deviation. This gives

$$\langle w_i^3 \rangle = \bar{w}^3 + 3\bar{w}s_N^2. \tag{17}$$

The expectation value of q is then proportional to

$$\langle q \rangle \propto \frac{1 + s_N^{*2}}{\bar{w}(1 + 3s_N^{*2})}, \tag{18}$$

where $s_N^* = s_N/\bar{w}$ is the normalized standard deviation of the channel width. Using this, we can obtain an estimate for the expected decrease in effectiveness given by

$$\Delta\varepsilon \approx 1 - \frac{1 + s_N^{*2}}{1 + 3s_N^{*2}}. \tag{19}$$

This expression corresponds well to the numerically calculated degradations of performance, even though the influence of conjugate heat transfer between neighboring channels and variations in the aspect ratio have been neglected. The greater s_N^* becomes, the larger the deviation of the analytical approximation becomes. This is because more conjugate heat transfer occurs when the degree of non-uniformity increases.

The peak utilization is plotted in Fig. 4 as a function of the porosity. The shift in peak position can be explained by considering the region of high heat transfer.

If we consider a regenerator, where the thermal mass of the fluid, $c_f m_f$ is much greater than the thermal mass of the solid, $c_s m_s$, the plate will cool down instantaneously as the fluid at the lower temperature progresses. Therefore, the peak in this limiting case can be expected to occur when $t = L/u_m$ – at a fluid displacement of 100% of the length. If the ratio $(c_f m_f)/(c_s m_s)$ is not infinite, however, the fluid will heat up as it moves through the regenerator, which slows the progression of the region of high heat transfer. This delay will be equal to $(c_s m_s)/(c_f m_f)$, which means that the peak will occur at a stroke length of $(1 + (c_s m_s)/(c_f m_f)) \cdot L$, which corresponds to the utilization

$$\Phi_{peak} = \frac{c_f m_f}{c_s m_s} + 1. \tag{20}$$

This function is also plotted in Fig. 4 and can be seen to correspond very well to the modeling results.

If the fluid displacement is less than $(1 + (c_s m_s)/(c_f m_f)) \cdot L$, the degradation of the effectiveness will always increase when the fluid displacement is increased. If the fluid displacement is greater, however, some of the loss will be recovered and the degradation of performance will decrease, reaching zero at the limit $\Phi \to \infty$, where non-uniformity has no effect.

The analytical approximation describes the general behavior of the peak with a certain accuracy. If detailed information of the peak shape, or the precise peak position is required, modeling is still necessary, especially for regenerators with small numbers of channels.

Since the coupled channel-to-channel heat transfer is neglected in the approximation, slight variations in the peak shape and position occur, even for large numbers of channels, and since $\Delta\varepsilon$ increases with s_N^*, these variations can also be expected to increase with s_N^* (as seen in Fig. 3).

However, it can also be seen that the variations due to the distributions being randomly generated are significantly larger than the variations that come from neglecting the coupled heat transfer. This effect is averaged out by taking the mean of 20 simulations (which corresponds to having a regenerator with a large number of channels), but for regenerators with small numbers of channels, the $\Delta\varepsilon$-curve may depend strongly on the particular distribution rather than being a function of only the standard deviation.

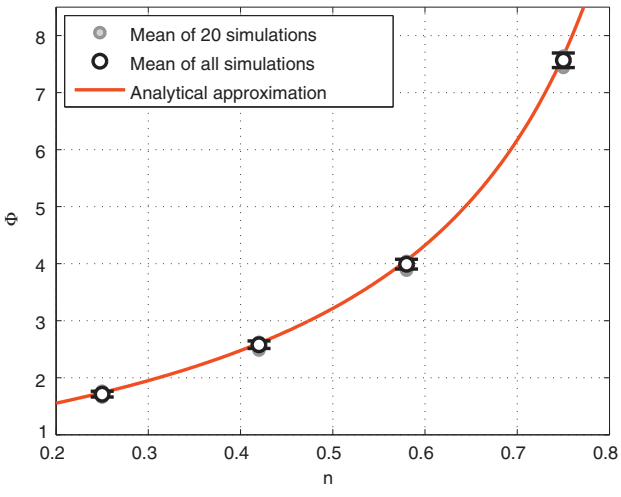

Fig. 4. Peak position as a function of porosity. The gray points are mean values for the 20 equivalent simulations and the white points are mean values for all simulations with the same relative standard deviation.

The analytical expressions give a generalized description of how $\Delta\varepsilon$ behaves as a function of s_N^*, AR, and n, which can be useful for optimization purposes and for the general understanding of the coupled heat transfer in non-uniform systems.

Furthermore, the effectiveness investigated in this paper is for a single blow operation with a simple initial condition. For regenerative processes, the absolute effectiveness may differ from the single blow effectiveness and cumulative effects can occur. It is our ongoing work to validate the descriptions of the heat transfer in regenerators, both experimentally and numerically.

6. Conclusion

In this paper, simulations of a single blow process of a regenerator with simplified initial conditions have been presented for variations of regenerator aspect ratio and porosity. A number of regenerators with normal distributions of plate spacings have been modeled and the effects of varying the standard deviation as well as the aspect ratio and porosity have been investigated.

It has been found that the decrease in single blow effectiveness of a regenerator can be estimated well with simple analytical approximations that neglect the conjugate heat transfer that takes place between channels.

Furthermore, if the relative fluid displacement of a single blow is smaller than the ratio of the thermal masses, it has been found that the degradation will increase for increasing displacement, but if is larger, part of the loss will be recovered, leading to a smaller decrease in effectiveness due to non-uniformity.

Acknowledgement

The authors would like to acknowledge the support of the Programme Commission on Energy and Environment (EnMi) (Contract No. 2104-06-0032) which is part of the Danish Council for Strategic Research.

References

[1] R. Radebaugh, Development of the pulse tube refrigerator as an efficient and reliable cryocooler, in: Proceedings of the Institute of Refrigeration, London, 1999, pp. 11–31.
[2] S. Jain, P.L. Dhar, S.C. Kaushik, Evaluation of liquid desiccant based evaporative cooling cycles for typical hot and humid climates, Heat Recov. Syst. CHP 14 (6) (1994) 621–632.
[3] D.A. Reay, A review of gas–gas heat recovery systems, Heat Recov. Syst. 1 (1980) 3–41.
[4] K.A. Gschneidner, V.K. Pecharsky, Thirty years of near room temperature magnetic cooling: where we are today and future prospects, Int. J. Refrig. 31 (6) (2008) 945–961.
[5] C.R.H. Bahl, A. Smith, N. Pryds, S. Linderoth, Magnetic refrigeration – an energy efficient technology for the future, in: Proceedings Risø International Energy Conference, 2009, pp. 107–115.
[6] J.E. Coppage, A.L. London, The periodic-flow regenerator – a summary of design theory, Trans. Amer. Soc. Mech. Eng. 5 (1953) 779–787.
[7] T.E.W. Schumann, Heat transfer: a liquid flowing through a porous prism, J. Franklin Inst. 208 (3) (1929) 405–416.
[8] A.J. Willmott, Digital computer simulation of a thermal regenerator, Int. J. Heat Mass Transfer 7 (1964) 1291–1302.
[9] R.K. Shah, D.P. Sekulic, Fundamentals of Heat Exchanger Design, John Wiley & Sons Inc., 2003.
[10] B.S. Baclic, P.J. Heggs, Unified regenerator theory and reexamination of the unidirectional regenerator performance, Adv. Heat Transfer 20 (1990) 133–179.
[11] J.B. Jensen, K. Engelbrecht, C.R.H. Bahl, N. Pryds, G.F. Nellis, S.A. Klein, B. Elmegaard, Modeling of parallel-plate regenerators with non-uniform plate distributions, Int. J. Heat Mass Transfer 53 (2010) 5065–5072.
[12] B.P. Rao, P.K. Kumar, S.K. Das, Effect of flow distribution to the channels on the thermal performance of a plate heat exchanger, Chem. Eng. Process. 41 (2002) 49–58.
[13] D. Gedeon, Flow circulations in foil-type regenerators produced by non-uniform layer spacing, Cryocoolers 13 (2004) 421–430.
[14] S. Backhaus, G.W. Swift, Fabrication and use of parallel plate regenerators in thermoacoustic engines, in: Proceedings of the 36th Intersociety Energy Conversion Conference, ASME, 2001, pp. 453–458.
[15] K. Engelbrecht, J.B. Jensen, C.R.H. Bahl, N. Pryds, Experiments on a modular magnetic refrigeration device, in: Proceedings of the Third International Conference on Magnetic Refrigeration at Room Temperature, IIR/IIF, Des Moines, IA, USA, 2009, pp. 431–436.
[16] Comsol Multiphysics User's Guide, ver. 3.5a, Comsol AB, Göteborg, Sweden, 2008.
[17] MATLAB, version 7.10.0, The MathWorks Inc., Natick, Massachusetts, 2010.
[18] C.R.H. Bahl, K. Engelbrecht, R. Bjørk, D. Eriksen, A. Smith, N. Pryds, Design concepts for a continuously rotating active magnetic regenerator, in: Proceedings of the Fourth International Conference on Magnetic Refrigeration at Room Temperature, IIR/IIF, Baotou, China, 2010, pp. 1–7.
[19] P. Clot, D. Viallet, F. Allab, A. Kedous-Leboc, J.M. Fournier, J.P. Yonnet, A magnet-based device for active magnetic refrigeration, IEEE Trans. Mag. 39 (2004) 3349–3351.
[20] Y.B. Tang, Y.G. Chen, B.M. Wang, Q.X. Xue, M.J. Tu, A room-temperature magnetic refrigerator using heat exchange of free convection, in: A. Poredos, A. Sarlah (Eds.), Proceedings of the Second International Conference on Magnetic Refrigeration at Room Temperature, IIR/IIF, Portoroz, Slovenia, 2007, pp. 359–361.
[21] F.M. White, Fluid Mechanics, sixth ed., McGraw Hill, 2008.
[22] J. Pitman, Probability, Springer, USA, 1993.

B.3 Experiments on a Modular Magnetic Refrigeration Device

This article has been accepted for publishing in the Journal of Mechanical Engineering (Strojniški vestnik). It was originally published in the proceedings of the *Third IIF-IIR International Conference on Magnetic Refrigeration at Room Temperature*, but an adapted version was subsequently invited for publication in the Journal of Mechanical Engineering.

The article describes the test machine and a test of two different regenerator housings. One of the tested housings had hollow walls and the other housing had solid walls. It was investigated whether the hollow walls would inhibit the heat losses from the regenerator to the surroundings significantly under various conditions of different ambient temperatures and fluid velocities. The study showed that the heat losses do not affect the performance significantly as long as the temperature difference is below 10°C.

Strojniški vestnik - Journal of Mechanical Engineering Volume(2010)No, StartPage-EndPage Paper received: 06.07.2010
DOI:10.5545/sv-jme.2010.151 Paper accepted: 23.06.2011

Experiments on a Modular Magnetic Refrigeration Device

K. Engelbrecht[1,*] - J. B. Jensen[1] - C. R. H. Bahl[1]
[1] Fuel Cells and Solid State Chemistry Division,Risø National Laboratory for Sustainable Energy, Technical University of Denmark – DTU, Roskilde, Denmark

An experimental magnetic refrigeration test device has been built at Risø DTU. The device is designed to be modular, and thus all parts of the device can easily be replaced depending on the experiment. This makes the device highly versatile, with the possibility of performing a wide variety of different experiments. The test device is of the reciprocating type, and the magnetic field source is provided by a permanent Halbach magnet assembly with an average flux density of 1.03 Tesla. This work presents experimental results for flat plate regenerators made of gadolinium and sintered compounds of $La(Fe,Co,Si)_{13}$ and experimentally investigates the effect of thermal conduction through the regenerator housing walls. Each regenerator was tested over a range of hot reservoir temperatures under no load conditions for a regenerator comprised of gadolinium. The test machine was also tested with two different compositions of $La(Fe,Co,Si)_{13}$ compounds. Test results are presented for a regenerator made of a single $La(Fe,Co,Si)_{13}$ material and a two-material regenerator, and the results are compared to the same system using gadolinium.

Keywords: experiment, magnetic refrigeration, gadolinium, regenerator

0 INTRODUCTION

Active magnetic regenerative (AMR) refrigerators are a potentially environmentally-friendly alternative to vapor compression technology that could potentially be used for air-conditioning, refrigeration, and heat pump applications. Rather than using a gaseous refrigerant, AMRs use magnetocaloric materials (MCMs) that have a coupling between their thermodynamic properties and internal magnetic field. The magnetization of an MCM is analogous to the compression of a gas in that the material's state becomes more ordered. With magnetization, the material's entropy is lowered, and the temperature increases if conditions are adiabatic. AMRs are still a developing technology and there is much research effort currently focused on improving AMR performance through the development of new MCMs and system designs. Gadolinium has been the most commonly used MCM in recent AMR machines [1], but many new materials are being developed and characterized [2]. One MCM with the potential to improve system performance over Gd is the $La(Fe,Co,Si)_{13}$ series of materials. This work compares the two materials in a prototype AMR.

A single regenerator reciprocating AMR test machine has been built and used to test different magnetocaloric materials and regenerator designs. The volume of the regenerator, not including housing and external hardware, is approximately 15 cm^3, and the magnetic field is provided by a Halbach cylinder type permanent magnet with an average flux density in the bore of 1.03 T. The magnet, which is described by [3], has a bore of 42 mm and a height of 50 mm. Magnetization and demagnetization of the regenerator are achieved by moving the regenerator vertically relative to the stationary magnet by use of a stepper motor. The test device is described in detail by [4] and was designed such that the regenerator housing can be easily changed, allowing a range of regenerator designs to be tested quickly. However, only flat plate regenerators have been tested up to this point. In order to test the machine's performance over a range of operating temperatures and to better control the experimental conditions, the device has been placed in a temperature controlled cabinet with the hot reservoir in thermal contact with the air in cabinet. In this work, the air inside the temperature controlled cabinet is considered ambient. This paper presents no-load temperature span measurements for a test machine using a flat plate gadolinium regenerator and a regenerator made of plates of two sintered $La(Fe,Co,Si)_{13}$ materials.

*Corr. Author's Address: Risø DTU, Frederiksborg 399, 4000 Roskilde, Denmark, kuen@risoe.dtu.dk

A simple schematic of the test machine is given in Fig. 1. The regenerator has a Perspex tube screwed onto each end, with the hot reservoir located in the tube above the regenerator and the cold reservoir in the tube below. There is a resistance heater installed in the regenerator's cold reservoir to simulate a cooling load. Heat transfer fluid is moved through the regenerator by means of a displacer in the cold reservoir.

The entire device is placed in contact with the same ambient temperature; however, the hot reservoir is thermally linked to ambient via a forced convection heat exchanger while the cold reservoir is insulated from ambient using foam tubing. All thermal losses through the regenerator housing and cold reservoir will go to the ambient temperature. This test machine was used to measure the no-load temperature span of a flat plate regenerator for a range of operating conditions using regenerators made of gadolinium and one and two-material regenerators made of $La(Fe,Co,Si)_{13}$ and the results are presented below.

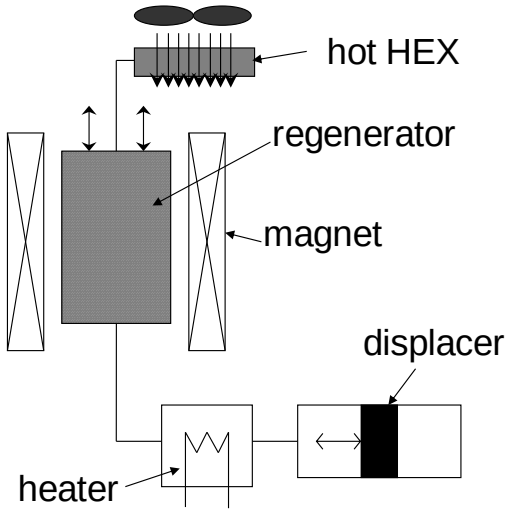

Fig. 1. *Schematic of the test machine*

1 THE REGENERATOR HOUSING

The goal of the test machine described here is to test a range of AMR designs quickly when subjected to consistent conditions. The regenerators were fabricated using rapid prototyping techniques. Rapid prototyping was chosen because a range of detailed geometries can be produced in a single piece, eliminating fluid leakage. Some types of rapid prototyping processes use plastics with relatively low thermal diffusivities, such as acrylic or nylon, which should reduce interactions between the heat transfer fluid and regenerator housing. The regenerator is 40 mm in the direction of flow with a rectangular flow opening 23 mm wide by 17 mm high. Each plate is held in place by a 1 mm tall slot that runs the entire length of the regenerator. Plate spacing is controlled by ribs between each slot, and the height of each rib can be no less than 0.5 mm due to manufacturing limitations. The regenerator houses 11 plates with the top and bottom plates in direct contact with the housing to reduce interactions between the heat transfer fluid and regenerator housing. The heat transfer fluid is a mixture of 75% water and 25% automotive antifreeze. Consumer antifreeze, which is based on ethylene glycol, was chosen over laboratory grade ethylene glycol because it has corrosion inhibitors that reduce the corrosion of several of the magnetocaloric materials under consideration in this paper.

This paper shows results for 0.9 mm thick commercial grade Gd plates held in place in two different regenerator housings. The first is made using a PolyJet process, where droplets of an acrylic-based polymer are deposited in layers with a thickness of approximately 0.02 mm and hardened after each deposition. The second is made using a selective laser sintering (SLS) process, where layers of nylon powder 0.1 mm in thickness are selectively sintered to form the final part. The SLS process was chosen because it could be used to produce a regenerator housing with hollow walls, which should reduce thermal conduction to the ambient. The PolyJet process could not be used to make the hollow-walled regenerator housing because the process uses a wax support structure that would be difficult to remove from the space inside the walls. A CAD cross-section of the hollow regenerator is show in Fig. 2. As shown in the figure, there must still be a support structure for the regenerator plates, but the overall conduction path is reduced by using a hollow wall. Assuming that the hollow volume is filled with quiescent air, the thermal resistance through the hollow housing and solid housing can be estimated. Using an average distance occupied by the air, the thermal resistance through the hollow regenerator wall is approximately 4 times greater than through the solid regenerator housing. The minimum wall thickness is 2.2 mm for the hollow regenerator housing. The PolyJet

regenerator has the same geometry as the one shown in Fig. 2, with the exception that the wall between the opening for the regenerator plates and the outside is solid.

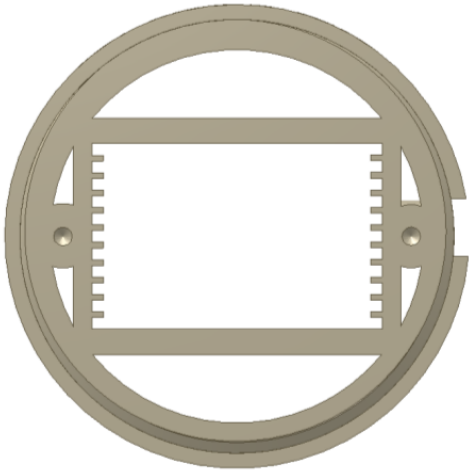

Fig. 2. *CAD drawing of a regenerator with hollow walls made with SLS*

2 EXPERIMENTAL RESULTS

2.1 Flat Plate Gadolinium Regenerator

The solid and hollow regenerators were tested over a range of ambient temperature to determine the optimum temperature span of the test device. Both regenerators were tested with 0.9 mm thick commercial grade gadolinium plates with a spacing of 0.5 mm. In order to determine operating parameters that are near optimal, the solid PolyJet regenerator was used for a range of experiments where the fluid flow rates and cycle times were varied. Operating conditions that result in the optimal no-load temperature span were determined experimentally and they are shown in Table 1. The AMR cycle is broken into four separate processes for the test machine presented here. The cold-to-hot blow starts only when the regenerator is fully magnetized, and the hot-to-cold blow starts after the regenerator is moved fully out of the magnetic field. Therefore, if the time for any single process is changed, the cycle time is also changed.

Table 1. *Operating conditions for ambient temperature variation experiment using the commercial grade gadolinium flat plate regenerator*

Parameter	Value
Fluid velocity	8.2 mm/s
Cycle time	8 s
Utilization	0.55

The regenerator utilization, U, is defined as [5]:

$$U = \frac{v_f A_f \tau_2 \rho_f c_f}{V_s \rho_s c_s} \quad (1)$$

where τ_2 is the time for a blow period, v_f is the fluid velocity, A_f is the cross-sectional area available for fluid flow, ρ_f and ρ_s are the fluid and solid densities, respectively, c_f and c_s are the specific heats of the fluid and solid, respectively, and V_s is the volume of the solid regenerator material. The average specific heat of gadolinium is assumed to be 260 J/kg-K based on data from [6].

The ambient temperature was varied in a range around the Curie temperature of Gd (21 °C) and the no-load temperature span was measured for the solid and hollow regenerators. The results are shown in Fig. 3. The hot heat exchanger generally maintains the hot reservoir to approximately 1 °C or less above ambient temperature.

Fig. 3 shows that the maximum temperature span is achieved at an ambient temperature of approximately 25 °C for both regenerators. It has previously been reported that the optimum hot-end temperature is just above the Curie temperature [7]. At an ambient temperature of 24 °C, the regenerator operates approximately between 16 and 25 °C. The Curie temperature is close to the middle of this range, meaning that the entropy change with magnetization of the material is maximized. The hollow regenerator housing generally performs slightly better than the solid housing, but the difference is near the experimental uncertainty for the device which is estimated at approximately 0.2 °C. As the temperature span of the device increases, the performance of the hollow housing may improve relative to the solid housing. However for a temperature span below 10 °C, the

benefit of the hollow regenerator housing is relatively small.

The effect of ambient temperature relative to the hot and cold reservoirs was also tested. The device was run at the same operating conditions but with a reduced pump speed in the hot heat exchanger, and the resulting temperature span was measured. With the hot heat exchanger effectiveness reduced, the ambient temperature was set to 22.5 °C and the regenerator produced a no-load span of 10.2 °C between 15.6 °C and 25.8 °C. The temperature span that was achieved when the hot reservoir was allowed to rise more than 3 °C above ambient increased the device's temperature span by more than 1 °C. This could be due to the reduced temperature difference between the cold reservoir and ambient or the reduced temperature difference between any location along the regenerator and ambient. Because the losses through the regenerator wall were shown to be relatively small, it is possible that there is a thermal leak from the cold reservoir to the ambient that causes a noticeable reduction in performance.

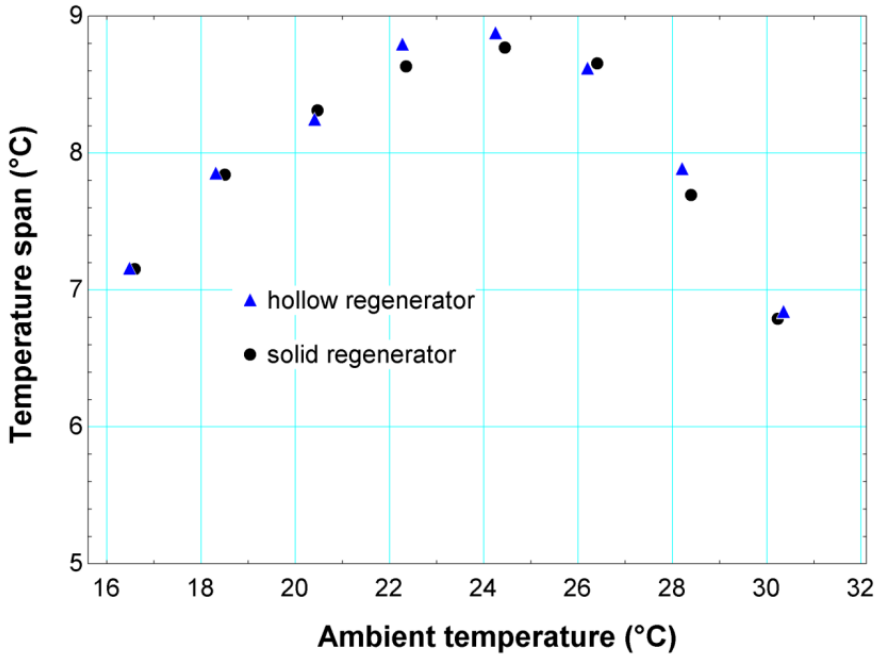

Fig. 3. *No-load temperature span as a function of ambient temperature for the operating conditions shown in Table 1*

2.2. Experimental Results for a Two-Material Regenerator

Plates of 0.9 mm thickness have been made by Vacuumschmelze of two compositions of sintered $La(Fe,Co,Si)_{13}$ with Curie temperatures of approximately 3 °C and 16 °C. The properties of the T_C = 3 °C material tested here are given by [8]. $La(Fe,Co,Si)_{13}$ materials are attractive materials for AMR systems because they have a higher entropy change with magnetization than gadolinium, although they exhibit a smaller adiabatic temperature change upon magnetization. Each plate is 0.9 mm thick and 20 mm long or half the length of the gadolinium plates discussed above. The layered bed is constructed by simply butting two plates of different materials together. The solid regenerator housing was run with a regenerator made of only the T_C = 16 °C material and the system reached a no load temperature span of 7.9 °C, with the regenerator operating between 10.1 and 18.0 °C while the ambient temperature was set to 15.6 °C.

The layered bed was tested at an ambient temperature of 13 °C for a range of utilizations and heat transfer fluid velocities, and the no-load temperature span was measured. The cycle time is a function mostly of fluid velocity and utilization. Thus, for the same utilization, the cycle time will be longer for a lower fluid velocity. Testing of

the layered La(Fe,Co,Si)$_{13}$ showed that the system was most sensitive to fluid velocity, with cycle time and utilization having relatively small effects on system performance for conditions tested here. The experimental results are shown in Fig. 4. The dependence on fluid velocity may be due to the increased time for heat transfer between the fluid and solid when the velocity is lower. Changing the ambient temperature for this experiment does not significantly affect the results, provided it lies between the Curie temperatures of the two materials. The

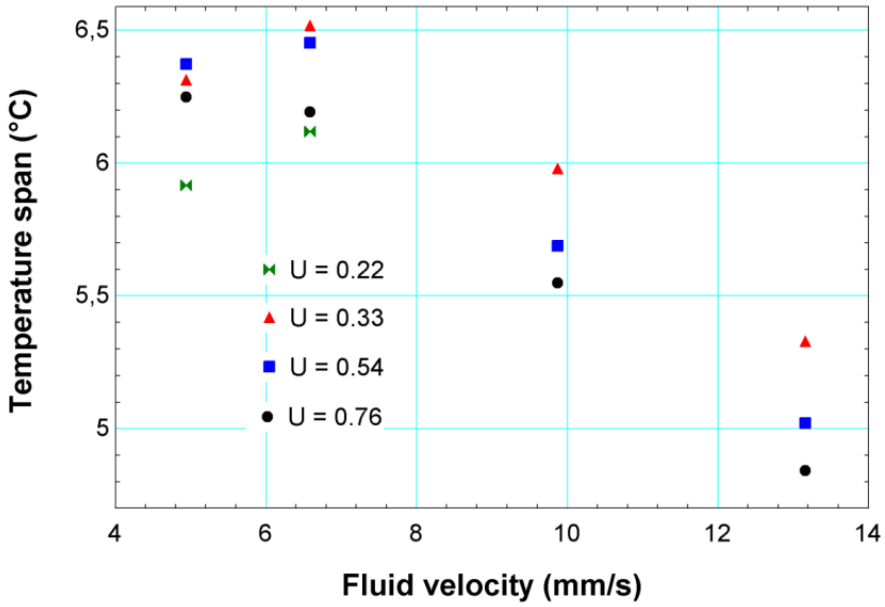

Fig. 4. *No load temperature span as a function of fluid velocity for a two-material La(Fe,Co,Si)$_{13}$ regenerator*

insensitivity to operating temperature may be due to the fact that the difference between the Curie temperatures of the two materials is higher than the temperature span that can be achieved by this regenerator design.

Examination of Fig. 4 shows that the no-load temperature span is similar for a range of utilizations when the fluid velocity is held constant. However, the results are dependent on fluid velocity, achieving the largest temperature span with a fluid velocity of 6.6 mm/s. The system showed very little dependence on cycle time. For example, the case with a utilization of 0.33 and fluid velocity of 6.6 mm/s has a cycle time of 9.2 s while the experiment with a utilization of 0.76 and the same fluid velocity had a cycle time of 17 s, but the temperature span showed a difference of only 0.3 °C. There is a much more drastic change in performance as the fluid velocity is changed. The maximum temperature span for the layered regenerator is 6.5 °C, which is 1.5 °C lower than the temperature span for a single material La(Fe,Co,Si)$_{13}$ regenerator. The layered regenerator probably did not perform as well as the single material bed because the Curie temperatures of the magnetocaloric materials are too far apart for this regenerator design. Because the regenerator cannot produce a large enough temperature span to reach the temperature where the low-Curie-temperature material has high magnetocaloric performance, the potentially higher temperature span for the layered regenerator was not realized.

During operation of the test machine, the La(Fe,Co,Si)$_{13}$ plates were more prone to break than the gadolinium plates that were also tested. It is not clear if the plates were broken during assembly/disassembly or during operation, but brittleness should be a concern when designing a system using La(Fe,Co,Si)$_{13}$ materials.

3 CONCLUSIONS

No-load temperature spans have been presented for two different regenerator designs and two different regenerator materials. By testing a regenerator with hollow walls, it was shown that thermal losses through the regenerator wall to ambient do not significantly affect the test machine's performance when the temperature span is less than 10 °C. However as the temperature span increases, losses through the regenerator wall will also increase and reducing the conduction through the regenerator housing may have a larger impact on performance. Tests presented in this paper show that a single-material AMR performs best when the Curie temperature is within the working temperature span of the machine. The test machine presented is able to control the operating temperature of the AMR and therefore is able to test a given MCM in its optimum temperature range and provide a meaningful comparison between potential new working materials with different Curie temperatures.

Single-material and layered bed regenerators were made from $La(Fe,Co,Si)_{13}$ compounds, and the no load temperature span was found to be lower than that of gadolinium when both materials operated near their respective Curie temperatures. Also, the layered regenerator provided a lower temperature span than the single material regenerator because the two materials had Curie temperatures that were too far apart for the regenerator design that was tested. However, $La(Fe,Co,Si)_{13}$ compounds exhibit relatively high entropy change with magnetization and still hold promise for AMR systems provided the materials are chosen correctly.

4 ACKNOWLEGEMENTS

We thank Mr. Jørgen Geyti for his technical help. Also, we thank Vacuumschmelze GmbH & Co. KG, 63450 Hanau, Germany for supplying the plates of $La(Fe,Co,Si)_{13}$. The authors further acknowledge the support of the Programme Commission on Energy and Environment (EnMi) (Contract No. 2104-06-0032), which is part of the Danish Council for Strategic Research.

5 REFERENCES

[1] Gschneidner Jr, K.A., Pecharsky, V.K., Tsokol, A.O. (2005). Recent developments in magnetocaloric materials. *Rep. Prog. Phys*, vol. 68, p. 1479-1539.

[2] Engelbrecht, K.L., Nellis, G.F., Klein, S.A., Zimm, C.B. (2007). Recent developments in room temperature active magnetic regenerative refrigeration. *HVAC&R Res.* vol. 13**,** p. 525-542.

[3] Bjørk, R., Bahl, C.R.H., Smith, A., Pryds, N. (2010). Review and comparison of magnet designs for magnetic refrigeration. *Int. Journal of Refrigeration*, vol. 33, p. 437-448.

[4] Bahl, C.R.H., Petersen, T.F., Pryds, N., Smith, A. (2008). A versatile magnetic refrigeration test device. *Rev. Sci. Instrum.* vol. 79, no. 093906.

[5] Dragutinovic, G.D., Baclic, B.S. (missing year). *Operation of counterflow regenerators*. Computational Mechanics Inc., Billerca.

[6] Dan'kov, S.Y., Tishin, A.M., Pecharsky, V.K., Gschneidner, K.A. (1998). Magnetic phase transitions and the magnetothermal properties of gadolinium. *Physical Review B*, vol. 57, no. 6, p. 3478-3490.

[7] Rowe, A. Tura, A. (2008). Active magnetic regenerator performance enhancement using passive magnetic materials. *J. Magn. Magn. Mater.*, vol. 320, p. 1357-1363.

[8] Hansen, B.R., Katter, M., Theil Kuhn, L., Bahl, C.R.H., Smith, A., Ancona-Torres, C. (2009). Characterization study of a plate of the magnetocaloric material $La(Fe,Co,Si)_{13}$. *ProcEedings of 3rd International Conference on Magnetic Refrigeration at Room Temperature, IIF/IIR*, p. ??- ??.

B.4 Degradation of the Performance of Microchannel Heat Exchangers Due to Flow Maldistribution

This article was submitted to Applied Thermal Engineering in August 2011. It describes the simulations presented in Chapter 9 and a series of experiments that have been performed on the experimental regenerators that were produced.

Degradation of the performance of microchannel heat exchangers due to flow maldistribution

K.K. Nielsen[1], K. Engelbrecht[1], D.V. Christensen[1,2], J.B. Jensen[1] A. Smith[1], C.R.H. Bahl[1]

[1] Fuel Cells and Solid State Chemistry Division
Risø National Laboratory for Sustainable Energy
Technical University of Denmark
Frederiksborgvej 399, DK-4000 Roskilde, Denmark

[2] Niels Bohr Institute, University of Copenhagen
Blegdamsvej 17, DK-2100 Copenhagen, Denmark

Abstract

The effect of flow maldistribution on the performance of microchannel parallel plate heat exchangers is investigated using an established model and cyclic steady-state experiments. It is found that as the variation of the individual channel thickness in a particular stack (heat exchanger) increases the actual performance of the heat exchanger decreases significantly, deviating from the expected nominal performance. We show that this is due to both the varying fluid flow velocities in each individual channel and the thermal cross talk between the channels transverse to the direction of the flow.

Keywords: micro-channels, flow maldistribution, thermal crosstalk, parallel plates

1. Introduction

Microchannel heat exchangers show promise of theoretically large heat transfer coefficients and provide the ability to design compact devices. These are two very central parameters in the areas of, e.g., cryocoolers, dehumidifiers, Stirling engines, solar power, electronics cooling and magnetic refrigeration [1, 2, 3, 4, 5, 6, 7].

Parallel plate heat exchangers are considered, from a theoretical standpoint, to have a good ratio between heat transfer properties and pressure drop. In order to reach sufficient values of the number of transfer units (NTU) and heat transfer coefficient, h, the flow channels defined by the parallel plates, or similar geometries, must be made into the sub-milimeter regime. This is due to the fact that, assuming a constant Nusselt number, the only parameter that can increase h is a decrease in the hydraulic diameter, D_{H}. The required flow rate, specified through operating frequency and thermal utilization of the heat exchanger, defines a minimum value of h and thus D_{H} for a given value of the NTU. In many applications it is thus important to have quite small channels (hydraulic diameters down to or even below 100 μm are not unrealistic in many applications) [8].

The range of hydraulic diameters from 1 μm to 1 mm is commonly defined as microchannels [9]. Significant discrepancies are, however, often observed between experiments and theory in this range. This has led to a quite significant amount of research into various aspects of the governing physics at the relevant scales.

1.1. Relevant physical effects at the microscale level

Several explanations for the relatively large deviations of the predicted heat transfer performance and that experimentally observed on the microscale have been suggested. These include physical effects not previously considered such as, e.g., whether the continuum assumption breaks down, the influence of surface roughness in the channels etc. In [9] these issues are reviewed and it is concluded that for incompressible laminar flows with aqueous fluids no new physical phenomena happen in microchannels. This is backed up by careful experiments performed on single-channel tubes and square channel heat exchangers in the microchannel range [9, 10, 11].

A range of assumptions are usually made in order to model the coupled fluid-flow and heat transfer problem in heat exchangers in general. These issues are discussed in great detail in [9] and references therein. Here, we will briefly summarize them:

- Entrance effects
- Temperature dependent properties
- Viscous dissipation
- Surface roughness
- Conjugate heat transfer
- Uneven flow in flow manifolds

The entrance effects cover both hydrodynamic and thermal issues. It is important to investigate whether the flow may be considered fully developed

and, in the case of a 1D model, also whether the thermal entrance length is relatively short.

Temperature dependent properties may influence the performance in several ways. If the viscosity of the heat transfer fluid varies significantly then the pressure drop in an actual experiment may be somewhat different than predicted. Similarly, if the specific heat and the mass density are sensitive to temperature then that may cause substantial deviations between the results observed experimentally and those predicted by a numerical model neglecting these effects.

The viscous dissipation is the irreversible conversion of mechanical energy to heat in the fluid due to the pressure drop. If this effect is considerable and not taken into account in a numerical model, then the heat transfer will be incorrectly predicted. A general criterium for estimating the importance of viscous dissipation is to calculate the pressure drop and use that to find the associated energy release. Comparing this number to the total amount of transfered heat in the system is a good estimate of the possible importance of the viscous heating.

The surface roughness is indeed difficult to model exactly. Several investigations have shown, however, that the impact of surface roughness on the heat transfer effectiveness may be either positive or negative depending on the characteristics of the roughness [12, 13, 14]. It is generally concluded that surface roughness increases the pressure drop [9].

The issue of conjugate heat transfer is the effect of thermal conduction in the flow direction in the heat exchanger solid. For small Reynolds numbers this effect may be quite significant and using simple Nusselt-Reynolds

correlations may not sufficiently describe the actual heat transfer [9, 11, 15].

Finally, in a microchannel heat exchanger with several channels flow maldistribution in the channels can be significant. If the channels are nominally small their spacing may be manufactured with a relatively large uncertainty. The resulting performance of the heat exchanger is difficult or even impossible to predict without the help of a numerical model resolving the heat transfer problem in at least two dimensions.

While much research on heat transfer and fluid flow modeling in microchannels generally studies a single channel [16, 17], entire microchannel heat exchangers with practical manufacturing tolerances have received less attention. How fluid maldistribution in microchannel manifolds affects heat transfer performance was studied using a 3D model [18]. A 1D heat exchanger model was used to predict how flow maldistribution affects vapor compression system performance [19, 20]. This method predicts that two individual plate stacks with different spacing will have poorer heat transfer performance than an equivalent stack with average plate spacing of the two. However, the parallel heat exchanger approach cannot capture the effect of thermal interactions (cross talk) between adjacent fluid channels with different channel heights. The effect of cross talk on microchannel stack performance is not well understood. The existing literature on microchannel heat exchangers lacks an in-depth theoretical analysis of how varying channel heights influence bulk heat transfer performance in a heat exchanger. Other research has focused on flow maldistribution on the air side of a microchannel heat exchanger [21]. Flow and temperature distribution in parallel channels were studied numerically when obstructions such as bubbles or debris were placed

in one of the channels [22]. The outlet temperature profile was shown to be affected by obstruction in one of the channels, but the change in heat transfer performance was not quantified.

In this paper we investigate the influence of flow maldistribution and the associated conjugate heat transfer using the 2-dimensional heat transfer and fluid flow model presented in [23, 24] on four custom made parallel-plate heat exchanger stacks built from commercial aluminum sheets. The four stacks all have the same plate thickness of 0.4 mm and number of plates but different nominal plate spacings ranging from 0.1 to 0.74 mm. The performance as passive thermal regenerators is investigated experimentally in a setup that allows a periodic flow in the system, and the performance evaluated at cyclic steady state.

The numerical model simulates a single-blow process in a given inhomogeneous stack of parallel plates. The reduction in heat transfer coefficient due to the inhomogeneity of the stack is determined through comparison with the ideal single channel case. This reduction factor is found at varying flow rates in order to probe the influence of flow maldistribution as a function of Reynolds number.

2. Experimental

2.1. Construction of aluminum regenerators

The flat plate stacks were fabricated from 0.4 mm thick commercial grade Al plates that were laser cut to the dimensions 40×25 mm^2. Thin wires were used as spacers to regulate the plate spacing, and the sections of wire of varying diameter were stretched slightly to produce a straight wire with no sharp bends. Each stack was made with two wires sandwiched between

each plate in a simple rig to facilitate easy plate stacking. After all the plates were stacked, the stack was compressed slightly to reduce the effects of slight bending of the wires and the plates were bonded with epoxy on both sides along the entire length of the plates in the flow direction (40 mm). Each stack was placed in a nylon housing and sealed around the periphery of the stack with silicone to prevent heat transfer fluid from bypassing the stack. The fabrication and test procedure for the stacks is discussed in more detail in [25, 26].

A Vantage Laser Scanner was used to scan the cross sections at both ends of each stack. The resolution along the direction of the stacking of the aluminum plates was set to 5 μm and along the transerve direction it was set to 20 μm. The laser scanner is designed to measure surface topology. However, in this case the data from the scanner was truncated to two values; one representing solid aluminum, the other representing void space, i.e. flow channel. In this way the channel and plate thicknesses were found through analyzing the 2-dimensional maps of the cross sections of the stacks. The processed maps of each stack configuration are shown in Fig. A.8 in Appendix Appendix A.

The distance between each plate in each stack configuration is found for each measured point along the transverse direction. From these, the mean and standard deviation values for each channel are then found. In Tab. I the mean separation and standard deviation values are provided for each stack configuration. The standard deviations on the thicknesses of the plates are more than an order of magnitude smaller than the channel spacings and it may therefore be safely assumed that the plates are homogeneous and

Table I: Summary of the nominal plate spacing, the actually measured mean plate spacing (μ), the absolute standard deviation (σ), the relative standard deviation and the maximum and minimum channel spacings. Measurements are given for both the up and down (dn) faces of the stack.

Nom. sep. [mm]	0.7 (up)	0.7 (dn)	0.4 (up)	0.4 (dn)	0.2 (up)	0.2 (dn)	0.1 (up)	0.1
μ [mm]	0.743	0.755	0.407	0.415	0.211	0.214	0.116	0
σ [mm]	0.046	0.043	0.053	0.036	0.026	0.027	0.027	0
σ/μ [%]	6.1	5.7	13.1	8.7	12.2	12.5	23.3	2
Min. sep. [mm]	0.631	0.694	0.310	0.353	0.161	0.186	0.044	0
Max. sep. [mm]	0.815	0.852	0.496	0.484	0.263	0.263	0.159	0

identical.

From Tab. I it is seen that the absolute value of the standard deviation actually decreases as the nominal plate spacing decreases. However, the difference is within a factor of two for a change in nominal spacing of more than a factor of seven. The relative standard deviation, therefore, shows a clear increase as the nominal plate spacing decreases. The stack with a nominal spacing of 0.1 mm has a standard deviation of the plate spacings of 24 % whereas the stack with a nominal spacing of 0.74 mm has a standard deviation of about 6 %.

2.2. Periodic flow test machine setup

A modular device built originally for use as an active magnetic regenerator test machine [27] is used to test the stacks as thermal regenerators in passive mode. A reciprocating piston provides oscillating flow through the regenerator between the hot and cold thermal reservoirs while a heater maintains a temperature gradient. The device and passive regenerator experiments are described in more detail in [26]. Below the regenerator a piston is situated such that the heat transfer fluid flow may be controlled. The device has been modified slightly for the experiments presented here. The heater

location has been moved from the face of the piston to a fixed location near the regenerator inlet. A mesh screen was also added to the ends of the regenerators in order to achieve a better flow distribution in the regenerators and more even fluid inlet temperature. When operated as a passive regenerator the end with the piston (and heater) is thus the hot end, whereas the end with the constant-temperature heat exchanger is the cold end. The temperature is measured by type E thermocouples at both ends. A heater power and oscillating fluid flow are applied to each regenerator and the resulting temperature span is measured. Higher temperature spans correspond to higher regenerator effectiveness and thus to better heat transfer performance in the regenerator.

3. Numerical analysis

One major goal of this paper is to theoretically demonstrate the effect on bulk heat transfer in a microchannel heat exchanger or regenerator caused only by non-uniform channel spacing. The work here is based on a CFD model of a stack of plates with varying channels reported in [23]. In the model the following assumptions are made:

- the fluid is aqueous with properties assumed temperature-independent
- the fluid flow is single phase, incompressible, laminar and fully developed
- the fluid at the inlet and outlet of the heat exchanger has a constant pressure and a well-distributed flow
- the heat exchanger inlet and outlet are adiabatic

- the fluid and solid do not interact thermally with the ambient or the heat exchanger housing
- viscous dissipation of pump power inside the heat exchanger is negligible
- each solid plate is flat with uniform thickness and no roughness
- each fluid channel is uniform in the flow direction but the height of each flow channel can vary
- perfect fluid mixing at the heat exchanger outlet

According to [28] it is valid to treat fluid in channels with the heights considered here as a continuum. Applying finite element analysis of fluid and heat transfer phenomena to microchannel heat exchangers has been shown to produce accurate results [29]. Viscous dissipation effects become more significant as channel spacing is reduced and the fluid flow rate is increased. For the cases considered, the maximum pumping loss is 0.3 W/m, which represents 0.5 % of the energy transferred during the simulated blow process and is therefore assumed to have minimal effects on the predicted results.

A method to determine when conjugate heat transfer must be considered is to calculate the Maranzana number [30]

$$\mathrm{Ma} = \frac{k_\mathrm{s} A_\mathrm{s}}{k_\mathrm{f} A_\mathrm{f} \mathrm{RePr}}, \tag{1}$$

where Pr is the Prandtl number, k is the thermal conductivity, A is surface area and the subscripts s and f refer to solid and fluid, respectively. For conditions in this study, Ma is generally of the order of 5. Values of less than

0.01 correspond to situations where conjugate heat transfer can be ignored, thus conduction along the aluminum plates cannot be ignored in this study.

The numerical model comprised of a number of identical plates separated by fluid channels with varying spacing has been implemented in COMSOL [31]. The fluid and solid in the heat exchanger are initialized with a uniform low temperature and the bed is subjected to a step increase in fluid temperature and fluid flow at time = 0. This numerical heat transfer model, presented and validated in [23], is used to predict how each microchannel stack with channel thicknesses corresponding to the laser measurements presented above and to compare the performance to that of ideal stacks of uniform fluid channels. Each cross section measured with the laser scanner is assumed to be an independent heat exchanger that maintains the specific cross section along the entire length of the stack. In this way, a total of eight heat exchangers are investigated, as each set of nominal channel thickness, stacks denoted by "up" and "down", respectively, are individually analyzed. It is expected that each pair will perform somewhat similarly, however, as the data presented in Appendix Appendix A indicate, the "up" and "down" stacks are not identical. Because laser measurements could not be obtained for each flow channel, the number of channels used in the numerical model is different than the number in the actual regenerator. Here the number of channels in the numerical model is the same as the number of channels that could be measured with the laser technique, which is 17 channels for the 0.7 mm spacing, 14 channels for the 0.4 mm spacing, 15 channels for the 0.2 mm spacing, and 17 channels for the 0.1 mm spacing.

The model solves the coupled 2-dimensional transient heat transfer equations of both the solid and heat transfer fluid with the resolved dimensions being the direction of the flow (denoted x) and the direction of the stacking of the plates (denoted y). Therefore, the microchannels are treated as infinitely wide parallel plates. The governing heat transfer equations in the fluid and solid are

$$\rho_{\mathrm{f}} c_{\mathrm{f}} \left(\frac{\partial T_{\mathrm{f}}}{\partial t} + \mathbf{u} \cdot \nabla T_{\mathrm{f}} \right) = k_{\mathrm{f}} \nabla^2 T_{\mathrm{f}} \tag{2}$$

$$\rho_{\mathrm{s}} c_{\mathrm{s}} \frac{\partial T_{\mathrm{s}}}{\partial t} = k_{\mathrm{s}} \nabla^2 T_{\mathrm{s}}. \tag{3}$$

Here, T is temperature and t is time. The mass density, specific heat and thermal conductivity, denoted ρ, c and k, respectively, are assumed constant at all times and temperatures. The fluid flow, represented by the velocity field, $\mathbf{u}$, is assumed to be laminar, incompressible and fully developed. The velocity field thus reduces to

$$\mathbf{u} = (u_x(y), 0, 0), \tag{4}$$

The velocity in the ith channel, $u_{x,i}(y)$, is then found analytically,

$$u_{x,i}(y) = \frac{3}{2} \tilde{u}_i \left(1 - 4 \frac{(y - H_{\mathrm{f},i}/2)^2}{H_{\mathrm{f},i}^2} \right), \tag{5}$$

where $H_{\mathrm{f},i}$ is the height of the ith fluid channel and y_i is the coordinate in the resolved direction, orthogonal to the flow direction being zero at the boundary between the fluid channel and the lower plate and equal to $H_{\mathrm{f},i}$ at the similar boundary between the upper plate and the fluid channel. The mean fluid velocity in the channel is denoted $\tilde{u}_i$. For a given distribution of

channels and a volumetric flow rate per unit width of the regenerator, $\dot{V}'$, the mean fluid velocity in the ith channel is found by assuming that the pressure drop is the same in each channel:

$$\tilde{u}_i = N\dot{V}' \frac{H_{\mathrm{f},i}^2}{\sum_{i=1}^{N} H_{\mathrm{f},i}^3}, \tag{6}$$

where N is the number of channels.

The heat transfer equations, (2–3), are coupled at the boundary interfaces between the solid and the fluid domains through the boundary condition

$$k_{\mathrm{s}} \frac{\partial T_{\mathrm{s}}}{\partial y} = k_{\mathrm{f}} \frac{\partial T_{\mathrm{f}}}{\partial y}, \tag{7}$$

valid on the internal boundaries only. In this way the non-slip boundary condition is implicitly assumed and, furthermore, no temperature jumps are assumed at the boundaries between solid and fluid.

The transient equations governing heat transfer in the microchannels (Eq. 2 - 7) are solved over a finite element grid using COMSOL. Details about the mesh parameters and solver package used for the numerical analysis are given in Table. II. The hot fluid is allowed to flow through the heat exchanger until the temperature at the heat exchanger outlet is within 0.005 K of the inlet temperature. The blow time depends on fluid flow rate and channel spacing.

3.1. Evaluating the performance of the parallel plate heat exchangers

Single blow testing has previously been used to experimentally measure the heat transfer in heat exchangers with complex geometries, such as packed particles, where direct measurement of the heat transfer coefficient is difficult. The single blow method described in, e.g., [32] measures the thermal response

Table II: Parameters used to run the single blow heat exchanger model.

Parameter	Value
Number of fluid channels	14-17
Plate length	40 mm
Plate thickness	0.4 mm
Plate specific heat	903 J/kgK
Plate thermal conductivity	235 W/mK
Plate density	2704 kg/m^3
Fluid specific heat	4200 kg/m^3
Fluid thermal conductivity	0.6 W/mK
Fluid density	1000 kg/m^3
Mass of aluminum plates	0.0195 kg
Number of elements in flow direction	128
Number of vertical elements in each channel	8
Number of vertical elements in each plate	1
Maximum time step	0.005
Solver package	UMFPack
Solver absolute tolerance	0.001
Solver relative tolerance	0.0001

of a heat exchanger subjected to a step change in inlet temperature. If the inlet condition is well known, the outlet temperature profile measured as a function of time can be used to determine the average heat transfer in the heat exchanger. Some of the advantages of treating the entire plate stack using a single blow method are that it characterizes the heat transfer in the entire heat exchanger, rather than each flow channel individually, and that it allows for the interaction between channels of different heights to influence overall heat transfer performance. The thermal reaction of a heat exchanger made of a distribution of non-uniform channels subjected to a step change of fluid flow and temperature at the inlet is modeled. The bulk average outlet

temperature is calculated and used to characterize the average heat transfer in the heat exchanger using the same standard techniques applied in single blow experiments.

Characterizing the performance of a specific parallel plate stack exposed to certain conditions may be done in several ways. Fundamentally, as the flow propagates through the heat exchanger the temperature of the fluid at the output, $T_{\mathrm{o,f}}$, changes from the initial temperature, T_{i}, until it eventually reaches the input temperature, $T_{\mathrm{i,f}}$. $T_{\mathrm{o,f}}$ is defined as the average temperature at each time step at the outlet of the flow channel. The total volumetric average value, assuming a constant specific heat, is equal to

$$T_{\mathrm{o,f}}(t) = \frac{\sum_{i=1}^{N} T_{\mathrm{o,f},i}(t)\tilde{u}_i H_{\mathrm{f},i}}{\sum_{i=1}^{N} \tilde{u}_i H_{\mathrm{f},i}}, \tag{8}$$

where $T_{\mathrm{o,f},i}(t)$ is the average outlet temperature of the ith channel at time t.

This temperature response curve is key to understanding the heat transfer performance, however it is not a direct measurement of heat transfer in the heat exchanger. In [32] a set of experimental techniques to evaluate the regenerator performance using this curve is discussed. The methods are focused on various properties of the temperature response curve and each has its own justification, depending on the experimental conditions. For this work, it was decided to consider two of the methods. These are denoted the M and S methods, respectively. The former is focused on the steepest gradient of the temperature response curve and the latter considers the difference in time between the breakthrough of 20 and 80 % of the temperature curve, respectively.

The "M method" may mathematically be written as [32]

$$\mathrm{M} = K\max\left(\frac{\mathrm{d}T_{\mathrm{o,f}}}{\mathrm{d}t}\right). \tag{9}$$

Here K is a function of the volumetric flow rate and the thermal properties.

The "S-method" may be written as

$$\mathrm{S} = C\left(\tau_{80} - \tau_{20}\right), \tag{10}$$

where C is again a function of the volumetric flow rate and the thermal properties of the solid and fluid. τ_{20} and τ_{80} mark the 20 and 80% breakthrough times of the outlet curve, $T_{\mathrm{o,f}}$.

To determine the average heat transfer in the heat exchanger, the values of M and S must be matched to the corresponding values of an output curve for a heat exchanger with known heat transfer characteristics. The known geometry chosen in this work is a single uniform channel with a half plate at either side made from the same materials as the multiple plate heat exchanger. A single microchannel has been shown experimentally to agree with its theoretical performance [11] and experiences nominally the same conjugate heat transfer as a microchannel stack with varying channel heights, making it a preferable condition to compare M and S values.

Fitting the output curves of the full non-uniform stack presents a challenge. Conjugate heat transfer can become significant due to the high conductivity of the solid and the shape of the outlet fluid curve for both the single and multiple channel models can be sensitive to a range of modeling parameters. Four modeling scenarios in which the heat transfer between solid and fluid can be varied were considered for fitting M and Svalues: a 1D regen-

erator model with a user-specified heat transfer coefficient, a 2D model of a single channel with varying plate spacing, a 2D model of a single channel with varying fluid thermal conductivity, and a 2D model of a single channel with a varying thermal resistance between the solid and fluid boundaries. The 1D model did not provide adequate results because the axial conduction in the 1D and 2D model seemed to affect the model results in different ways. The 1D model ignores temperature gradients normal to the fluid flow direction in the solid and fluid as well as the velocity profile in the fluid, which likely caused small discrepancies between the two models under certain operating conditions. Using a 2D model and varying the plate spacing to vary the heat transfer was also investigated. However, this technique has the disadvantage that changing the plate spacing also changes the porosity and average fluid velocity in the channel, thus changing several transport properties in the heat exchanger. Using a 2D model and varying the fluid thermal conductivity effectively varies the heat transfer in the regenerator, but it also changes the rate in which heat is transferred from the fluid at the wall into the bulk fluid stream. This also artificially changes thermal transport in the fluid, making it less than ideal for a fitting model. Adding a thermal resistance between the fluid and solid domains in a 2D model allows the effective heat transfer between the solid and fluid to vary while preserving the same regenerator geometry and heat transport in both the solid and fluid domains. Therefore, all curve fitting was done using the thermal resistance method. The single channel model is, of course, run at the average channel height of the multiple channel model. The thermal resistance acts as a reduction in the heat transfer coefficient between the fluid and solid. This may be formulated

mathematically as a Nusselt number scaling factor

$$\mathrm{Nu}_{\mathrm{scl}} = \frac{1/h}{1/h + d/k}, \tag{11}$$

where d is the thickness of the virtual thermal resistance layer and k is the conductivity. The convective heat transfer coefficient may be found from the Nusselt number relation.

$$h = \frac{\mathrm{Nu}k_{\mathrm{f}}}{D_{\mathrm{H}}}, \tag{12}$$

The mean Nusselt number for a parallel plate duct at constant wall temperature varies along the flow direction [33]; however, for the operating conditions considered here the average Nusselt number varies less than 1 % over the range of flow rates and channel thicknesses. In order to illuminate the impact of flow maldistribution on the heat transfer performance of the parallel plate heat exchanger h is therefore calculated based on the constant Nusselt number, 7.541.

M and S can then be found as a function of the Nusselt number scaling factor in the heat exchanger. An example of this is given in Fig. 1. In this way, the average heat transfer in a stack of varying microchannels can be summarized as having the same heat transfer performance as a single channel having a reduced effective heat transfer coefficient yielding the same value of M or S. In order to compare M and S values for single channel and multiple channel heat exchangers, the average fluid flow per channel must be equal. Note that larger channels in the multiple channel heat exchangers will receive a larger portion of the fluid flow, but the average channel fluid flow in the multiple channel heat exchanger must be the same as the single

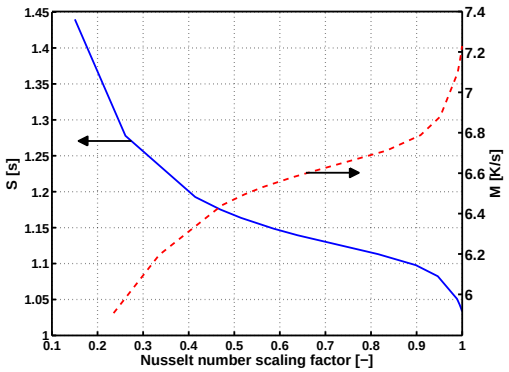

Figure 1: Example of the M and S values as a function of Nusselt number reduction factor at a volumetric flow rate of 9 $\mathrm{mm^2 s^{-1}}$ and a channel thickness of 0.2 mm.

channel heat exchanger.

The curves for $\mathrm{M}(\dot{V}_0', \mathrm{Nu_{scl}}, H_\mathrm{f})$ and $\mathrm{S}(\dot{V}_0', \mathrm{Nu_{scl}}, H_\mathrm{f})$ may thus be found at a given volumetric flow rate, $\dot{V}_0'$, and nominal plate spacing, H_f. In order to quantify the performance of an inhomogeneous regenerator, the values of $\mathrm{M_{reg}}$ and $\mathrm{S_{reg}}$ are extracted from the breakthrough temperature curve of that particular regenerator (and at $\dot{V}_0'$). The Nusselt number scaling factor is then found through interpolation in the $\mathrm{M}(\dot{V}_0', \mathrm{Nu_{scl}}, H_\mathrm{f})$ and $\mathrm{S}(\dot{V}_0', \mathrm{Nu_{scl}}, H_\mathrm{f})$ single channel data, respectively. The effective heat transfer coefficient then becomes

$$h_\mathrm{eff} = \mathrm{Nu_{scl}} \frac{7.541 k_\mathrm{f}}{D_\mathrm{H}} \tag{13}$$

The Nusselt number scaling factor determined from the M and S values, respectively, were found to generally agree.

4. Results and discussion

4.1. Experimental results

The aluminum regenerator experiments were designed to compare model predictions with experimental results. For a passive regenerator with con-

stant material properties, the regenerator effectiveness is a function of utilization and NTU [34]. When the fluid flow rate and the mass of the solid heat exchanger material are held constant, the only factor that affects regenerator effectiveness is the heat transfer coefficient between solid and fluid, which is directly proportional to NTU. Therefore, a higher effective heat transfer coefficient will result in a more effective regenerator.

The four aluminum stacks detailed above were tested in the active magnetic regenerator test device described in Sec. 2.2 as passive regenerators. For each stack two flow rates and four different values of the thermal utilization were tested. The thermal utilization is defined as

$$\varphi = \frac{\dot{m} c_{\mathrm{f}}}{2 f c_{\mathrm{s}} m_{\mathrm{s}}}, \tag{14}$$

where $\dot{m}$ is the fluid mass flow rate, f is operating frequency and m_{s} denotes the mass of solid material.

Figure 2 gives the results in the form of steady-state temperature spans as a function of the nominal channel thickness at a fixed heater power of 2.1 W. If each regenerator were fabricated with uniform plate spacing, it is expected that the regenerator temperature span should increase as the plate spacing decreases. However, for the non-uniform regenerators tested here, the stack nominally spaced with 0.2 mm has the best performance, indicating the highest effective heat transfer in the regenerator, in all cases, and the performances of the 0.1 mm and 0.4 mm stacks are quite similar with a tendency that the 0.4 mm stack performs slightly better than the 0.1 mm does. The 0.74 mm stack has overall the poorest performance. The experimental performance suggests a severe reduction in the heat transfer coefficients from

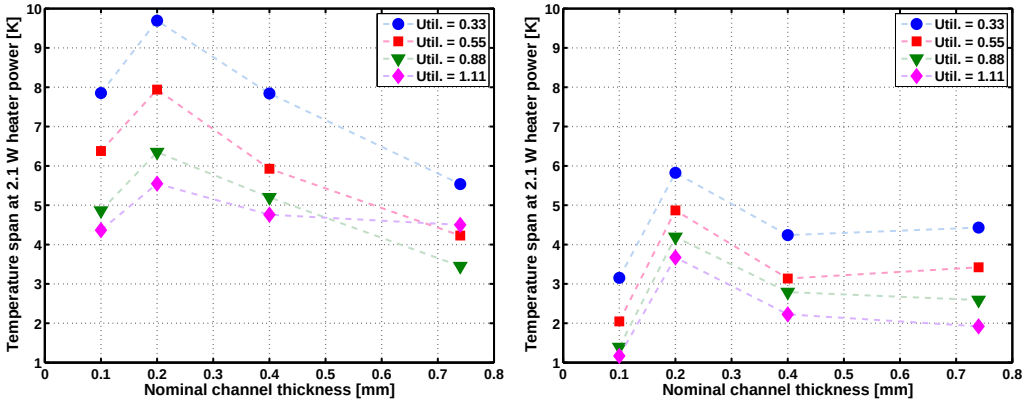

Figure 2: Steady-state temperature spans at a fixed heater power (2.1 W) as a function of mean channel thickness, thermal utilization and flow rate (a): 1.6 mm^2s^{-1}, (b): 6.4 mm^2s^{-1}. The ambient temperature and thus the cold end was set to 288 K.

the expected values as the nominal channel thickness decreases from 0.2 to 0.1 mm.

4.2. Analysis of aluminum regenerators

The aluminum regenerators are analyzed using measured plate spacing in order to compare the predicted performance to the measured performance in the passive regenerator test. In the experiment, commercial grade aluminum and a mixture of 25% ethylene glycol and 75% water were used. The properties used for this study are given in Tab. III. The model predictions for the effective heat transfer coefficient for both the up and down sides of each regenerator at both fluid flow rates that were tested are summarized in Fig. 3.

In Fig. 3 the effective heat transfer coefficient is plotted as a function of the mean (or nominal) channel thickness for the down (Fig. 3(a)) and up (Fig. 3(b)) stacks at different flow rates. The effective heat transfer coeffi-

Table III: Material properties used for simulation of the passive regenerator experiments.

Parameter	Value
Plate specific heat	902 J/kgK
Plate thermal conductivity	218 W/mK
Plate density	2700 kg/m^3
Fluid specific heat	3811 J/kgK
Fluid thermal conductivity	0.486 W/mK
Fluid density	1031 kg/m^3

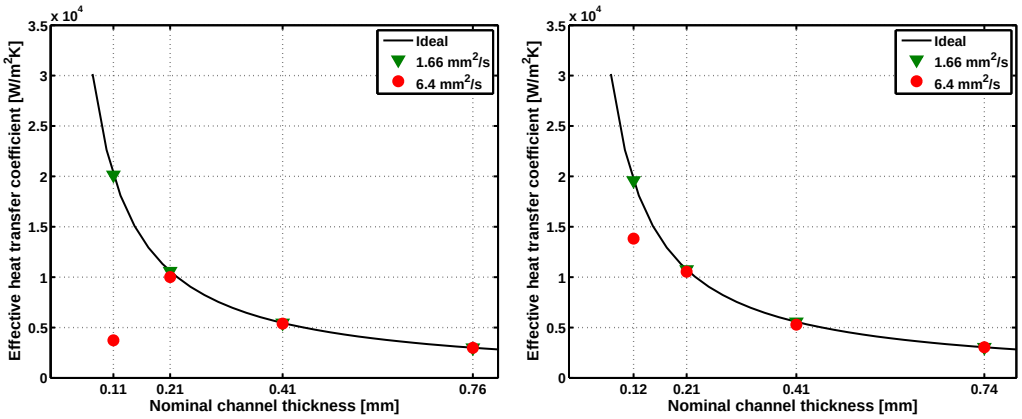

(a) (b)

Figure 3: The predicted convective heat transfer coefficient as a function of nominal, i.e. mean, channel thickness for the down stacks (a) and the up stacks (b) at different flow rates. The heat transfer coefficient for a uniform ("ideal") plate stack is plotted for comparison. The flow rates are indicated in the figure legends.

cient is seen to deviate drastically from the ideal case as the nominal channel thickness decreases (and thus the relative standard deviation increases). It is also apparent from the figure that the flow rate has a significant influence on the effective heat transfer coefficient. At the lowest flow rate almost no deviation from the ideal case is observed whereas at the larger flow rates the deviation becomes as much as a factor of four at the smallest nominal channel thickness.

At the higher experimental flow rate, the model is in very good agreement with experiment, which both predict that the 0.2 mm regenerator has the highest performance, the 0.1 mm and 0.4 mm stacks having similar performance, and the 0.7 mm stack having the lowest performance. The lower flow rate results do not agree as well with experiment. The model predicts that the 0.1 mm stack will have the highest performance, while the 0.2 mm stack exhibited the best performance experimentally. It was found that the solid thermal conductivity has a large influence on heat transfer degradation, and the discrepancy between model and experiment may be partially caused by the commercial aluminum conductivity being lower than the value used in the model. Accurately measuring the thermal conductivity of the aluminum plates is considered outside the scope of this paper.

4.3. A plate stack with constant absolute standard deviation

The analysis of the experimental regenerators is expanded to quantify the effect of reducing the plate spacing on heat transfer performance. 14 random numbers were chosen from a distribution with a mean of 0 mm and a standard deviation of 35 μm. The numbers, shown in Tab. IV, are used to create a distribution of channel thicknesses. For each channel distribution, the absolute standard deviation is held constant while the average thickness is varied. By holding the deviations in channel thickness constant the effect of decreasing nominal plate spacing while using the same fabrication technique is simulated. In this section, pure aluminum properties and pure water properties as found in Tab. IV are used in the simulations.

Regenerators comprised of 14 channels with nominal plate spacings from 0.075 mm to 0.8 mm with spacing distributions that are calculated using the

Table IV: The 14 normally distributed channels with a mean value of 0 mm and a standard deviation of 0.035 mm.

Channel no.	1	2	3	4	5	6	7	8	9	10	11	12	13	1
Deviation from nominal [μm]	6	-25	-3	10	-27	-9	11	-55	31	73	29	-9	13	-3

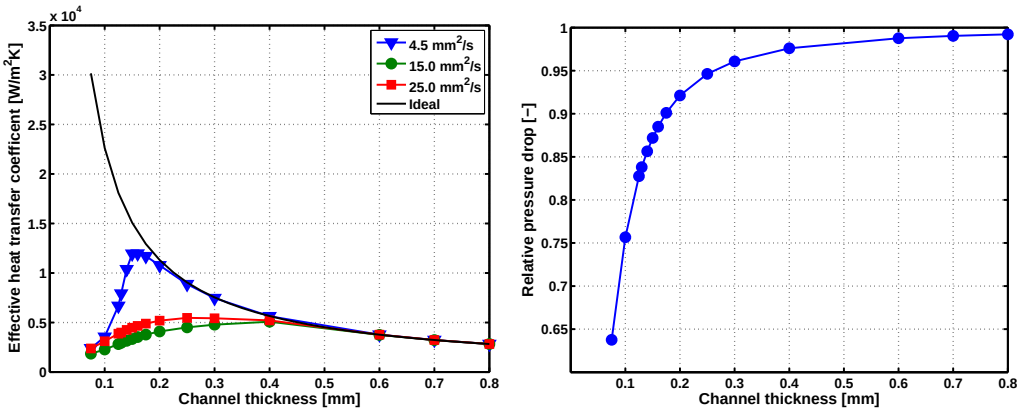

(a) (b)

Figure 4: The effective heat transfer coefficient (a) and the relative pressure drop (b) both as a function of the nominal channel thickness compared to a uniform (ideal) stack. The relative standard deviation varies while the absolute standard deviation is kept constant at 0.035 mm. The relative pressure drop is calculated as the ratio between the pressure drop of the inhomogeneous stack and that of the equivalent homogeneous stack with a channel spacing equal to the mean spacing of the inhomogeneous stack.

deviation values from Tab. IV were simulated in the CFD model for several fluid flow rates. The output curves were used to calculate the effective heat transfer coefficient in the regenerator by Eq. 13 and the results are shown in Fig. 4(a).

When considering the absolute heat transfer coefficient for the flow rates (Fig. 4(a)) it is observed that for the larger flow rate a certain value of the nominal channel thickness / relative standard deviation exists where the heat transfer coefficient has a maximum. At lower channel thicknesses the

effective heat transfer coefficient actually decreases. This is because as the nominal plate spacing decreases, the relative non-uniformity increases. At some value of plate spacing the heat transfer losses caused by non-uniformity effects become larger than the increase in heat transfer performance due to smaller plate spacing. Figure 4(a) also shows that when the flow rate is low, the heat transfer performance is less affected by non-uniform plate spacing. This may be because the heat exchanger is dominated by conduction losses, which outweigh convection losses due to non-uniformity.

The ratio between pressure drop and heat transfer coefficient is commonly used as a measure of the quality of a particular heat exchanger geometry at a certain set of operating conditions. In Fig. 4(b) the pressure drop is not reduced accordingly and for the inhomogeneous stack normalized with the nominal pressure drop is plotted. Although the ratio of pressure drop of non-uniform to uniform plate spacing does decrease as the nominal channel thickness decreases (due to the fact that individual channels in the distribution become relatively large) the decrease is clearly smaller than those of the effective heat transfer coefficient, particularly at the larger flow rates. It may thus be concluded that not only does the heat transfer become significantly degraded as the channel thickness decreases, but the pressure drop still remains relatively large. Thus with increasing relative non-uniformity, both a severe reduction in heat transfer coefficient is observed at the same time as the quality parameter (heat transfer / pressure drop fraction) is significantly decreased.

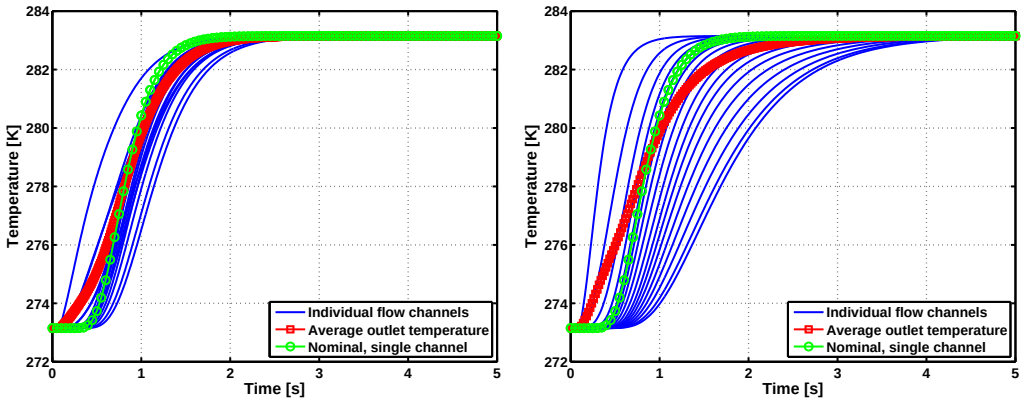

Figure 5: Examples of the breakthrough curves of the individual channels in the 0.1 mm (down) stack unsorted (a) and sorted (b). Overplotted are the resulting breakthrough curves for each stack (as calculated using Eq. 8) and the single channel breakthrough curve found by applying the mean (nominal) spacings of the respective stacks.

4.4. Influence of thermal cross-talk

The flow maldistribution in an inhomogeneous parallel plate stack causes what may be denoted thermal cross talk. The thermal waves of each individual channel will propagate at different speeds due to the different fluid velocities. Heat transfer will therefore be present orthogonal to the direction of the flow through the solid. The significance of this effect is of course dependent on the actual materials properties as well as the degree of flow maldistribution.

The 0.1 mm (down) and 0.7 (down) stacks are applied in two modes. In the first mode they are run with the channel heights arranged in the same order as the actual plate stack at a flow rate of 15 $\mathrm{mm^2 s^{-1}}$ whereas in the other mode their individual channels are sorted after size. In this way the cross talk will differ between the two modes, keeping everything else the same. The high flow rate is chosen to reduce the relative effect of conduction.

Table V: M and S values for the 0.1 down and 0.7 down stacks both for the original stacks and when they are sorted. Furthermore, the single channel corresponding values are provided.

	0.1 dn, sorted	0.1 dn	0.1 single	0.7 dn, sorted	0.7 dn	0.7 single
S [s]	0.86	0.69	0.45	1.37	1.36	1.30
M [K/s]	8.4	10.35	15.75	5.83	5.88	6.26

Considering Fig. 5 the difference between the two modes for the 0.1 mm (down) stack are clearly observed. The resulting outlet temperature curve is plotted as are each of the individual channel outputs. Furthermore, the nominal (single channel) output curve is overplotted for comparison. The average output curve of the sorted stack (Fig. 5(b)) does breaks through sooner than that of the unsorted stack (Fig. 5(a)). However, it is clearly seen that both the steepest part of the curve and the time interval between the 20 and 80 % breakthroughs indicate a poorer performance than that of the unsorted stack. In Table V the M and S values are given.

In the case of the sorted stack the individual channels behave closer to being individually isolated channels than in the case of the unsorted stack. In this way the majority of the channels have breakthroughs that are significantly slower in the case of the sorted stack compared to the case of the unsorted stack. This means that the resulting average breakthrough curve is extended. In terms of the thermal cross talk this means that the unsorted, or random, stack overall experiences more cross talk than the sorted stack does. In that way the stack that is non-ideal may be helped somewhat in terms of the cross talk that seems to smooth out the effect of the flow maldistribution.

In Fig. 6 the breakthrough curves for the 0.755 mm (down) stack in both

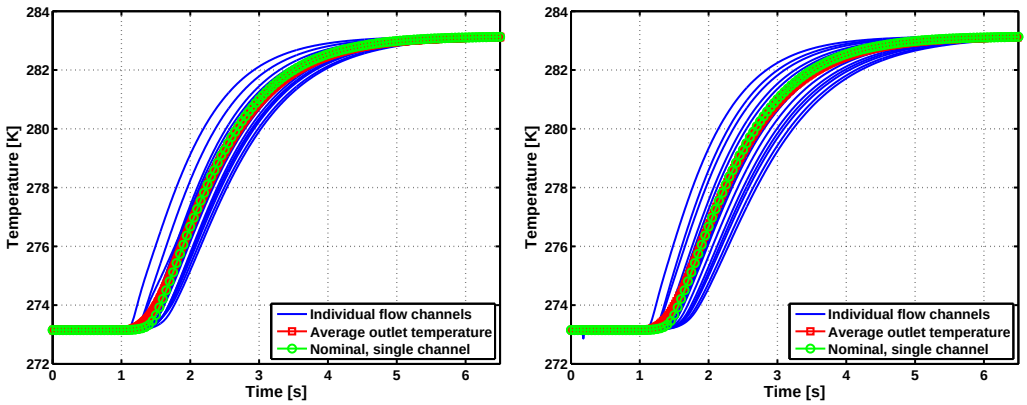

Figure 6: Breakthrough curves of the 0.755 mm (down) of the individual flow channels unsorted (a) and sorted (b). As in Fig. 5, the resulting breakthrough curves of the overall stacks and the single channel breakthrough curves are plotted.

the unsorted and sorted modes are plotted in the same manner as Fig. 5 where the 0.112 mm (down) stack was considered. The trend is the same as for the nominally smaller channel thickness stack, however, the effect of sorting the channels is significantly smaller (see Tab. V). This is simply due to the fact that the thermal waves moving perpendicular to the direction of the flow are exposed to a much larger thermal resistance since the flow channels are roughly seven times larger than in the former case.

A direct comparison of the influence of the thermal cross talk may be done by considering Fig. 7. Here, the breakthrough curves of the two extreme channels from the 0.112 mm (down) stack are plotted for the two modes (unsorted and sorted). In the same figure the corresponding nominal breakthrough curves are plotted. It is clearly observed that the thermal cross talk is more pronounced in the unsorted stack. The effect is that the individual extreme breakthrough curves are brought closer together and thus

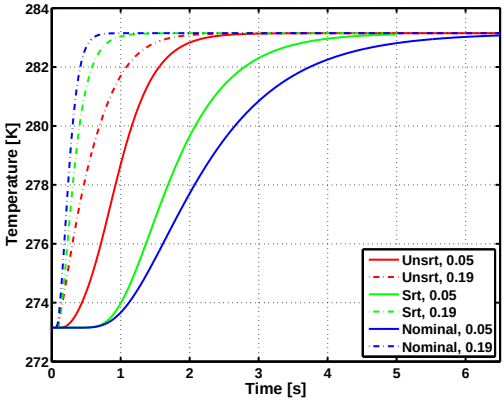

Figure 7: The breakthrough curves of the two extreme channels from the 0.112 mm (down) stack plotted for both the unsorted and sorted modes. The nominal curves indicate the corresponding single channel heat exchangers with the same fluid velocity as present in the respective channels in the stacks. The thicknesses of the two channels are 0.05 and 0.19 mm, respectively.

further from their respective nominal curves.

5. Conclusions

This paper presents a numerical method to quantify the heat transfer degradation associated with non-uniform flow channel thickness in a two-dimensional stack of flat plates using a single blow technique to characterize bulk heat transfer in the heat exchanger. The resulting heat transfer degradation can then be used in a simpler 1D or single-channel 2D model to model more complex systems using microchannel heat exchangers. Simulations showed that large decreases in heat transfer performance can occur when flow channels are not uniformly spaced, which may explain the lower-than-expected performance of microchannel heat exchangers reported in the literature. These effects are unrelated to many previous explanations of reduced microchannel performance, such as break-down of the continuum fluid

assumption and temperature dependent properties in the fluid. The CFD model presented was validated on flat plate heat exchangers tested as passive regenerators. The model predicted that as the channel spacing was decreased using a given fabrication technique, the gap between the ideal and actual heat transfer performance increases with decreasing plate spacing, which was observed experimentally in a cyclic steady-state test apparatus.

This paper also studied the effects of thermal cross talk between fluid channels. The cross talk was shown to improve performance of a microchannel heat exchanger compared to a series of fluid channels that are thermally isolated from each other. The range of channel thickness affects microchannel performance, but the arrangement of the various channel thicknesses can also be important. Results in this paper are presented only for heat exchangers consisting of aluminum and a water-based heat transfer fluid. Results for materials with different properties may vary by a large degree and should be considered individually.

Acknowledgements

The authors thank the support of the Programme Commission on Energy and Environment (EnMi) (Contract no. 2104-06-0032) which is part of the Danish Council for Strategic Research. The technical assistance from Johan Hjelm, Risø DTU, is gratefully appreciated. K.K. Nielsen also wishes to thank The Danish Council for Independent Research — Technology and Production Sciences (Contract no. 10-092791) for financial support.

References

[1] R. Radebaugh. Development of the pulse tube refrigerator as an efficient and reliable cryocooler. *Proc. Institute of Refrigeration*, 96:11–31, 1999-2000.

[2] M. J. White, G. F. Nellis, S. A. Klein, and Y. Zhu, W. Gianchandani. An experimentally validated numerical modeling technique for perforated plate heat exchangers. *J. Heat Transfer*, 132:111801, 2010.

[3] Sanjeev Jain, P.L. Dhar, and S.C. Kaushik. Evaluation of liquid dessicant based evaporative cooling cycles for typical hot and humid climates. *Heat Recovery Systems & CHP*, 14(6):621–632, 1994.

[4] Rodger W. Dyson, Scott D. Wilson, Rodger W. Dyson, Roy C. Tew, Scott D. Wilson, and Roy C. Tew. Review of computational stirling analysis methods. *Collect. Tech. Pap. Int. Energy Convers. Eng. Conf.*, 1:511–531, 2004.

[5] Bancha Kongtragool and Somchai Wongwises. A review of solar-powered stirling engines and low temperature differential stirling engines. *Renewable & Sustainable Energy Reviews*, 7(2):131–154, 2003.

[6] Ryan J. McGlen, Roshan Jachuck, and Song Lin. Integrated thermal management techniques for high power electronic devices. *Applied Thermal Engineering*, 24(8-9):1143–1156, 2004.

[7] K.A. Gschneidner and V.K. Pecharsky. Thirty years of near room temperature magnetic cooling: Where we are today and future prospects. *International Journal of Refrigeration*, 31:945–961, 2008.

[8] M. P. Mitchell, D. Gedeon, G. Wood, and M. Ibrahim. Results of tests of etched foil regenerator material. In *Cryocoolers*, volume 14, pages 381–387, 2007.

[9] P. Rosa, T.G. Karayiannis, and M.W. Collins. Single-phase heat transfer in microchannels: The importance of scaling effects. *Applied Thermal Engineering*, 29(17-18):3447–3468, 2009.

[10] Gian Luca Morini. Scaling effects for liquid flows in microchannels. *Heat Transfer Eng*, 27(4):64–73, 2006.

[11] Andrei G. Fedorov and Raymond Viskanta. Three-dimensional conjugate heat transfer in the microchannel heat sink for electronic packaging. *International Journal of Heat and Mass Transfer*, 43(3):399–415, 2000.

[12] Giulio Croce and Paola D'Agaro. Numerical analysis of roughness effect on microtube heat transfer. *Superlattices and Microstructures*, 35(3-6):601–616, 2004.

[13] Giulio Croce and Paola D'Agaro. Numerical simulation of roughness effect on microchannel heat transfer and pressure drop in laminar flow. *J. Phys. D: Appl. Phys.*, 38(10):1518–1530, 2005.

[14] J. Koo and C. Kleinstreuer. Analysis of surface roughness effects on heat transfer in micro-conduits. *International Journal of Heat and Mass Transfer*, 48(13):2625–2634, 2005.

[15] Poh-Seng Lee, Suresh V. Garimella, and Dong Liu. Investigation of heat transfer in rectangular microchannels. *International Journal of Heat and Mass Transfer*, 48(9):1688–1704, 2005.

[16] Gabriel Gamrat, Michel Favre-Marinet, and Dariusz Asendrych. Conduction and entrance effects on laminar liquid flow and heat transfer in rectangular microchannels. *International Journal of Heat and Mass Transfer*, 48(14):2943–2954, 2005.

[17] Weilin Qu and Issam Mudawar. Analysis of three-dimensional heat transfer in micro-channel heat sinks. *International Journal of Heat and Mass Transfer*, 45(19):3973–3985, 2002.

[18] J.H. Ryu, D.H. Choi, and S.J. Kim. Three-dimensional numerical optimization of a manifold microchannel heat sink. *International Journal of Heat and Mass Transfer*, 46(9):1553–1562, 2003.

[19] Wiebke Brix, Martin Ryhl Kærn, and Brian Elmegaard. Modelling refrigerant distribution in microchannel evaporators. *International Journal of Refrigeration*, 32(7):1736–1743, 2009.

[20] Wiebke Brix, Martin Ryhl Kærn, Brian Elmegaard, and Martin Ryhl Kærn. Modelling distribution of evaporating CO_2 in parallel minichannels. *International Journal of Refrigeration*, 33(6):1086–1094, 2010.

[21] Liang-Liang Shao, Liang Yang, Bo Gu, Liang Yang, and Chun-Lu Zhang. Numerical modeling of serpentine microchannel condensers. *International Journal of Refrigeration*, 32(6):1162–1172, 2009.

[22] Mathieu Martin, Chris Patton, John Schmitt, and Sourabh V. Apte. Direct simulation based model-predictive control of flow maldistribution in parallel microchannels. *Journal of Fluids Engineering, Transactions of the ASME*, 131(11):1112011–11120117, 2009.

[23] Jesper B. Jensen, Kurt Engelbrecht, Christian R.H. Bahl, Nini Pryds, Gregory F. Nellis, Sanford A. Klein, and Brian Elmegaard. Modeling of parallel-plate regenerators with non-uniform plate distributions. *International Journal of Heat and Mass Transfer*, 53(24-24):5065, 2010.

[24] J. B. Jensen, C. R. H. Bahl, K. Engelbrecht, B. Elmegaard, and N Pryds. Analysis of single blow effectiveness in non-uniform parallel plate regenerators. *Int. J. Heat and Mass Transfer*, 54:4746–4751, 2011.

[25] K. Engelbrecht, K. K. Nielsen, and N. Pryds. An experimental study of passive regenerator geometries. In P. W. Egolf, editor, *Fourth International Conference on Magnetic Refrigeration at Room Temperature*. International Institute of Refrigeration, 2010.

[26] K. Engelbrecht, C. R. H. Bahl, K. K. Nielsen, and N. Pryds. Experimental results for a magnetic refrigerator using three different types of magnetocaloric material regenerators. *International Journal of Refrigeration*, Accepted, 2010.

[27] C. R. H. Bahl, T. F. Petersen, N. Pryds, and A. Smith. A versatile magnetic refrigeration test device. *Review of Scientific Instruments*, 79(9):093906, 2008.

[28] J.D. Jones. Optimization of stirling engine regenerator design. *Proceedings of the 25th Intersociety Energy Conversion Engineering Conference*, pages 359–65 vol.5, 1990.

[29] Poh-Seng Lee and Suresh V. Garimella. Thermally developing flow and heat transfer in rectangular microchannels of different aspect ratios. *In-*

ternational Journal of Heat and Mass Transfer, 49(17-18):3060–3067, 2006.

[30] Gael Maranzana, Isabelle Perry, and Denis Maillet. Mini- and micro-channels: influence of axial conduction in the walls. *International Journal of Heat and Mass Transfer*, 47(17-18):3993–4004, 2004.

[31] Comsol. *Comsol Multiphysics Model Library, third ed.* COMSOL AB, Chalmers Teknikpark 412 88 G., 2005.

[32] P.J. Heggs and D. Burns. Single-blow experimental prediction of heat transfer coefficients - a comparison of four commonly used techniques. *Experimental Thermal and Fluid Science*, 1(3):243–251, 1988.

[33] Markus Nickolay and Holger Martin. Improved approximation for the Nusselt number for hydrodynamically developed laminar flow between parallel plates. *International Journal of Heat and Mass Transfer*, 45(15):3263–3266, 2002.

[34] G. D. Dragutinovic and B. S. Baclic. *Operation of Counterflow Regenerators*. Computational Mechanics Inc., Billerica, MA, 1998.

Appendix A. Resulting laser measurements of the regenerator stacks

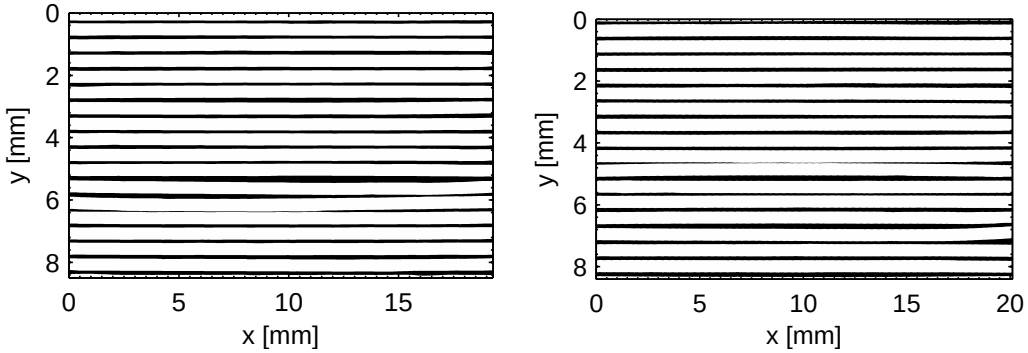

(a) 0.112 mm, down

(b) 0.116 mm, up

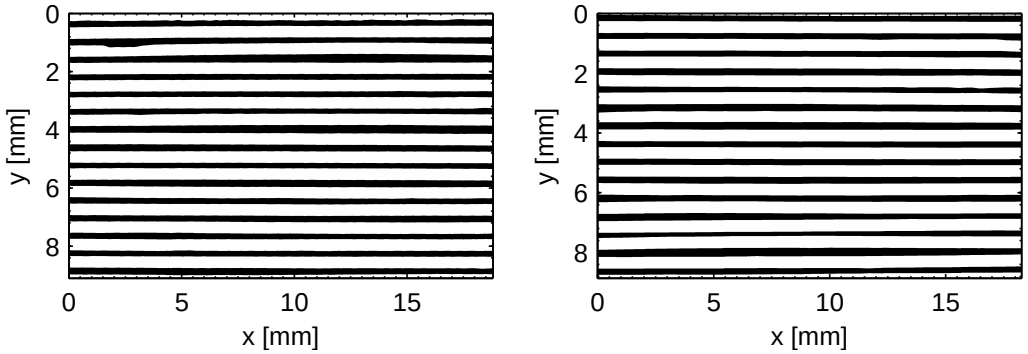

(c) 0.214 mm, down

(d) 0.211, up

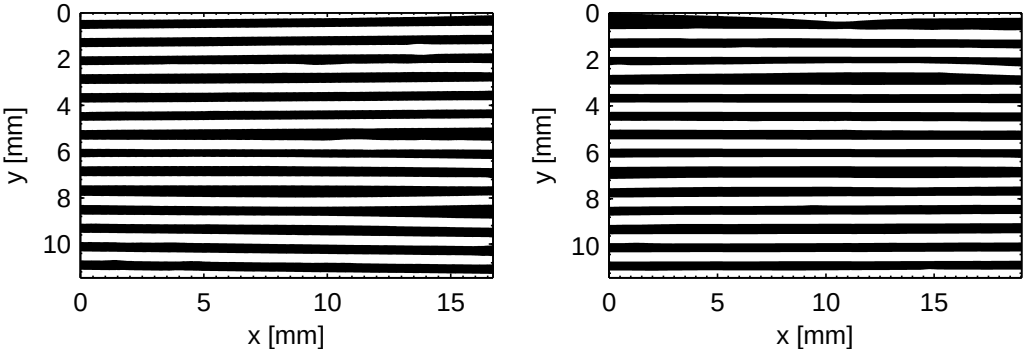

(e) 0.415, down

(f) 0.407, up

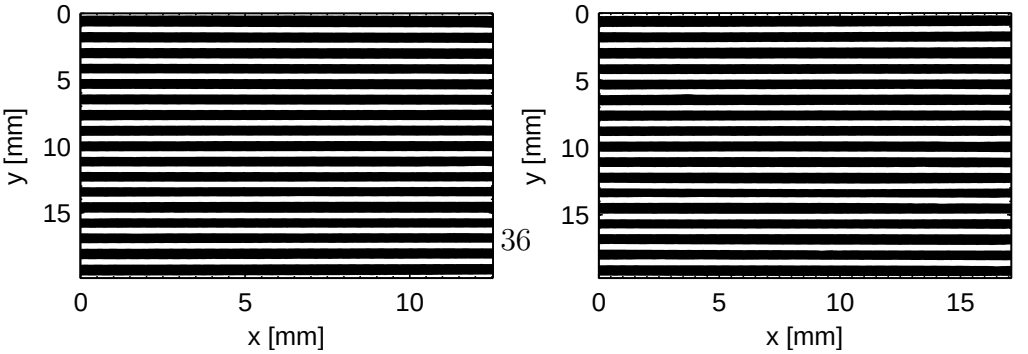

(g) 0.755, down

(h) 0.743, up

Figure A.8: The laser-measured cross sections of each of the eight regenerators considered. The mean plate spacings and the labels (up and down, respectively) are indicated in the sub-figure captions.

B.5 Magnetic Cooling at Risø DTU

This article was written for the *8th IIR Gustav Lorentzen Conference on Natural Working Fluids*, which was held in September 2008 in Copenhagen, Denmark. The article describes the status of the magnetic cooling research at Risø DTU at the time. An early version of the test machine is described in this article. The most significant differences between this version and the version used for the work described in the thesis, is that this version does not have a heat exchanger or any insulation. A different heater, which was eventually replaced due to problems with the sealing, was used in the piston and the regenerator housing consisted of solid plastic and featured flow guides at the ends of the plates. Furthermore, a 2D reciprocating model of the regenerator running as an active magnetic regenerator and the Hallbach magnet that is used in the machine are described.

Magnetic cooling at Risø DTU

K.K. Nielsen[a,b], R. Bjørk[b], J.B. Jensen[b], C.R.H Bahl[b], N. Pryds[b], A. Smith[b], A. Nordentoft[b], J. Hattel[a]

[a] Technical University of Denmark, Department for Mechanical Engineering, Produktionstorvet, building 425 room 024, 2800 Kgs. Lyngby, Denmark, kaspar.kirstein.nielsen@risoe.dk

[b] Department for Fuel Cells and Solid State Chemistry, Risø National Laboratory for Sustainable Energy, Technical University of Denmark - DTU, building 232, Frederiksborgvej 399, 4000 Roskilde

ABSTRACT

Magnetic refrigeration at room temperature is of great interest due to a long-term goal of making refrigeration more energy-efficient, less noisy and free of any environmentally hostile materials.
A refrigerator utilizing an active magnetic regenerator (AMR) is based on the magnetocaloric effect, which manifests itself as a temperature change in magnetic materials when subjected to a varying magnetic field.
In this work we present the current state of magnetic refrigeration research at Risø DTU with emphasis on the numerical modeling of an existing AMR test machine. A 2D numerical heat-transfer and fluid-flow model that represents the experimental setup is presented. Experimental data of both no-heat load and heat load situations are compared to the model. Moreover, results from the numerical modeling of the permanent magnet design used in the system are presented.

1. INTRODUCTION

The magnetocaloric effect (MCE) was discovered by E. Warburg in 1881. Warburg found that iron got heated up when placed in a magnetic field and when the magnetic field was removed the iron sample cooled down (Warburg 1881). The basic principle of the MCE is that the ordering of the magnetic moments is increased when an external magnetic field is applied to a magnetic material. This means that the spin-entropy decreases. The process is virtually adiabatic if the field is applied rapidly. This means that the total entropy of the system must remain constant and thus the lattice and electron entropies must increase, which is equivalent to an increase in temperature. The process is reversible (for some materials) and thus the opposite will take place when the field is removed again (i.e. the ordering of the magnetic moments decrease and the temperature thus decreases). The MCE is strongest at the phase-transition between the ferromagnetic and the paramagnetic phases. This phase transition takes place at the Curie temperature T_C, which can vary significantly depending on the material. In the past materials have been used mainly for cryogenic applications, but some 30 years ago research into the MCE at room temperature was commenced (Brown 1976) .
The MCE yields, for the benchmark magnetocaloric material (MCM) gadolinium (Gd), an adiabatic temperature change of about 3.6 K at room temperature for a 1 tesla (T) magnetic flux density. This rather low temperature change is obviously too small for direct usage in a cooling device. However, if the material is used in an AMR it is possible to achieve, due to regeneration, a higher temperature difference (Brown 1976). In his experiments Brown reached a temperature span of 46 K using Gd with the hot end at 319 K using a 7 T magnetic flux density from a super conducting magnet. The MCE of Gd is proportional to the magnetic flux density to the power of 0.7 (Pecharsky and Gschneidner 2006). Today's state-of-the-art permanent magnets yield a magnetic flux density of about 1.5 T (Tura and Rowe 2007). Therefore it is crucial to develop a high-performing and efficient AMR.
This work is primarily concerned with developing a model describing an existing AMR test machine based on parallel plates, and using a permanent magnet based on the Halbach design yielding around 1.1 T (Halbach 1980) . In Section 2 the experimental test machine is described. In Section 3 the corresponding numerical model is presented. In Section 4 results from the test machine and the model are compared both including no-load and load-situations. In Section 5 the results are discussed and the work is concluded with some future aspects briefly discussed.

2. EXPERIMENTAL SETUP

Figure 1 shows photos of the test machine, which consists of a regenerator core in the middle of a plastic tube with outer diameter 40 mm and inner diameter 34 mm. The regenerator core is built up of 13 plates of 99.9 % pure Gd (obtained from China Rare Metal Materials Co). The plates with dimensions 40x0.9x25 mm have a total mass of 92 g. At both ends of the Gd plates (in the flow direction) 20 mm long plastic flow guides are placed to ensure a fully developed laminar flow across the plates. The plates and flow guides are fixed by precision machined grooves and are stacked with a spacing of 0.8 mm, which is then the height of the fluid channel.

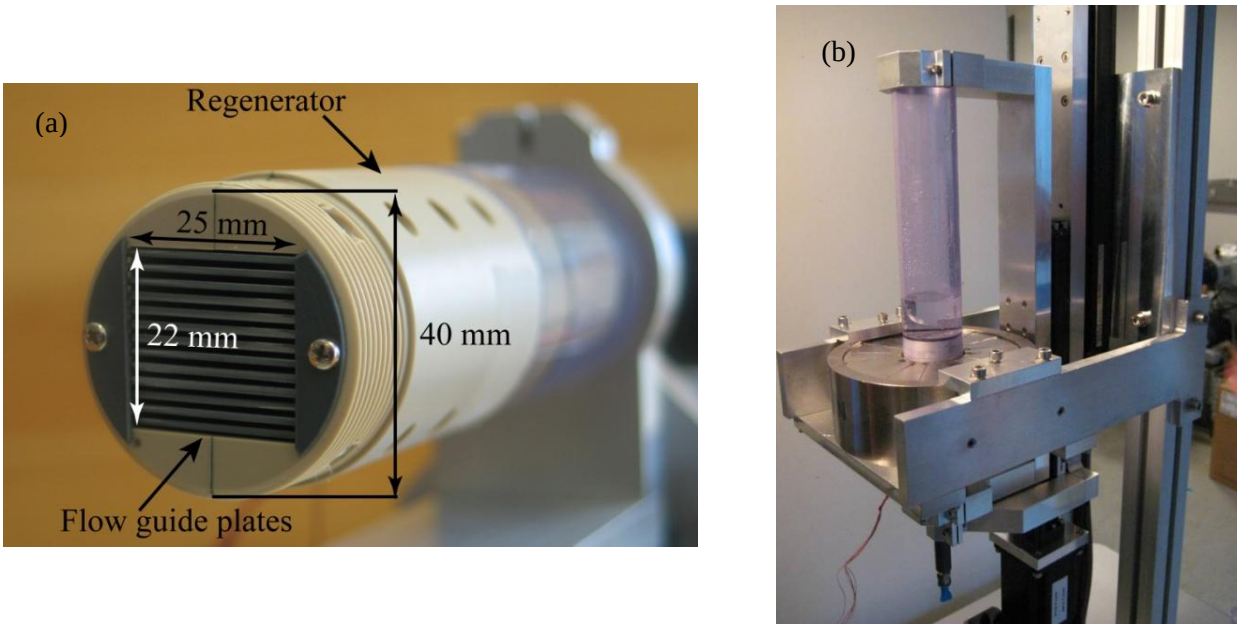

Figure 1: Figure (a) shows a close-up of the experimental AMR test machine where the 13 parallel channels can be seen as well as the plastic tube. Figure (b) is a picture of the machine in its operational environment. The permanent Halbach magnet can be seen with the plastic tube including the regenerator core penetrating it.

The heat transfer fluid is moved by a piston. The regenerator block and its parent plastic tube are suspended vertically in a mounting as shown in Figure 1b and can be moved in and out of the field of the permanent Halbach magnet using stepper motors. This magnet has a maximum magnetic flux density of 1.1 T.
One of the most important results of the experiment – as well as in the model – is to be able to measure the temperature gradient across the regenerator core. This is done via five type E thermo-couples placed equidistantly in the center flow channel as sketched in Figure 2a.

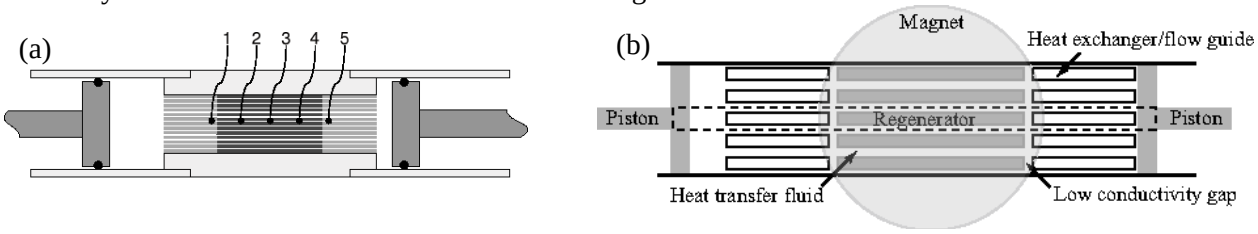

Figure 2: Drawing (a) is a schematic of the regenerator pictured in Figure 1a. The locations of the five thermo-couples are indicated with their appropriate numbers. Thermo-couples 1and 5 are placed at the cold and hot ends respectively. Figure (b) shows how the numerical model represents the full geometry of the AMR. The model breaks the geometry down into a single replicating cell consisting of one half of a complete flow channel (indicated with a dashed line in the figure and magnified in Figure 3).

The system evolves transiently through a number of AMR cycles until cyclic steady-state has been reached. Each cycle consists of four different steps, which have four different characteristic times τ_1, τ_2, τ_3 and τ_4. The cycle is symmetric meaning that $\tau_1 = \tau_3$ and $\tau_2 = \tau_4$. In the first step the magnetic field is applied thus increasing the temperature of the MCM and at this stage the fluid is stationary. In the second step, the pistons move the fluid for τ_2 seconds towards the hot end of the regenerator to reject heat. At the third step the magnetic field is switched off and thus the temperature in the MCM decreases and again at this stage the fluid is stationary. Finally, the piston pushes the fluid towards the cold end for τ_4 seconds. The total cycle-time is $\tau_{total} = 2(\tau_1 + \tau_2)$. In this way the MCM is used as the active material in a regenerator and a

temperature gradient is built up. The magnitude of this gradient depends mainly on the geometry, material and operational properties, i.e. the piston stroke length, τ_1 and τ_2, the height of the fluid channel, the MCM, and how strong the magnetic field is. It is therefore quite a challenge to predict the behavior of a certain system for different process parameters.

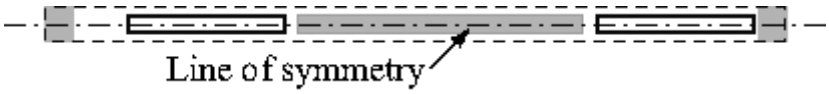

Figure 3: A close-up of the line of symmetry from the replicating cell marked with a dashed line in Figure 2b.

The geometrical simplicity of such an experimental setup makes it ideal for studies of parallel plate regenerators, facilitating direct comparison to the numerical model. Validating the model against the experiment is crucial since a high-quality model can predict the performance of configurations otherwise not thought of and span a much larger parameter-space than possible with the experiment.

3. NUMERICAL MODELING

3.1 Thermal model of the regenerator

The numerical model is "2.5-dimensional" as illustrated geometrically in Figure 4 and Figure 5. For technical reasons the heat transfer fluid is chosen to be stationary and the solid domains are moved relative to this. Thus, the piston movement is modeled as a coordinate transformation of the solid domains with a suitable convective term in the thermal equation for the fluid. The spatial discretization is the classical 2nd order finite difference scheme with a equidistant grid where $\Delta x = 1\,\mathrm{mm}$ and $\Delta y = 0.05\,\mathrm{mm}$, and the temporal integration is done using an Alternate Direction Implicit (ADI) solver with a timestep chosen to be 0.001 second. Since the system includes moving boundaries it is extremely important to make sure that there is energy conservation. Therefore the finite difference (FD) formulation is preferred and validation-tests show that the energy-conservation is virtually the precision of the computer. The computational time on a 2.0 GHz Intel Core 2 Duo CPU is roughly 0.7 CPU-seconds pr physical second in the model.

Due to symmetry considerations only half a replicating cell is modeled (as indicated in Figure 3). This is a good assumption at least for the central channels and plates (which have virtually no loss through the top and bottom of the regenerator).

Figure 4a and Figure 5 show a schematic of the boundary conditions of the model in the (x,y)-plane and (x,z)-plane respectively. The various thermal resistances are labeled with their respective names.

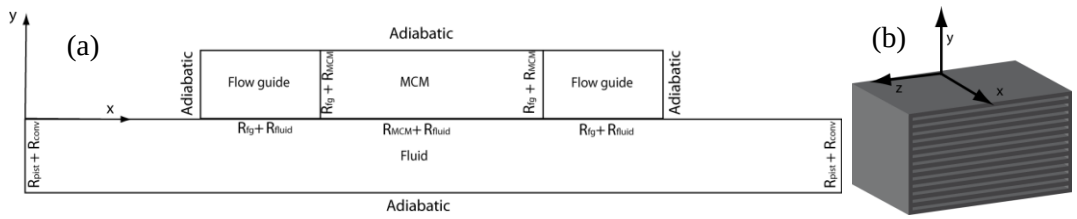

Figure 4 : Figure (a) shows a schematic of the modeled domain in the (x,y)-plane, i.e. half a replicating cell with the boundaries being either adiabatic (symmetry boundaries) or coupled via thermal resistances to the ambient. The x-direction is the direction of the flow and the y-direction is orthogonal to the plates (labeled MCM). The left end is defined as the cold end and the right end as the hot end. Figure (b) shows a 3D sketch of the regenerator block with the coordinate system visualized.

The governing equations for the thermal system are

$$\frac{\partial T_{fl}}{\partial t} = \frac{k_{fl}}{\rho_{fl} c_{p,fl}} \nabla^2 T_{fl} - (\boldsymbol{u} \cdot \nabla) T_{fl} \tag{1}$$

$$\frac{\partial T_s}{\partial t} = \frac{k_s}{\rho_s c_{p,s}} \nabla^2 T_s \tag{2}$$

where the temperatures of the fluid and solid domains are denoted by T_{fl} and T_s respectively. For simplicity all the solid domains are labeled with an s, although they have different physical properties. The thermal properties, i.e. the thermal conductivities k_{fl} and k_s, the mass densities ρ_{fl} and ρ_s and the heat capacities $c_{p,fl}$ and $c_{p,s}$ are all assumed constant except the heat capacity of Gd, which varies as function of both temperature and magnetic field (see Figure 6). The material properties used are given in Table 1.

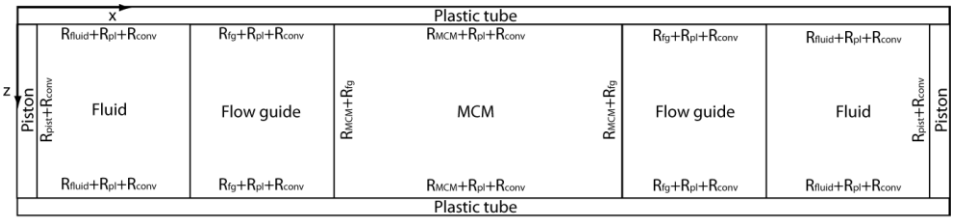

Figure 5 : The model in the (x, z)-plane. The z-direction is only resolved by one grid cell meaning that the model is effectively 2.5-dimensional with the x- and y-dimensions being the two regular dimensions and the finite extension of the z-direction as the half dimension (and most importantly including losses via boundary conditions).

The velocity field in the fluid is denoted by $\boldsymbol{u} = (u, v)$ and is prescribed by the analytical expression for a parallel-plate laminar flow with piston velocity u_p, see e.g. (T. F. Petersen 2007):

$$u = \frac{H_{fl}^2}{2\mu}\frac{\partial p}{\partial x}\left(1 - \frac{y^2}{H_{fl}^2}\right) + u_p \tag{3}$$

$$v = 0 \tag{4}$$

$$\frac{\partial p}{\partial x} = \frac{96}{Re}\,\rho_{fl}\,\frac{1}{4H_{fl}}\,\frac{u_p^2}{2} \tag{5}$$

The Reynolds' number $Re = u_p 4H_{fl}\rho_{fl}/\mu$, ρ_{fl} is the mass density of the fluid, H_{fl} is half the height of the fluid channel, μ is the viscosity of the fluid and y is the vertical coordinate, i.e. orthogonal to the flow direction.

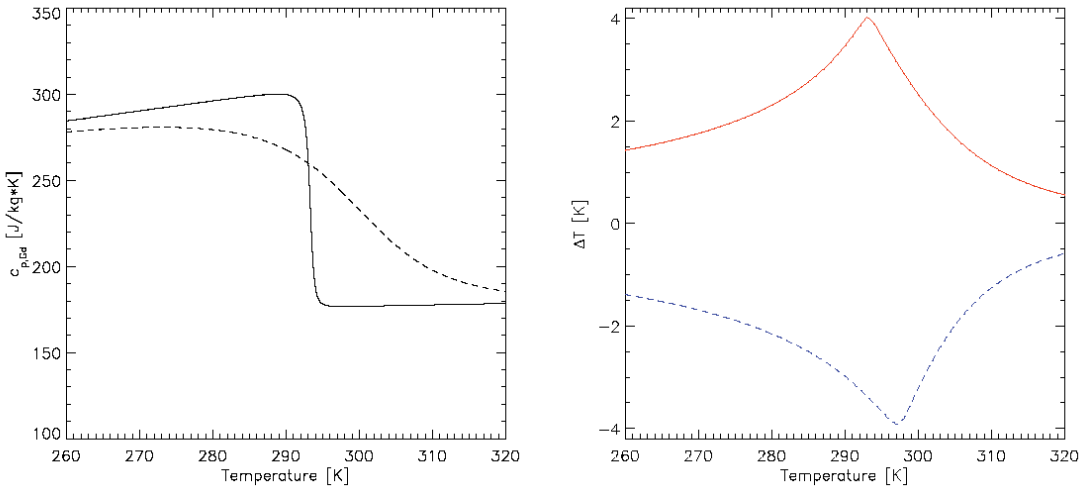

.

Figure 6 : Left: c_p for Gd as function of temperature in zero field (solid line) and in a 1 T field (dashed line). The change around 293 K is rather significant and is actually the definition of the Curie temperature. Right: The adiabatic temperature change of Gd around room-temperature in a 1 T field. The red/solid line is the temperature increase when the field is applied and the blue/dashed line is the corresponding curve for when the field is removed. The data are calculated from the mean field model of Gd compiled in e.g. (Petersen, et al. 2008).

The internal boundaries between the fluid domain and the solid domains are implemented through thermal resistances in Fourier's law of thermal conduction:

$$q_{bd} = -\frac{T_1 - T_2}{R_1 + R_2}. \tag{6}$$

Here the flux across the boundary between two domains (e.g. fluid and MCM) is denoted by q_{bd}, the temperature of the boundary cells in the two adjacent domains are T_1 and T_2 and their corresponding thermal resistances are R_1 and R_2 respectively. The thermal resistance is simply given by the distance from the grid cell's centre to the boundary face divided by the thermal conductivity of the material multiplied by the area of the face boundary.

Table 1 : Material properties used in the model obtained from (Petersen, et al. 2008) and (Holman 1987).

Material	k [W/m · K]	ρ [kg/m^3]	c_p [J/kg · K]	μ [kg/m · s]
Water/ethanol mixture	0.52	981	4330	$8.91 \cdot 10^{-4}$
Plastic	0.2	1200	840	n/a
Gd	10.5	7900	170-300	n/a

The outer boundaries are either adiabatic, if they are symmetry boundaries, or they simulate heat loss in the z-direction, which is not directly resolved (hence this is what we call a 2.5-dimensional model). These losses are calculated via thermal resistances and they contain the thicknesses and thermal conductivities of the particular domain (fluid or solid) and the insulating material surrounding the entire system. On the outer part of the insulating material there is assumed to be natural convection modeled via the parameter h_{conv}, which has a value in the range $5 - 20$ W/Km^2 and corresponds to free convection of air on a plate (Holman 1987).

3.2 The permanent magnet

The magnetic field that generates the MCE can be produced by an electromagnet or a permanent magnet assembly. For this machine we have chosen the latter as this requires no external power source to produce a strong magnetic field. The requirement of the permanent magnet assembly is that it must produce a strong homogenous magnetic field in a confined region of space and a very weak field elsewhere. The design known as a Halbach cylinder (Mallinson 1973), (Halbach 1980) fulfills these requirements and has therefore been chosen for the test machine. An ideal Halbach cylinder consists of a permanent magnetic material with a bore along the cylinder symmetry axis. The magnetic material is magnetized such that the direction of magnetization varies as shown in Figure 7. This produces a strong homogeneous field in the cylinder bore. In the case of an infinitely long cylinder the flux density in the bore is given by $B = B_r \ln\left(\frac{r_{ex}}{r_{in}}\right)$. An ideal Halbach cylinder is not physically realizable, as it is both necessary to make the Halbach cylinder of a finite length and to divide the continuously magnetized cylinder into parts consisting of permanent magnets each with their own directions of magnetization. Based on the design of the regenerator the Halbach cylinder for the test machine consists of 16 blocks of permanent magnets and with dimensions $r_{in} = 2.1$ cm, $r_{ex} = 6$ cm, and $L = 5$ cm.

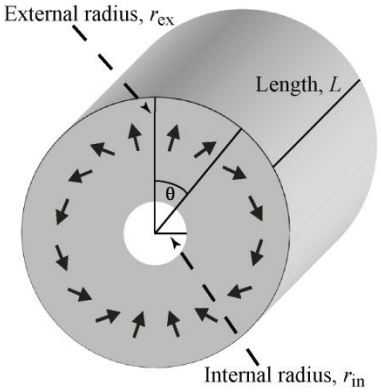

Figure 7: A drawing of a Halbach cylinder showing the internal radius, r_{in}, external radius, r_{ex}, and length, L. Also shown are arrows in the direction of the remanent magnetization of the magnetic material. This varies as 2θ. The figure is from (Bjørk, et al. 2008)

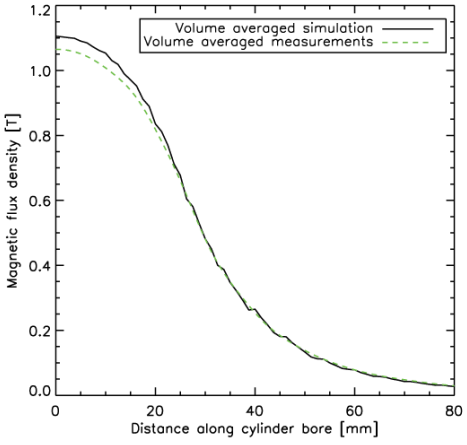

Figure 8: Flux density for the simulated and the physical Halbach cylinder for the test machine. There is good agreement between data.

To investigate the magnetic field produced by this Halbach cylinder we have performed numerical simulations using the commercially available finite element multiphysics program, *Comsol Multiphysics* (Comsol 2005), see also (Bjørk, et al. 2008) for details.

As well as modeling the magnet assembly we have also performed measurements of the flux density of the physical magnet assembly, seen in Figure 1. In Figure 8 the average flux density of the magnetic field as a function of distance from the center of the Halbach cylinder for both simulation and measurement is shown. As can be seen from the figure the numerical simulation and the experimental measurements agree, and show that a high flux density is produced in the center of the cylinder bore.

4. RESULTS

The experimental and modeling results are divided in two parts. First a sensitivity analysis of how far the regenerator is taken out of the Halbach's magnetic field is addressed under no-load conditions. Secondly a load-situation is investigated.

4.1 Sensitivity to the magnetic field

Since the magnetic field of the Hallbach magnet strays outside of the central bore in the cylinder (see Figure 8), the distance which the regenerator block is moved away from the centre of the Halbach must have some influence on the performance of the regenerator. The experiments were adjusted to move the regenerator out of the magnetic field with a distance varying from 30 mm to 150 mm (see Figure 9). The operating conditions were the same for each experiment, which was allowed to reach steady-state in each case (see Table 2). The model was set with the same parameters and the varying magnetic field was implemented via a volumetric source term in the heat equation for the MCM:

$$\frac{dQ_{MCM}}{dt} = -\rho_{Gd} T_{Gd} \frac{\partial \sigma}{\partial T} \frac{dB}{dt}. \tag{7}$$

This is obtained from the mean field theory of Gd, see e.g. (Petersen, et al. 2008). The change with respect to temperature of the magnetization is denoted by $\partial\sigma/\partial T$ and the magnetic flux density is denoted by B. The magnetic field only varies in the x-direction in the regenerator. The crucial term in this formulation is the time variation of the magnetic field. This is implemented simply using the finite extent of the regenerator block and the velocity of which the regenerator is moved in and out of field.

As seen in Figure 9 there is one series of experimental data and two model series. The data sets show the no-load steady-state temperature span between thermo-couples one and five as function of how far the regenerator is taken out of the magnetic field. It is seen from the experimental data that at distances above 70 mm the temperature span does not increase anymore; hence, the full yield of the magnet is utilized.

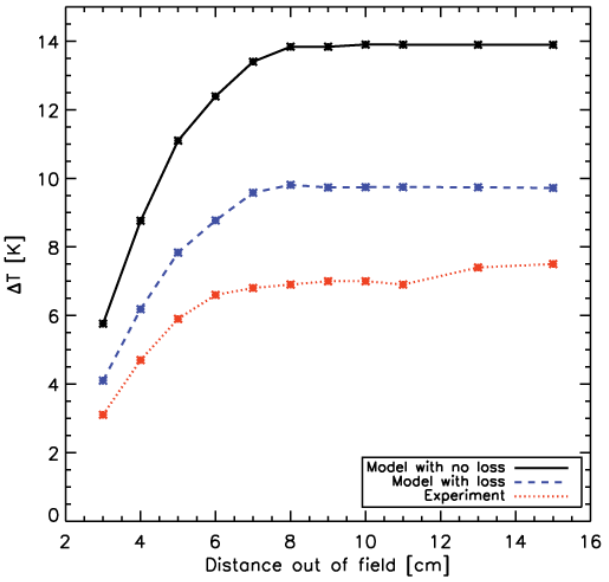

Figure 9: The figure shows how the steady-state and no-load temperature span behaves when the regenerator is not taken completely out of the magnetic field (the red/dotted line). Each asterisk in the graph represents a data point. Also included are the results of two slightly different numerical simulations; one without losses (the black/solid line) and one with ideal losses (blue/dashed line). The tendencies are clearly the same on all three graphs. The absolute values of the temperature spans differ somewhat, however, including losses is seen to improve the correspondence between experiment and model significantly.

The model simulations were done for two cases: One with no loss to the surroundings, i.e. perfect thermal insulation, and one with realistic losses via the boundary conditions described in Section 3.1. The tendencies of all three data sets are virtually the same, which clearly shows that the numerical model catches many of the aspects of the magnetic regeneration. It is not surprising that the ideal adiabatic model overestimates the temperature span somewhat as significant losses to the ambient are expected in the test device. When the losses are included, however, the model comes much closer at the experimental values still showing the exact same tendency.

Table 2 : The operational properties of the two experiment series.

Experiment	Effective piston stroke length (% of plate length)	τ_1(s)	τ_2(s)
Magnetic field variation	40 %	3.0	2.9
Heat load experiment	53 %	1.5	2.9

4.2 Load experiment

The piston at the cold end has been equipped with a copper plate connected to a power supply which makes it possible to apply a heat load through ohmic dissipation to the water. An experiment was run with the

parameters given in Table 2 and heat loads from 0 to 1.6 W. The model was set with the same parameters and a spatially constant magnetic flux density of 1 T. Figure 10 shows both an example of the transient evolution of a specific heat load experiment (left-hand) and the results of the heat-load series (right-hand).

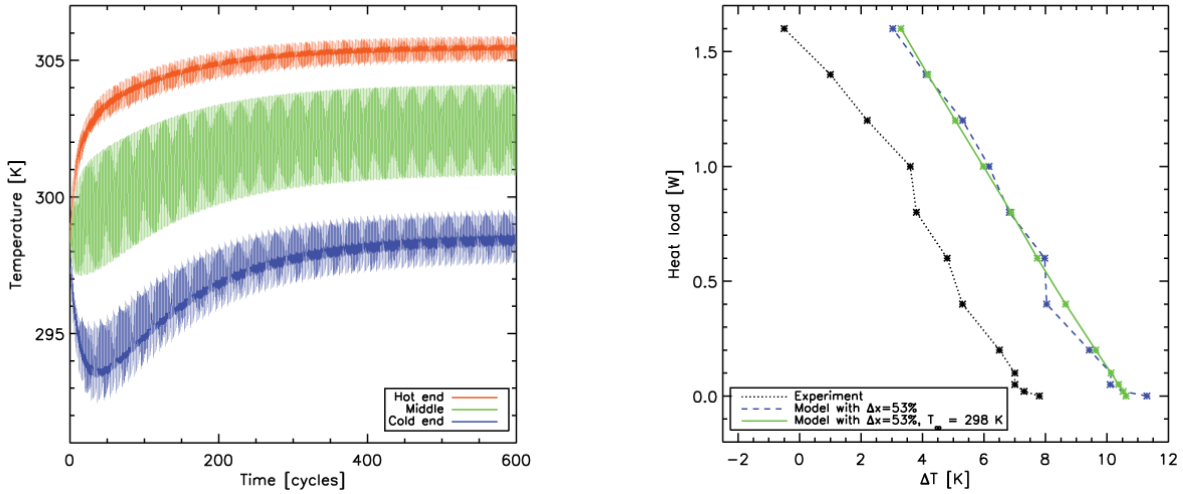

Figure 10: Left: The transient evolution of the cold, middle and hot parts of the regenerator (simulated). The particular example is for a piston stroke (Δx) of 53% with a load of 0.8 W. Right: A load-experiment and the corresponding model results. The model assumed $h_{conv} = 20\,W/m^2K$. *Note that there are two model-series in the right graph. The green/solid line data set was performed with a constant ambient temperature whereas the blue/dashed line data set corresponds directly to the circumstances during the experimental data acquisition (black line/dotted).*

The experimental series was performed over a period of two days since it takes around an hour to reach steady-state for each configuration. Therefore the ambient temperature T_∞ varied slightly (from 296-299 K). This is possible to adjust in the model as well, and therefore the two data sets are directly comparable. The model and the experimental data are very similar in behavior, though the model over-estimates the temperature span. Generally the temperature span decreases linearly with the increasing cooling capacity as one would expect. There are, however, minor fluctuations in the linearity. If the experimental data are considered isolated, the small variations may be regarded as experimental noise. However, when compared to the model data, virtually the same variations are seen. To investigate this, a model-series was performed with the ambient temperature set to the constant value 298 K. This is seen as the green/solid line in the right graph of Figure 10. Thus, the variations away from the linearly decreasing cooling capacity are interpreted as a result of the fluctuations in the ambient temperature. The slopes of each of the three graphs were found by linear regression. The values are all -0.2 $\pm$0.01 W/K.

5. DISCUSSION, CONCLUSIONS AND OUTLOOK

5.1 Discussion

The numerical model has been successfully validated against real experiments in different situations including no-load and load-experiments, varying the magnetic field and some of the operational parameters, namely piston stroke length, τ_1 and τ_2. The discrepancies between the model and the experiment seen in Figure 9 and Figure 10 are, however, something that should be considered and the model should be improved to minimize these. We have used an ideal model for the behavior of Gd in terms of c_p and ΔT_{ad}. We have independently measured the actual adiabatic temperature change of the Gd used in the test machine and it has turned out that due to impurities the actual adiabatic temperature change is roughly 20 % lower than in the ideal mean field model used in the numerical model. We have chosen not to include this in the present work since we have not yet performed enough measurements of the utilized Gd in order to cover the range in magnetic fields and temperature span needed.

A result of this work is that the model is directly capable of catching the effect of the ambient temperature on the system. This may have been interpreted as an experimental feature (e.g. noise) if the model had not caught it and if not the constant-ambient temperature modeling had resulted in the completely straight line seen in the right part of Figure 10.

5.2 Conclusions and outlook

The experimental AMR at Risø DTU has been demonstrated to be quite versatile in terms of operational parameters and various aspects of the cooling capacity. The corresponding numerical model is to a large extent successful in predicting the behavior of the system. Many interesting aspects still need to be investigated though. They include obtaining more reliable and realistic data of the Gd we actually use in our test machine, testing other potential MCM materials and changing the thickness of the plates and the fluid channels as well as the operating parameters. Having a powerful numerical model that predicts the behavior seen experimentally is crucial for the further development of a new AMR with significantly improved performance. The fact that there is a very strong correspondence between the experimental and modeling results in both series presented in Section 4 strongly indicates that the model indeed captures the general behavior of the parallel-plate AMR system.

ACKNOWLEDGEMENTS

The authors thank Mr. Jørgen Geyti for his technical assistance. Furthermore the authors would like to acknowledge the support of the Programme Commission on Energy and Environment (EnMi) (Contract no. 2104-06-0032) which is part of the Danish Council for Strategic Research.

REFERENCES

Bjørk, R., C.R.H. Bahl, A. Smith, and N. Pryds. "Optimization and improvement of Halbach cylinder design." *Journal of Applied Physics, in press*, 2008.

Brown, G. V. "Magnetic heat pumping near room temperature." *Journal of Applied Physics* (AIP) 47 (1976): 3673-3680.

Comsol. *Comsol Multiphysics Model Library, third ed.* COMSOL AB, Chalmers Teknikpark 412 88 G., 2005.

Halbach, K. "Design of permanent multipole magnets with oriented rare earth cobalt material." *Nuclear instruments and methods* 169 (1980).

Holman, J.P. *Heat Transfer.* 6. McGraw-Hill, 1987.

Mallinson, J. C. "One-sided Fluxes - A Magnetic Curiosity?" *IEEE Transactions on magnetics* 9 (4) (1973): 678-682.

Pecharsky, V. K., and K.A. Gschneidner. "Advanced magnetocaloric materials: What does the future hold?" *International Journal of Refrigeration* 29 (2006): 1239-1249.

Petersen, T. F., N. Pryds, A. Smith, J. Hattel, H. Schmidt, and H.J.H Knudsen. "Two-dimensional mathematical model of a reciprocating room-temperature Active Magnetic Regenerator." *International Journal of Refrigeration* 31 (2008): 432-443.

Petersen, Thomas Frank. "Numerical modelling and analysis of a room temperature magnetic refrigeration system." PhD Thesis, Risø National Laboratory and Technical University of Denmark, 2007.

Tura, A., and A. Rowe. "Design and Testing of a Permanent Magnet Magnetic Refrigerator." *2nd International Conference on Magnetic Refrigeration at Room Temperature.* 2007. 363-370.

Warburg, E. "Magnetische untersuchungen." *Ann.Phys (Leipzig)* 13 (1881): 141-164.